ADDIS ABABA UNIVERITY

ADDIS ABABA INSTITUTE OF TECHNOLOGY

SCHOOL OF CHEMICAL AND BIO ENGINEERING

CATALYTIC HYDROPROCESSING OF *BRASSICA CARINATA* OIL TO PRODUCE BIO-JET FUEL: INVESTIGATION OF ALTERNATIVE FEEDSTOCKS, AND SYNTHESIS, CHARACTERIZATION, AND EVALUATION OF SUPPORTED MESOPOROUS CATALYSTS

PH.D. DISSERTATION

ZINNABU TASSEW REDDA

ADDIS ABABA, ETHIOPIA

AUGUST 2024

Catalytic Hydroprocessing of *Brassica carinata* Oil to Produce Bio-Jet Fuel: Investigation of Alternative Feedstocks, and Synthesis, Characterization, and Evaluation of Supported Mesoporous Catalysts

by

ZINNABU TASSEW REDDA

A PH.D. DISSERTATION

Submitted to the School of

Chemical and Bio Engineering of Addis Ababa Institute of Technology,

Addis Ababa University, Addis Ababa, Ethiopia

in Partial Fulfilment of the Requirements

for the Degree of

DOCTOR OF PHILOSOPHY

in

CHEMICAL ENGINEERING (PROCESS ENGINEERING)

August 2024

STATEMENT OF THE AUTHOR

By my signature below, I declare and affirm that this doctoral dissertation is my work. It has not been submitted for any degree or examination at any other university. I have adhered to all ethical guidelines, which are in line with the university's regulations, and meet the accepted requirements for originality and quality.

Citations have been used to acknowledge every scholarly content incorporated in the thesis. I confirm that every source I utilized when writing this thesis has been cited and referenced. This thesis has been prepared with every great precaution to avoid plagiarism.

Zinnabu Tassew Redda		29/08/2024
Ph.D. Candidate	**Signature**	**Date**

APPROVAL SHEET

The dissertation, entitled **"Catalytic Hydroprocessing of *Brassica carinata* Oil to Produce Bio-Jet Fuel: Investigation of Alternative Feedstocks, and Synthesis, Characterization, and Evaluation of Supported Mesoporous Catalysts"** prepared and submitted by Zinnabu Tassew Redda in partial fulfillment of the requirements for the Degree of Doctor of Philosophy in Chemical Engineering complies with the regulations of the university and meets the accepted standards with respect to originality and quality.

Approved by the Examination Committee

Prof. Dr. Nigus Gabbiye		August 31, 2024
Internal Examiner	**Signature**	**Date**
Prof. Dr. Frank Behrendt		August 29, 2024
External Examiner	**Signature**	**Date**
Dr. Eng. Abubeker Yimam		01.11.2024
Major Advisor	**Signature**	**Date**
Prof. Dr. Asnakech Laß-Seyoum		*September 06, 2024*
Major Advisor	**Signature**	**Date**
Prof. Dr. -Ing. Mirko Barz		24.10.2024
Co-Advisor	**Signature**	**Date**
Dr. Shimelis Kebede		01.11.2024
Chair Person	**Signature**	**Date**

DEDICATION

I dedicate my dissertation work to my family and many friends. I am profoundly thankful to my loving parents, Mr. Tassew Redda Kahsay and Mrs. Asefu Molla Mengesha, whose unwavering support, encouragement, and love have sustained me throughout every stage of my life.

This dissertation is also dedicated to my wife, Mrs. Medhanit Nigusie Araya, younger brother, Haftu Tassew Redda, younger sister, Marzeneb Tassew Redda, and many other family members and friends whose words of support and inspiration for tenacity ring in my ears, always remain by my side, and are truly special.

ACKNOWLEDGEMENTS

Above everything, my biggest and highest thanks should go to the Almighty God without whom nothing would have been ever possible. Next, I am extremely thankful and appreciative to my supervisors, Dr. Eng. Abubeker Yimam from Addis Ababa University, Ethiopia, Prof. Dr. Asnakech Laß-Seyoum and Prof. Dr.-Ing. Mirko Barz from the University of Applied Sciences (HTW) Berlin, Germany for their compassion, guidance, and unwavering support throughout my doctoral studies. Their invaluable daily suggestions/comments, immense knowledge, and gigantic experience have been tremendously helpful to me at all levels of study and provided me with abundant experience for my academic research career.

Furthermore, my unalloyed appreciation goes to Prof. Asnakech Laß-Seyoum for her voluminous and invaluable contributions and guidance throughout my studies. Prof. Laß-Seyoum, I hold all of your day-to-day suggestions, remarks, and encouraging words close to my heart; they will never be forgotten. Your high degree of freedom and your words of hope to me in the course of this study were extremely invaluable. In general, I am at a loss for words to properly express your contributions to the study and myself. Prof. Mirko Barz, I cannot quantify your contributions and support throughout the course of the study, your co-supervision has left no vacuum. I am exceptionally thankful for all of your incredible efforts and support.

For their excellent support, I would additionally like to extend my heartfelt thanks to all of the technical and administrative colleagues at Faculty I, University of Applied Sciences (HTW), Berlin, Germany. My friend, Mr. Steffen Kadow, of HTW Berlin deserves very special recognition for his persistent help and relentless commitment during the study.

The success of the study can also be largely attributed to Mr. Daniel Brennecke and his colleagues at the Fritz-Haber-Institute of Max-Planck-Society (FHI), Berlin, Germany; Mr. Carsten Prinz and Mrs. Annett Zimathies, Federal Institute for Materials Research and Testing (BAM), Berlin, Germany; and Prof. Dr. rer. nat. Hartmut Wesenfeld and Prof. Dr. Monika Buchholz, Berlin University of Technology (BHT), Berlin, Germany, for which I would like to take this opportunity to sincerely appreciate them.

I am also especially profoundly indebted to my employer institution, Addis Ababa University, for covering my full-time study. In addition, I must not fail to sincerely appreciate and acknowledge the academic and administrative colleagues of the School of Chemical and Bio Engineering of the university. I also would like to express my sincere gratitude to DAAD for providing me with the financial assistance required to fully fund the 2018 Ethio-German Home-Grown Ph.D. Scholarship Program.

Additionally, the Holetta Agricultural Research Center in Holetta, Ethiopia, deserves a great deal of recognition for providing me with the various *Brassica carinata* oilseed crops that are the primary subjects of the study. Mr. Birhanu Mengistu Aboye deserves particular acknowledgment for his efforts.

For their financial support when the DAAD Scholarship program came to an end, I am especially indebted to Prof. Asnakech Laß-Seyoum, Mr. Detlev Laß, and Mr. Hartmut Welke (CEO of Pneumatik Berlin GmbH PTM) in Berlin, Germany. Your financial assistance has greatly aided my stay in Germany and enabled me to successfully complete my studies. I am incredibly grateful for this.

I am also incredibly grateful to the following individuals: Mrs. Katharina Becker, Mr. Marco Haupt, and Mr. Tobias Fries, University of Applied Sciences (HTW) Berlin, Berlin, Germany; Mrs. Susanne Hoffmann, Institute for Energy Technology, Technical University of Berlin, Berlin, Germany; Dr. Sven Schaller, Dr. Özge Mutlu, and other colleagues of the German Biomass Research Centre (DBFZ), Leipzig, Germany; Mr. Hintsa Selassie Seife, Mr. Aklilu G/Hawaria, Mr. Samson Addisu, Dr. Estifanos Ele Yaya, Mrs. Senait Dagne, and Mr. Debebe Hailu, Addis Ababa University, Addis Ababa, Ethiopia.

LIST OF ACRONYMS, AND ABBREVIATIONS

AJF	Alternative Jet Fuel
ATJ	Alcohol-To-Jet
ATR	Attenuated Total Reflectance
BET	Brunauer-Emmett-Teller
BF	Bright Field Scanning
BJH	Barrett-Joyner-Halenda
CHR	Carbothermal Hydrogen Reduction
deCO	Decarbonylation
$deCO_2$	Decarboxylation
DIN	Deutsches Institut fur Normung (German Institute for Standardisation)
DRS	Diffuse Reflectance Spectroscopy
DSC	Differential Scanning Calorimetry
DSCH	Direct Sugar-to-Hydrocarbon
DTA	Differential Thermal Analysis
DTG	Differential Thermogravimetric Analysis
DTGS	Deuterated Triglycine Sulfate
EDS	Energy-dispersive X-ray spectroscopy
FT	Fischer–Tropsch
FT-BTL	Fisher-Tropsch Biomass to Liquid
FWHM	Full-Width Half Maximum
GC-TCD	Gas Chromatography Thermo-Conductivity Detector
GTJ	Gas-To-Jet
$GtCO_2$	Gigaton of Carbon Dioxide
HAADF	High Angle Annular Dark Field Scanning
HDN	Hydrodenitrogenation
HDO	Hydrodeoxygenation
HEFA	Hydroprocessed Esters and Fatty Acids
HHV	Higher Heating Value
FT	Fischer–Tropsch

HRJ	Hydroprocessed Renewable Jet
HTL	Hydrothermal Liquefaction
IATA	International Air Transport Association
ICAO	International Civil Aviation Organization
ICP-OES	Inductively Coupled Plasma Optical Emission Spectroscopy
IEA	International Energy Agency
IWI	Incipient Wetness Impregnation
JCPDS	Joint Committee on Powder Diffraction Standards
LHSV	Liquid Hourly Space Velocity
LRS	Laser Raman Spectroscopy
MFC	Mass Flow Controller
MSI	Metal-Support Interaction
NCV	Net Calorific Value
OTJ	Oil-To-Jet
SAF	Sustainable Aviation Fuels
SIP	Synthesized Iso-Paraffins
SPK	Synthetic Paraffinic Kerosene
STEM	Scanning Transmission Electron Microscope
TCR	Thermo-Catalytic Reforming
TEM	Transimision Electron Microscope
TGA	Thermogravimetric Analysis
TG-MS	Thermogravimetric And Mass Spectroscopy
TMC	Transition Metal Carbide
TPD	Temperature–Programmed Desorption
TPO	Temperature–Programmed Oxidation
TPR	Temperature Programmed Reduction
TPRC	Temperature Programmed Reduction Carburization
WHSV	Weight Hourly Space Velocity
XPS	X-Ray Photoelectron Spectroscopies
HRJ	Hydroprocessed Renewable Jet

TABLE OF CONTENTS

LIST OF TABLES

LIST OF FIGURES

LIST OF TABLES IN THE APPENDIX

LIST OF FIGURES IN THE APPENDIX

LIST OF PUBLICATIONS AND CONFERENCES

Peer-Reviewed Publications

1. **Redda, Z.T.**, Laß-Seyoum, A., Yimam, A. *et al.* Solvent extraction and characterization of *Brassica carinata* oils as promising alternative feedstock for bio-jet fuel production. *Biomass Conv. Bioref.* **14**, 12207–12226 (2024). https://doi.org/10.1007/s13399-022-03343-x
2. **Redda, Z.T.**, Laß-Seyoum, A., Yimam, A. *et al.* Characterization of Hexane-Defatted *Brassica carinata* Oilseed Meals to Explore Their Potential for Valorisation Towards a Sustainable Circular Bioeconomy. *Waste Biomass Valor* **15**, 1185–1197 (2024). https://doi.org/10.1007/s12649-023-02248-8
3. **Redda, Z.T.**, Laß-Seyoum, A., Yimam, A. *et al.* Pyrolysis-Based Synthesis and Characterization of Bio-Oil From *Brassica Carinata* Oilseed Meals and Its Application to Produce Bio-Jet Fuel. *Bioenerg. Res.* **17**, 1328–1343 (2024). https://doi.org/10.1007/s12155-023-10703-6
4. **Redda, Z.T.**, Brennecke, D., Prinz, C. *et al.* Synthesis and Characterization of $AlPO_4$-18 Supported Mesoporous and Crystalline β-Mo_2C, Ni_3C, and WC Nanoparticles. *Catal Lett* (2024). https://doi.org/10.1007/s10562-024-04791-y
5. **Redda, Z.T**., Kadow S., Barz M., Yimam A. *et al.* Catalytic hydroprocessing of Yellow Dodolla oil using thermally stable and mesoporous $AlPO_4$-18 supported β-Mo_2C, Ni_3C, and WC nanoparticles to produce bio-jet fuel. Under review.
6. **Redda, Z. T.**, Gizaw, D. G., Periyasamy, S., Isabel, J. B., & Karthik, V. (2023). Sustainable aviation biofuels. In Environmental Sustainability of Biofuels (pp. 363–388). Elsevier. https://doi.org/10.1016/B978-0-323-91159-7.00003-5

Conference Presentation

1. **Redda, Z. T**., Laß-Seyoum, Asnakech; Yimam, Abubeker; Barz, Mirko: Suitability of *Brassica carinata* oils as alternative feedstocks for bio-jet fuel production. In: In: Proceedings of the 8th International Conference on Sustainable Energy and Environment (SEE 2022): The Road to Net-Zero: Energy Transition Challenges and Solutions, S. 1 - 14, Bangkok, Thailand, 2022, ISBN 978-974-456-820-5. Oral presentation.

EXECUTIVE SUMMARY

The aviation industry, which is one of the biggest drivers of economic growth, offers a considerable contribution to the global economy. However, over the past few decades, the industry has played a significant role in driving up a significant portion of greenhouse gas emissions into the atmosphere, contributing significantly to global CO_2 emissions. The transition from fossil-derived jet fuels to sustainable aviation fuels is one of the most viable strategies to decarbonize the industry and mitigate CO_2 emissions generated by fossil fuel combustion. Consequently, as environmental concerns pertaining to the effects of CO_2 emissions from fuels derived from carbon resources that originate from fossil fuels are growing, the endeavor to explore renewable carbon sources has been spurred. As a fossil fuel substitute, bio-jet fuel, one of the most significant forms of renewable and green energy that can be potentially derived from renewable and alternative feedstocks, has the potential to improve energy security, reduce carbon footprint, and promote agricultural economy and social development.

In this doctoral study, comprehensive experimental investigations were conducted on a variety of *Brassica carinata* oilseed crops (indigenous to Ethiopia) derived coproducts, including non-food vegetable oils, oilseed meals, and bio-oils to evaluate their potential industrial applications, particularly in the aviation industry. Following their successful synthesis, supported transition metal carbide catalysts, distinguished for their superior properties, were evaluated for their ability to produce bio-jet fuel. Under appropriate reaction conditions, a lab-scale designed fixed-bed reactor system was used to transform the oil feedstock, Yellow Dodolla oil (one of the most remarkable inedible *Brassica carinata* vegetable oils), into the bio-jet fuel.

The non-food *Brassica carinata* vegetable oils were extracted using a solvent extraction method involving the Response Surface Methodology with Box-Behnken Design in an isothermal batch reactor. After extraction, physicochemical characterization, fatty acid profiling, ultimate analysis, metal and phosphorus concentration analysis, Fourier-transform infrared spectroscopy characterization, and calorific value studies were used to investigate the qualities of the oils. As a result, it was found that oil yields varied between 35.93 and 45.25%. Erucic acid was the most prevalent fatty acid in all oils, representing 42–50% in Derash and Yellow Dodolla oils, respectively, making Yellow Dodolla oil a super-high erucic acid oil. The characterization results also showed that the *Brassica carinata* oils have better physicochemical qualities, exceptional fatty

acid profiles, and extremely low concentrations of metals, phosphorous, and heteroatoms (nitrogen, and sulfur). As a result, the oils—most notably Yellow Dodolla oil—are of the highest caliber and offer a viable alternative feedstock for upgrading them into bio-jet fuel using a hydroprocessing route. However, the bio-jet fuel plant's output streams, such as solvent defatted oilseed meals, may be utilized as an effective resource utilization approach, to produce a wide range of co-products. Thus, a comprehensive study was conducted on these meals using bomb calorimetric digestion, proximate analysis, ultimate analysis, inductively coupled plasma optical emission spectroscopic analysis, and determination of energy densities. Characterization results verified that the meals' highly distinguishing characteristics enable them better options than other oilseed meals.

However, through valorization, the solvent-defatted oilseed meals can be employed as a useful resource utilization strategy which could subsequently support the development of a carinata-based circular bio-economy. Four different hexane-defatted meals were characterized and valorized for their substantial potential valorization options. Proximate analysis, ultimate analysis, inductively coupled plasma optical emission spectroscopic analysis, bomb calorimetric digestion, and energy densities, were used to characterize the meals. As a result, analysis results demonstrated that the meals had distinct features, making them ideal alternative feedstocks for valorization into a variety of industrial applications.

The solvent-defatted oilseed meals were further used to produce bio-oils using a non-catalytic slow pyrolysis approach at various temperatures (350−500 °C). The pyrolysis experiments showed that the highest temperature (550 °C) yielded the maximum bio-oil product (55.01%), while the lowest temperature (350 °C) yielded the maximum bio-char (34.93%) and gas (45.84%) yields. The properties of the bio-oils were studied using physicochemical characterization, ultimate analysis, atomic ratios analysis, heating value analysis, inductively coupled plasma-optical emission spectrometry analysis, gas chromatograph-mass spectroscopy, and Fourier-transform infrared spectroscopy. Analysis results showed that the bio-oils had moisture (35.38−48.64%), pH (8.50), kinematic viscosity (14.10−16.05 cSt), ash content (0.17−0.208%), carbon (55.4−62.3%), hydrogen (9.02−9.29%), nitrogen (6.08−6.20%), sulfur (0.61−0.69%), oxygen (21.47−28.56%), and higher heating value (26.98−30.45MJ/kg). Furthermore, it was found that the major classes of compounds identified include saturated hydrocarbons (13.56−14.52%), saturated fatty acids (2.33−3.67%), monounsaturated hydrocarbons (30.28−34.62%), monounsaturated fatty acids

(6.54−11.23%), polyunsaturated fatty acids (1.41−2.82%), and Others (such as nitrogenated compounds) (38.44−39.62%).

However, since a catalytic hydroconversion technique will be applied for transforming the oil feedstock, high-efficiency, high-stability, and low-cost deoxygenation and hydrocracking catalytic materials must be developed. Aluminophosphate ($AlPO_4$-18), a zeolite-like molecular sieve, was used as a catalyst support for the synthesis of carbon-coated β-Mo_2C, Ni_3C, and WC nanoparticle catalytic materials. The nanoparticles were synthesized using an incipient wetness impregnation followed by a temperature-programmed reduction-carburization approach, which involved cracking a hydrocarbon gas, propane, in a hydrogen environment. The synthesis parameters were a 1:7 propane/hydrogen reductive-carburizing gas stream, 15 wt. % metal loading, an 800 °C carburization temperature ramped-up at a heating rate of 10 °C min^{-1}, 2 hours holding time, and a 1-hour holding time in a hydrogen environment. The nanoparticles were characterized by thermogravimetry mass spectroscopy coupled with temperature-programmed oxidation (TPO TG-MS), nitrogen physisorption at 77 K, X-ray diffraction (XRD), and transmission electron microscopy (TEM) coupled with energy-dispersive X-ray spectroscopy (EDS) methods.

Consequently, TPO TG-MS, nitrogen physisorption, TEM, and XRD characterization results proved that atomic carbon was successfully incorporated into the lattice interstitials, resulting in the development of thermally stable $AlPO_4$-18 supported well-dispersed, crystalline and mesoporous β-Mo_2C, Ni_3C, and WC nanoparticles. Moreover, XRD analysis showed how the structural evolution occurred during the reduction-carburization, revealing average crystallite sizes of the metal-containing particles to be 8.2–9.22, 6.64–8.50, and 6.03–7.56 nm for β-Mo_2C/$AlPO_4$-18, Ni_3C/$AlPO_4$-18, and WC/$AlPO_4$-18, respectively, with these values did not significantly deviate from the results of high-resolution TEM analysis. After the reduction-carburization process, the nanoparticles' surface areas dropped and were categorized in decreasing order as WC/$AlPO_4$-18 > Ni_3C/$AlPO_4$-18 > β-Mo_2C/$AlPO_4$-18, with values of 193.79, 169.05, and 66.57 m^2 g^{-1}, respectively.

Following the successful synthesis of the nanoparticles, a single pot oil-to-jet catalytic hydroprocessing upgrading approach was employed to evaluate the nanoparticles' catalytic activities. The catalytic activities were carried out on Yellow Dodolla oil to transform it into bio-jet fuel. The deoxygenation and hydrocracking reactions were carried out at different reaction

temperatures (300 and 500 °C) and an elevated hydrogen pressure (21 bar) in a laboratory-scale designed three-phase continuous fixed-bed reactor system. The remaining variables, including the volumetric flow rates of the oil feedstock (0.30 mL min^{-1}), hydrogen gas (350 mL min^{-1}), the hydrogen gas-to-oil ratio (1,667 mL H_2 gas per mL oil), the catalyst-to-oil ratio (0.14 g catalyst per g oil), the liquid hourly space velocity (LHSV) (2.41 h^{-1}), the weight hourly space velocity (WHSV) (2.78 h^{-1}), and the residence time (2.5 h), were all kept constant throughout the experiments.

Consequently, the hydrodeoxygenation, hydrodecarbonylation, decarboxylation, and hydrocracking/polymerization reactions resulted in a conversion of 71.57–79.76 wt. %, with the highest conversion was achieved by $Ni_3C/AlPO_4$–18 catalyst at the maximum temperature. The results of these catalytic reactions showed that the rate of deoxygenation varied from 8.08 to 11.67 wt.% at 300 °C, with nickel catalyst achieving the highest rate and molybdenum having the lowest. Yet, the rate of deoxygenation rose sharply to 96.67, 62.44, and 57.31 wt. %, respectively, via molybdenum, nickel, and tungsten catalysts as the temperature rose to 500 °C. Moreover, it was determined that bio-jet fuel (C_8-C_{16}) exhibited remarkably higher yields (23.34–27.31 wt.%) and selectivity (37–45 wt.%) at the maximum temperature when compared to biogasoline (2.63–8.72 wt.%) and biodiesel (1.18–4.58 wt.%). The $WC/AlPO_4$-18 catalyst produced the highest yields and selectivity of the jet fuel. Furthermore, characterization findings of products revealed that, in comparison to conventional jet fuels, they had nearly identical physicochemical properties, chemical compositions, hydrogen-to-carbon atomic ratio (H/C) (1.90–1.92), oxygen-to-carbon atomic ratio (O/C) (0.002–0.030), and gravimetric energy density, net, (41.35–42.89 MJ kg^{-1}) compared to conventional jet fuels.

In conclusion, the comprehensive investigation carried out on the various *Brassica carinata* coproducts—vegetable oils, oilseed meals, and bio-oils—showed that they are highly significant and viable alternative feedstocks for various industrial uses, particularly in the aviation industry. Because of the fierce competition for resources on a global scale, which is rendering aviation fuels unsustainable in the long run, the use of a hydroconversion approach involving low-cost, high-efficiency, and high-stability transition metal carbide nanocatalyst alternatives on *Brassica carinata* coproducts can be considered one of the most promising decarbonization strategies.

Keywords: *Brassica carinata* Oil; Oilseed Meal; Catalyst Synthesis; Catalyst Characterization; Transition Metal Carbide Catalyst; Nanoparticle; Fixed-Bed Reactor; Sustainable Aviation Fuel.

CHAPTER ONE

INTRODUCTION

1.1 Background

Energy has evolved into an essential component of long-term economic prosperity and a high standard of living for human beings [1]. Nations use considerably more energy in the twenty-first century than they did in the past for domestic demands, transportation, and industrial expansion [2]. Nowadays, fossil fuels, which will remain the biggest source of energy for the next two to three decades, are a major component of the global economy [2]. For all the world's energy demands, even though these fuels are indispensable, their prices are unstable and they are not sustainable. Furthermore, the most important global environmental challenges produced by the combustion of fossil fuels are currently influenced by global warming, precipitation of acid rain, and pollution [1].

This century will see an increase in the global population from 6 billion to 11 billion people, a doubling of life expectancy over the previous two centuries, and a 35-fold rise in energy demands [3]. Thus, global issues such as overcrowding, air pollution, freshwater pollution, coastal pollution, deforestation, biodiversity loss, and deteriorating climate change have become the forefront of the development of energy [4]. However, in the present day, fossil fuels supply nearly 81% of commercial energy consumption, with oil accounting for 34.3%, coal for 26.0%, and gas for 20.5%. Nuclear energy and hydroelectric power account for 6.2% and 2.2%, respectively, with the remainder of 10.8% split between renewable energy sources such as biomass (like biofuels), the solar, wind, and geothermal energy [5].

Transportation, after industry, is the globe's second-biggest energy-consuming industry, consuming approximately 30% of the total global energy supply, with road transport accounting for 80% as reported in [6]**.** Predictions also state that this industry will have the fastest-growing energy consumption and consume approximately 60 percent of the world's oil. The majority of fossil fuels utilized in the transportation sector—roughly 97.6%—come from oil, with very little coming from natural gas. This industry is predicted to account for around three-fourths of the increase in oil demand between 2006 and 2030 [6].

In light of the pivotal role of air travel in the contemporary world, the global aviation sector is predicted to grow steadily in the years to come. According to the International Air Transport Association (IATA), 53.9 million metric tons of goods worth over $5.5 trillion and nearly 3.8 billion passengers were moved in 2016 [7]**.** As per the 2017 IATA annual report, $3.0 trillion in economic activities and 67.7 million employments were generated by commercial aviation in 2016. By 2034, it is predicted that commercial aviation will consistently grow, generating 90 million employment and around $6 trillion in yearly economic activity (compared to $3 trillion in 2016). This huge increase in air traffic necessitates a substantial volume of aviation fuel (jet fuel); yet, the widespread usage of conventional oils in recent times has culminated in a significant drop in petroleum reserves [7].

Even though the aviation industry contributes significantly to the global economy, providing approximately 57 million employment and USD 2.2 trillion in GDP [8], its high reliance on petroleum-based liquid fuels, along with the continued boom in demand, has resulted in a relentless increase in the sector's greenhouse gas emissions (GHG) [9]. As a result, according to [10], jet fuel consumption will double and CO_2 emissions will spike six times by 2050 as a result of the anticipated 3-5% annual growth in passenger and 10% annual growth in freight air travel over the next 30 years. Governments are issuing directions to encourage the use of jet fuels derived from biomass, or bio-jet fuels, in an effort to lessen the aviation sector's reliance on petroleum and reduce the accompanying GHG emissions [10]. Based on the Three Global Goals and Four Pillars outlined in [11], the aviation sector most significantly acknowledged the need to address the global challenge of climate change and approved a set of ambitious targets to minimize CO_2 emissions from air transport in 2009.

However, crude oil prices, feedstock availability and cost, conversion technology yields and costs, and governmental regulations are some of the biggest constraints to investment in sustainable aviation fuel (SAF) production [12]. In other words, raw materials cost accounts for a significant quantity of the entire cost of bio-jet production [13], rendering commercial bio-jet fuel production economically challenging. In contrast to traditional aviation fuel, which has a cost per liter of $0.55, the price of SAF may vary from $0.44 to $8.45, based on the feedstocks used, yield variations by location, and conversion technology [14], [15], [16]. However, in another study reported by [17], it was shown that the minimum fuel selling price (MFSP) of a bio-jet fuel produced using the

HEFA approach primarily depends on the feedstock utilized during the process. As a result, a readily available supply of feedstocks is required to lower production expenses and enhance market supply [18].

Nowadays, used cooking oil, animal fats, and vegetable oils are the main sources of alternative jet fuels (AJF) produced by the hydroprocessed esters and fatty acids (HEFA) pathway [19]. Ling et al. [20] investigated 20 different feedstocks for triglyceride production, and their findings demonstrate that the majority of the oils derived from these feedstocks consist of C_{16} and C_{18} fatty acids. *Brassica carinata* A. Braun, often known as "Ethiopian mustard", "Ethiopian rape", "Abyssinian mustard", or simply "carinata", is being explored as a non-food and oil-based feedstock related to camelina and soybean and is identified as a new potential feedstock for SAF production [21,22]. Carinata, unlike soybean and canola, does not have a food-versus-fuel controversy because it is not appropriate for direct human consumption [23]. More importantly, carinata oil has a fatty acid profile of $C_{16:0}$ to $C_{22:1}$ [24], and the oil's 22-carbon chain can also be split into two biofuel hydrocarbons, doubling the fuel output for each erucic acid molecule [25], making it more advantageous than other feedstocks.

Moreover, carinata is an excellent oilseed crop for crop rotation and intercropping with food crops such as wheat, chickpeas, barley, and sorghum [26], [27], [28]. Carinata is employed as a cover crop to enhance soil health and mitigate soil erosion [29]. It is more agronomically superior and frost-resistant than other oilseed crops and mustards. In addition, it is extremely tolerant to a wide range of biotic (like disease and insect pests) and abiotic factors (like drought and cold tolerance) [29]. In comparison to canola (1456 kg/ha) and camelina (952 kg/ha), carinata has the maximum seed yield, 2800 kg/ha [30]. Moreover, it contains a very high oil content (36–45%) and a greater erucic acid concentration (42–50%) [24].

Catalytic hydroprocessing of esters and fatty acids (HEFA) is the most well-established of the American Society for Testing and Materials (ASTM)-approved and certified processes for producing alternative aviation fuels [31]. More attention has been paid to this conversion pathway because of its high product yield, lower technological complexity, lower cost of production, greater energy efficiency, and high level of maturity and reliability compared to other technologies including alcohol-to-jet (ATJ), direct sugar to hydrocarbon (DSHC), gasification and Fischer Tropsch process (GFT), and fast pyrolysis (FP) [31], [32]. Bio-derived synthetic paraffinic

kerosene (Bio-SPK) or hydroprocessed renewable jet (HRJ) were the original terms used to describe hydroprocessed esters and fatty acids (HEFA). However, because the term "hydroprocessed esters and fatty acids" (HEFA) better accurately describes the feedstock and the method of production, HRJ fuels were redesignated as HEFA during the evaluation and approval process [33]. Moreover, bio-aviation fuel (also referred to as bio-jet fuel, renewable jet fuel, or aviation biofuel) a kind of biofuel for the air transport industry, is identified as a short- to medium-term strategy for reducing the sector's overall GHG emissions [8]. Bio-aviation fuel is a biomass-derived synthetic paraffinic kerosene (SPK) that is blended with traditionally petroleum-derived jet fuel [7].

Hydroprocessed esters and fatty acids are a complex set of catalytic reactions that are carried out in the presence of hydrogen gas and transform lipids (vegetable oils and animal fats) into HRJ fuel [34], [35]. Hydrogenation reactions often take place on metal surfaces, where hydrogen gas is dissociated and subsequently reacts to remove the dissolved oxygen of feedstocks [36], [37]. High pressures are employed to guarantee proper solubility of hydrogen, and to increase its availability in the vicinity of the catalyst [37], and may also help to reduce the rate of coke formation [38]. Based on [39], the production of hydrocarbons via hydroprocessing technology necessitates the use of heterogeneous catalysts with simultaneous hydrogenation and cracking properties.

Over the past few decades, transition metal carbides (TMCs) have garnered a lot of attention for a variety of scientific applications in numerous sectors, including heterogeneous catalysis [40]**.** Because of their unique and intriguing physical and chemical properties, such as the extreme hardness of covalent solids, high melting temperature of ionic crystals, excellent electrical, and thermal conductivity, and catalytic properties [41]**,** they have recently been investigated in a variety of areas, including biomass conversions, particularly in the cleavage reactions of C-C, C-O-C, and C-O-H bonds [42].

1.2 Statement of Problem

The development of alternative transportation fuels is being propelled by several variables including economic sustainability, environmental sustainability, competition for energy resources, and diversity in the energy supply, with geographical location affecting the relative relevance of the drivers [43]. Despite improvements in airplane fuel efficiency, the amount of GHG produced by domestic and international aviation has increased continuously since 1970. This trend is

predicted to continue [44]. The aviation industry uses approximately 3% of the globe's fossil fuels, produces 2% of anthropogenic GHG emissions, and contributes between 11% and 12% of all transportation-related CO_2 emissions worldwide. The International Energy Agency (IEA) predicts that in 2019, aviation produced 1.03 $GtCO_2$, of which 36% came from domestic flights and 64% from international flights. Due to COVID-19 lockdowns, emissions fell to 0.61 $GtCO_2$ in 2020 but slightly increased to 0.7 $GtCO_2$ in 2021 [45].

Over the past few decades, the aviation industry has played a significant role in driving up carbon dioxide (CO_2) emissions, which in 2019 accounted for almost one gigaton (Gt) of CO_2, or 2−3% of all CO_2 emissions globally [46]. By 2050, the industry aims to reduce the CO_2 emissions to half from 2005 levels, in response to growing public awareness of greenhouse gas emissions and climate change [47]. According to [48], as environmental concerns become more severe and fossil fuel resources become more constrained, research and commercial efforts toward the development of alternative fuels through the utilization of renewable sources have been stimulated.

Fuel expenditures are among the biggest operating expenses in the aviation industry, accounting for around 30% of total costs, as only premium paraffinic fuels are suitable for use in aircraft [49], [50]. Furthermore, GHG emissions are currently at their highest levels ever, and they are the main reason why climate change is such a prominent issue [51]. As a result, with a growing demand to cut emissions, the aviation sector has advocated for developing aviation biofuel, or bio-jet fuel. Because the organic material used to make most bio-jet absorbs CO_2 as it grows, bio-jet has the potential to cut lifecycle CO_2 emissions by up to 80% when compared with conventional jet fuel [44].

The introduction and industrialization of alternative aviation fuels derived from vegetable oils, which are among the oilseeds showing promising potential for producing liquid aviation fuels, could contribute to efforts to address the depletion of petroleum-based fuels. However, because biofuels compete with food sources, non-food vegetable oils that do not pose a threat to the food industry must be used as feedstock for the production of renewable hydrocarbon jet fuels. Since the rapidly escalating worldwide rivalry for resources is also posing tremendous hurdles to the long-term viability of aviation fuel, one of *Brassica carinata*'s coproducts could potentially be used to sustain the industry's economy. Notable characteristics are among the primary reasons why feedstock is a promising alternative resource for the aviation industry. The physical and chemical

properties of *Brassica carinata* oil, an inedible vegetable oil feedstock, are identical to those of petroleum-based fuels [52]. Furthermore, the oil has low levels of saturated fatty acids and a high concentration of erucic acid (>40%), a fatty acid that readily cleaves into two hydrocarbon molecules [53].

Despite their high catalytic activity and stability, noble metals like platinum, ruthenium, rhodium, iridium, and palladium are impractical for commercial applications due to their high costs and limited availability [54], [55]. Developing appropriate, affordable, and environmentally acceptable catalysts that retain their chemical functionality and energy for extended use in a variety of industrial processes is one of the most significant research gaps in the field of renewable and sustainable energy [56]. For this, transition metal carbides (TMCs) have garnered significant attention over the past three decades due to their remarkable properties, including exceptional mechanical hardness, excellent thermal stability, high melting point, good conductivity, and catalytic activity [57], [58]. In addition, these metal carbides have shown to be efficient catalysts for hydrogenolysis, hydrogenation, isomerization reactions, electrocatalytic hydrogen evolution, and hydrodeoxygenation (HDO) of biomass-derived oxygenates, their qualities have drawn more attention recently than those of noble metal catalysts [37].

The choice of catalyst support is crucial in determining the overall performance and efficiency of a catalytic process. Because well-selected support can offer several advantages, including enhanced catalyst dispersion, improved catalyst stability, tailored catalyst properties, cost-effectiveness, environmental benefits, and process optimization (regeneration and recyclability). To ensure the stability of these carbon-coated catalysts, a thermally stable aluminophosphate (a zeolite-like molecular sieve) was employed as a catalyst support. These nanoscale transition metal carbide catalysts (β-Mo_2C/$AlPO_4$-18, Ni_3C/$AlPO_4$-18, and WC/$AlPO_4$-18) demonstrate exceptional performance, durability, and cost-efficiency in deoxygenation and hydrocracking processes. The various synthesis methods and their corresponding parameters were meticulously ascertained. To achieve this, the temperature-programmed reduction-carburization (TPRC) method, a low-cost and flexible technique, was utilized.

A lab-scale three-phase fixed-bed reactor was constructed to facilitate catalytic evaluations and produce bio-jet fuel using the hydroprocessing method for oil feedstock upgrading. Hydrodeoxygenation (HDO) and hydrocracking are essential processes for converting this

biomass-derived feedstock into bio-jet fuel. Identifying optimal parameters for these reactions is crucial to maximizing product yield and quality. As a result of the judicious selection of parameters, liquid-phase products were generated and comprehensively analyzed following catalytic processes.

1.3 Scope and Limitations of Study

The scope of the study is to perform experimental research on the catalytic hydroconversion of *Brassica carinata* oil to produce bio-jet fuel. Within the framework of this scope, the main investigational components are the extraction and characterization of vegetable oils, the oilseed meal valorization process, the non-catalytic slow pyrolysis and the characterization of *Brassica carinata* bio-oils; and, ultimately, the synthesis, characterization and catalytic performance evaluation of aluminophosphate supported metal carbide catalysts to generate bio-jet fuel.

Ethiopia grows a variety of *Brassica carinata* oilseed crops, yet only four of these species are investigated in this study since these seed cultivars appear to have a greater potential for industrial applications. Although the study performed an extensive evaluation of the potential use of bio-oils derived from *Brassica carinata* oilseed meals via non-catalytic slow pyrolysis and demonstrated that they have exceptional properties for producing bio-jet fuel, upgrading these bio-crudes into advanced fuels was beyond the purview of this study.

In light of some potential constraints, such as the scope of the thesis, only one of the oil feedstocks, Yellow Dodolla oil, was transformed into a sustainable aviation fuel. The upgrading process involved the utilization of different catalysts, hydrotreatment (particularly deoxygenation), and hydrocracking reactions at selective temperatures, an elevated partial pressure of hydrogen, while keeping other reaction conditions fixed. The heavy molecular weight oil feedstock was hydrotreated and hydrocracked, producing a variety of different hydrocarbon and non-hydrocarbon molecules. After these catalytic reactions, the catalysts' performance was evaluated using conversion, yield, selectivity, and deoxygenation rate.

Furthermore, another potential limitation of the study could be the use of fractional distillation to separate each of the middle distillate hydrocarbon fuels (i.e., biogasoline, bio-jet fuel, and biodiesel), obtained via hydrocracking reactions. Although the liquid phase products were thoroughly analyzed, the resulting gas fraction products have not been extensively studied, which may be considered one of the study's few potential limitations. This allowed for a limited evaluation

of the various forms of deoxygenation pathways, including hydrodeoxygenation, hydrodecarboxylation, and hydrodecarbonylation processes. Because it is an experimental investigation, evaluating reaction kinetics likewise remains out of the scope of the present study.

1.4 Objectives of Study

1.4.1 General objective of study

The overall objective of this study is the catalytic hydroprocessing of *Brassica carinata* oil for the production of bio-jet fuel utilizing robust supported transition metal catalysts.

To achieve this primary objective, five secondary specific objectives were formulated.

1.4.2 Specific objectives of study

The specific objectives of the study include:

- Solvent extraction and characterization of *Brassica carinata* oils as promising alternative feedstock for bio-jet fuel production
- Characterization of hexane-defatted *Brassica carinata* oilseed meals to explore their potential for valorization towards a sustainable circular bio-economy
- Pyrolysis-based synthesis and characterization of bio-oil from *Brassica carinata* oilseed meals and its application to produce bio-jet fuel
- Synthesis, and characterization of thermally stable and mesoporous $AlPO_4$-18 supported β-Mo_2C, Ni_3C, and WC nanoparticles for bio-jet fuel production using Yellow Dodolla oil
- Catalytic hydroprocessing of Yellow Dodolla oil using thermally stable and mesoporous $AlPO_4$-18 supported β-Mo_2C, Ni_3C, and WC nanoparticles to produce bio-jet fuel

1.5 Expected Significance and Implications of Study

The present investigation involves an experimental study of the appropriateness of novel alternative and sustainable feedstocks for the aviation industry, as well as the development of low-cost and viable catalytic materials (i.e., β-$Mo_2C/AlPO_4$-18, $Ni_3C/AlPO_4$-18, and $WC/AlPO_4$-18) for the

catalytic transformation of these newly introduced alternative feedstocks into sustainable aviation fuel. As a result, because the aviation industry is committed to continuing to reduce carbon emissions, the current investigation, which falls under one of the International Civil Aviation Organization's (ICAO's) Four Pillar policies, as shown in Figure 1.1 [59], has the potential to make significant contributions and implications to the industry. Accordingly, the introduction of novel feedstocks and an alternative SAF to the industry is an incredible achievement of the current study, given that sustainable aviation fuels (SAFs) are among the most significant facilitators of decarbonization in the aviation industry and that they have the potential to lower emissions by up to 80% [60].

Generally speaking, various stakeholders are thought to value the following aspects of the investigative work:

A. Academia. Researchers could use the research work's findings as a basis for further study and a reference to spark other investigations in the area.

B. Policymakers/regulatory bodies. For policymakers and regulatory authorities, it is alert signaling that the natural environment is at its most vulnerable due to GHG emissions and that development plans need to be revised or modified, as well as corrective actions taken based on the evidence gathered from the study.

C. Industrialists/operators. For them to take appropriate action or make the necessary process adjustments to act in an environmentally friendly and socially acceptable manner—without which their business and/or development activity would not be sustained—it highlights the environmental and societal status of their companies as well as any gaps related to the realization of the adopted sustainability management technologies.

D. Community. The potential for leveraging the expansion of the agricultural sector for wider rural development can be achieved through the commercial production of sustainable aviation fuels, without having an impact on food production. Along the bio aviation value chain, agriculture offers employment opportunities due to its labor-intensive nature, which can potentially stimulate green economic development.

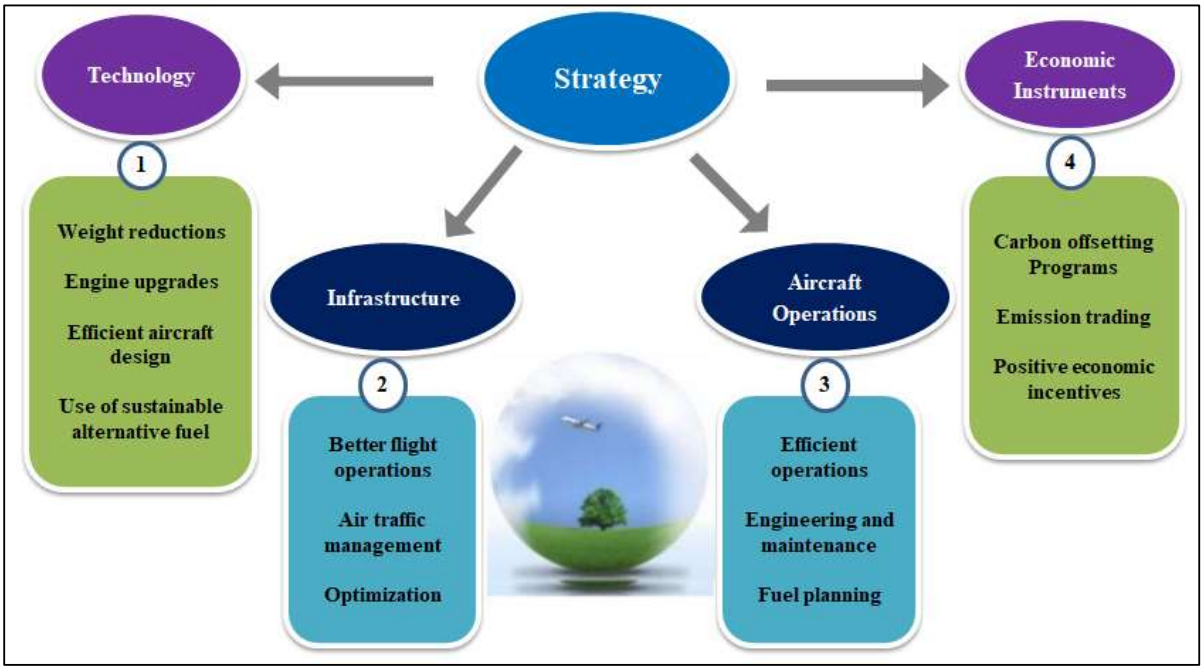

Figure 1.1 IATA`s four-pillar strategy (redrawn).

1.6 Organization of Dissertation

This dissertation work, as detailed below, is organized into eight major chapters.

The study's experimental work is outlined in Chapters Three, Four, Five, Six, and Seven, with Chapters Three to Five addressing the potential industrial applications of *Brassica carinata* (Amharic: ጎመን ዘር) oilseed crops. However, the remaining chapters (i.e., Chapters Six and Seven) emphasize the synthesis, characterization, and performance evaluation of supported transition metal carbide catalysts to produce a bio-jet fuel using one of the inedible *Brassica carinata* vegetable oils. In general, the dissertation is organized as follows:

Chapter One constitutes the initial segment of the general introduction section, encompassing the study's background, justification of the study regarding the focus on bio-jet fuel, scope and limitations of the study, objectives, and expected significance and implications.

Chapter Two before initiating any experimental effort, a review of pertinent literature and other sources is carried out to determine whether any similar studies or research has already been carried out. With a primary focus on the fundamentals of both conventional and bio-jet fuels as well as

global trends in the catalytic hydroprocessing of bio-jet fuel production, this comprehensive literature review offers invaluable insight into contemporary aviation fuel production technologies. Lastly, a summary of the main discoveries has been provided.

Chapter Three presents published work on the applicability of vegetable oils derived from four inedible *Brassica carinata* oilseed crops that are indigenous to Ethiopia to establish their viability as alternative feedstocks for the production of a sustainable aviation fuel. For this, an isothermal batch reactor was used to extract *B. carinata* oils using a response surface methodology (RSM) with three levels of Box-Behnken Design (BBD), and finally, a compressive characterization study was carried out.

Chapter Four provides a published study on four different hexane-defatted *Brassica carinata* oilseed meals that could have been obtained from the output streams of a bio-jet fuel facility. Characterization results were utilized to valorize how best to utilize the *Brassica carinata* meals (BCM) for their diverse potential industrial applications.

Chapter Five presents a published study investigating bio-oils derived from streamside products using thermochemical conversion techniques such as non-catalytic pyrolysis. Following slow pyrolysis at temperatures at a range of temperatures (350, 450, and 550 ℃), which produced product yields (bio-oil, biochar, and gas), a thorough analysis of the unique properties of the bio-oils was conducted to establish their viability for usage as potential alternatives to advanced fuels such as jet fuel production.

Chapter Six covers a study whose paper is already published. Through the use of incipient wetness impregnation (IWI), and temperature-programmed reduction carburization (TPRC) approach, the synthesis of aluminophosphate ($AlPO_4$-18) supported transition metal carbide nanoparticles is being investigated in this work. Following synthesis, *ex-situ* state-of-the-art characterization methods were applied to study the thermal, structural, microscopic, and textural properties of the supported metal carbide nanoparticles.

Chapter Seven contains an in-depth examination of a work being reviewed for publication. The catalytic performance of the supported metal carbide nanoparticles was evaluated on Yellow Dodolla oil under various reaction conditions. Following a detailed analysis to evaluate the

catalytic activity of the nanoparticles, a thorough characterization of the liquid phase products was performed.

Chapter Eight is the final component of the dissertation, and it summarizes the study's conclusions as well as recommendations/future outlooks for further study. After this final component, the bibliography section, which covers all references cited throughout the entire dissertation, is included.

The document contains significant supplements for the Supplementary Information of the experimental studies, which can be accessed in the List of Appendices. The document also includes a List of Annexes and a Glossary of Terms.

CHAPTER TWO

LITERATURE REVIEW

2.1 Basics of Vegetable Oil-Based Triglycerides

Researchers are getting increasingly interested in using biomass materials as an alternative energy source in the present day [61], [62]. This is true because biomass is a carbon-neutral energy source. After all, it emits a similar amount of CO_2 into the environment during growth as it does during photosynthesis [63]. Several investigations have been conducted on the process of transforming biomass into useful biofuels, which typically involve many different approaches [64].

Vegetable oils, commonly known as triglycerides, contain the chemical structure shown in Scheme 2.1, consisting of 98% triglycerides and a small proportion of mono- and diglycerides [65]. Triglycerides are composed of one molecule of glycerol and three molecules of fatty acids. With a carboxyl group at the end, the latter has a long chain of carbon atoms linked by single bonds and attached to hydrogen [66]. The relative positioning of fatty acids on the glycerol and the composition of fatty acids determine the characteristics of triglycerides [67]. Based on the type of oil, different fatty acid chains have different degrees of unsaturation (number of double bonds) and different carbon distributions.

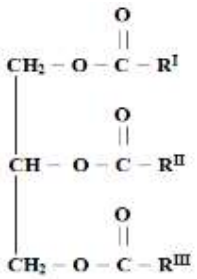

Scheme 2.1 Chemical structure of a typical triglyceride molecule [68].

Oils and fats are triglycerides composed primarily of glycerin and saturated and unsaturated fatty acids (chain lengths ranging from C_8 to C_{20}, with 16, 18, and 20 carbons being the most prevalent) [69]. Vegetable oils are typically extracted from plant seeds or fruits (such as rapeseed, sunflower, and olive) via pressing and/or solvent extraction. They are classified as nonpolar and lipophilic

systems, with extremely varied and complicated compositions depending on origin, quality, and production processes [70]. The type of fatty acids bonded to the triglyceride molecule is the main distinguishing factor among vegetable oils. The percentage of unsaturated/saturated content and molecular weight of vegetable oils are also determined by the chemical composition of fatty acids. Carbon chains (triacylglycerides) in vegetable and other plant oils (including algae) are too long and viscous to allow for proper flow and combustion. They must be transformed into low-viscosity fuels to be used as transportation fuels [71]. The extended carbon chain and big molecules containing oxygen atoms in vegetable oils give them a high viscosity. These oils have densities ranging from 0.84 g/mL to 0.97 g/mL and higher heating values of 37.1 MJ/kg to 40.6 MJ/kg, respectively, [72]. It was also discovered that vegetable oils have an oxygen content ranging from 10.5% to 14.5%.

2.2 Vegetable Oil-Based Triglycerides for Alternative Jet Fuels

A multitude of factors influence the production of biofuel, one of which is the accessibility of feedstock in the locality. The availability, affordability, and climate in each country are the primary factors in determining the feedstock [73]. Vegetable oil's composition is a significant factor in determining its suitability as a feedstock. The composition of the oil subsequently governs the qualities of the biofuel produced. Several varieties of edible vegetable oils, as well as non-edible oils having a variable composition in fatty acids, are utilized to produce biofuel [74].

Vegetable oils are advantageous because they are liquid, portable, renewable, easily obtainable, have minimal sulfur and aromatic content, and are biodegradable. Nonetheless, there are still hurdles preventing vegetable oil from being used as jet fuel, such as its high viscosity, high freezing point, and poor energy density. Jet fuel must have a low freezing point (-40 °C), a high flash point, high energy density, exceptional fluidity, and compatibility with the materials used in aircraft engines. Generally, raw vegetable oils must be refined to eliminate undesirable components while enhancing their qualities to meet aviation fuel specifications [75], [76]. Other potential sources, including microalgae, cellulose, and agricultural waste, are also accessible; however, the energy efficiency of collecting these materials and the technology for converting them into high-quality fuels have yet to be examined and developed. Many vegetable oils have undergone extensive hydrogenation, mostly to produce biofuels that are chemically identical to fuels generated from petroleum so there are no regulatory limitations on their usage in conventional engines [77].

The increasing need for energy has prompted researchers and energy companies to look for sustainable alternative energy sources. Hence, many types of oils and fats have been investigated as promising biofuel sources [78]. Due to their affordability and ability to facilitate a variety of chemical reactions at double bonds, ester groups, and allylic positions, vegetable oils represent one of the most significant classes of renewable raw resources [79]. The composition of vegetable oil feeds varies considerably on their origin, but in general, these feeds consist of triglycerides composed of various (even-numbered) (un)saturated fatty acids [80].

2.2.1 *Brassica carinata*

The global transition to alternative renewable energy sources has been necessitated by the demand for energy independence, environmental stewardship, viable economics, supplementing oil supplies, long-term unsustainability of non-renewable energy sources, and global warming concerns [81]. The search for suitable feedstocks has focused on cultivatable crops that can meet both technical and economic criteria. Non-edible oil crops that can be grown on marginal land requiring minimal agricultural inputs, tolerant to drought and extreme temperatures as well as resistant to pests and diseases while producing high oil yield are ideal. Commercial-scale bio-jet fuel production requires a reliable and consistent feedstock supply to be a sustainable, long-term alternative to petroleum-based conventional jet fuels.

Carinata (*Brassica carinata*), commonly referred to as Abyssinian Mustard and Ethiopian Mustard, is an oil-based feedstock that is similar to soybean and camelina and has been proposed as a new alternative feedstock for the production of SAF [22]. Its production advances sustainable agriculture because it strives to complement, not replace, summer food crops like soybeans, corn, peanuts, and corn, and so provide farmers with additional income, while minimizing topsoil erosion and improving the soil microbiome [82]. Comparative field experiments carried out in North Florida indicate that among oilseeds like camelina (952 kg ha^{-1}) and canola (1456 kg ha^{-1}) carinata has by far the highest seed output (2800 kg ha^{-1}) [83].

Carinata may offer an array of additional benefits, including enhanced water quality, protected soil, reduced weed growth, elevated soil carbon, and support for pollinator health [84]. Crop production for bioenergy has gained popularity globally as an alternative source of energy to mitigate greenhouse gas emissions [85]. The high erucic acid concentration of the seed oil makes this crop deemed sustainable for biofuel production [86], making biofuel conversion more successful than

conventional oils such as soybean and corn oils [52]. The potential application of carinata as a high-energy biofuel crop for jet fuel production has been studied [87], considering the current constraints of high production costs and limited alternative aviation biofuels [88].

The primary component of the oil, erucic acid, can also be used as a feedstock for producing nylon fibers, lacquers, plasticizers, herbicides, surfactants, and lubricants [82]. In addition to the oil, other components of the carinata seed, such as the biomass content of CM, need to be valorized to enhance the economics of carinata biofuels and enable large-scale carinata deployment [89]. The CM, which is primarily made of protein and lignocellulosic biomass, can be used as an animal feed supplement as well as a source of cellulosic biomass and sinapic acid [82].

To boost the overall economics of the carinata value chain, the biomass carbohydrates in CM may also be transformed into useful chemicals like propionic acid and other organic acids through thermochemical pretreatment and subsequent enzymatic hydrolysis [82]. The yearly requirement for propionic acid is roughly 300,000 metric tons, with over half of that being utilized as preservatives in grain and animal feed, while the rest is used to synthesize plastics, herbicides, fungicides, flavoring, fragrances, and pharmaceuticals [82].

2.3 Basics of Conventional Jet Fuels

Crude oil, often known as conventional petroleum, is refined to make most of the jet fuel used today. Thin, light crudes often have lower densities, higher concentrations of volatile compounds (such as kerosene and gasoline), and lower sulfur and nitrogen content [43]. Thicker, heavier, and darker crudes may and are refined into valuable, volatile, clean products by more intensive processing, but there are economic and environmental consequences associated with the increased processing [43].

Jet fuel consists of a wide variety of hydrocarbon compounds. It is mostly composed of C_8 to C_{16} hydrocarbons, with chemical components including alkanes, iso-alkanes, naphthenic or naphthenic derivatives, and aromatic chemical compounds [43]. A specific amount of aromatics is required to prevent leaks in the fuel system seals, even though high aromatic content may enhance the development of soot. Jet fuels that are certified for use in engines normally have an aromatic level of 15–23% [90]. After the refining and blending operations are finished, the bulk physical qualities of the fuel are determined by the mass contribution of each of these groups to the fuel's total

chemical composition [91]. There exists a clear correlation between the characteristics of the jet fuel and the content of each component.

Jet fuel is an aviation fuel developed primarily for commercial and military aircraft. Conventional jet fuel is produced by the distillation of crude oil at temperatures ranging from 205 to 260 °C [92]. The degree of isomerization and composition can affect properties including freezing point, flash point, and viscosity [93]. It is the different ratios of the hydrocarbons that make up the different jet fuel types. Similar to other petroleum products, jet fuel has a variable chemical composition and must adhere to certain standards depending on its intended purpose. Figure 2.1 shows the carbon number and boiling point for motor gasoline, jet, and diesel fuels. [94]. Evidently, motor gasoline is the lightest liquid fuel for transportation, with jet and diesel coming in second and third, respectively. The C_4 to C_{12} range applies to gasoline. From C_9 to C_{16}, the jet is the next heaviest. The C_9 to C_{24} range corresponds to diesel fuel.

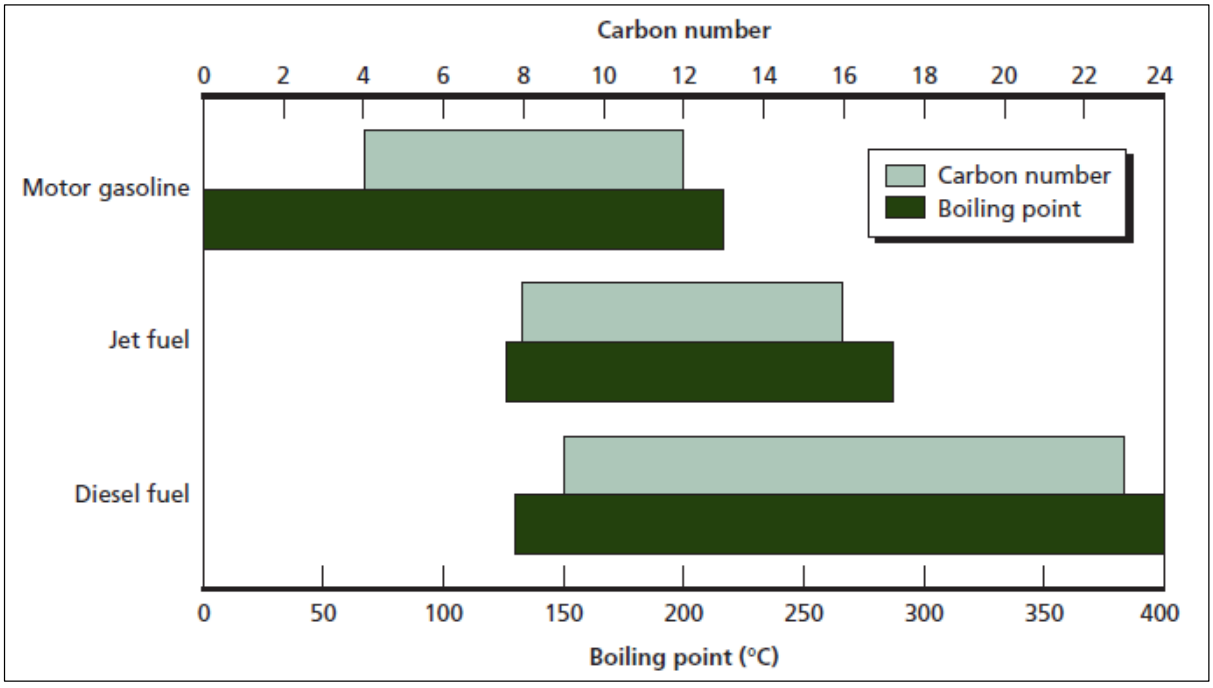

Figure 2.1 The boiling point and carbon number of motor gasoline, jet, and diesel fuels

The thorough investigation into four *Brassica carinata* oilseed crops which are only grown in Ethiopia such as *Brassica carinata* 'Yellow Dodolla', *Brassica carinata* 'Holleta-1', *Brassica carinata* 'Derash', and *Brassica carinata* 'Tesfa', which is covered in the later chapters (Chapters 3,

4, and 5) of the study, provide evidence for their promising industrial applications, especially for the aviation industry. This is highly acknowledged as a factor in the strong competition for resources that are rapidly expanding throughout the globe, posing tremendous hurdles to the long-term sustainability of many industrial products, including aviation fuel, which may then depend on one of carinata's coproducts to maintain its environment and economy sustainability. Consequently, the comprehensive study on the various coproducts including vegetable oils, oilseed meals, and bio-oils derived from the aforesaid Ethiopian-origin *Brassica carinata* oilseed crops turned out to be novel due to the lack of accessible reported studies.

2.4 Composition and Properties of Sustainable Aviation Fuels

Alternative aviation fuels, often known as sustainable aviation fuels, are low-carbon alternatives used in the aviation sector. The term "sustainable aviation fuels" (SAF), in turn, is most commonly used to describe a broad spectrum of drop-in kerosene alternatives that can be synthesized from multiple feedstocks, despite the lack of an internationally recognized definition for the term [95]. To satisfy its commitments to global efforts to mitigate the effects of climate change, the aviation sector requires effective and long-term solutions. Bio-jet fuels generated from biomass feedstocks might thus dramatically cut GHG emissions and increase energy security in the aviation industry [96]. These fuels, on the other hand, must have lower carbon emissions throughout their lifecycles and can achieve significant reductions while requiring no changes to current aircraft and infrastructure, which are by far the most affordable and immediate option for a rapidly decarbonizing industry [97].

The "drop-in" fuels, which satisfy the requirements for kerosene derived from oil, are the short- and medium-term substitute fuels for aviation. On the other hand, non-drop-in fuels and drivetrains (such as solar, hydrogen, FC, etc.) call for new aircraft and ground support. Bio-jet fuels are more compatible with conventional engines and fuel systems than other alternative fuels (such as ethanol): Bio-jet fuels don't require engine modifications for use, and they won't cause problems with fuel quality [98]. Because of its poor fuel characteristics, ethanol is inappropriate for use as aviation fuel. Furthermore, the main challenge is a lack of compatibility with the existing mechanical systems. Upgrading them all to run on a new fuel would require a trillion dollars [43].

The physicochemical properties of jet fuels are significantly influenced by the molecular structure and composition of their constituents. For example, almost all physical properties are affected by straight-chain hydrocarbons, whereas density, heating value, freezing point, and aniline point are affected by cyclanes and arenes [99]. The components of jet fuels also affect how efficiently an aircraft operates. For example, alkanes and alkenes help with better engine starting performance, and arenes enhance the sealability of fuel systems. Because of this, there are stringent regulations governing the chemical makeup and structure of jet fuel constituents [99]. Performance-related characteristics (such as energy content, combustion characteristics, stability, lubricity, fluidity, viscosity, freezing point, volatility, and non-corrosiveness) and safety-related characteristics (such as cleanliness, flash point, and electrical conductivity) are the most prevalent physicochemical characteristics of bio-jet fuels.

2.5 Recent and Emerging Sustainable Aviation Upgrading Technologies

Numerous bio-jet fuel conversion techniques are described in the literature, spanning from those in the demonstration, research, and development, to commercial stages. An in-depth comprehension of all upgrading technologies—approved and pending—from laboratory to commercial scale is needed to accurately assess the current state of progress for biomass-to-jet fuel development. The conversion routes can be broadly categorized into four groups based on the feedstocks and conversion processes: (1) the oil-to-jet (OTJ), (2) the gas-to-jet (GTJ), (3) the alcohol-to-jet (ATJ), and (4) the sugar-to-jet (STJ) [100]. The subsequent sections go into the specifics of these upgrading pathways, with Table 2.1 providing a summary of these methods.

2.5.1 Oil-to-jet (OTJ) fuel

The three most frequently utilized approaches in this OTJ transformation process are: HRJ, also known as HEFA; catalytic hydro-thermolysis (CH), also known as hydrothermal liquefaction; and hydro-treated depolymerized cellulosic jet (HDCJ), also known as rapid pyrolysis with jet fuel upgrading [100]. Since the HEFA upgrading route is utilized in the present investigation, the next section provides an in-depth review of this production method.

Table 2.1 The description of the typical synthesis pathways of several SPK fuels.

Type of Platform	SPK	Descriptions	Reference
Oil-to-jet	HEFA-SPK	Hydroprocessing after deoxygenation of mono-, di-, and triglycerides, free fatty acids, and fatty acid esters	[101], [102]
Gas-to-jet	FT-SPK	Gasification to produce Syn-gas ($CO+H_2$), coupled with Fisher-Tropsch (FT) to produce paraffins and olefins, then finally hydroprocessing	[7], [103]
	FT-SPK/A	The aromatic composition is purposely enhanced by introducing alkylated and bio-based aromatics in combination with the FT-SPK.	[104], [105]
Alcohol-to-jet	ATJ-SPK	Hydrolysis to get fermentable sugars; fermentation of sugars for iso-butanol and ethanol production, followed by dehydration, oligomerization, hydrogenation, and fractionation	[106]
Sugar-to-jet	SIP-SPK	Hydrolysis to produce simple sugars; sugar fermentation for farnesene synthesis; hydroprocessing and fractionation	[107]

HEFA: Hydroprocessed Esters and Fatty Acids. SPK: Synthetic Paraffinic Kerosene. FT: Fischer–Tropsch. SIP: Synthesized Iso-Paraffins. 30% blend for ATJ fuels, 50% blend for HEFA.

2.5.2 Gas-to-jet (GTJ) fuel

This can be defined as the Fisher-Tropsch biomass to liquid (FT-BTL) process**.** By use of biomass gasification, the gas-to-jet platform produces syngas, which is further converted via the Fischer-Tropsch production pathway (FT) into paraffinic and olefinic hydrocarbons, and hydroprocessed to produce FT-SPK. FT-SPK/A can also be produced using the gas-to-jet platform by adding alkylated and bio-based aromatics [7]. Moreover, current research suggests that transforming biomass to synthetic fuels via FT technology could provide a viable carbon-neutral substitute for conventional diesel, kerosene, and gasoline [100]. One of the most significant barriers to the FT-SPK route is the economic viability of bio-based feedstocks in light of the necessary gasification

technology and syngas clean-up processes. There are currently no commercially available gasified bio-jet fuels produced from biomass [108].

2.5.3 Alcohol-to-jet (ATJ) fuel

The process of producing an alcohol-to-jet (ATJ) platform or process entails hydrolyzing biomass to yield fermentable sugars, which are subsequently fermented to produce alcohol. The alcohols are subsequently dehydrated, oligomerized, hydrogenated, and fractionated to produce ATJ-SPK [7]. Since kerosene is composed of hydrocarbons with carbon values ranging from C_8 to C_{16} or even C_{19}, these treatment processes are necessary since the feedstock alcohols are oxygenated molecules with carbon numbers varying from C_1 to C_4 [106]. The physical and chemical properties of the final product must be similar to those of typical aviation fuel to transform bio-based ethanol into drop-in bio-jet fuel. Because of this, the first step in converting alcohol is to use the dehydration method to remove oxygen from the ethanol molecules [109].

2.5.4 Sugar-to-Jet (STJ) fuel

Sugar-to-jet (STJ) fuel is an environmentally sound aircraft fuel derived from sugar feedstocks [110]. The method of Direct Sugar-to-Hydrocarbon Jet Fuel Synthesis (DSCH), also referred to as the Sugar-to-Jet upgrading platform, begins with the hydrolysis of fermentable sugars from biomass. Then, these sugars are fermented to farnesene, which is further hydroprocessed and fractionated to produce SIP-SPK [7]. It can be considered a sustainable alternative to traditional jet fuel because it can reduce carbon emissions and dependency on fossil fuels. The STJ fuel approach consists of several processes, such as feedstock selection, fermentation, conversion, and purification [110].

2.6 Recent Advances in Catalytic Hydroprocessing

2.6.1 Hydroprocessing catalysts

The variables that follow may be taken in mind while developing new catalysts for transforming vegetable oils, even if the commercial catalysts used to produce renewable fuels have been tuned to process petroleum feedstocks: a) high activity toward deoxygenation, b) minimization of coke formation, c) water resistance, d) capability to regenerate in single processes, e) high tolerance to

chemical poisons, f) scalability in any commercial process [111]. The selection of a catalyst for hydrotreating depends on a variety of factors, including catalyst life, activity toward desired or unwanted side reactions, pressure drop, ease of activation, regeneration, and cost. In general, choosing a catalyst requires a thorough analysis of the particular circumstances [112]. The application and intended activity/selectivity are taken into consideration when selecting a catalyst.

In the past, Group VIII and VIB metal elements—specifically, noble metals like platinum (Pt), palladium (Pd), rhodium (Rh), ruthenium (Ru), etc.—and transition metal catalysts like nickel (Ni), cobalt (Co), molybdenum (Mo), and tungsten (W) have been used as hydrogenation components [113]. Nowadays, transition metal carbide, nitride, boride, and phosphide catalysts have become increasingly important in hydroprocessing [114], [115]. More significantly, transition metal carbides are currently the hottest material in the emerging catalytic material sector because of their remarkable catalytic performance, high melting point, remarkable hardness, and unique electronic structure [116]. A type of interstitial compound known as a transition metal carbide is formed when carbon atoms are introduced into the transition metal lattice. It has unique geometries and physicochemical characteristics similar to those of costly noble metals like Pt [116]. The interstitial compounds, as opposed to salinic, intermediate compounds, are characterized by unique properties due to special bonding between carbon and transition metal atoms [117].

This process generates chemical interactions between metal atoms and carbon atoms within metal-metal bonds. Because of their distinct structure, these carbides have different catalytic properties than their parent metals and metal oxides [118]. These TMCs have demonstrated remarkably high activity, stability, and selectivity as catalytic materials for a variety of hydrogen-related reactions, including hydrodesulfurization, hydrogenation, hydrogenolysis, and dehydrogenation [119]. The catalytic properties of transition metal carbide (TMC) catalysts are analogous to those of noble metal-based materials, yet they can be synthesized at lower costs [118].

The most popular and frequently used method for producing metallic carbide catalysts following incipient wetness impregnation (IWI) is the temperature programmed reduction (TPR) approach, which was developed by J. S. Lee, Oyama, and Boudart [120], with the method involving carburization temperatures often varying from 973 K to 1000 K. Thus, after being transformed into the active form such as sulfide, carbide, phosphide, or nitride, the oxide precursors are utilized in the hydrodeoxygenation of the biobased liquid feedstocks. For this, one or more heat treatments in

the air or a controlled environment—such as an inert, reducing, or oxidizing atmosphere—are typically part of the process.

The synthesized catalysts can be characterized using N_2 adsorption measurements (BET), UV–vis diffuse reflectance spectroscopy (DRS), Laser Raman spectroscopy (LRS), temperature-programmed reduction (TPR), X-ray photoelectron spectroscopies (XPS) and NO chemisorption [121], [122]. Furthermore, the following temperature-programmed techniques including thermogravimetry (TG), differential scanning calorimetry (DSC), differential thermal analysis (DTA), temperature–programmed oxidation (O_2-TPO), and temperature–programmed desorption (H_2-TPD), temperature–programmed desorption (O_2-TPD), and temperature–programmed reduction (H_2-TPR) are particularly helpful in studying this process because they can reveal changes in the properties of the catalyst, such as decomposition, melting, crystallization, and the loss of volatile compounds [123], [124]. The utilization of these approaches can give information on catalyst/support interaction, dispersion of catalyst on a support, the oxidation state of the metal, the role of promoters, number, and strength of binding sites, catalyst acidity, and reaction mechanisms [123].

2.6.2 Hydroprocessed esters and fatty acids (HEFA)

The HEFA, an oil-to-jet transforming pathway, produces HEFA-SPK by deoxygenating oils and fats and subsequently hydroprocessing them [7]. Hydroprocessing has been a well-known and commonly used technique in petroleum refineries for several decades [125]. The technique of catalytic hydroprocessing liquid biomass provides great adaptability to meet the ever-growing needs of the biofuels industry. Various liquid biomass, such as animal fats, leftover cooking oil, raw vegetable oils, and algae oils, can be converted into high-yield biofuels [126]. The upgrading techniques employed in hydroprocessing, including hydrotreating, isomerization, and hydrocracking, are readily available and have developed to a quite advanced stage. In the present day, refineries often use these processes to produce transportation fuels [127].

Hydrotreatment is a reaction of several hydrogenation reactions, such as transforming double/triple bonds into saturated hydrocarbons, converting heavy fraction hydrocarbons into light fraction hydrocarbons, and removing contaminants such as sulfur, nitrogen, oxygen, and metals [128]. Hydrogenation reactions often take place on metal surfaces, where H_2 is dissociated and then reacts.

However, unlike C-C bond hydrogenolysis, which produces compounds with the same skeletal identity, hydrocracking causes considerable structural rearrangements. For hydrocracking to occur, a catalyst with dual functions is required, one for hydrogenation and the other for cracking, with the latter being provided by protonic (Brønsted) acid sites on the support [112].

The hydroprocessed esters and fatty acids (HEFA) utilize a propane cleavage mechanism to transform triglycerides into hydrocarbons. This involves breaking the carbon-carbon bonds in the triglycerides with hydrogen gas, resulting in the production of water, propane, and longer-chain hydrocarbons that are classified as jet fuel [31]. The feedstock's triglycerides are hydrodeoxygenated to produce straight-chain alkanes, which are further catalytically hydrocracked and hydroisomerized to produce light, branched alkanes to meet jet fuel standards [129]. As demonstrated in Figure 2.2, triglyceride conversions over hydrotreating catalysts in the presence of hydrogen have complex reaction routes that involve parallel and/or sequential reaction types such as saturation, cracking, decarboxylation, decarbonylation, and/or hydrodeoxygenation [130]. Hydrocracking is a more severe form of hydrotreating. It transforms heavier feedstocks into more valuable, low-boiling products. In the hydrocracking process, cracking and hydrogenation reactions occur simultaneously on a dual-function catalyst; the catalyst's acid sites are required for isomerization and cracking activities, while its metallic sites are required for hydrogenation and dehydrogenation reactions [131].

A catalyst that has lost its capability to catalyze reactions and maintain product selectivity is said to be deactivated. Regenerating or replacing the catalyst can come at a high cost. The deactivation takes place due to: (1) poisoning of active sites because of chemisorption of heteroatoms, (2) coking due to deposition of coke on catalyst surface, (3) sintering/thermal deposition due to breakdown of catalyst and support surface area because of crystalline growth, (4) loss of internal pores during crushing, (5) vapor compound formation accompanied by transport [132].

The generation of coke is correlated with the acidity of the catalysts, and coking rises as catalyst acidity increases. Because of its significant interaction with the coke precursors and comparatively high acidity, alumina acidic support deactivates more quickly than inert supports like SiO_2. Catalytic deactivation, which happens when carbon deposits, or coke, obstruct acid sites on the catalyst's surface, is the main cause for concern during catalytic upgrading. Researchers concur that

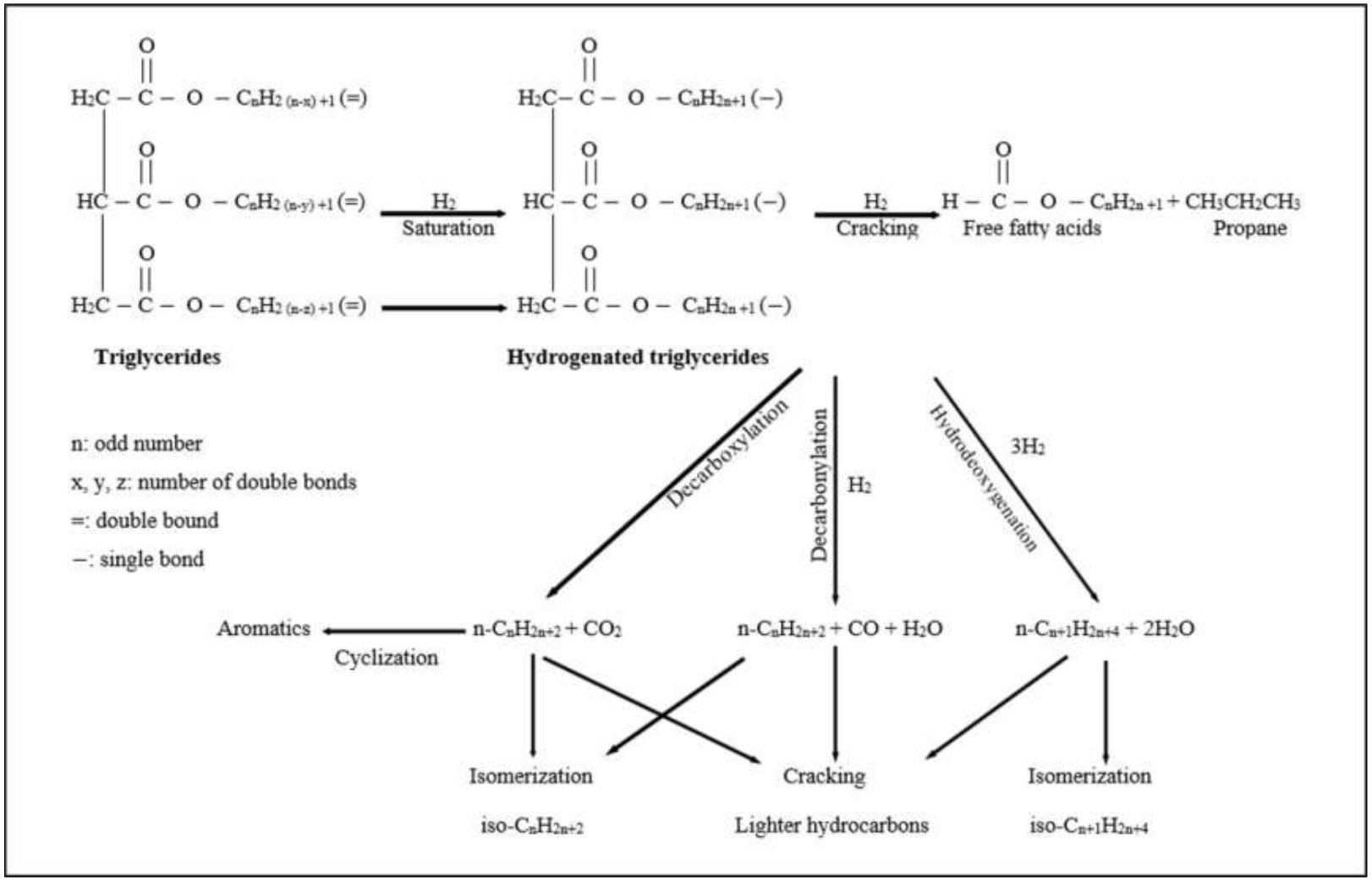

Figure 2.2 Possible reaction pathways of triglycerides over hydrotreating catalyst.

the physicochemical characteristics of the catalyst, including its acidity and pore structure, and the reaction conditions play a major role in coke formation [133], [134]. In broad terms, catalysts are deactivated in three ways: mechanically, thermally, and chemically [135].

When feedstock contains alkalis cations without a charge-compensating inorganic anion, catalyst activity gradually decreases. This can be attributed to alkalis depositing on the catalyst surface, which causes electronic interactions that limit hydrogenation [136]. This would inhibit both the hydrogenation of double bonds and the hydrodeoxygenation route. Alkalis were found to deposit on the exterior surface of catalyst particles [137] and calcium has been observed to cause deactivation in hydrogenation, hydrocracking, hydrodesulfurization, and hydrodeoxygenation [138]. Furthermore, several alkali molybdates, tungstates, and aluminates were identified as thermodynamically plausible compounds that formed on hydroprocessing catalysts in the presence of alkali particles. Yet, their stability and behavior under hydroprocessing conditions remain unknown [137].

One of the most frequent catalyst regeneration approaches is the oxidation or the calcination of the catalyst in a furnace or reactor in air at high temperatures (500–600 °C). Some researchers washed the used catalysts with acetone before calcination, which may help eliminate some contaminants (e.g., oil) deposited on the used catalysts [139]. The proper regeneration of used catalysts could assist minimize the cost of biofuel production from vegetable oil processing.

A significant effort was undertaken to look into catalytic hydroprocessing of some recent developments reported in the literature, which may help to identify and address the gaps with the help of the current study. Because there were no previous investigations that utilized feedstock, catalyst, catalyst support, and reaction conditions identical to those used in the present investigation, recent advancements in hydroprocessing involving various feedstocks, various supported catalysts, and a diversity of reaction conditions were reviewed. As a result, the discussion in the paragraphs that follow strives to highlight the recent advances in catalytic hydroprocessing reactions employing diverse forms of catalysts with varied feedstocks and reaction conditions.

A study on *Brassica carinata* oil that was upgraded using a single-step thermal/catalytic cracking and hydroprocessing using noble and transition metal catalysts such as Ni/SiO_2-Al_2O_3, Ni/C, Ru/C, and Pd/C indicated the highest wax yields of 80, 15, 83, and 85% over Ni/SiO_2-Al_2O_3, Ni/C, Ru/C, and Pd/C, respectively, [140]. Their analysis showed that the rapid hydrogenation of C–C bonds in

triglycerides was responsible for the significant levels of wax formation (waxy products at room temperature with a melting point of around 35 ℃). Furthermore, these findings suggest saturated glycerides could hinder the cracking reaction by obstructing the active catalyst sites [140]. On the other hand, they also employed a two-step thermal/catalytic cracking strategy, followed by hydroprocessing, with the same catalysts (Ni/SiO_2-Al_2O_3, Ni/C, Ru/C, and Pd/C), and found liquid yields of 81, 72, 68, and 60%, respectively, indicating that Ni catalyst had the highest cracking activity when compared to the noble metal catalysts [140].

Vegetable oils were found to be difficult to crack at low reaction temperatures in the preliminary catalytic cracking tests, with typical reaction temperatures for this process ranging from 380 to 525 ℃ [141]. According to [141], the highest hydrocarbon content found in sunflower oils from seed and meat is 63.05% and 76.98%, respectively, for two different sunflower oils used as a feedstock and ZSM-5 catalyst at reaction temperatures of 450 ℃, 500 ℃, and 550 ℃. The soybean oil triglycerides were completely converted at 650 psi and 360−450 ℃ using a bimetallic hydrocracking carbide NiMo/ZSM-5 catalyst. A low reaction temperature (360 °C) yielded a significant increase in selectivity for hydrocarbon fuels. After a 4-day reaction, only 3−5% of hydrocarbon fuels were generated, along with a significant amount of carboxyl acids (up to 140 mg KOH g^{-1}) [142].

A study on the hydrodeoxygenation of stearic acid employing 7.5% α-MoC_{1-x}/CNF and 7.5% β-Mo_2C/CNF catalysts was also carried out, and the results indicated that the intrinsic activities of both phases were identical [143]. Nevertheless, after 240 minutes, α-MoC_{1-x}/CNF achieved 80% stearic acid conversion, whereas the β-Mo_2C/CNF catalyst reached the same conversion after 360 minutes [143].

Adjaye & Bakhshi [144] proposed that the maximum distillate yield could be achieved at 370 ℃ using a ZSM–5 zeolite in a fixed-bed microreactor, despite several research recommending reaction temperatures exceeding 500 ℃ to maximize the liquid oil yield. T. Li, Cheng, Huang, Zhou, and Cen [145] explored three different aspects of mesoporous zeolite formation. Meso-Y, Meso-H-beta, and Meso-HZSM-5 supported nickel catalysts enabled the synthesis of hydrocarbon-like jet fuels. They found that among the three catalysts, the Ni/Meso-Y catalyst produced the highest yields of aromatic hydrocarbons (9.47%) and alkanes (55.32%) in the jet fuel range. The acid density and surface area of Meso-Y zeolites, which are notably higher than those of other

zeolites, were identified as the cause of the shift in jet fuel production. On the other hand, the jet fuel range alkane yields from Ni/Meso-H-beta and Ni/Meso-HZSM-5 catalysts were lower (29.95% and 4.96%) while the aromatic hydrocarbon yields were greater (40.3% and 89.43%).

The potential of a nickel-based catalyst to upgrade waste cooking oil into aromatic hydrocarbons suitable for jet fuel range was studied using three distinct types of zeolites: Meso-Y, SAPO-34, and HY [146]. The alkane selectivity (C_8–C_{16}) of the jet range over Ni/Meso-Y, Ni/SAPO-34, and Ni/HY was found to be 53%, 58%, and 53%, respectively. Additionally, Ni/HY demonstrated a significantly higher yield of aromatic hydrocarbons to 23% of the jet-fuel hydrocarbons selectivity (C_8–C_{16}) and a lower heating value among these three catalysts, while Ni/SAPO-34 demonstrated the lowest yield of aromatic hydrocarbons of jet-fuel selectivity at 6.1%, resulting in poor lubricating properties. The Ni/Meso-Y catalyst was also shown to have an average aromatic hydrocarbon selectivity for jet fuel hydrocarbons (13.4%) [146].

Additionally, Bezergianni, Voutetakis, and Kalogianni [147] conducted catalytic hydrocracking of fresh and used cooking oil over commercial sulfide hydrocracking catalysts at 350–390 °C. The results produced a roughly 17% kerosene jet at 390 °C and 2000 psi, along with an extremely high H_2/oil ratio (1069 Nm^3/m^3). It is frequently stated that greater catalyst concentrations lead to improved catalytic activity because more catalytic sites become available for the reactants.

In conclusion, this review has provided a comprehensive overview of recent advancements in the hydroprocessing of oil feedstocks to produce advanced fuels. Table 2.2 further highlights the current progress in this area, showcasing the diverse range of feedstocks, catalyst forms, and reaction conditions being explored. Consequently, the following paragraphs highlight several key research gaps and discuss the potential contributions of this study.

It is commonly known that a variety of factors, including the type of feedstock, the catalyst, the support and promoter, the activity and selectivity of the catalysts, the reactor type, the operating parameters of the hydrotreatment and hydrocracking reactions, and catalyst deactivation, affect the production of the highest yield of hydrocarbon biofuels, particularly the middle distillate products (gasoline/naphtha, jet, and diesel range hydrocarbon fuels). As a result, several research gaps that can be addressed in the current investigation have been identified after meticulously evaluating the reviewed research gaps.

As indicated in the above paragraphs, one of the most important elements influencing the production of the maximum yield of middle distillate fractions is the kind of feedstock, and the current study used Yellow Dodolla oil, which is one of the most notable non-food vegetable oils, to solve the issue. Because the type of catalyst support is the other crucial factor that should be taken into account, aluminophosphate ($AlPO_4$-18), which is one of the most significant zeolite-like molecular sieves with extremely distinctive thermal stability qualities, was employed in the present study. Another significant aspect related to this is the type of catalyst; in the current study, transition metal carbides supported over this catalytic support, have been used. According to prior studies' assessments outlined above, selectivity concerns are among the most critical problems. Furthermore, product distributions, particularly chain length distributions for each class of hydrocarbon, are a key aspect of the identified study gap. These and other critical issues are carefully studied and attempted to be addressed in the current study.

Table 2.2 Recent advances in hydroprocessing of vegetable oils to hydrocarbon biofuels.

Feedstock	Catalyst	Reaction conditions	Conversion (wt. %)	Yield/ Selectivity (wt. %)	Reference
Brassica carinata	Ni/SiO_2-Al_2O_3 Ni/C Ru/C Pd/C	Single-stage cracking and hydroprocessing (T = 400, P = 1000 psig (ca. 68.947 bar), t = 60 min)	-	Y_{wax} = 80 Y_{wax} = 15 Y_{wax} = 83 Y_{wax} = 85	[140]
Brassica carinata	Ni/SiO_2-Al_2O_3 Ni/C Ru/C Pd/C	two-step thermal/catalytic cracking followed by hydroprocessing (T = 400, P = 1000 psig (ca. 68.947 bar), t = 15 min)	-	Y_{liquid} = 81 Y_{liquid} = 72 Y_{liquid} = 68 Y_{liquid} = 60	[140]
Stearic acid	7.5 wt. % α-MoC_{1-x}/CNF	T=350 °C, 30 bar H_2	80 (after 240 min)	-	[143]
Stearic acid	7.5 wt. % β-Mo_2C/CNF	T=350 °C, 30 bar H_2	80 (after 360 min)	-	[143]
Methyl palmitate	Mo_2C/CNTs	batch reactor, 240 °C, 2 h, 15 bar H_2	-	$Y_{hexadecane}$ = 57	[148]
Palm oil	3 wt. % catalyst ratio, Ni-Mo/SiO_2	400 °C, 30-50 bar, 2 h	98.21	Y_{jet} = 45.17 S_{jet} = 45.46	[149]

Table 2.2 Continued.

Feedstock	Catalyst	Reaction conditions	Conversion (wt. %)	Yield/ Selectivity (wt. %)	Reference
Sewage sludge bio-oil	NiW/SiO_2-Al_2O_3	mini-bench top high-pressure batch reactor,	-	$Y_{kerosine} = 25$	[150]
Soybean oil	8 wt.% Ni/SAPO-11	370 °C, 40 bar H_2, LHSV = 1, h^{-1}	100	$Y_{OLP} = 75$ $S_{C7\text{-}C14} = 16$	[151]
Palm oil	10 wt.% Ni/SAPO-34	390 °C, 52 bar H_2, 8 h	97	$Y_{C8\text{-}C16} = 41$	[152]
FAMe from Nannochloropsis	10 wt.% Ni/meso Y-HPW	255 °C, 20 bar H_2	97.2	$Y_{jet} = 63.1$	[153]
Jatropha oil	2 wt.% Pt/SAPO-11	410 °C, 50 bar H_2, LHSV = 1.2 h^{-1}, H_2/oil ratio = 1000 mL/mL	100	$S_{C8\text{-}C16} = 59$	[154]
Palm oil	0.5 wt.% Pd/Al_2O_3	400 °C, 60 bar H_2, 2 h		$Y_{kerosene} = 43$, $Y_{diesel} = 50$	[155]
Jatropha	Ni-W/SiO_2-Al_2O_3	420 °C, 60 bar	-	$Y_{Biokerosene} = 25$–30	[156]
Soybean	Ni-Mo/ZSM-5	36–450 °C, 45 bar	-	$Y_{HC\ biofuel} = 50$	[157]

CHAPTER THREE

Solvent Extraction and Characterization of *Brassica carinata* Oils as Promising Alternative Feedstock for Bio-Jet Fuel Production

3.1 Introduction

Presently, it is projected that the worldwide demand for biofuels will increase by 41 billion liters, or 28%, between 2021 and 2026. One-fifth of this demand surge is due to a return to pre-COVID-19 consumption levels [158]. However, despite a large rise in production (i.e., from just 7 million liters in 2018), commercial volumes of bio-jet fuel are still rather low (i.e., roughly 140 million liters/year (2019)), which is less than 1% of fuel currently used by the sector. This is associated with several factors, including the sluggish pace of technological advancement and the high price of these fuels [159].

Due to the sustainability and environmental friendliness of bio-jet fuels, they are regarded as a viable alternative to conventional jet fuels [7]. The significant potential for sustainable fuels to decrease the industry's influence on the environment stems from their potential to cut CO_2 emissions by up to 80% over their lifecycle [60]. This has a great contribution to the industry, reaching a 50% decrease in CO_2 emissions by 2050 compared to 2005 levels [47]. By eliminating oxygen from biomass, which results in the production of bio-based oxygen-free hydrocarbons, the detrimental impact of oxygen-containing biofuels may be reduced. Various techniques with varying degrees of complexity may be used to remove all or some oxygen from bio-based feedstocks for the production of biofuels [160]. The resultant oxygen-free hydrocarbons are compatible with fossil fuels.

The composition of vegetable oil is a key parameter for determining its appropriateness as a feedstock. The composition of the oil, in turn, affects the characteristics of the biofuel produced [74]. Because of the possible benefits such as high energy density, low moisture content, and high relative stability, vegetable oils are promising feedstocks for the production of bio-jet fuels. Moreover, they may also be converted into saturated, unbranched, and long-chain hydrocarbon fuels [161]; however, high viscosity and high freezing point are some of the undesirable qualities of vegetable oils for use as jet fuel [75], [76]. In the production of bio-jet fuels, the first crucial

stage is the recovery of high-quality vegetable oil from the oilseeds [162], [163]; accordingly, it is vital to investigate an economical extraction technique for effectively obtaining the necessary oils [164]. The Brassicaceae family comprises one of the most commercially significant plant groups [165]. *Brassica carinata* (A. Braun) is a plant species under the Brassicaceae family that evolved in the central highlands of Ethiopia at elevations ranging from 2200 to 2800 m above sea level, and it is a high yielding, disease, and pest-resistant oilseed crop [166].

In Ethiopia, the main growing regions include Arsi, Bale, Gonder, Gojam, Wello, Shewa, Sidamo, and Wellega; over the previous five years (CSA 2011/12 – 2015/16), 550,000 –750,000 quintals were produced from a total area coverage of 30,000 to 45,000 hectares [167]. *B. carinata* has quite high oil contents (25–47%) [168], [169], and its oil is a non-food vegetable oil having a very long-chain fatty acid composition suitable for conversion to biofuel [170]. Furthermore, *B. carinata* has a high percentage of erucic acid (35–51%), making it unsuitable for human consumption [171], [172]. Erucic acid (EA) is difficult to digest and absorb in the human body. Both glucosinolates and EA are harmful to health and can induce sickness, hence regulatory organizations have set severe limits on the maximum EA concentration of oils. Researchers have widely focused on increasing the EA level in Brassicaceae oilseeds to meet commercial uses while decreasing the EA concentration to assure food safety [173].

Brassica carinata provides coproduct molecules with functions apart from fuel that have major potential advantages, which is known as the coproduct-driven carinata bioeconomy strategy [30]. This is the reason why *B. carinata* oil's high erucic acid concentration is suitable for industrial use and important raw material for the production of commercial products such as plasticizers, detergents, surfactants, and polyesters among others [174]. Furthermore, the non-edible nature of the oil makes it an important bio-industrial crop that can be used for the production of bio-jet fuels where the 22-carbon chain of the oil may be broken down into two biofuel hydrocarbons, thereby doubling the fuel output for each erucic acid molecule [175], [176].

The existence of naturally appearing impurities in vegetable oils such as phosphorus (P), alkalis (alkali and alkaline-earth metals) (e.g., Ca, Mg, Na, K), and Sulphur (S), have great impacts on the deactivation of hydrodeoxygenation catalysts [177]. The occurrence of the alkali in the catalyst deactivation because of their accumulation on the catalyst surface gives rise to blocking/poisoning of active sites. Phosphorus resulted in an even doubling of the consequence; however, they have

pointed out that the occurrence of sulfur was observed to markedly increase the stability of the catalyst activity [177]. Calcium was observed to bring about deactivation in hydrogenation, hydrocracking, hydrodesulfurization, and hydrodeoxygenation processes [138].

To the authors' knowledge, no existing research has comprehensively investigated the in-depth solvent extraction and characterization of oils from four Ethiopian-indigenous *Brassica carinata* cultivars. The primary objectives of this research were to systematically evaluate the effects of various solvent extraction parameters, including temperature, solvent-to-solid ratio, time, and particle size, on the oil yield and properties of different *Brassica carinata* cultivars, with the ultimate goal of determining their suitability as a feedstock for bio-jet fuel production.

3.2 Materials and Methods

3.2.1 Collection and preparation of samples

Seed samples of four *B. carinata* cultivars (i.e., *Brassica carinata* 'Yellow Dodolla', *Brassica carinata* 'Holleta-1', *Brassica carinata* 'Derash', and *Brassica carinata* 'Tesfa') were collected from the Holetta Agricultural Research Centre in Holetta, Ethiopia. In this study, the seed feedstock particle sizes of 150–355, 355–500, and 500–710 μm were prepared and used for the experimental analysis. The local names of the cultivars (i.e., Yellow Dodolla, Holetta-1, Derash, and Tesfa) are used to elucidate them.

3.2.2 Design of experiments for solvent extraction, and statistical analysis

Response surface methodology (RSM) with three levels of Box-Behnken Design (BBD) was applied to study the effects of extraction parameters (i.e., temperature, solvent-to-solid ratio, time, and particle size) on oil yield. An isothermal batch reactor (Armfield CEX Chemical Reactor) was used to extract the oil. The extraction unit was outfitted with a temperature regulator (thermostat), mixer, and rpm controller. The design parameters were temperature (25, 46.5, 68 °C), solvent-to-solid ratio (6:1, 8:1, 10:1 mL/g), time (30, 60, 90 min), and particle size (150–355, 355–500, 500–710 μm). The solvent, n-hexane, was first added to the unit, heated, and continually stirred. After reaching the required temperature, 25 g of powdered sample was introduced to the unit and left for a fixed period. Following extraction, the oilseed cake was vacuum filtered to separate the mixture

of oil and solvent where the oil was then separated from the solvent using a simple distillation method. Extracted oil yields were calculated using Equation 2.1.

$$Extracted\ oil\ yield(\%) = \frac{Mass\ of\ oil}{Mass\ of\ sample} \times 100 \quad (2.1)$$

3.2.3 Characterization of oils

3.2.3.1 Physicochemical characterization

Experiments were run in two replicates and each of the mean ± standard deviation values was reported as numbers corrected to two decimal places. Association of Official Analytical Chemists [170] standards were applied to characterize the properties of the samples.

A. Physical properties

Approximately 5 g of an oil sample was used to measure the total moisture content (%) by oven drying method (AOAC 925.10) in an oven (D-6450 Hanau, Heraeus Instruments, Germany). The determination of pH was based on the AOAC 960.19 method in a pH meter (Jenway 3505, Fisher Scientific, UK). Two drops of an oil sample were used to measure the refractive index at 20°C using AOAC 921.08 in a refractometer (RFM960, Bellingham Stanley). The pycnometer method as described in AOAC 920.212 method was applied to determine the density and specific gravity of samples at 15 °C using a 50 cm^3 standard volumetric pycnometer. The kinematic viscosity (mm^2 s^{-1}) was carried out following ASTM standard D445 using a Vibro viscometer (SV10, A & D Company Ltd, Tokyo, Japan). Kinematic viscosities were measured at three different temperatures (i.e., 25, 40, and 100°C) to observe the effect of temperature.

B. Chemical properties

Approximately 10 g of a sample was applied to measure the total ash content following method AOAC 923.03 using an electrically heated Nabertherm furnace (L5/C6, Nabertherm GmbH, Germany). Hanus method as defined in AOAC 920.158 method was used to determine the iodine value (IV) of the oils. For the titration, approximately 0.25 g of an oil sample was used. According to ISO 660:2009, ca. 20 g of a sample was used to measure the acid value (AV). The methods AOAC 965.33 and AOAC 920.160 were used to estimate the peroxide value (PV) and

saponification value (SV), respectively. Approximately, 5 g of samples were used for each of these analyses.

3.2.3.2 Fatty acids profiling

AOAC 996.06 was applied for the qualitative and quantitative determination of fatty acid methyl esters (FAMEs) of *B. carinata* oils in an Agilent Technologies' gas chromatography (7820A GC) equipped with a mass selective detector (HP 5977), and a DB-5MS capillary column (60 m, 0.25 mm ID., 1.4 μm thickness). Helium was employed as the carrier gas, with a constant flow rate of 1 mL/min, and a 1μL injection volume. The injector and detector temperatures were 250°C, and 280°C, respectively. The oven temperature was set to 50°C (isothermal for 4 min), then increased to 280°C at 30°C/min for 10 min, isothermal at 280°C, and the mass scan range was set at 29-800 amu [170].

3.2.3.3 Ultimate analysis

DIN 51732 (2014-07), DIN 51732 mod. (2014-07), DIN EN 14582 (2016-12), and DIN 51733 (2016-04), were used for CH, N, S, and O, respectively. Analysis for CHN, S, and O, was performed using a CHNS analyzer (Vario EL Cube, Elementar, Germany), bomb calorimeter (C6000, IKA-Werke, Germany), and by difference [i.e., 100 − (C + H + N + S + ash content)], respectively. For CHN and S analyses, approximately 150 mg and 0.5 g of each sample were employed, respectively.

3.2.3.4 Analysis of metals and phosphorous contents

Concentrations of the various metals (i.e., Na, K, Ca, Mg, Al, Fe, Zn, Ni), and P were determined by DIN ISO 22036:2009-06. Aqua regia flux digestion (DIN EN 13657 (2003-01)) in a microwave digester (ETHOS. Lab, Germany), followed by inductively coupled plasma optical emission spectroscopy (ICP-OES) (Vista MPX, Varian Deutschland GmbH, Germany) was used. Approximately 0.3 g of each sample was used for analysis.

3.2.3.5 FT-IR characterization

An FT-IR Spectrometer (Spectrum 100, PerkinElmer, UK) was used for the qualitative characterization of functional groups, and Spectrum software (Version 6.1.1.0045) was employed

for instrument monitoring and data acquisition. The FT-IR was outfitted with a deuterated triglycine sulfate (DTGS) detector that scanned at a resolution of 4 cm^{-1} over a frequency range of 4000 to 550 cm^{-1}. A single drop of the sample was applied to the diamond surface, a crystal with a high refractive index.

3.2.3.6 Measurement of calorific value

Samples of known moisture and ash contents were used for the determination of gross calorific value (GCV) and net calorific value (NCV). The determination of these calorific values was performed using DIN 51900-1 (2000-04 + Correction 2004-02) (C6000, IKA-Werke GmbH & Co. KG, Staufen, Germany) in a bomb calorimeter. Measurements were carried out in two replicate experiments using 0.5 g of each sample.

3.3 Results and Discussion

Storage of seeds of *B. carinata* cultivars, statistical data analysis for solvent extraction, and characterization of the oils are the three main components of this section.

3.3.1 Storage of *B. carinata* cultivars

In the present work, since the mean moisture and oil contents were determined, based on previously reported seed storage potential factors, the moisture and oil contents can indicate how long the seeds of the cultivars may be stored. Several variables affect seed quality during storage, including environmental conditions at the time of seed production, pests, diseases, oil content, moisture content, mechanical damage to seed during processing, packaging materials, pesticides, air temperature, and relative air humidity [179]. However, during storage, seeds also age primarily through autoxidation. This autoxidation happens as a result of the peroxidation of polyunsaturated fatty acids, which produce free radicals and reactive oxygen species (ROS). Changes in the concentrations of saturated and unsaturated fatty acids were attributable mostly to oxidative degradation during storage. Due to the lack of double bonds in their structure, the saturated fatty acids content was only marginally impacted. Changes in the unsaturated fatty acid proportion, however, were more apparent [180].

In addition, due to the direct relationship between free fatty acid levels and seed vigor and viability, its measurement is a valuable qualitative indication of seed degradation during storage [181]. Seeds with high oil content could be kept for 4-5 years at temperatures ranging from 0 to 35°C, with an average of 18 °C. The recommended moisture content of seeds with high oil content was less than 5% moisture content [182]. The cultivars of the current study are very high oil-content oilseed crops and their mean moisture contents were found to be ca. 5%. Therefore, because of the various potential seed storage factors, especially aging and improper storage, the quality of bio-jet fuel produced from these cultivars may be significantly impacted.

3.3.2 Statistical data analysis for solvent extraction

3.3.2.1 Model fitting and ANOVA analysis

Mathematical models were fitted to the observed data to generate regression models, and second-order polynomial equations (Table 3.1) were presented for each of the oil yields. For the oil yields of Yellow Dodolla, Holetta-1, Derash, and Tesfa, the coefficients of determination (R^2) were determined to be 0.9522, 0.9756, 0.9551, and 0.9589, respectively, with a non-significant lack of fit at $p>0.05$. The model F-value and the lack of fit F-value were used to determine the relevance of each of the coefficient terms (p-value).

Table 3.1 Quadratic polynomial equations of oil yields in terms of coded factors.

Responses	Equations	
Y_{Yellow}	$Y_{Yellow} = +40.89 + 0.51A - 6.20B + 0.28C + 2.15D + 1.51AB + 1.92AC + 1.36AD + 1.06BC + 0.075BD - 0.61CD - 1.05A^2 - 2.98B^2 - 0.45C^2 - 1.28D^2$	(2.2)
$Y_{Holetta,}$	$Y_{Holetta} = +32.69 + 0.52A - 6.19B + 0.33C + 1.75D + 0.67AB + 1.17AC + 1.26AD + 1.41BC + 0.52BD - 0.34CD - 1.15A^2 - 3.09B^2 - 1.09\ C^2 - 0.69\ D^2$	(2.3)
Y_{Deras}	$Y_{Derash} = +39.75 + 0.60A - 6.02B + 0.15C + 1.99D + 1.18AB + 1.06AC + 1.47AD + 1.86BC - 0.095BD - 0.17CD - 0.87A^{2\,-}\ 3.50B^2 - 0.64C^2 - 1.35D^2$	(2.4)
Y_{Tesfa}	$Y_{Tesfa} = +40.89 + 0.51A - 6.08B + 0.22C + 2.15D + 1.51AB + 1.92AC + 1.36AD + 1.26BC + 0.075BD - 0.61CD - 0.99A^2 - 3.10B^2 - 0.57C^2 - 1.22D^2$	(2.5)

Y_{Yellow}, $Y_{Holetta}$, Y_{Derash}, and Y_{Tesfa} are responses for Yellow Dodolla, Holetta-1, Derash, and Tesfa oil yields, respectively.

3.3.2.2 Diagnostic analysis for model validation

Diagnostic analysis was used to check the validity and reliability of the developed models. Figures 3.1 (a) –3.4 (a) showed that the normal probability plot of residuals was adequately approximated along a straight line with no sign of non-normality, showing that the normality plot of residuals fulfilled the requirement for model adequacy tests. The experimental values were well fit by the model equations (Table 3.1) as evidenced by the random scatter and uniform distribution of residuals (i.e., plots of residuals versus predicted values) shown in Figures 3.1 (b) –3.4 (b). Another significant test for determining the adequacy of predictive models is a comparison of predicted and actual values based on the coefficient of determination values (R^2). Since the linear correlation plots between the predicted and experimental values were quite close to the regressed diagonal line, the values of R^2 were very high. This confirmed that the goodness of fit was excellent ($p<0.0001$), indicating a high level of agreement between the predicted and actual values.

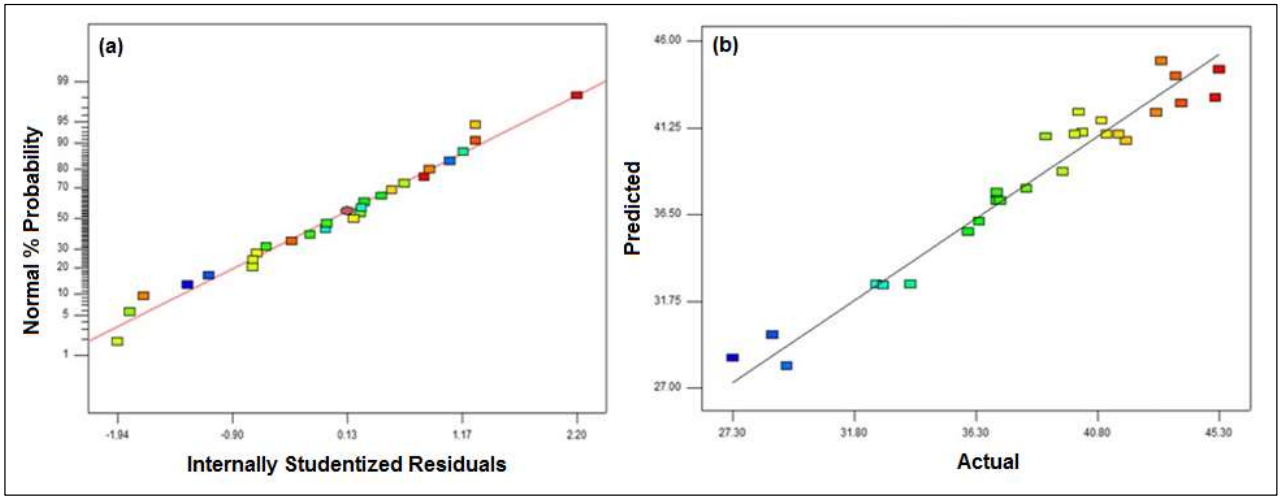

Figure 3.1 Adequacy test plots for Yellow Dodolla oil yield (%) (a) Normal probability distribution, (b) Predicted vs. actual values

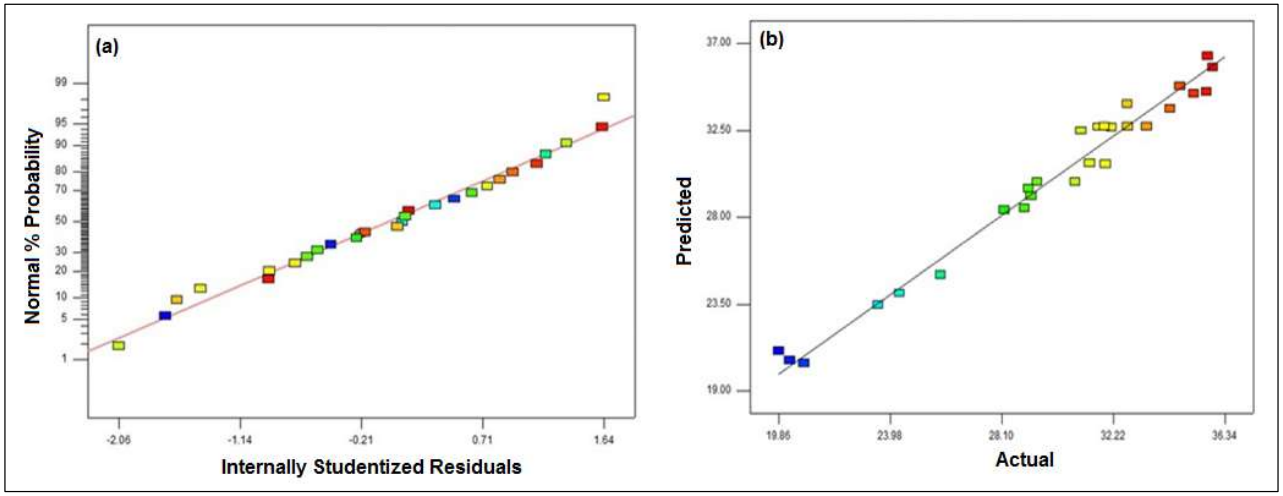

Figure 3.2 Adequacy test plots for Holetta-1 oil yield (%) (a) Normal probability distribution, (b) Predicted vs. actual values

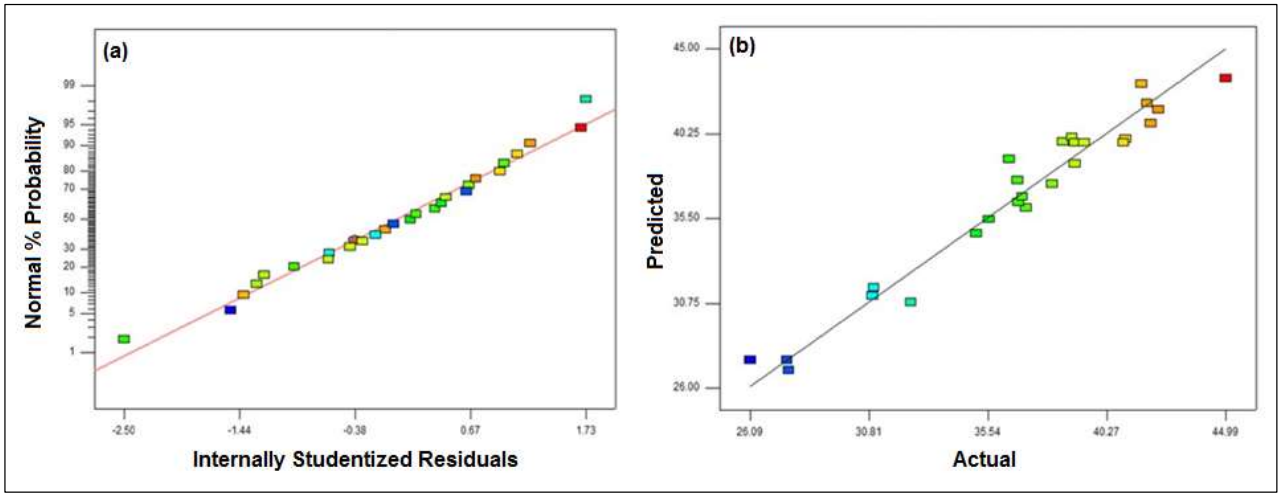

Figure 3.3 Adequacy test plots for Derash oil yield (%) (a) Normal probability distribution, (b) Predicted vs. actual values

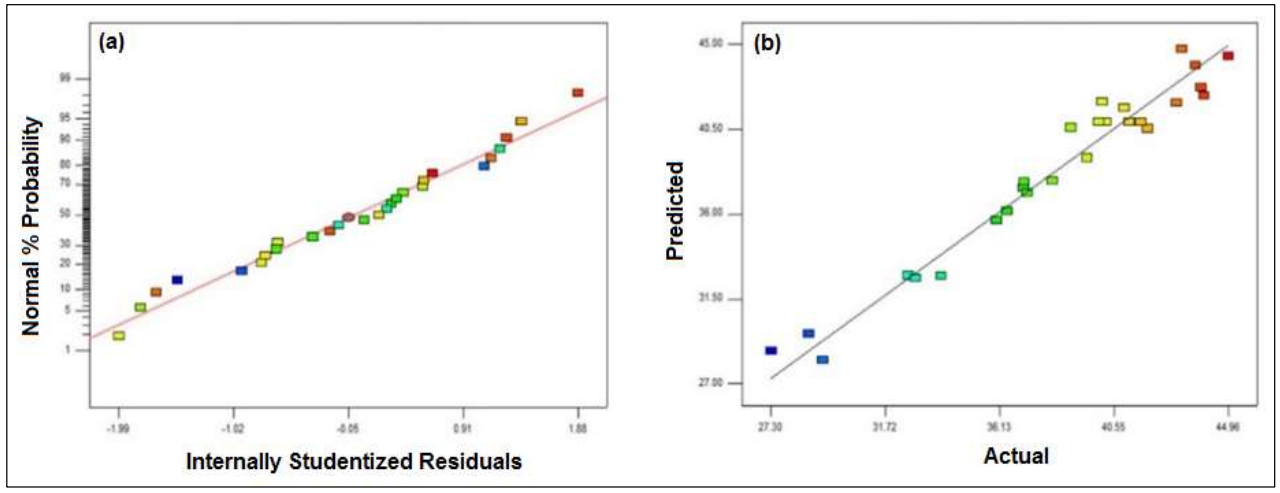

Figure 3.4 Adequacy test plots for Tesfa oil yield (%) (a) Normal probability distribution, (b) Predicted vs. actual values

3.3.2.3 Analysis of response surface and contour plots

For all types of oil yields, the single factor particle size (i.e., 150–355 μm) was shown to be statistically highly significant ($p<0.0001$). The solvent-to-solid ratio was also shown to be significant for Yellow Dodolla ($p=0.0005$), Holetta-1 ($p=0.0001$), and Tesfa ($p=0.0003$) oil yields. Figure 3.5 (a–d) shows 3D response surface plots that reveal statistically significant two-parameter interactions. Among the two-parameter interactions, the 3D surface plots of the combined effects of temperature and time ($p=0.0329$) (Yellow Dodolla), particle size and time ($p=0.0247$) (Holetta-1), temperature and solvent to solid ratio ($p=0.0396$) (Holetta-1), particle size and time ($p=0.0303$) (Derash), temperature and time ($p=0.0238$) (Tesfa), were significant factors. Table 3.2 shows the optimum parameters and their corresponding optimum oil yields. According to the study, further increases above the optimum values (e.g., solvent-to-solid ratios) have not brought any changes in the oil yields. This might be owing to mass transfer resistances that occurred after the optimal levels were reached. This was confirmed by a previously reported work, where higher solvent-to-solid ratios resulted in a greater concentration gradient during mass transfer within solids, leading to faster diffusion rates [183]. The combined effects of temperature and time, and particle size and time were significant. Higher temperatures and longer extraction times, increase solvent vaporization losses and reduce extraction yields [184]. The maximum and optimum oil yields were obtained at temperatures somewhat higher than room temperature (35.52–38.94 °C), particle size (150–355 μm), shorter extraction times (30.00–39.38 min), and relatively lower solvent-to-solid ratios (8.63–9.20 mL/g). Since Soxhlet extraction is a time-consuming extraction process (6–24 h) [185], in the current study, however, an isothermal batch reactor, was employed and it was possible to drastically reduce the long Soxhlet extraction time to an extremely low extraction time (i.e., 30 min). According to the results (Table 3.2), very short extraction times were achieved, and maximum oil yields were obtained without reaching hexane's boiling point [186]. This confirmed that lower temperatures close to room temperatures can be applied to extract oils, and hence, the technique can also be used for the extraction of heat-sensitive compounds. Even though recovery of products by filtration is a drawback when compared to Soxhlet extraction, it is simple to use and requires no thimbles. For validation of the optimization results, experiments with the optimum parameters were carried out; and the mean ± standard deviation verification values for Yellow Dodolla, Holetta-1, Derash, and Tesfa oil yields, were determined to be 45.65 ± 0.47, 35.85 ± 0.16, 44.28 ± 0.10, and 44.05 ± 03, respectively, in percentages.

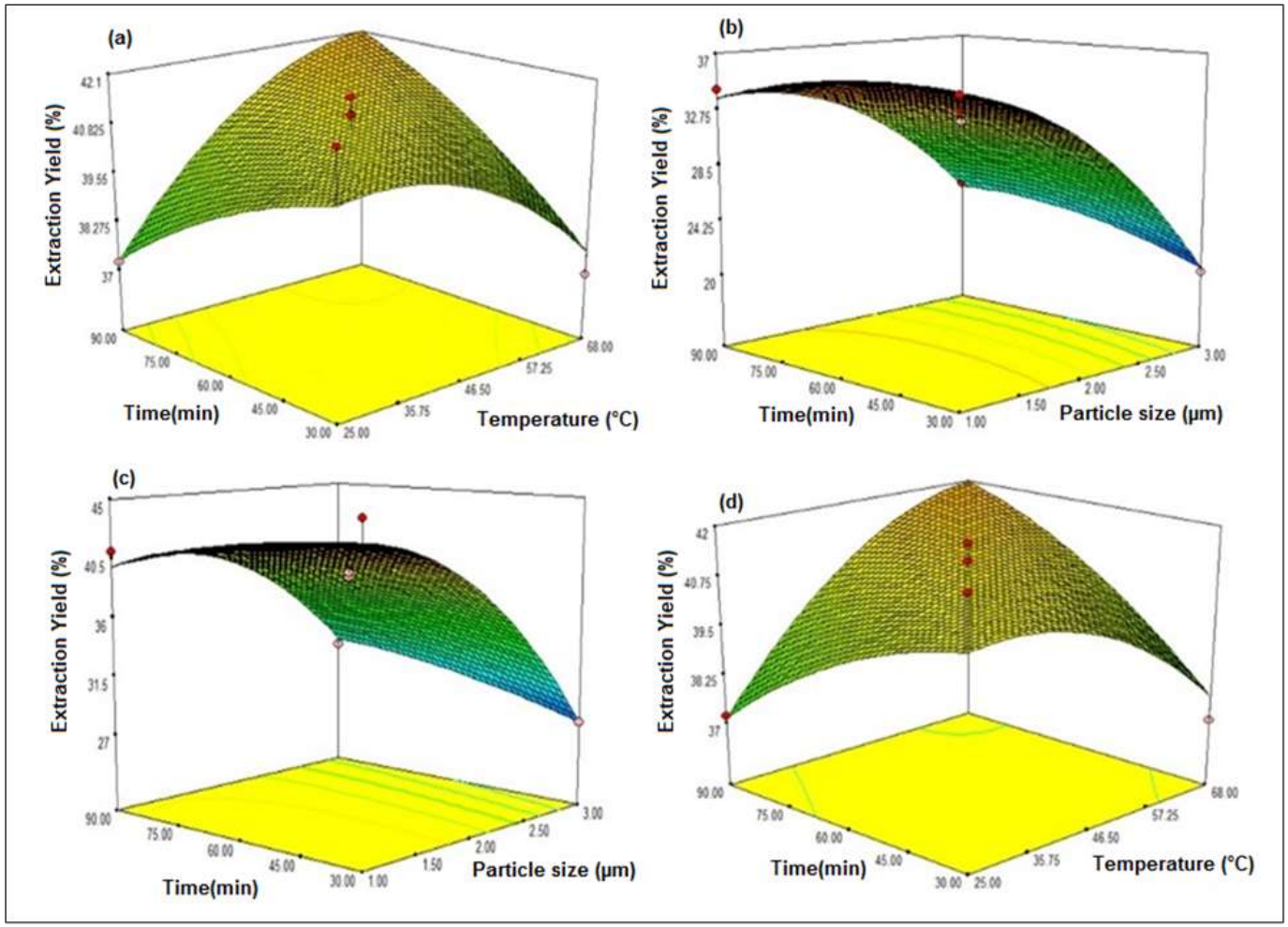

Figure 3.5 3D response surface plots (a) Temperature and time (Yellow Dodolla), (b) Particle size and time (Holetta-1), (c) Particle size and time (Derash), (d) Temperature and time (Tesfa).

Table 3.2 Optimum values of factors and predicted responses.

Name of variety	Optimum values of factors				Response (%)		Desirability
	Temperature (°C)	Particle size (µm)	Time (min)	Solvent-to-solid ratio (mL/g)	Exp.	Pred.	
Yellow Dodolla	38.94	150–355	35.20	8.96	45.30	45.25	1
Holetta-1	35.52	150–355	39.38	8.63	35.88	36.34	1
Derash	37.27	150–355	30.00	9.20	44.99	43.34	0.967
Tesfa	36.95	150–355	37.35	8.72	44.96	43.74	1

3.3.3 Characterization of oils

3.3.3.1 Physicochemical characterization

Table 3.3 shows the characterization results of the *B. carinata* oils. Table 3.3 also includes the literature values for Mustard and Jatropha oils. The *B. carinata* oils have very low moisture contents (i.e., <1%), and nearly the same pH values which make them less strong acidic oils. The refractive index (RI) of oils is affected by molecular weight, fatty acid chain length, degree of unsaturation, and degree of conjugation [187]. The RI of *B. carinata* oils is higher than that of the reported values of *Jatropha curcas* and Mustard measured at 28 °C and 25 °C, respectively. The RI of the oils is also greater than that of Soybean [188] measured at 30 °C (1.459 ± 0.00). The kinematic viscosities ($mm^2 s^{-1}$) of the oils were determined at 25, 40, and 100 °C. At 25 °C, the oils are more viscous than those from jatropha and mustard, while the temperature of mustard was not specified. At 40°C, the kinematic viscosities of Holetta-1 and Derash were very close to the kinematic viscosity of *B. carinata* oil (61.85 $mm^2 s^{-1}$) [189]; however, Yellow Dodolla was found to be slightly more viscous than this reported value and Tesfa is the least viscous one compared to the reported value of *B. carinata* oil. On the other hand, the kinematic viscosities of Holetta-1 and Tesfa were close to the kinematic viscosity of *B. carinata* oil (55.07 $mm^2 s^{-1}$) [190]; however, Yellow Dodolla and Derash were slightly more viscous than these reported values.

Table 3.3 Physicochemical properties of *B. carinata* oils.

Properties	**Experimental values**				**Reported values**	
	Yellow Dodolla	**Holetta-1**	**Derash**	**Tesfa**	**Jatropha**[191]	**Mustard**[192]
Moisture content (%)	0.20 ± 0.01	0.32 ± 0.04	0.41 ± 0.01	0.69 ± 0.02	5.58	0.05 ± 0.002
pH	5.33 ± 0.01	5.15 ± 0.01	5.20 ± 0.010	5.18 ± 0.01	–	–
Refractive index @ 20 °C	1.473 ± 0.00	1.473 ± 0.00	1.472 ± 0.00	1.477 ± 0.00	1.458	1.4652 ± 0.001
Kinematic viscosity ($mm^2\ s^{-1}$)						
25 °C	109.39 ± 0.00	108.49 ± 0.00	103.84 ± 0.00	88.44 ± 0.00	49.85	61.30 ± 0.02
40 °C	69.46 ± 0.08	57.28 ± 0.00	61.20 ± 0.00	51.41 ± 0.00	–	–
100 °C	12.89 ± 0.00	12.34 ± 0.00	14.80 ± 0.00	10.14 ± 0.00	–	–
Density @ 15 °C (kg/m^3)	907.75 ± 0.00	907.90 ± 0.00	905.25 ± 0.00	904.55 ± 0.00	915.00	0.8867 ± 0.3
Specific gravity @ 15 °C	0.914 ± 0.00	0.914 ± 0.00	0.912 ± 0.00	0.911 ± 0.00	–	0.9021 ± 0.01
Ash content (%)	0.02 ± 0.00	0.03 ± 0.00	0.03 ± 0.00	0.02 ± 0.01	–	–
Iodine value (g I2/100 g oil)	95.15	96.78	96.89	93.93	96.3	121.3 ± 0.32
Acid value (mg KOH/g)	0.45	0.5	0.22	9.20	2.9	0.4 ± 0.02
Peroxide value (meq. O_2/kg oil)	10.00	17.98	5.99	21.96	1.1	2.84 ± 0.13
Saponification value (mg KOH/g)	171.73	176.51	178.23	174.02	202.87	–

The higher level of unsaturation from monounsaturated fatty acids, which will be addressed in the following sections, may be the reason for the *B. carinata* oils' higher viscosities, especially, that of Yellow Dodolla. The oils have a little lower density than jatropha but a slightly higher density than mustard. The iodine value (IV) of the oils, an indication of the degree of unsaturation, may be primarily derived from the erucic acid and is much lower than Soybean [188] (127.55 ± 0.74 g I2/ 100 g), but much higher than the different mustard oilseed varieties such as BARI Sarisha-15, BARI Sarisha-16, and BARI Sarisha-17 whose IV are 72.50, 70.60, and 73.44, respectively, [193]. Although lower than the Mustard oil [192], the IV of the oils is in good accord with that of Jatropha. The IV of the oils is slightly lower than that of *B. carinata* (111.7 g I2/ 100 g) and *B. napus* (100.1 g I2/ 100 g) [194], but much lower than that of *B. juncea* (125.3 ± 0.32 g I2/ 100 g) [195]. The *B. carinata* oils have also very low ash levels, indicating that the oils' inorganic content is quite low, and this can be related to the lower metals´ concentrations. Except for Tesfa oil, the oils' acid values, which is the susceptibility to rancidity for higher values as free fatty acids, are identical to that of Mustard [192] but lower than that of Jatropha (Table 3.3), Mustard (3.82 ± 0.10 mg KOH/g oil) [196] and *B. juncea* oils (3.90 ± 0.32 KOH/g) [195]. The peroxide values (PV) of Holetta-1 and Tesfa are much higher than those of Soybean (2.1 ± 0.11 meq. O2/kg oil) [188], Jatropha, and Mustard oils [192]. The higher acidic and peroxide values of Tesfa may be due to the possible oxidation of the oil. The reported saponification values (SV) of *B. carinata* (177.60 mg KOH/g) and *B. napus* (190.95 mg KOH/g) [194] are higher than that of the experimental oils; however, the SV of *B. carinata* are much lower when compared to that of Soybean (225.56 ± 0.42 mg KOH/g) [188]. The *B. carinata* oils have high-quality physicochemical properties which enable them to be applied in the production of bio-aviation fuels.

3.3.3.2 Fatty acids profiling

The characteristics of vegetable oils, notably fatty acid profiles (FAP), are affected by oilseed species, oil extraction processes, and processing conditions [161]. Fatty acids may impact the properties of vegetable oil, such as viscosity, oxidative stability, boiling point, and combustion energy, consequently, vegetable oil with a high FAP can be readily converted into a suitable hydrocarbon fuel at a low cost and with high efficiency [197], [198]. Fatty acid profiles of the *B. carinata* oils (i.e., Yellow Dodolla, Holetta-1, Derash, and Tesfa) are shown in Tables 3.4–3.7, respectively. The mass spectrum of the various fatty acids (FA) illustrated in Figure 2.6 (a–d) showed narrow elution times, but the separation was adequate to avoid coelution.

Based on the qualitative analysis of the FA, carbon lengths of C16:0, C18:0, C18:1, C18:2, C18:3, C20:1, and C22:1 are found in the *B. carinata* oils (Tables 3.4–3.7); however, carbon lengths of 16:0, 18:0, 18:1, 18:2 in algal [199], 16:0, 18:0, 18:1, 18:2, 18:3 in *Jatropha curcas* [200], and 16:0, 18:0, 18:1cis-9, 18:1, 18:2, 18:3 in Castor oils [201] are found. Palmitic (C16:0, 51%) [199], oleic (C18:1, 43%) [200], ricinoleic acids (C18:1, 87.7%) [201], and erucic acid (C22:1, 42.00–49.69%), are the highest concentrations of fatty acids found in algal, Jatropha, Castor and the experimental *B. carinata oils*, respectively. The total saturated fatty acids (SFA) content of the *B. carinata* oils (3.01-5.66%) is nearly the same as the SFA of Moroccan castor seed oil (5.2%) [202]. In addition, the total unsaturated fatty acids (UFA) content of this seed oil is also approximately the same as the UFA (94.34-96.99%) of the *B. carinata* oils. The presence of erucic acid in the *B. carinata* oils, therefore, makes them industrially significant feedstocks where these significant fatty acids are not common in many of the edible and non-edible oils.

Erucic acid, a long-chain monounsaturated fatty acid, has emerged as a promising candidate for sustainable aviation fuel (SAF) production. Erucic acid's long carbon chain (22 carbons) is a key factor contributing to its high energy content, making it an ideal candidate for jet fuel production. Moreover, the high erucic acid content enhances fuel properties, including cetane number and cold flow performance.

Table 3.4 Fatty acid profile of *B. carinata* 'Yellow Dodolla' oil.

Peak No	Retention Time (min)	Systematic Name	Cas No.	Molecular Formula	Shorthand Notation	Saturation/ unsaturation	Other Name	Area %	Qual
1	19.4349	Hexadecanoic acid, methyl ester	000112-39-0	$C_{17}H_{34}O_2$	C16:0	Saturated	Palmitic	3.0092	98
2	24.5131	9-Octadecenoic acid, methyl ester, (Z)-	002777-58-4	$C_{19}H_{36}O_2$	C18:1	mono	Elaidic	7.9235	99
3	24.63	9, 12-Octadecadienoic acid, methyl ester	002462-85-3	$C_{19}H_{34}O_2$	C18:2	poly	Linoleic	24.8872	99
4	25.0783	9, 12, 15-Octadecatrienoic acid, methyl ester, (Z, Z,Z)-	000301-00-8	$C_{19}H_{32}O_2$	C18:3	poly	Linolenic	10.597	99
5	29.941	cis-11-Eicosenoic acid, methyl ester	1000333-63-8	$C_{21}H_{40}O_2$	C20:1	mono	Eicosenoic	3.8935	99
6	35.1245	13-Docosenoic acid, methyl ester, (Z)-	001120-34-9	$C_{23}H_{44}O_2$	C22:1	mono	Erucic	49.6896	99

Table 3.5 Fatty acid profile of *B. carinata* 'Holetta-1'.

Peak No	Retention Time (min)	Systematic Name	Cas No.	Molecular Formula	Shorthand Notation	Saturation/ unsaturation	Other Name	Area %	Qual
1	19.402	Hexadecanoic acid, methyl ester	000112-39-0	$C_{17}H_{34}O_2$	C16:0	Saturated	Palmitic	3.6786	96
2	24.4789	9-Octadecenoic acid (Z)-, methyl ester	000112-62-9	$C_{19}H_{36}O_2$	C18:1	mono	Oleic acid	13.7337	99
3	24.5944	9,12-Octadecadienoic acid, methyl ester	002462-85-3	$C_{19}H_{34}O_2$	C18:2	poly	Linoleic	25.4673	99
4	24.9222	Methyl stearate	000112-61-8	$C_{19}H_{38}O_2$	C18:0	Saturated	Stearic	1.9791	95
5	25.0453	9,12,15-Octadecatrienoic acid, methyl ester, (Z,Z,Z)-	000301-00-8	$C_{19}H_{32}O_2$	C18:3	poly	Linolenic	8.3703	99
6	29.9074	cis-11-Eicosenoic acid, methyl ester	1000333-63-8	$C_{21}H_{40}O_2$	C20:1	mono	Eicosenoic	4.2913	96
7	35.0911	13-Docosenoic acid, methyl ester, (Z)-	001120-34-9	$C_{23}H_{44}O_2$	C22:1	mono	Erucic	42.4798	96

Table 3.6 Fatty acid profile of *B. carinata* 'Derash' oil.

Peak No	Retention Time (min)	Systematic Name	Cas No.	Molecular Formula	Shorthand Notation	Saturation/ unsaturation	Other Name	Area %	Qual
1	19.3984	Hexadecanoic acid, methyl ester	031604-55-4	$C_{17}H_{34}O_2$	C16:0	Saturated	Palmitic	4.0976	88
2	24.4691	9-Octadecenoic acid, methyl ester, (Z)-	002777-58-4	$C_{19}H_{36}O_2$	C18:1	mono	Elaidic	9.148	84
3	24.5906	9,12-Octadecadienoic acid (E,E)-, methyl ester	002566-97-4	$C_{19}H_{34}O_2$	C18:2	poly	Linolelaidic	28.7437	99
4	25.0395	9,12,15-Octadecatrienoic acid, methyl ester, (Z,Z,Z)-	000079-07-2	$C_{19}H_{32}O_2$	C18:3	poly	Linolenic	10.0951	83
5	29.8951	11-Eicosenoic acid, methyl ester	1000335-06-7	$C_{21}H_{40}O_2$	C20:1	mono	Eicosenoic	4.9996	83
6	35.0756	13-Docosenoic acid, methyl ester, (Z)-	001120-34-9	$C_{23}H_{44}O_2$	C22:1	mono	Erucic	41.997	98
7	35.4295	Amphetamine	000300-62-9	$C_9H_{13}N$	–	–	Amphetamine sulfate	0.919	49

Table 3.7 Fatty acid profile of *B. carinata* 'Tesfa' oil.

Peak No	Retention Time (min)	Systematic Name	Cas No.	Molecular Formula	Shorthand Notation	Saturation/ unsaturation	Other Name	Area %	Qual
1	19.3974	Hexadecanoic acid, methyl ester	000112-39-0	$C_{17}H_{34}O_2$	C16:0	Saturated	Palmitic	3.0954	98
2	24.4742	9-Octadecenoic acid, methyl ester, (Z)-	002777-58-4	$C_{19}H_{36}O_2$	C18:1	mono	Elaidic	8.3143	99
3	24.5902	9,12-Octadecadienoic acid (Z,Z)-, methyl ester	000112-63-0	$C_{19}H_{34}O_2$	C18:2	poly	Oleic	27.4425	99
4	24.9167	Methyl stearate	000112-61-8	$C_{19}H_{38}O_2$	C18:0	Saturated	Stearic	1.8042	97
5	25.0384	9,12,15-Octadecatrienoic acid, methyl ester, (Z,Z,Z)-	000301-00-8	$C_{19}H_{32}O_2$	C18:3	poly	Linolenic	10.1229	99
6	29.8994	11-Eicosenoic acid, methyl ester	003946-08-5	$C_{21}H_{40}O_2$	C20:1	mono	Eicosenoic	4.0452	98
7	30.0764	Methyl 9-eicosenoate	004605-14-5	$C_{21}H_{40}O_2$	C20:1	mono	Gadoleic	1.4611	53
8	35.0888	13-Docosenoic acid, methyl ester, (Z)-	001120-34-9	$C_{23}H_{44}O_2$	C22:1	mono	Erucic	43.7144	99

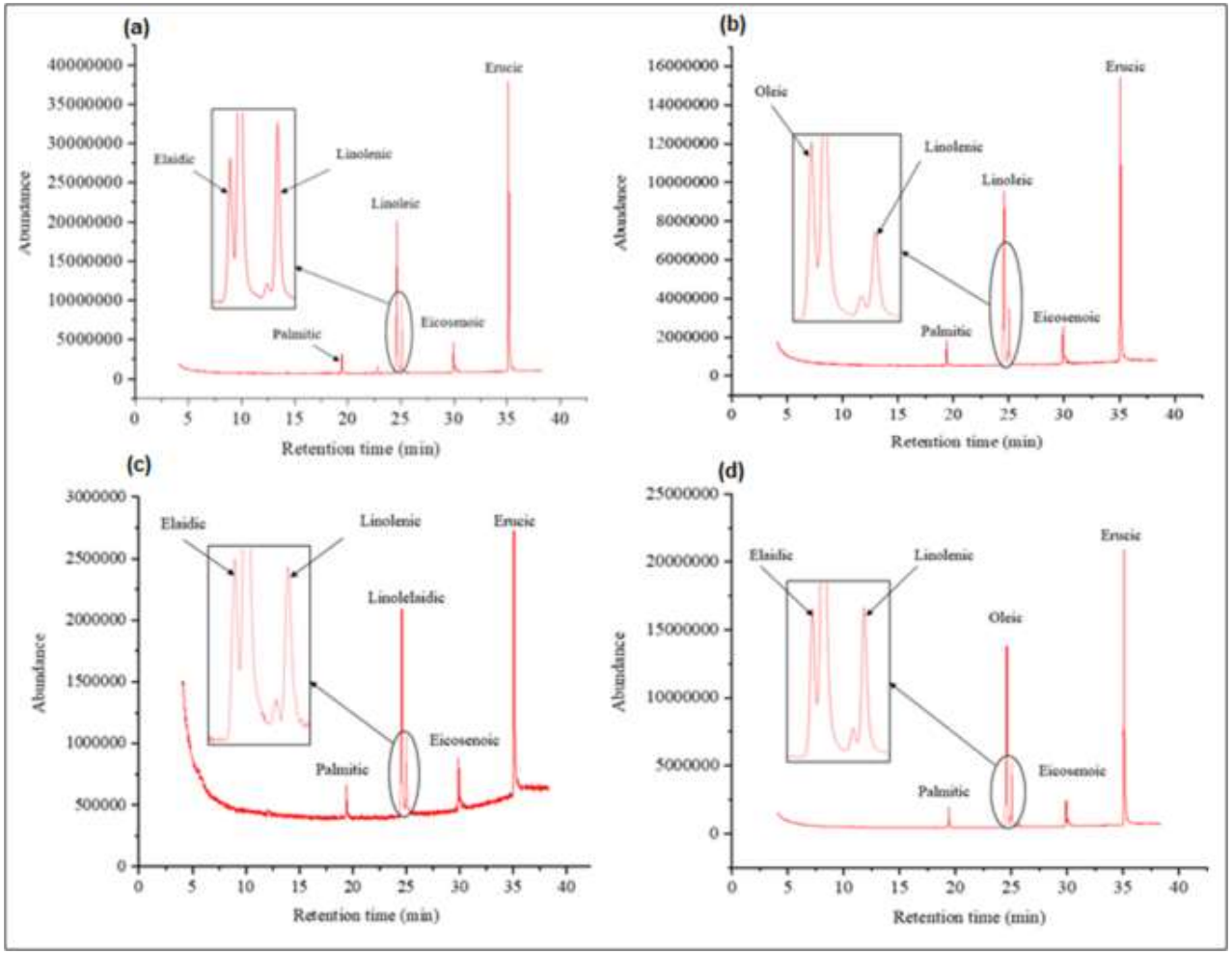

Figure 3.6 Chromatogram of methyl esters of *B. carinata* oils. (a) Yellow Dodolla, (b) Holetta-1, (c) Derash, (d) Tesfa.

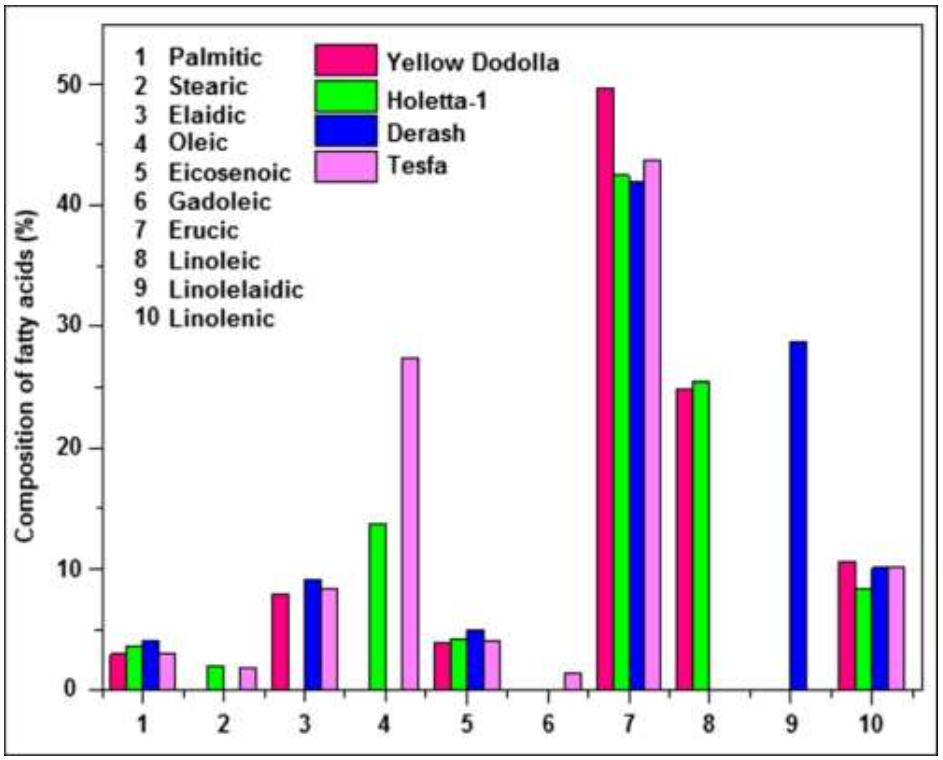

Figure 3.7 Comparison of FA composition of B. carinata oils.

Among all the different varieties and species of the Brassicaceae family, there are variations in the concentrations of fatty acids. This is mainly due to the intended purposes of the breeding programs. *B. carinata*, for example, are mostly developed either to have no erucic acid which will be used for human consumption, or developed to have high erucic acid or linoleic acid contents which will be applied in the biofuel processing industries [189], [52]. The erucic acid content of the *B. carinata* oils is compared with other previously reported *B. carinata* cultivars. As a result, the oils, and Yellow Dodolla oil, in particular, had somewhat greater erucic acid contents than what was reported (40.7–42.9%) by [29]. In the present study, erucic acid, eluted after 35 minutes, was the most prevalent FA in all oils, accounting for the lowest value (42.00%) from Derash to the highest level (49.69%) from Yellow Dodolla, making Yellow Dodolla a super-high erucic acid oil. After erucic acid, the next most dominant FA in Yellow Dodolla, Holetta-1, Derash, and Tesfa oils were linoleic (24.89%), linoleic (25.47%), linolelaidic (28.74%), and oleic (27.44%), respectively. The overall quantity of unsaturated (mono and poly) FA in each of the oils outnumbers the total number of saturated FA. Yellow Dodolla has the greatest percentage (96.99%) of total unsaturated FA (UFA) with >61% coming from total monounsaturated FA (MUFA), primarily, from erucic acid.

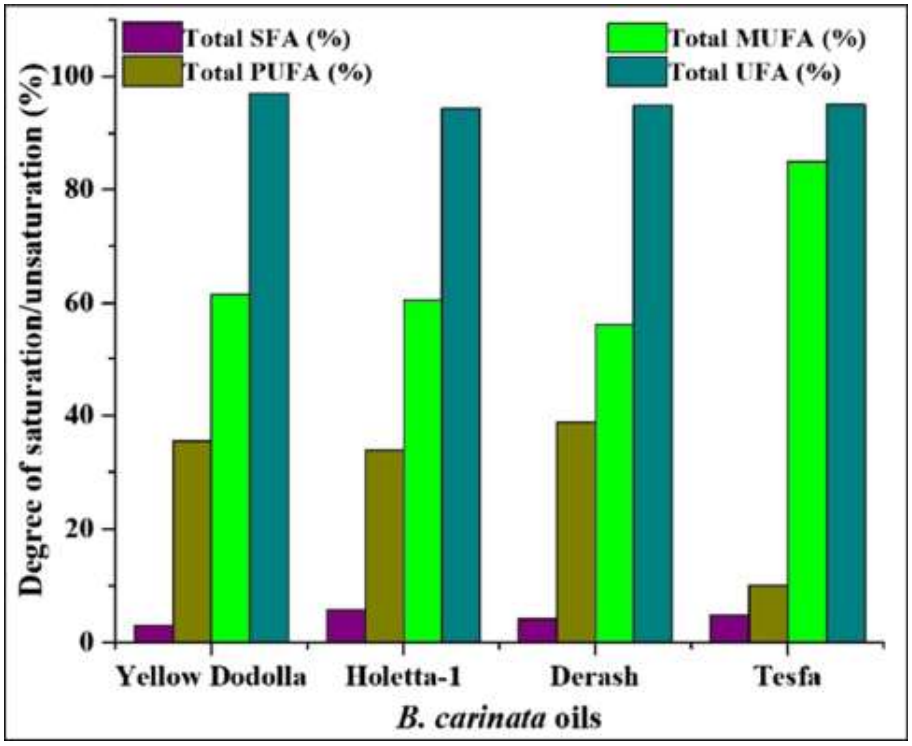

Figure 3.8 Degree of saturation/unsaturation of FA of *B. carinata* oils.

Since Yellow Dodolla is slightly more viscous at 25 and 40 °C than the other oils, this feature could be attributed to the maximum level of unsaturation, and hence to the lengthy carbon chains and big molecules containing oxygen atoms. In comparison to the other oils, this oil has the lowest total saturated FA content (SFA) (3.01%), which is even lower than the low saturated fatty acids (≤6%) found in other *B. carinata* oils [203]. Yellow Dodolla's combined qualities (i.e., lowest total SFA and highest total UFA) make it a suitable feedstock for the production of bio-jet fuels and biochemicals. Figures 3.7 and 3.8 indicate a comparison of compositions, and the degrees of saturation and unsaturation of the various FA, respectively. The highest UFA and lowest SFA levels of oils, especially Yellow Dodolla, have a wide range of practical applications. This is backed up by the following previously reported work. Because of the highly reactive properties of *B. carinata* oils UFA, they can easily form cycloparaffin and aromatic compounds, and their larger molecular weights resulted in more hydrocarbon fuel products and chemicals when compared to vegetable oils with longer 18-carbon chains, such as Soybean, Canola, or Jatropha oils [30]. In each of the experimental oils, total MUFA content > total PUFA content > total SFA content. Table 3.8

shows a comparison of saturated, unsaturated, total mono- and polyunsaturated FA, as well as their important ratios. Yellow Dodolla is indeed the most prominent cultivar among the four *B. carinata* cultivars due to its superior fatty acid profile for the production of bio-jet fuel.

Table 3.8 The total number of saturated/ unsaturated, and percentages of total saturated, unsaturated, mono- and polyunsaturated fatty acids.

Parameter	Yellow Dodolla	Holetta-1	Derash	Tesfa
Total number of SFA	1	2	1	2
Total number of UFA	5	5	5	6
Total MUFA (%)	61.51	60.50	56.14	57.53
Total PUFAs (%)	35.48	33.84	38.84	37.57
Total SFA (%)	3.01	5.66	4.10	4.90
Total UFA (%)	96.99	94.34	94.98	95.10
MUFA/PUFA	1.73:1	1.79:1	1.45:1	1.53:1
PUFA/SFA	11.79	5.98	9.48	7.67
UFA/SFA	32.23:1	16.68:1	23.18:1	19.41:1

3.3.3.3 Ultimate analysis

Results (Table 3.9) of the concentrations of C, H, N, S, O, H/C, and O/C atomic ratios indicated that each of these elements and atomic ratios differed according to C (77.6-79.8%), H (12.0-12.3%), N (0.01-0.14%), S (0.004%), O (7.80-10.30%), H/C (1.84-1.86), and O/C (0.07-0.10). These results were compared to edible and non-edible vegetable oils, and bio-oil published in the literature. There were no significant variations in carbon and hydrogen concentrations when compared to the reported values of the edible oil, Canola oil (Table 3.9); however, the concentrations of each of N, S, and O were smaller than that of Canola oil (Table 3.9); but higher

Table 3.9 Ultimate analysis results, H/C and O/C atomic ratios of *B. carinata* oils.

Element	Experimental values (wt. %)				Literature values (wt. %)			
	Yellow Dodolla	**Holetta-1**	**Derash**	**Tesfa**	**Canola** [204], [205] **(edible)**	**Pongamia** [206] **(non-edible)**	**Carinata** [207] **(non-edible)**	**Biomass** [208] **pyrolysis oil**
C	79.8	77.6	79.7	78.1	78.3	77.2 ± 0.24	78.33±0.14	40.8
H	12.3	12.0	12.3	12.0	12.2	11.4 ± 0.03	11.64±0.08	6.1
N	0.14	0.02	0.01	0.01	0.43	–	0.37±0.24	<0.1
S	0.004	0.004	0.004	0.004	0.02	–	–	<0.1
O	7.80	10.30	8.00	9.80	11.5	11.2 ± 0.21	9.67±0.18	53.1
H/C	1.85	1.86	1.85	1.84	–	1.78	–	–
O/C	0.07	0.10	0.08	0.09	–	–	–	–

than that of refined Rapeseed oil (0.0003%) [209]. Additionally, the oils' C, H, O, and H/C ratios were compared to that of Pongamia oil, whose values are presented in [206].

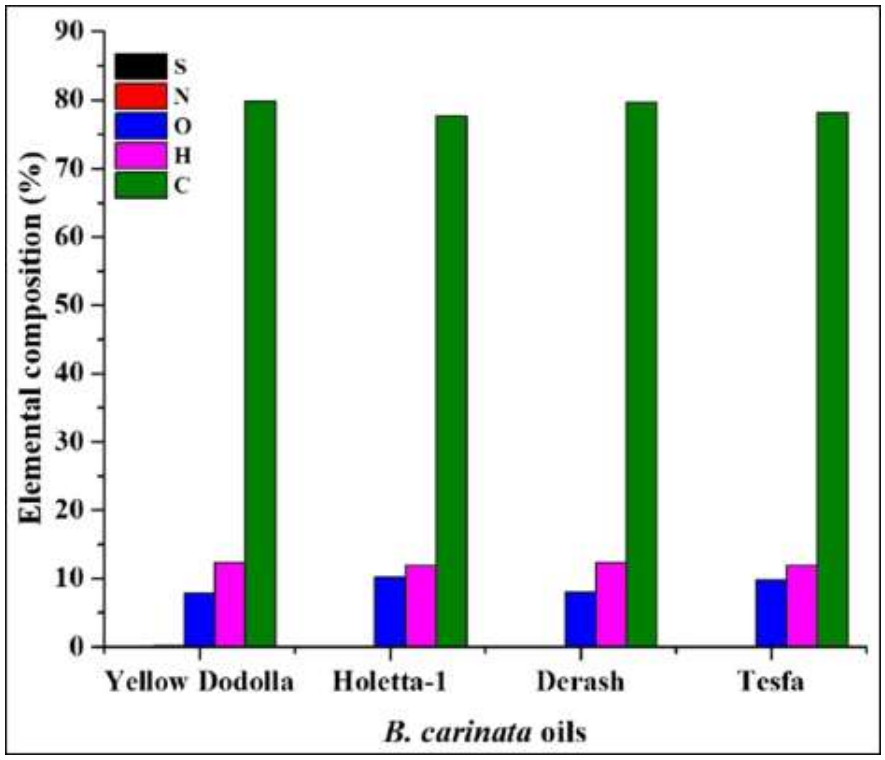

Figure 3.9 Ultimate analysis results of B. carinata oils.

Although Pongamia oil has a little higher oxygen concentration than the *B. carinata* oils, its C, H, and H/C ratios are in good agreement with that of these oils. As can be seen in Table 3.9, the ultimate analysis results of the oils are also compared to the literature values of *B. Carinata* (Table 2.9) and biomass-pyrolysis oils [208], where except for the nitrogen content of the *B. carinata* oil, which is slightly higher than that of the experimental oils, the *B. carinata* and these experimental oils have nearly the same C, H, and O contents. This is not the case with biomass pyrolysis oil, though. The C and H concentrations of the experimental oils are significantly greater than those of the pyrolysis oil, and their oxygen level is substantially smaller. The oxygen concentration of the oils is similarly quite low when compared to liquid fuels such as bioethanol (35%), and FAME biodiesel (11%) [210]. Based on the foregoing discussion, *B. carinata* oils have excellent ultimate analysis results with greater H/C and lower O/C atomic ratios, as well as very low N and S levels, all of which make the oils very useful feedstocks.

Comparisons were also performed among the *B. carinata* oils, where significant variations were not observed in their C, H, S, N, and H/C atomic ratio results except for the value of N, which is slightly greater in Yellow Dodolla oil. Although the N content of Yellow Dodolla appears to be slightly greater when compared to the other oils, its value is still lower than that of the edible Canola oil (Table 3.9). The oils have very small and identical S contents; however, the solvent-extracted oilseed meals of these cultivars have higher S concentrations, which will be further investigated in our upcoming work. Even though the oils have lower O concentrations, the concentration of O in Yellow Dodolla is the lowest. The *B. carinata* oils, in general, offer excellent ultimate analysis results, especially, since their lower O levels require reduced hydrogen gas consumption during upgrading in the deoxygenation of the oils.

3.3.3.4 Analysis of metals and phosphorous contents

Table 3.10 shows the ICP-OES results of metals and phosphorous concentrations. These results are also shown in Figure 3.10. Regardless of their concentrations, all these elements were found in all of the *B. carinata* oils. The concentrations of the elements Na, K, Ca, Mg, Al, Fe, Zn, Ni, and P were compared to previously reported values of edible NRO (neat rapeseed oil, fresh oil after extraction) [177], non-edible (e.g., *B. carinata*, and Waste Rapeseed Oil (WRO)), and used cooking oils (UCO) (Table 3.10). Na levels in the *B. carinata* oils are less than those in NRO, but they are practically identical to those in Waste Rapeseed Oil (WRO) (4.5 mg/kg) [177]. Except for Tesfa oil, the K content in the *B. carinata* oils is lower than that found in NRO but almost equivalent to that of WRO (4.00 mg/kg) [177]. The oils have relatively higher Ca contents than those of *B. carinata* oil and UCO, although the concentrations are quite low compared to the value in NRO. The Mg concentration is comparatively larger than that of WRO (0.91 mg/kg) [177], *B. carinata*, and UCO [211].

Table 3.10 ICP-OES elemental analysis results of *B. carinata* oils.

Elements	Experimental values (mg/kg)				Literature values (mg/kg)		
	Yellow Dodolla	**Holetta-1**	**Derash**	**Tesfa**	**NRO[177] (edible)**	**Carinata[211] (non-edible)**	**UCO[211] (Used cooking oil)**
Na	3.00	3.00	3.00	4.00	7.20	–	–
K	5.00	7.00	5.00	20.00	24.60	–	–
Ca	20.00	30.00	30.00	50.00	146.00	1.4 ± 0.6	7.2 ± 0.5
Mg	4.00	6.00	4.00	10.00	45.90	<0.011	0.85 ± 0.10
Al	3.00	4.00	4.00	6.00	–	0.47 ± 0.09	1.1 ± 0.2
Fe	6.00	4.00	3.00	7.00	–	0.2 ± 0.05	7.4 ± 0.2
Zn	12.00	7.90	4.00	0.00	–	–	–
Ni	0.21	<0.20	<0.20	0.31	–	<0.18	<0.18
P	30.00	50.00	30.00	120.00	188.00	–	–

NRO: (neat rapeseed oil, fresh oil after extraction, edible) UCO: Used cooking oil.

The concentrations of Al in Yellow Dodolla, Holetta-1, and Derash are similar to those observed in *B. carinata* and UCO (Table 3.10), with just minor differences. The Ni content in the oils is quite low and is comparable to that of the *B. carinata* and UCO (Table 3.10). The concentration of Fe in the oils did not vary significantly, but it is somewhat higher than the levels reported for these *B. carinata* and UCO. Although Yellow Dodolla has a relatively higher Zn content, Zn was not detected in Tesfa. Even though the concentration of P in all the *B. carinata* oils, except for its value in Tesfa, was found to be close to the reported P level in a *B. carinata* oil (59 mg/kg) [52], and WRO (37.90 mg/kg) [177], its concentration was much smaller than what was reported for NRO. In general, the lower concentrations of the metals of the *B. carinata* oils may be correlated to the lower total ash contents of the oils discussed in the previous sections.

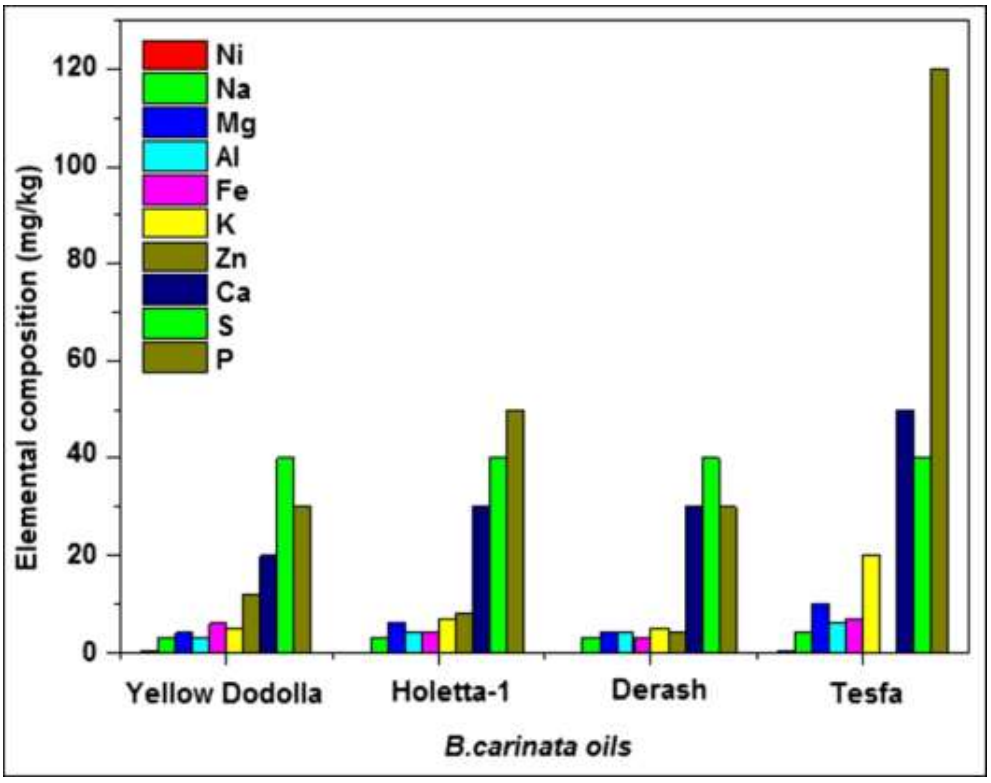

Figure 3.10 ICP-OES elemental analysis results of *B. carinata* oils.

3.3.3.5 FT-IR Characterization

Since FT-IR is a versatile analytical approach for the evaluation of a broad variety of materials, particularly for identifying unknown compounds [212], it provides details on unique chemical

bonds and functional groups [213]. Based on research performed on hydrocarbons, the physical and chemical characteristics are highly reliant on the functional groups, and the spectrum-functional group interactions offer the theoretical background for employing mid-IR spectra to determine fuel qualities [214]. Vegetable oils are susceptible to degradation due to factors such as oxygen, heat, light, and humidity. This instability can lead to various chemical reactions, making their preservation challenging. Therefore, proper production and storage methods are crucial for maintaining their quality [215]. As a result, this qualitative analysis may be used to estimate the relative purity of the oils.

Figures 3.11–3.14 show the FT-IR spectra of the *B. carinata* oils. Strong, medium, and weak infrared bands have been observed in all types of *B. carinata* oils, with the majority of the peaks being quite sharp (i.e., not broad) and quite strong, suggesting that the oil samples are exceptionally pure. The presence of an alkene was verified by the presence of a C-H stretching vibration, which is attributed to the medium peaks at 3008 cm^{-1}. The existence of an asymmetrical $–CH_2$ stretching vibration [216] indicated the presence of an alkane, which gives off a very strong peak at 2922 cm^{-1}. Likewise, the presence of a symmetrical $–CH_2$ stretching vibration, which is responsible for the strong and sharp peaks at 2853 cm^{-1}, showed the presence of an alkane [217]. Because of the presence of carboxylic acids [218], the oils show a peak at 1744 cm^{-1}, confirming quite sharp and quite strong vibration of –C=O bonds. The C=C stretching vibration that is attributed to the variable peak at 1654 cm^{-1} shows the presence of an alkene. The presence of C–C stretching vibration that leads to a peak at 1463 cm^{-1} confirmed the presence of an aromatic ring.

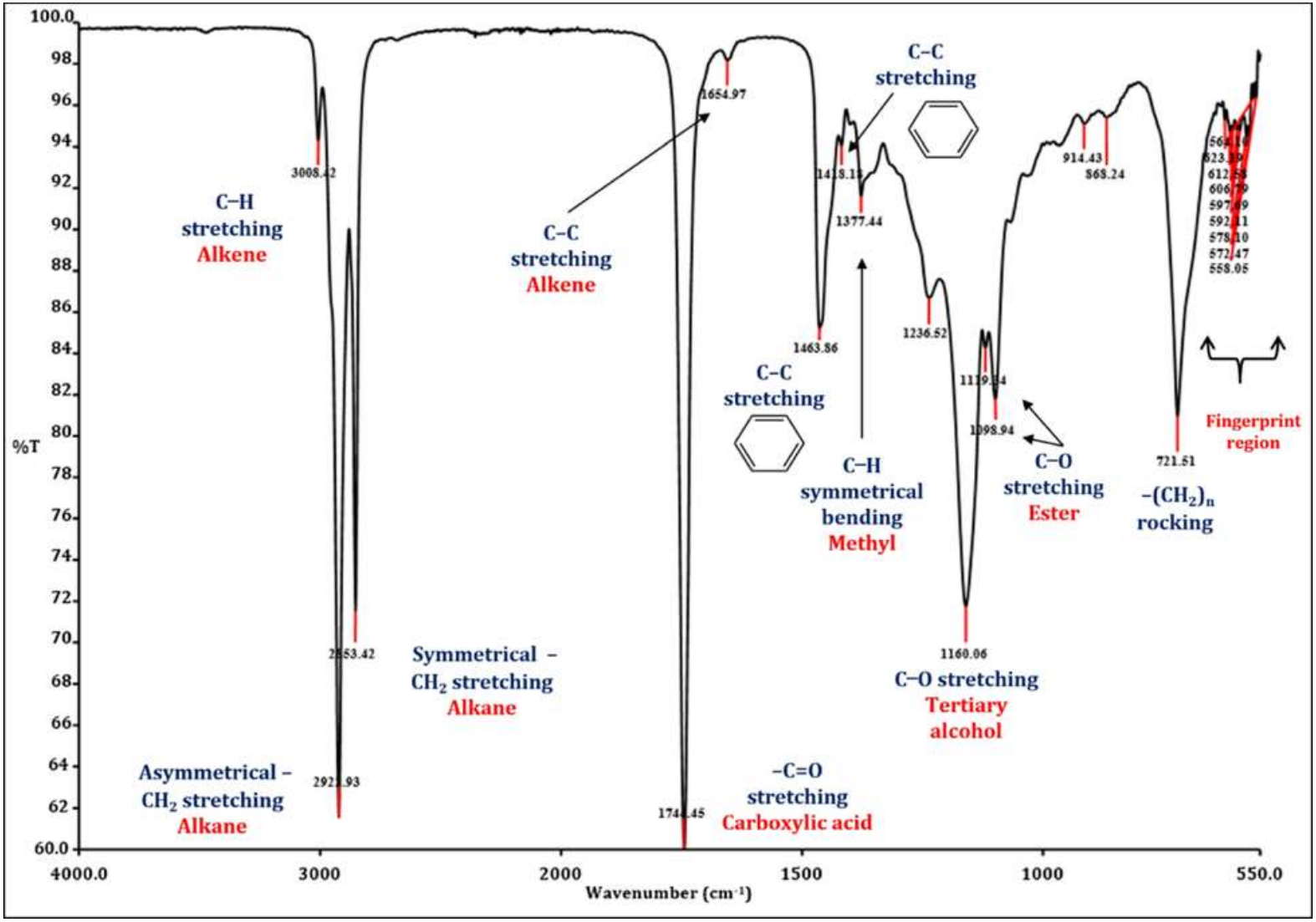

Figure 3.11 FT-IR spectrum of Yellow Dodolla oil.

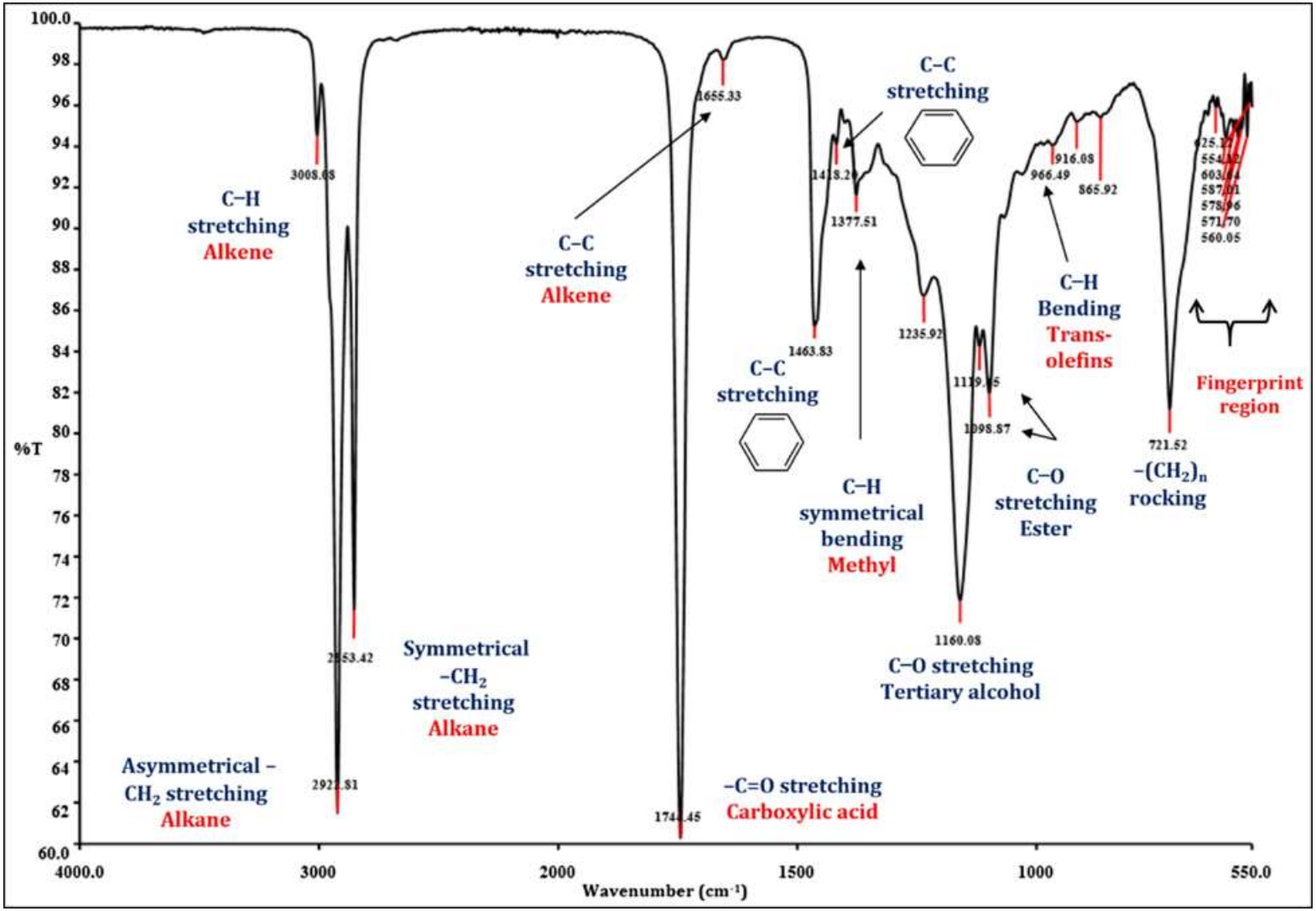

Figure 3.12 FT-IR spectrum of Holetta-1 oil.

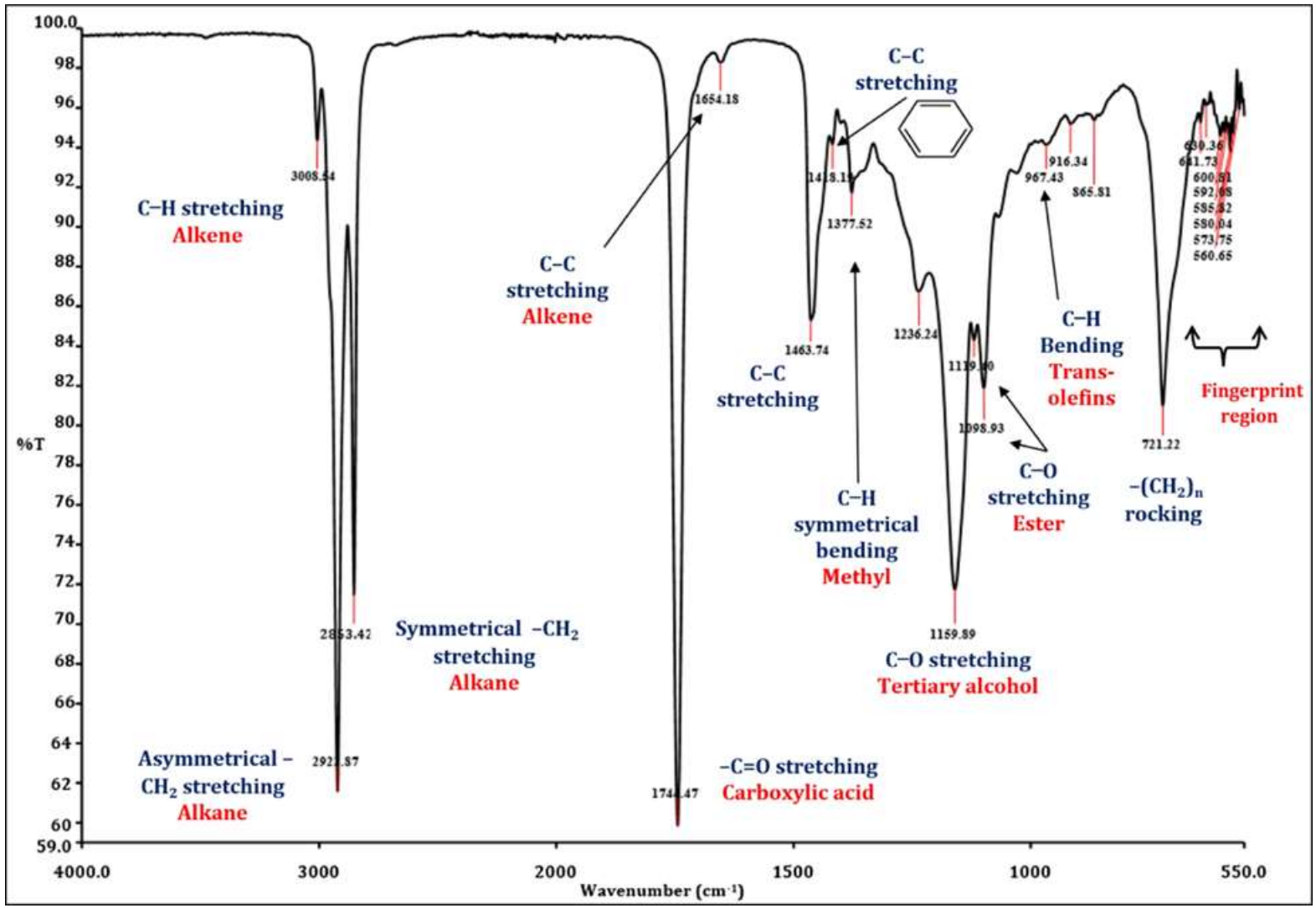

Figure 3.13 FT-IR spectrum of Derash oil.

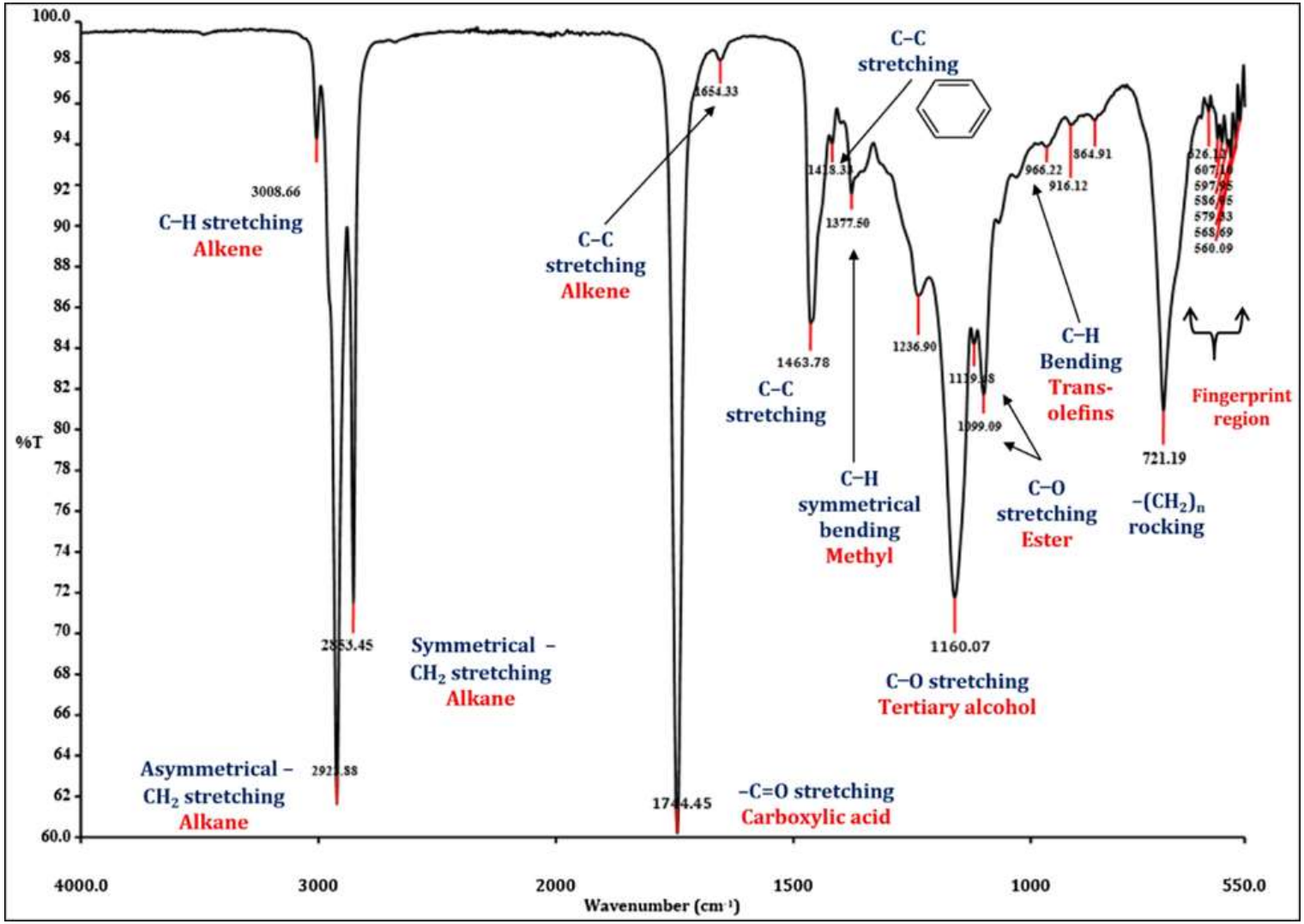

Figure 3.14 FT-IR spectrum of Tesfa oil.

The other absorption bands lower than 1463 cm^{-1} (Figures 3.11–3.14) are also discussed as follows: Except for the peaks at 1160, 1099, and 721 cm^{-1}, all other peaks are not strong. There is an aromatic ring (C–C stretching) in 1418 cm^{-1}, a methyl (C-H symmetrical bending) in 1377 cm^{-1} [219], an α, β-unsaturated ester (C–O stretching) in ca. 1236 cm^{-1}, tertiary alcohol (C–O stretching) in ca. 1160 cm^{-1}, an ester (C–O stretching) in the peaks 1119 cm^{-1} and ca. 1099 cm^{-1} [217]. Furthermore, the appearance of C–H bending vibration at a peak of 967 cm^{-1} confirms the presence of trans-olefins produced from mono- or polyunsaturated groups [220]; however, these olefins are not observed in Yellow Dodolla oil. There is a $–(CH_2)_n$ rocking vibration at a peak of 721 cm^{-1} [216]. There are intricate patterns of absorptions that are peculiar to the chemical compounds or molecules in the so-called "fingerprint region," which lies within the wavelength range of about 1500-500 cm^{-1} [221]. In the current study, the differences in the patterns of *B. carinata* oils are relatively insignificant outside of this region (i.e., bands above 721 cm^{-1}), thus they share the same functional groups and identical chemical compositions; yet, there are slight variations in the patterns of the oils in the fingerprint region (Figures 3.11–3.14), suggesting that the oils have different properties.

3.3.3.6 Analysis of calorific values

The gross calorific values (GCV) of the oils were determined to vary from 39.97 ± 0.32 (Holetta-1) to 40.08 ± 0.24 MJ/kg (Yellow Dodolla), and the net calorific values (NCV) of the oils were found to be closely identical, 37.45 MJ/kg. The GCV and NCV of the oils were compared to edible and non-edible vegetable oils, including those from *B. napus*, *B. carinata*, and Jatropha curcas oils. In light of this, the GCV of the present *B. carinata* oils is nearly comparable to that of *B. napus* (39.55 MJ/kg), *B. carinata* (39.93 MJ/kg) [194], and Jatropha curcas (38.8 MJ/kg) [222], although slightly higher than that of Pongamia oil (35.18 ± 0.12 MJ/kg) [206]. Similarly, the NCV of the *B. carinata* oils is nearly identical to that of *B. carinata* (37.39 MJ/kg) and *B. napus* (37.01 MJ/kg) [194]. In general, the higher calorific values of the oils mentioned thus far make them suitable alternative feedstocks for the production of bio-aviation fuels.

3.4 Conclusions

Response surface methodology (RSM) with three levels of Box-Behnken Design (BBD) in an isothermal batch reactor was applied for the extraction of *B. carinata* oils. Powdered samples (150–

710 μm) were heated and continuously stirred in n-hexane. Both heat energy and continuous mixing were applied, and hence, the potential mass transfer resistances (i.e., solid-solid, solid-liquid, and liquid-liquid) might have been greatly reduced and enhanced the rate of extraction. Accordingly, very short extraction times (30.00–39.38 min), and lower temperatures somewhat higher than room temperature (35.52–38.94 °C) were achieved to recover the maximum and optimum oil yields (35.93–45.25%) using particle sizes of 150–355 μm without reaching hexane's boiling point (ca. 69°C). The application of this extraction technique can result in the following significant benefits: (a) It is not necessary to raise the boiling point of the solvent; (b) It reduces the amount of time required to boil, condense, and reach the surface of the sample; (c) It avoids the potential solvent loss while boiling; (d) There is no evaporation, no solvent loss, and hence, no potential reduction in extraction yield; (e) It saves energy for boiling; (f) It may also be applied for the extraction of heat-sensitive components at temperatures slightly higher than room temperature. Moreover, it is also simple to use and requires no thimbles even though recovery of products by vacuum filtration is a drawback when compared to the Soxhlet extraction method.

Characterization results confirmed that the oils' better physicochemical properties, excellent fatty acid profiles (such as their high erucic acid contents, 42–50%), ultimate analysis (such as their low heteroatom contents and O/C ratio), lower metals and phosphorous concentrations, FT-IR characterization (which demonstrates the presence of various functional groups in the oils), and high gross and net calorific values make them promising alternatives to existing feedstocks in the aviation industry. These findings suggested that the oils, in particular Yellow Dodolla oil, a super-high erucic acid oil, would be used in our subsequent investigation of a hydroprocessing pathway for the production of bio-jet fuel because of their ideal properties. Yellow Dodolla is among the most significant cultivated non-food *B. carinata* oilseed crops introduced in 1986 by the Holetta Agricultural Research Centre in Holetta, Ethiopia. Normal hexane was used for oil extraction, and it was determined to be a suitable solvent to obtain maximum oil yields; however, iso-propanol was also tested for extraction, and it resulted in very low oil yields. Furthermore, higher yields of viscous and semi-solid-like components were extracted. Depending on the need (i.e., maximum oil content or the viscous and semi-solid-like components), we propose that future studies extract and evaluate these iso-propanol soluble components for they may be very valuable feedstocks for the production of significant industrial products.

CHAPTER FOUR

Characterization of Hexane-Defatted *Brassica carinata* Oilseed Meals to Explore Their Potential for Valorization Towards a Sustainable Circular Bioeconomy

4.1 Introduction

The co-product produced after the extraction of oil is *Brassica carinata* meal (BCM), which is of increasing interest to animal nutritionists. BCM is highly dependent on the demand for its oil for the jet plane and aviation industry [223]. It is becoming more and more interesting to experts in animal nutrition since the BCM contains high protein and low fiber levels [220,221], making it a good source of animal feed for animals including poultry, beef, and pig [72,160]. Although BCM is a key co-product that can be used as a source of protein for animal feeding, various additional economically viable value-added co-products (such as plasticizers, detergents, surfactants, polyesters, lubricants, organic fertilizer, and biofumigants [160,75,166,223], can also be produced across the entire *B. carinata* supply chain.

The biggest constraints to investing in sustainable aviation fuel (SAF) production are crude oil prices, feedstock availability, feedstock cost, conversion technology yields and costs, and governmental regulations [12]. Before commercial development is viable, the economics of aviation fuels can also be sustained by the income that can be made from the *B. carinata* co-products. The large-scale deployment of carinata will, therefore, be feasible as the profitability of biofuel increases [29]. As a result, it is essential to switch to a circular economic paradigm centered on the establishment of new methods for making the best use of these natural resources to overcome resource overexploitation, mismanagement, environmental degradation, ecosystem imbalance, and climate change [228].

Thus, based on the diverse applications of BCM, characterization, and valorization of four different oilseed meals of *B. carinata* cultivars (Ethiopian origin)—Yellow Dodolla, Holetta-1, Derash, and Tesfa, a conceivable realization of a circular bioeconomy with *B. carinata* cultivars is highly possible. The purpose of the present study was to characterize these samples using proximate

analysis, ultimate analysis, estimation of energy densities and other important values (such as H/C, O/C, and C/N atomic ratios), analysis of heating values, and organic nutrient profiles. Furthermore, by using these characterization results, an investigation was carried out to valorize how best to utilize the meals for their potential industrial applications, which might later serve as an essential component for the development of an integrated biorefinery based on these carinata cultivars.

4.2 Materials and Methods

4.2.1 Collection of *Brassica carinata* meal samples

The investigation used oilseed meals from four *B. carinata* seeds collected from the Holetta Agricultural Research Centre, Holetta, Ethiopia. These oilseed meals were obtained from n-hexane-extracted *B. carinata* oils that were previously investigated for their potential applications in the aviation industry [24]. Their scientific names were also mentioned in that previous study. In the present work, whenever applicable, the local names of the cultivars—Yellow Dodolla, Holetta-1, Derash, and Tesfa—are applied to refer to the corresponding oilseeds and oilseed meals.

4.2.2 Characterization of meals

4.2.2.1 Proximate analysis

AOAC Official Methods of Analysis [229] were applied for the determination of total moisture content (MC) (method 935.29) in a moisture analyzer (PCE-MA 100, PCE Instruments, Germany), crude fat (CF) (method 922.06) using Soxhlet extraction method, crude protein (CP) (method 992.23) by Kjeldahl technique using titration in HCl, total ash content (AC) (method 923.03) in an electrically heated chamber Nabertherm furnace (L5/C6, Nabertherm GmbH, Germany), crude fiber (method 962.09) by chemical digestion followed by filtration, ashing, and oven drying, and the total carbohydrate content was determined by difference (i.e., total carbohydrate (%) = 100 − % (crude protein + crude fat + total moisture + total ash + crude fiber)) [230]. The samples' volatile matter (VM) content was determined based on ASTM D1762-84(2021), the standard test method for chemical analysis of wood charcoal. Lids were placed on the crucibles to prevent anything from escaping and to prevent oxygen from entering the process. The VM content was calculated as in equation 4.1

$$VM\ (\%) = \frac{W_1 - W_2}{W_1} * 100\% \quad (4.1)$$

where W_1−initial weight of the sample and W_2−final weight of the sample. The proportion of material determined to have been removed while being tested for moisture, volatile matter, and ash is calculated as follows:

$$FC\ (\%) = 100 - \%\ (MC + AC + VM) \quad (4.2)$$

where FC−fixed carbon content (%), MC−moisture content (%), AC−ash content (%), VM−volatile matter (%). Approximately 2.5 g of sample for moisture content and 2 g for each of the other analyses have been used.

4.2.2.2 Chemical composition analysis and determination of atomic ratios

The weight percentage concentrations of total carbon (C), total hydrogen (H), and total nitrogen (N) were determined based on DIN 51732 (2014-07) in a CHN analyzer (LECO, Leco CHN 828 MC, USA). Inductively coupled optical emission spectroscopy (ICP-OES) (Vista MPX, Varian Deutschland GmbH, Germany) was applied for the determination of the concentration of total sulfur (S) based on DIN ISO 22036 (2009-06) in aqua regia flux digestion (DIN EN 13657 Verf. I (2003-01) [A]). The total oxygen (O) content was obtained by difference from 100 − % (C + H + N + S + ash content) using DIN 51733 (2016-04). Approximately, 150 mg of a sample was utilized for analysis. The atomic ratios (i.e., H/C, O/C, and C/N) were calculated from the results of the chemical constituents.

4.2.2.3 Analysis of calorific values

Even though it is possible to determine the calorific values from proximate and ultimate analysis through linear and non-linear empirical equations, the higher heating (HHV) and lower heating values (LHV) of samples were determined using a bomb calorimeter method (DIN 51900-1:2000-04) in an adiabatic bomb calorimeter (C6000, IKA-Werke GmbH & Co. KG, Germany). Each replicate experiment utilized about 0.5 g of a sample.

4.2.2.4 ICP-OES analysis of nutrient profiles

Nutrient profiles of samples were carried out by inductively coupled plasma optical emission spectroscopy (ICP-OES) (Vista MPX, Varian Deutschland GmbH, Darmstadt, Germany) based on

DIN ISO 22036:2009-06. For the ICP-OES analysis, samples were first digested by Aqua regia flux digestion (DIN EN 13657 (2003-01)) in a microwave digester (ETHOS. Lab, Germany). Approximately, 0.3 g of a sample was applied for analysis.

4.3 Results and Discussion

4.3.1 Characterization of meals

4.3.1.1 Proximate analysis

Figure 4.1 shows the *B. carinata* cultivars during the flowering stage, seeds after harvesting, and the n-hexane-extracted oilseed meals. The pictures in Figure 4.1 (a–d) were taken during our field visit to the Holetta Agricultural Research Center when the *B. carinata* cultivars were in their flowering stage.

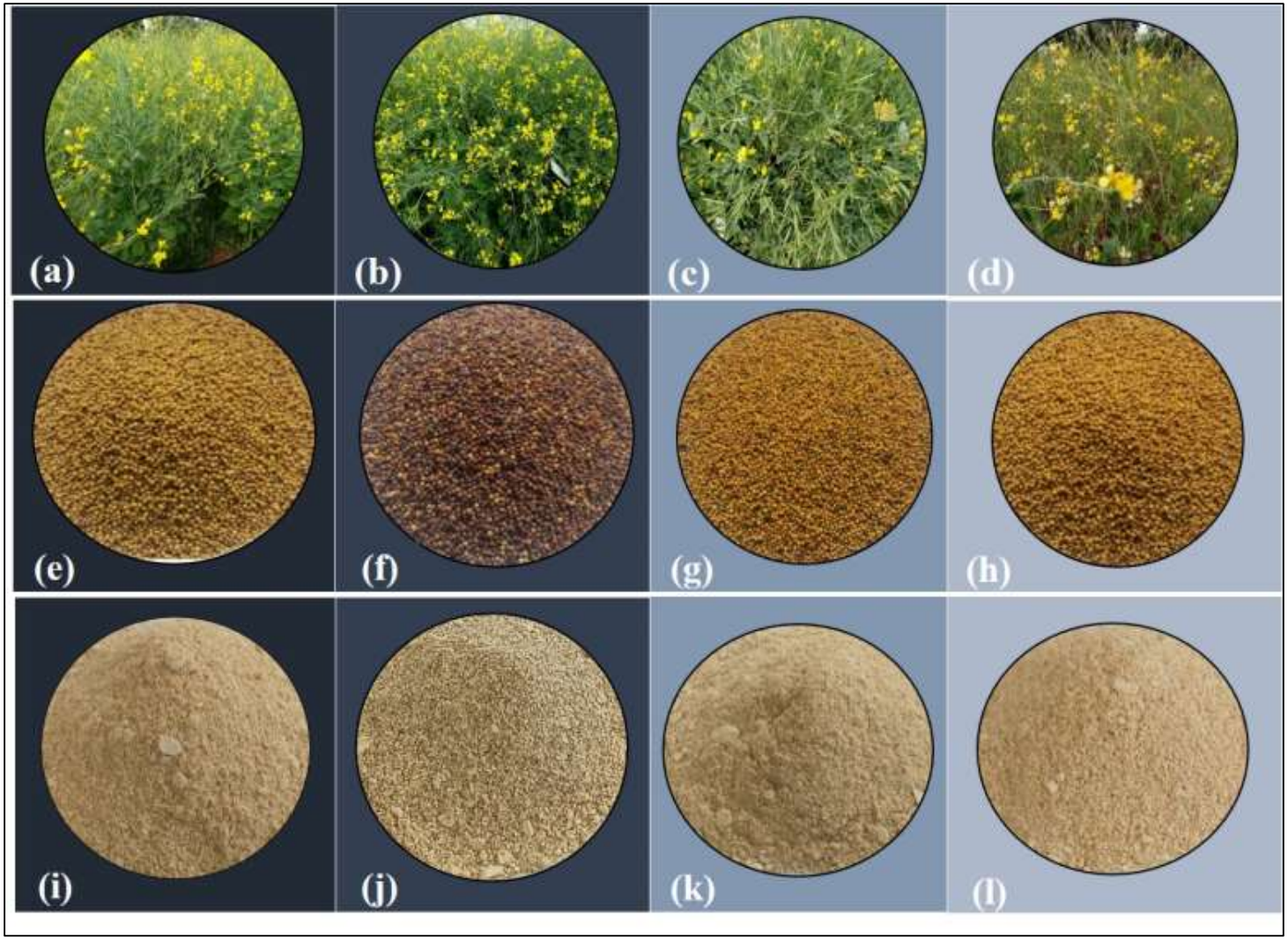

Figure 4.1 The *B. carinata* seed cultivars in their flowering stage: (a) Yellow Dodolla, (b) Holetta-1, (c) Derash, (d) Tesfa, Seed: (e) Yellow Dodolla, (f) Holetta-1, (g) Derash, (h) Tesfa, Meal: (i) Yellow Dodolla, (j) Holetta-1, (k) Derash, (l) Tesfa.

A. Carinata seeds

Table 4.1 shows the proximate analysis of the seeds. The mean total moisture content of the seeds is quite similar to that stated in our previous work [24]; nevertheless, it is lower than that of Jatropha seeds stored for twelve (8.28 ± 0.28%) and 60 months (11.6 ± 0.38%) [231]. Although the crude protein content of the meals (Table 4.2) is substantially higher than that of the seeds, the crude fat content of the seed samples was found to be higher than that of the meals. Comparisons with earlier studies indicated that the seed samples had lower total ash contents than *B. carinata* (4.08 ± 0.109 to 3.88 ± 0.363%) [232]. Furthermore, the ash content of the seeds was determined to be much lower than the ash content of mustard and rapeseed seed varieties (9.6–12.5%) [233]. This shows that the experimental *B. carinata* seeds have lower inorganic concentrations compared to the above-reported values. The ash contents of the seeds (on a wet basis) are remarkably similar to those of Pongamia seeds, which have ash concentrations ranging from 2.47 ± 0.03 to 3.30 ± 0.02% (dry basis) [206]. The samples' crude protein content, 25–26%, is substantially similar to the crude protein of *B. carinata* seeds (18.7–28.3%) [29]. The proximate analysis of the seeds is shown in Figure 4.2.

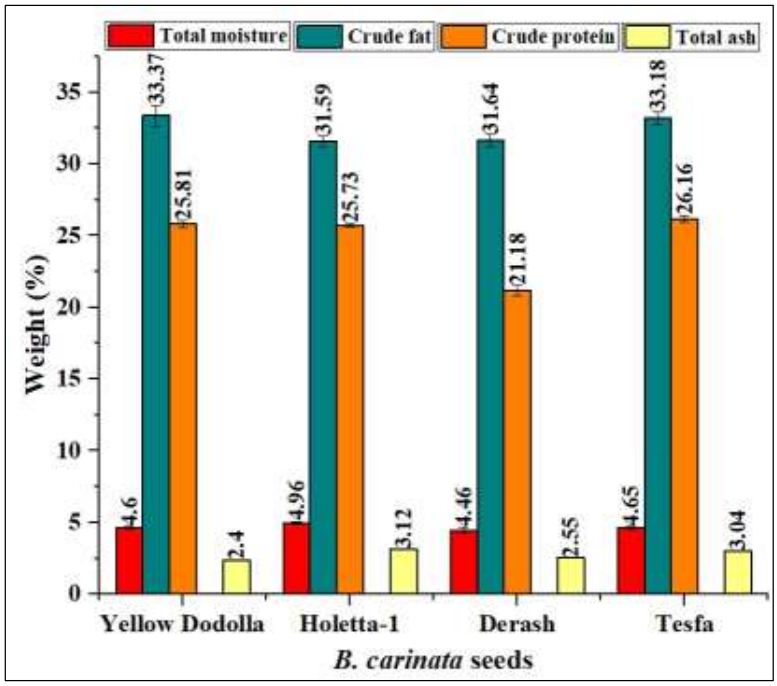

Figure 4.2 The proximate analysis of *B. carinata* seeds.

Table 4.1 Proximate analysis of *B. carinata* seeds.

Property (wt. %)	Yellow Dodolla	Holetta-1	Derash	Tesfa
Total moisture	4.86 ± 0.17	4.99 ± 0.17	4.67 ± 0.35	4.89 ± 0.14
Total ash	2.40 ± 0.00	3.12 ± 0.03	2.55 ± 0.00	3.04 ± 0.00
Crude protein	25.81 ± 0.25	25.73 ± 0.12	21.18 ± 0.36	26.16 ± 0.25
Crude fat	33.37 ± 0.73	31.59 ± 0.36	31.64 ± 0.42	33.18 ± 0.46

B. Carinata meals

Proximate analysis of the meals is shown in Table 4.2, and Figure 4.3. Each of the meals' mean total moisture contents is quite identical to the reported values of Rapeseed (8.7–11%) [234], [235] and Sunflower (5.6–11.1%) [234], [236]. Even though the Yellow Dodolla seed has the highest oil content (45.25%) [24], its meal has also the highest crude fat (CF) level when compared to the other meals. The total nitrogen contents of the meals determined by the Kjeldahl method using titration in HCl are practically identical to the total nitrogen contents determined by ultimate analysis (Table 4.3). According to their respective total nitrogen levels, the meals have very high crude protein contents, with Holetta-1 having the highest. Following solvent extraction, a significant increase in crude protein content (CP) was observed in the meals compared to the seeds, as illustrated in Tables 4.1 and 4.2. Comparing the meals' CP values to previously published results revealed that they are significantly higher than *B. carinata*'s (31%) [237] and slightly higher than Rapeseed's (37.6–38.2%) [238], the CP (Holetta-1) being considerably higher than these reported values. Additionally, it was determined that the meals' CP contents were higher than those of *B. napus* "black" (36.9%) and *B. napus* "yellow" (41.0%), but approximately close to those of *B. juncea* "yellow" (42.3%) [239].

The meals' crude fiber (CF) content is higher than that of Soybean (3.9–6.8%) comparable to the Sunflower meal's lower value, is higher than that of Soybean (3.9–6.8%) [234], and Rapeseed (11.5–12.7%) [234], [235], but lower than that of Sunflower (26.2–41.0%) [234], [236], except for Yellow Dodolla and Tesfa, whose values are comparable to that of the lower value of Sunflower meal. The total ash contents of the meals are smaller than that of Soybean (6.4–6.7%) [234], Rapeseed (6.3–7%) [234], [235], and Sunflower (5.3–6.5%) [234], [236]. Derash has the highest total carbohydrate content when compared to the other meals, even though all of the meals' levels

of fixed carbon and volatile matter are quite identical. The meals' volatiles are quite similar to that of the *B. napus* (Rapeseed) meal (82.60%), despite the meals' fixed carbon contents being slightly higher than those of the Rapeseed meal (7.90%) [240]. Yellow Dodolla and Tesfa may yield more bio-oil and non-condensable gases than the other meals due to their higher volatile and lower fixed carbon contents.

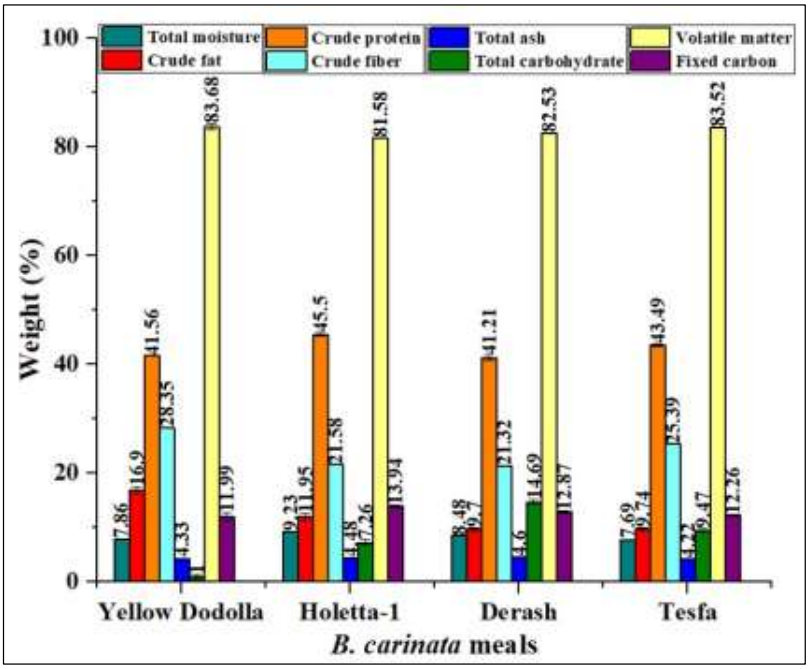

Figure 4.3 The proximate analysis of *B. carinata* meals.

Table 4.2 Proximate analysis of *B. carinata* oilseed meals.

Property (wt. %)	Yellow Dodolla	Holetta-1	Derash	Tesfa
Total moisture	7.86 ± 0.02	9.23 ± 0.10	8.48 ± 0.02	7.69 ± 0.13
Crude fat	16.90 ± 0.60	11.95 ± 0.68	9.70 ± 0.37	9.74 ± 0.33
Total nitrogen	6.65 ± 0.00	7.28 ± 0.06	6.59 ± 0.08	6.96 ± 0.04
Crude protein	41.56 ± 0.00	45.50 ± 0.37	41.21 ± 0.50	43.49 ± 0.25
Crude fiber	28.35 ± 0.07	21.58 ± 0.04	21.32 ± 0.02	25.39 ± 0.02
Total ash	4.33 ± 0.05	4.48 ± 0.04	4.60 ± 0.07	4.22 ± 0.01
Total carbohydrate	1.00 ± 0.43	7.26 ± 0.50	14.69 ± 0.44	9.47 ± 0.38
Volatile matter	83.68 ± 0.61	81.58 ± 0.01	82.53 ± 0.00	83.52 ± 0.03
Fixed carbon	11.99 ± 0.81	13.94 ± 0.22	12.87 ± 0.26	12.26 ± 0.20

4.3.1.2 Chemical composition analysis

Table 4.3 shows the chemical composition of the meal samples. These results are also clearly shown in Figure 4.4, with the weight (%) on the Y-axis scaled to 110, presented as stacked columns, and with the standard deviation values also displayed in each of the columns. Comparison with literature values reveals that the total concentrations of each of the chemical constituents are quite similar to those derived from a Rapeseed meal with C (52.25%), H (8.06%), N (3.91%), and O (35.78%) (Table 4.3), where it was found that the nitrogen levels of the experimental meals were higher.

The meals' C, H, N, and S contents were also compared with those of de-oiled solvent-extracted Pongamia cakes. Accordingly, the meals have higher C, N, and S contents and only marginally higher H content compared to the reported values of the cakes having C (42.97 ± 0.47% − 46.25 ± 0.53%), H (6.45 ± 0.01% − 6.83 ± 0.08%), N (4.98 ± 0.04% − 5.82 ± 0.02%), and S (0.23%–0.32%) (Table 4.3). The advantages of the higher nitrogen content are described in more detail in the subsequent sections.

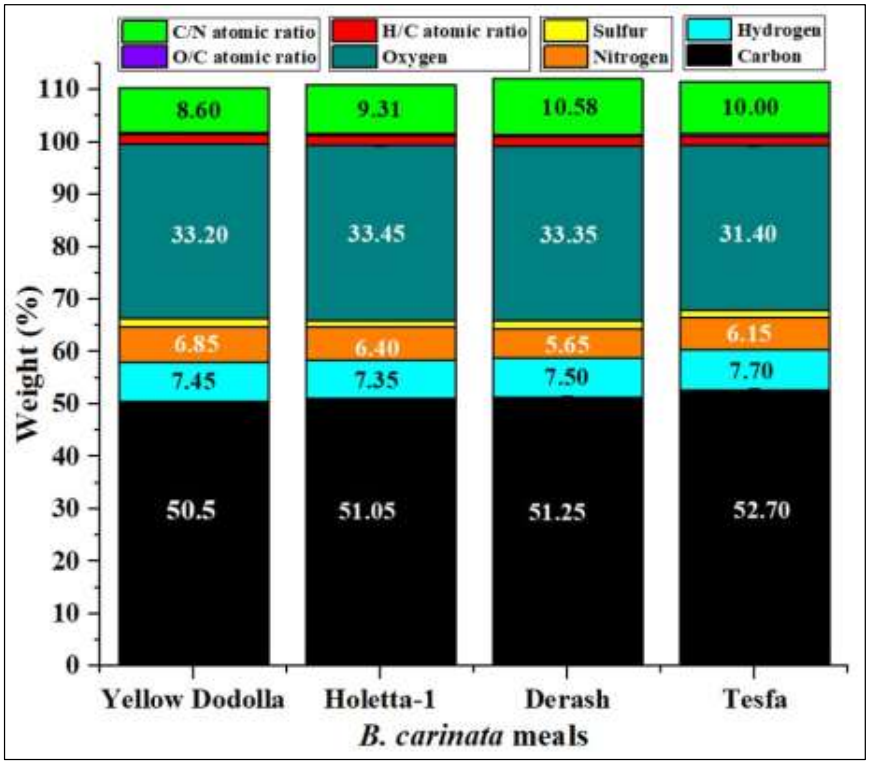

Figure 4.4 The ultimate composition, and atomic ratios of *B. carinata* meals.

Table 4.3 Chemical composition, and atomic ratio of *B. carinata* oilseed meals.

Ultimate composition/ Atomic ratio	**Experimental value (wt. %)**				**Literature value (wt. %)**	
	Yellow Dodolla	**Holetta-1**	**Derash**	**Tesfa**	**Rapeseed**[240]	**Pongamia cakes**[206]
C	50.5 ± 00	51.05 ± 0.21	51.25 ± 0.29	52.7 ± 0.14	52.25	42.97 ± 0.47% − 46.25 ± 0.53%
H	7.45 ± 0.07	7.35 ± 0.07	7.50 ± 0.00	7.70 ± 0.00	8.06	6.45 ± 0.01% − 6.83 ± 0.08%
N	6.85 ± 0.07	6.40 ± 0.00	5.65 ± 0.07	6.15 ± 0.07	3.91	4.98 ± 0.04% − 5.82 ± 0.02%
S	1.55 ± 0.01	1.13 ± 0.00	1.42 ± 0.01	1.38 ± 0.01	-	0.23%–0.32%
O	33.2 ± 0.00	33.45 ± 0.21	33.35 ± 0.07	31.4 ± 0.14	35.78	-
H/C	1.7702	1.7277	1.7561	1.7533	-	-
O/C	0.4931	0.4914	0.4880	0.4469	-	-
C/N	8.60	9.31	10.58	10.00	-	-

4.3.1.3 Estimation of energy densities using H/C and O/C atomic ratios

Apart from the proximate and ultimate analyses of biomass, lignocellulosic biomass differs from one another in terms of compositional formulations, which is a function of fuel efficacy. That is the capacity to generate appropriate energy in the form of heat and electricity [241]. A helpful method for understanding the calorific value of a fuel is the classification of atomic ratios of hydrogen, oxygen, and carbon employing diagrams like the H/C and O/C atomic ratio diagrams [242], [243]. The atomic H/C ratio is commonly used to differentiate between fuels (e.g., coals, biomass) and fuel-related chemicals such as soot [244]. The lower the atomic ratio values (H/C, O/C), the higher the energy content of fuel feedstocks [245]. Typically, biomass, a fuel composed of lignin and cellulose, has an atomic H/C ratio of about 1.5 [246]. Another application of the atomic H/C ratio is to predict potential bond arrangements [246].

The atomic ratios H/C, O/C, and C/N of the BCM samples are indicated in Table 4.3. Despite all samples having nearly comparable H/C atomic ratios, Holetta-1 was found to have a slightly lower H/C atomic ratio. Similarly, the O/C atomic ratios of all samples are virtually identical; Tesfa had a slightly lower O/C ratio, though. As a result, Holetta-1 and Tesfa meals have slightly higher energy densities and, thus, higher heating values than the other meals (Table 4.4). According to biomass's atomic O/C and H/C ratios, the higher concentration of oxygen and hydrogen relative to carbon lowers the energy value because carbon-oxygen and carbon-hydrogen bonds have lower energy contents than carbon-carbon bonds [247]. This means that in comparison to the other meals, Holetta-1 and Tesfa meals appear to contain more C-C bonds than C-H and C-O bonds due to the lower H/C of Holetta-1 and lower O/C of Tesfa, respectively.

Yellow Dodolla, on the other hand, has slightly higher H/C and O/C atomic ratios, which led to a decrease in its energy density and, presumably, its heating values (Table 4.4). The H/C ratio of the meals is also compared to previously reported results. The meals' H/C ratios are somehow greater than the H/C of a carinata meal residue (1.5) [248]. However, the meals' O/C atomic ratios are lower than that of this reported meal (0.73). The meals' H/C atomic ratios were also compared to those of solvent-extracted Pongamia cakes, and it was discovered that they were closely identical to the H/C values of these reported cakes (1.76–1.95) [206]. The H/C atomic ratios of the meals were comparable to those of conventional kerosene-based hydrocarbon fuels, falling within the range of 1.6 to 2.3 [249]

4.3.1.4 Analysis of heating values

It is crucial to ascertain the calorific values and percentages of C, H, N, S, and O in biofuels to assess whether they are suitable as ecologically sound energy sources and produce a specific bio-energy that can be utilized for industrial and residential process heat [250]. Table 4.4 and Figure 4.5 present the meals' HHV and LHV, also known as gross and net calorific values, respectively. The heating values of the meals were found to be very high, with Tesfa having the highest value, followed by Holetta-1 and Yellow Dodolla having the lowest of the samples. This is in perfect harmony with what was discussed in the section above (i.e., energy density) using the H/C and O/C atomic ratios. The HHV of the meals is generally comparable to that of a sub-bituminous type of coal (Wyoming coal) (21.385 MJ/kg), showing that the meals have an identical HHV to coals of this type [251].

Table 4.4 Heating (calorific) values of *B. carinata* oilseed meals.

Heating value (MJ/kg)	Yellow Dodolla	Holetta-1	Derash	Tesfa
Higher heating value	20.15 ± 0.07	23.10 ± 0.14	21.35 ± 0.49	23.75 ± 0.49
Lower heating value	19.65 ± 0.07	21.45 ± 0.07	19.90 ± 0.42	22.10 ± 0.42

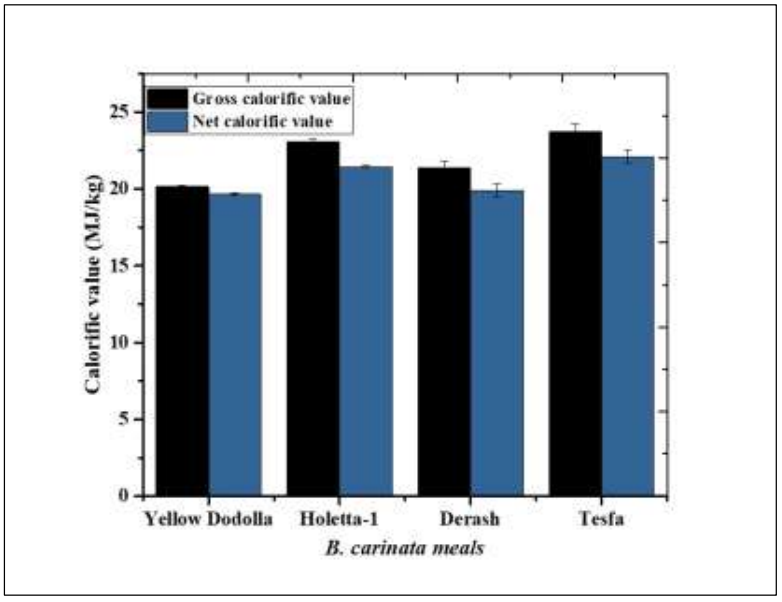

Figure 4.5 Calorific values of *B. carinata* meals.

High ash concentration is one of the factors that have a detrimental impact on biomass energy content [252]. Ash is an inorganic residue that remains after fuel is burned. Because ash indicates the fraction of the biomass that remained unburned, increasing the quantity of ash reduces the calorific value [253]. This is confirmed by the total ash contents of the meals (Table 4.2), which were shown to be relatively lower and had no impact on the calorific values. Comparisons with literature values show that the meals' HHVs are greater than that of Pongamia solvent de-oiled cakes, which range from 17.28 ± 0.12 to 18.38 ± 0.20 MJ/kg [206]. When the HHV of the meals is compared to that of hexane-extracted Jatropha cake (Kako WS (KkWSDCS/Hex), which has an HHV of 20.72 MJ/kg [254], the meals' HHV is found to be relatively greater. However, the HHV of the meals is significantly higher than the HHV (15.11 MJ/kg) of a carinata meal [248].

4.3.1.5 ICP-OES analysis of nutrient profiles

Table 4.5 and Figure 4.6 show the composition of the meals' various macro- and micronutrients. The results showed that the mineral nutrients with the highest concentrations were determined to be the macronutrients magnesium, calcium, phosphorous, and potassium, in increasing order, with potassium having the highest concentration; however, the concentrations of the remaining nutrients are a little lower. The meals' nutrient profiles were compared to those of previously published results. Although the Ca and P concentrations in BCM are slightly higher than the Ca (0.3%), and P (0.3%) concentrations in Soybean meal, the Mg (0.3%), Na (0.01%), and K (2.0%) values of Soybean meal were all nearly identical to those in BCM, with K concentration of the BCM remaining lower [255]. However, the meals' Ca, P, Mg, Na, and K concentrations are lower than those reported for canola, whose concentrations are Ca (0.7%), P (1.2%), Mg (0.6), Na (0.08), and K (1.29%), respectively (Table 4.5).

The micronutrient concentrations (such as iron and zinc) are also compared with those from earlier research. When compared to canola meal, which has Fe (0.0179%) and Zn (0.00621%), the BCMs have slightly higher levels of Fe and Zn, respectively (Table 4.5). Furthermore, the concentrations of each macronutrient in the BCM (i.e., Mg, Ca, P, and Na)—are relatively lower than those of the canola meal, which has Mg (0.58%), Ca (0.89%), P (1.11%), and Na (0.23%), respectively (Table 4.5). Similarly, the concentrations of Ca and P of the BCM were determined to be just relatively smaller than their respective values of *B. napus* "black" Ca (0.67%), P (0.95%), *B. napus* "yellow" Ca (0.55%), P (1.25%), and *B. juncea* "yellow" Ca (0.76%), P (1.04%) (Table 3.5).

Table 4.5 Mineral nutrient composition of *B. carinata* oilseed meals.

Nutrient	Experimental value (wt. %)				Literature value (wt. %)			
	Yellow Dodolla	**Holetta-1**	**Derash**	**Tesfa**	**Soybean**[255]	**Canola**[255]	***B. napus* "black"**[255]	***B. juncea* "yellow"**[255]
K	0.99	0.94	1.01	0.93	2.0	1.29	-	-
Ca	0.42	0.45	0.46	0.43	0.3	0.7, 0.89[256]	0.67	0.55
Mg	0.31	0.39	0.35	0.33	0.3	0.6, 0.58[256]	-	-
Na	0.011	0.009	0.008	0.010	0.01	0.08, 0.23[256]	-	-
P	0.55	0.69	0.68	0.62	0.3	1.2, 1.11 [256]	0.95	1.25
Al	0.008	0.004	0.009	0.004	-	-		
Fe	0.027	0.025	0.026	0.020	-	0.0179	-	-
Zn	0.0074	0.0082	0.0073	0.0075	-	0.00621	-	-

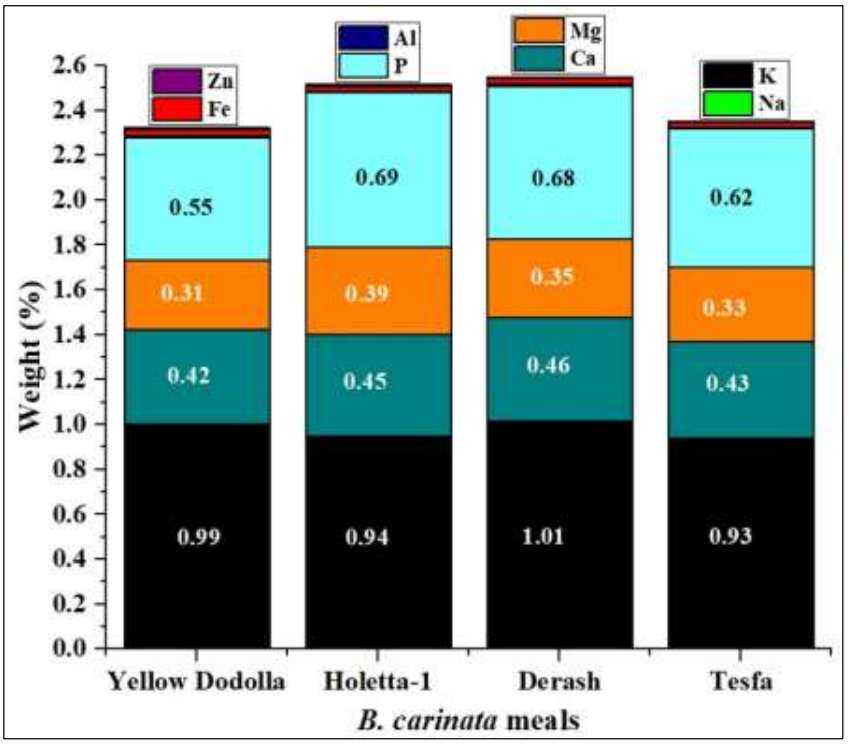

Figure 4.6 ICP-OES analysis of the nutrient profile of *B. carinata* meals.

4.3.2 Valorization of *B. carinata* meals

The side-stream products (i.e., the oilseed meals) of *B. carinata* oil production are the most significant co-products that can be valorized into a variety of industrial products. They may be applied either directly or by adding value to them, which may provide a sustainable option for efficient resource utilization. Since it may develop new market opportunities and use resources more effectively, this novel valorization strategy might be seen as one of the most promising routes to achieving a circular bioeconomy (CBE) [258]. Figure 4.7 depicts the various promising and potential alternative industrial applications of *B. carinata* meals, from which stallholders could benefit from the large-scale deployment of the routes of the biorefinery.

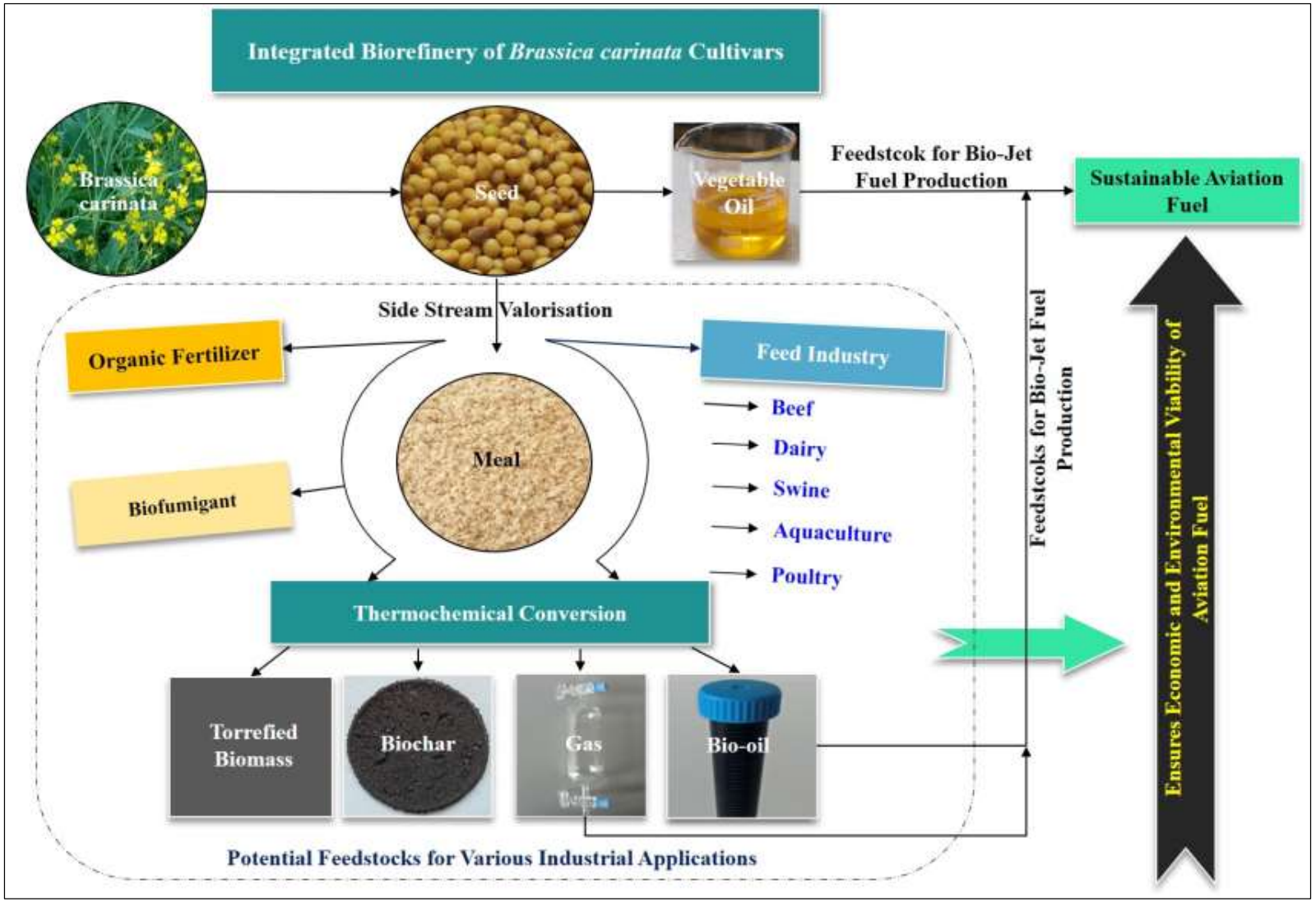

Figure 4.7 Potential industrial applications of *B. carinata* meals.

4.3.2.1 Source of protein supplement for animal nutrition

Solvent-extracted BCM can be used as a protein supplement for poultry, swine, aquaculture, and livestock feed industries due to its higher protein content provided that its glucosinolate level is lowered [171], [237], [259], [260]. Glucosinolates are a wide category of sulfur-containing secondary plant metabolites found in all economically important *Brassica* cultivars. Over 120 distinct glucosinolates have been identified to date [261]. According to [262], glucosinolate levels should be lowered before carinata meal can be utilized as animal feed, either by breeding or through solvent or mechanical extraction.

Based on [263], the total glucosinolate content of meals is affected by the oil extraction process due to different oil extraction conditions. Solvent-extracted meals included more glucosinolates than meals that were dehulled extracted, which in turn contained more than meals that were expeller-extracted. Because glucosinolates like sinigrin harm animal health by making food less palatable and preventing iodine uptake, carinata meal must have less than 2.0% erucic acid and less than 30 μmol of glucosinolates g^{-1} [263].

However, carinata meal pellets that had been extracted using a solvent were used in the study [264]. This meal had 28 μmol glucosinolates g^{-1} and 43.3% crude protein. Feeding the meal had no impact on ruminal pH, NH_3-N concentration, or total volatile fatty acids (VFA) concentration. Comparatively, the US Food and Drug Administration allows feedlot beef cattle to consume up to 100 g glucosinolates kg^{-1} of dietary dry matter, while the European Union limits the number of glucosinolates in feed for monogastric animals to 1.5 μmol glucosinolates g^{-1} obtained from *Camelina sativa* meal [265]. Furthermore, carinata's nutrient content is equivalent to that of other plant-based proteins (soybean, sunflower) and even some animal-based proteins (casein) [266]. It must be emphasized that these proteins (carinata) also offer useful functional properties [267], [268] for a variety of applications (e.g., encapsulation of bioactive substances, and medication delivery) [269].

The present samples' total glucosinolate content may have been significantly lowered as a result of the combined solvent extraction and mixing method used to produce them. As a result, this may make the meals a better source of supplemental protein for the feed industry. In addition, because of their very high crude protein and relatively lower crude fiber contents, the BCM may be,

therefore, a choice of significant interest in the greatly expanding demand for feed in the feed industry.

4.3.2.2 Alternative organic fertilizer and biofumigation

"Organic agriculture is a production system that promotes the health of soils, ecosystems, and people," as defined by the International Federation of Organic Agriculture Movements (IFOAM). It is based on biological processes, biodiversity, and rotations tailored to environmental conditions, instead of employing inputs with negative impacts [270]. The application of synthetic molecules including pesticides and mineral fertilizers is prohibited in this agricultural system [271], [272], and the use of organic amendments is advised for a positive balance of organic matter [273], [274], which is the basis of physical, chemical, and biological soil fertility [275], [276]. Chemical fertilizers that are soluble in water are quickly swept away by runoff and erosion. There is a projected environmental loss of 40–70% N, 80–90% P, and 50–70% K of fertilizers [277].

Although oilseeds derived from plants like the Sunflower (*Helianthus annuus* L.) and other Brassicaceae, like the *Brassica carinata* (A. Braun), are often fed to animals, several studies have proven their usefulness as organic fertilizers [278]. Although higher glucosinolate contents are not advised for animal feeding, according to [279], [280], a seed meal containing high glucosinolate levels (44–168 μmol g^{-1}) can be used as a soil amendment due to its biofumigant properties to reduce pest and disease activity. Brassica cells have a defense mechanism called glucosinolate myrosinase, which can produce a variety of physiologically active substances by enzymatic hydrolysis, including major isothiocyanates and, at lesser quantities, nitriles, and thiocyanates. These substances are recognized for their well-established ability to kill fungi, insects, and wireworms [270].

The green revolution and new farming techniques have greatly increased crop yields, but gradually reduced soil micronutrients including zinc, iron, and molybdenum [277]. Based on our analysis, we found that the meals had very high nitrogen concentrations (about 7%) (Table 4.3), and the meals were also determined to be a good source of magnesium, calcium, phosphorus, potassium, and other soil nutrients shown in Table 4.5. As a result, the hexane-extracted *B. carinata* meals, with their varied compositions and higher nitrogen levels, can be used as promising and alternative organic fertilizers and soil amendments, potentially increasing crop yields while minimizing the disadvantages and costs of chemical fertilizers.

4.3.2.3 Alternative feedstock for thermochemical conversion processes

Currently, biomass is only a cheap fuel when it is a waste product or byproduct of a higher-value activity or product. The higher costs associated with the fuel and its use are only partially offset by the benefits, which may include credits for lower CO_2, SO_x, and heavy metal emissions. Because of technology (lower heating value, flame instability due to the high reactivity and volatile matter content, fouling, slagging, and corrosion phenomena), economic and other issues, direct burning of biomass fuels is troublesome and rarely used [281]. It has been determined that the crop residue of *B. carinata* (straw) offers a potential alternative for energy production (i.e., biofuel or for electricity and heat cogeneration), particularly in rural parts of developing countries that might boost growers' income. Similarly, compared to a wood pellet, the carinata pellet derived from crop residues has been determined to be modestly suitable for energy usage, making it possible to sustain the beneficial outputs of local agro-energy chains [282].

As the *B. carinata* meals employed in the present investigation are easily accessible (i.e., leftovers from an oil extraction facility), and because of their higher calorific values (Table 4.4), they may be utilized for many thermochemical conversion applications. In particular, thermochemical conversion products such as bio-oil, bio-char, torrefied biomass, and syngas of varying economic relevance can be produced. Several pyrolysis products were added to Figure 4.7 to demonstrate that the meals could be converted into a variety of thermochemical conversion products which could then be used to produce other significant industrial products. According to the nutrient profiles of the BCM, a comparison of compositions of some of the nutrients (particularly metals) with those of Soybean, Canola, and B. napus described in the preceding section revealed that the BCM had relatively lower levels. This gives bio-oils (produced from BCM) an advantage since, following [283], during the catalytic upgrading of the oils, the catalysts may become deactivated due to the deposition of alkali metals and the adsorption of inorganic species such as sulfur or nitrogen.

4.4 Conclusions

The current investigation used normal hexane-defatted *Brassica carinata* oilseed meals from indigenous (Ethiopia) cultivars whose characterization properties were determined to be unique. As a result, they were found to be suitable feedstocks for a wide range of economically viable

value-added products or direct applications. The meals contain a significant amount of nitrogen, potassium, and other macro-and micro-plant nutrients, making them promising alternatives compared to the expensive and negatively impacting chemical fertilizers. The oilseed meals can also serve as promising feedstocks for the production of other important intermediate products (such as bio-oil, biochar, syngas, and torrefied biomass) after employing a thermochemical valorization. These intermediate products can, in turn, be transformed into a variety of commercial products (e.g., advanced fuels from bio-oil, and syngas). Moreover, it was found that meals were shown to be a significant option concerning the feed industry's rapidly growing demand for feed. All these side-stream valorization routes can be incorporated into a biorefinery, which ultimately establishes carinata-based circular bioeconomy, with the aviation industry being one of the facilities that may embrace the integrated biorefinery. Thus, the biorefinery might help in sustaining, particularly the economic viability, while maintaining the environmental sustainability of the aviation sector from the potential use of bio-oil and syngas-derived jet fuels as they are. We encourage researchers to continue their work on the study of the concentration of total glucosinolates and erucic acid, issues relating to the digestibility of proteins and fibers, and other anti-nutritional factors of the meals to enhance their appropriateness.

CHAPTER FIVE

Pyrolysis-Based Synthesis and Characterization of Bio-Oil from Brassica carinata Oilseed Meals and Its Application to Produce Bio-Jet Fuel

5.1 Introduction

About 2 billion barrels of petroleum are used annually by the aviation industry, which accounts for a significant portion of greenhouse gas emissions into the atmosphere and contributes significantly to global CO_2 emissions, releasing 669 million tons of CO_2 annually [284]. Furthermore, air travel demand is predicted to grow at a rate of 3−5% for passengers and 10% for freight during the next 30 years, tripling consumption of jet fuel and increasing CO_2 emissions sixfold by 2050. However, in response to such global concerns, high-value bio-based products are getting more attention, particularly in developed nations, and bioenergy is considered vital, given its capacity to mitigate global warming [285]. On the other hand, modern bioenergy's global primary energy consumption grew from 374 Mtoe (million tonnes of oil equivalent) in 2000 to 737 Mtoe in 2018 [286].

Because of its renewable nature and potential as a substitute for fossil fuels, biomass has drawn and continues to draw the interest of researchers and companies looking for sustainable sources of energy [287]. It has emerged as the fourth major energy resource after fossil fuels such as natural gas, oil, and coal, accounting for around 10% of the world's primary energy resources [288]. For this, pyrolysis is a promising technology because of its simple operating procedures and low prices, even though gasification generates well-defined products and requires less [289]. It involves converting biomass at a high temperature into a condensable mixture of oxygenated chemicals, light gases, and char, with the distribution of the end product being governed by process parameters [290]. In the process of pyrolyzing biomass, several steps such as depolymerization, monomer conversion, vaporization, and product conversion from vapors to final products are involved [291].

To produce high-performance products from the pyrolysis of biomass, the process is required to be tuned in terms of temperature, heating rate, process time, and type of biomass [291]. The pyrolysis process can either be catalyzed [292], or not catalyzed process [293]. The product from the pyrolysis process is known as "bio-oil" which is often a dark brown organic liquid that flows and

has a higher calorific content than the original material while being simple to store and transport. It may be used to produce chemicals as well as a potential alternative for fuel oils in several industrial applications such as heating and power generation [294]. Similar to how petroleum-based products are stored, pumped, and delivered, bio-oil can also be burned directly in boilers, gas turbines, and slow and medium-speed diesel engines for heat and power purposes [294].

Bio-oil is a mixture of over 200 different types of major and minor organic compounds, and is a source of some pure chemicals including phenol, organic acids, alcohol, and aldehyde, among others [295]. It typically comprises 50−65 wt.% organic components, including acids, aldehydes, ketones, furans, phenolics, guaiacols, syringols, and sugars; 15−30 wt.% moisture; and 20 wt.% colloidal fraction [296]. These compounds' oxygen content results in detrimental characteristics such as reduced energy density, instability, high viscosity, and corrosion [297]. Low volatility, high viscosity, coking, corrosiveness, and cold flow are major problems when employing bio-oils as fuel; however, these problems can be overcome with appropriate upgrading techniques [294]. It has the potential to be exploited for the production of advanced biofuels notwithstanding its unfavorable qualities (thermal lability, high acidity, low heating value, high water, and oxygen contents) [290].

Because of its properties, the oil cannot be directly processed as a fuel precursor in conventional refineries if it is to be used as fuel [298]. However, it can be upgraded using conventional bio-oil upgrading techniques including physical and chemical methods, such as emulsification, solvent addition, hydrotreatments, steam reforming, catalytic cracking, and supercritical fluid reforming [299]. More specifically, catalytic hydrodeoxygenation (HDO), an alternative method for upgrading the oil, can be used. In the presence of an active catalyst, catalytic HDO consists of a series of reactions involving oxygenated organic molecules that result in less oxygenated compounds [290]. The method, which uses hydrogen in a high-pressure catalytic upgrading process to remove oxygen, is a potential route for improving oil [300].

Nevertheless, one of the major economic factors and one of the biggest hurdles to be overcome in the scaling-up of alternative jet fuel (AJF) production is the availability of feedstocks [18]. For production costs to be reduced and market supply to be increased, lignocellulosic feedstocks must be easily accessible [18]. Presently, the vast majority of AJF is produced by the hydroprocessed esters and fatty acids (HEFA) pathway from used cooking oil, animal fats, and vegetable oils (such

as camelina and canola). Due to their limited availability, only 8% more of these feedstocks are projected to be available by 2020 (from 3.8 to 4.1 million tons/year) [19].

The Brassicaceae family is one of the most economically valuable plant families [301]. *Brassica carinata* (A. Braun) is a species of plant in the Brassicaceae family that originated in the central highlands of Ethiopia between 2200 and 2800 meters above sea level. It is a highly productive, disease- and pest-resistant oilseed crop [166], and due to the inedibility of its vegetable oils, *Brassica carinata* is a valuable bio-industrial crop that can be utilized for producing bio-jet fuels [302]. Because of these significant industrial applications, the earlier study [24] conducted on these vegetable oils (indigenous to Ethiopia) examined their potential as a feedstock for the production of a bio-jet fuel. In addition, even though the oilseed meals that were left over after hexane extraction of these oils were investigated for their diverse valorization options [303], thermochemical conversion via slow pyrolysis has not yet been performed on these meals.

The objective of the present study was to produce bio-oils from these meals using a slow pyrolysis process carried out at a range of temperatures (350, 450, and 550 °C). Product yields (i.e., yields of bio-oil, biochar, and gas) were also determined following the pyrolysis experiments. Furthermore, an in-depth evaluation of the bio-oils' various properties was performed to determine their suitability for use as prospective alternatives to producing advanced fuels. The present study is a continuation of the earlier work on the vegetable oils and oilseed meals (*Brassica carinata*) described above. The findings of the investigation may thus help to ensure that *Brassica carinata* meals (BCM)—streamside products of a bio-jet fuel facility—are potential alternative feedstocks for the aviation industry, thereby minimizing the competition for low-carbon fuel sources in the sector.

5.2 Materials and Methods

5.2.1 Raw materials

The current investigation used finely ground powders (150–355 μm) of hexane-defatted *Brassica carinata* oilseed meals. These meals were the streamside products of the previous study [24]. Since they exhibit remarkable characterization features as reported in [303], the feedstocks (locally known as Yellow Dodolla and Holetta-1) were used in the current study's thermochemical conversion method.

5.2.2 Thermogravimetric (TG)/derivative thermogravimetric (DTG) analysis

Thermogravimetric (TG) and derivative thermogravimetric (DTG) analysis were performed on the meal samples to study their thermal behaviors using a Thermal Gravimetric Analyzer (HCT-1, Bjhenven, China). For the analysis, 10 mg of each sample was utilized. In a nitrogen environment, the working temperature was raised from room temperature (25 ℃) to 1000 ℃ at a constant heating rate of 20 ℃ min^{-1}.

5.2.3 Pyrolysis of *B. carinata* meals

Before pyrolysis, the moisture level of the meals was measured to reduce the negative effects of moisture content on the pyrolysis with an AOAC Official Methods of Analysis [229] (PCE-MA 100, PCE Instruments, Germany) applied. The main parameters that affect the yield and composition of pyrolysis products are particle size, heating rate, pyrolysis temperature, gas flow rate, feed rate, and holding time. These factors influence the various chemical reactions that occur during pyrolysis, leading to different product distributions [304]. A study on polymer pyrolysis determined that temperature is a primary factor influencing the process. It directly controls the cracking reaction of polymer chains, breaking them down into smaller molecules [305]. However, the temperature should not be excessively high to prevent secondary reactions such as thermal cracking, repolymerization, and recondensation of the char residue, which can reduce bio-oil yield. Therefore, rapid removal of vapors from the reaction zone is crucial to minimize secondary reactions [304].

Since the highest oil yield for the pyrolysis of biomass typically occurs between 500 and 550 ℃ for a variety of heating conditions, sizes, and types [306], three different pyrolysis temperatures (350, 450, and 550℃) were utilized in the present study to examine the effect of temperature on bio-oil yield. The temperature of the lab-scale reactor (i.e., pyrolizer) was raised to each of the required temperatures at a rate of 10 ℃/min and then maintained at that temperature for 5 min. The reactor was mounted inside an electrically heated chamber Nabertherm furnace (L5/S, Nabertherm GmbH, Germany), which supplies heat energy to the reactor. In the present study, the terms "oil," "bio-oil," and "pyrolysis oil" were used interchangeably; however, the term "vegetable oil" appears when referring to vegetable oil. The yields of products (i.e., bio-oil, bio-char, and gas) were calculated using the following equations:

$$\text{Bio} - \text{oil yield (wt.\%)} = \frac{\text{Weight of liquid product}}{\text{Weight of sample}} * 100 \quad (5.1)$$

$$\text{Bio} - \text{char yield (wt.\%)} = \frac{\text{Weight of solid product}}{\text{Weight of sample}} * 100 \quad (5.2)$$

$$\text{Gas yield (wt.\%)} = 100 - (\text{Bio} - \text{oil yield, wt.\%} + \text{bio} - \text{char yield, wt.\%}) \quad (5.3)$$

5.2.4 Bio-oil characterization

5.2.4.1 Physicochemical characterization

The total moisture content (%) of a sample was determined using an oven drying method, AOAC 925.10, in an oven (Memmert GmbH + Co.KG, Schwabach, Germany), with about 2.5 g of a sample was used for the analysis. AOAC 960.19 method was used to determine pH using a pH meter (Jenway 3505, Fisher Scientific, UK). The refractive index (RI) of samples was measured at 20℃ based on AOAC 921.08 in a refractometer (RFM960, Bellingham Stanley). The total ash content of samples was determined using AOAC 923.03 in an electrically heated chamber Nabertherm furnace (L5/C6, Nabertherm GmbH, Germany), with approximately 5 g of sample utilized for analysis. The pycnometer method, as specified in the AOAC 920.212 method, was used to determine density and specific gravity at 20℃. A standard volumetric pycnometer with a volume of 5 cm^3 was utilized for the analysis. At 40°C, the kinematic viscosity of bio-oil is commonly evaluated to determine its fluidity characteristics. As a result, the kinematic viscosity of the bio-oils was measured at 40°C following the ASTM D445 standard method using a Pro rotational viscometer (DV II, AMETEK Brookfield, Germany).

5.2.4.2 Chemical composition analysis and determination of atomic ratios

CHNS determination was performed using DIN EN ISO 16948:2015-09 in a CHNS analyzer (Vario MACRO cube, Elementar, Langenselbold, Germany) in the German Biomass Research Centre (DBFZ), Leipzig, Germany. The oxygen content was found by difference [i.e., 100 − (C + H + N + S + ash content)] based on DIN 51,733 (2016–04). Approximately, 1.5 g of a sample was used for analysis. Equations 5.4−5.6 were used to calculate the atomic ratios.

$$\frac{\text{H}}{\text{C}} = \frac{\%\text{Hydrogen}/\text{Atomic weight of hydrogen}}{\%\text{Carbon}/\text{Atomic weight of carbon}} \quad (5.4)$$

$$\frac{O}{C} = \frac{\%\text{Oxygen}/\text{Atomic weight of oxygen}}{\%\text{Carbon}/\text{Atomic weight of carbon}} \quad (5.5)$$

$$\frac{C}{N} = \frac{\%\text{Carbon}/\text{Atomic weight of carbon}}{\%\text{Nitrogen}/\text{Atomic weight of nitrogen}} \quad (5.6)$$

5.2.4.3 Analysis of heating values

Following the unified equation for solid, liquid, and gaseous fuels developed by [307], the higher heating value (HHV) of the oils was calculated using equation 5.7.

$$\text{HHV (MJ/kg)} = 0.3491 * C + 1.1783 * H + 0.1005 * S - 0.1034 * O - 0.0151 * N - 0.0211 * AC \quad (5.7)$$

where C-carbon, H-hydrogen, S-sulphur, O-oxygen, N-nitrogen, and AC-ash content.

5.2.4.4 Inductively coupled plasma optical emission spectroscopy measurements

Metals such as sodium (Na), potassium (K), calcium (Ca), magnesium (Mg), aluminum (Al), iron (Fe), nickel (Ni), lead (Pb), zinc (Zn), and non-metallic element phosphorous (P), were analyzed using inductively coupled plasma optical emission spectroscopy (ICP-OES) CID Spectrometer (iCAP 6300, Thermo Scientific, Waltham, USA) at the German Biomass Research Centre (DBFZ), Leipzig, Germany following the DIN EN 16170 method. However, nitric acid digestion applying DIN EN 13,657 (2003-01) was performed before ICP-OES measurements.

5.2.4.5 Gas chromatography-mass spectroscopy characterization

The various components, both qualitative and quantitative, were identified using the AOAC 996.06 official method of analysis [178] in a GC-MS (7820A GC) equipped with a mass selective detector (HP 5977) and a DB-5MS capillary column (60 m, 0.25 mm ID, 1.4 m thickness), in the Instrument Laboratory, Department of Chemistry, Addis Ababa University (AAU), Addis Ababa, Ethiopia. With a constant flow rate of 1 mL/min and a 1 L injection volume, helium was used as the carrier gas. Temperatures for the injector and detector were 250°C and 280°C, respectively. The mass scan

range was set to 29-800 amu and the oven temperature was set to 50℃ (isothermal for 4 min), 280℃ at 30℃/min for 10 min, and isothermal at 280℃. 0.5 g of a sample was used for the analysis.

5.2.4.6 Fourier transform infrared spectroscopy characterization

In a Fourier Transform Infrared Spectroscopy (FT-IR) spectrometer (Spectrum 100, PerkinElmer, UK), the attenuated total reflectance (ATR) sample method was used to perform the qualitative analysis of functional groups by ASTM E1252-98(2021). For instrument monitoring and data input, 6.1.1.0045 version Spectrum software was used. A deuterated triglycine sulfate (DTGS) detector was installed in the FT-IR, which scanned at a resolution of 2 cm^{-1} spanning the frequency range of 4000 to 550 cm^{-1}. The surface of a diamond, a crystal with a high refractive index, was treated with a drop of the sample. The analysis was performed at the Organic Chemistry Laboratory, Pharmaceutical, and Chemical Engineering Department, Berlin University of Technology (BHT), Berlin, Germany.

5.2.5 Characterization of gaseous products

Offline gas analysis was performed using micro-gas chromatography coupled with a thermo-conductivity detector (GC-TCD) (5 HayeSep A), which was set at 30−165℃ and 1.4 mbar to qualitatively and quantitatively analyze the gas mixture. Due to several calibration constraints, such as the lack of calibration gases for all pyrolysis gases that may be present in the gas mixture, the calibration was limited to H_2, CO_2, and CH_4 gases and moisture content (H_2O) where argon was used as a carrier gas. The analysis was performed at the Organic Chemistry Laboratory, Department II, Berlin University of Technology (BHT).

5.3 Results and Discussion

5.3.1 Thermogravimetric and derivative thermogravimetric analysis

Any lignocellulosic biomass's ability to thermally decompose depends entirely on the nature and composition of its structural components such as cellulose, hemicellulose, and lignin. Even though there are no clearly defined zones for moisture release, devolatilization, and char degradation, the TG/DTG profiles demonstrate the typical degradation profile of the meal samples. As a result, the samples underwent three primary stages of thermal degradation based on the TGA of the pyrolysis

characteristics. The first step, which eliminated moisture, very light volatile components, and structural rearrangements, causing only minor changes in mass, took place between room temperature and 200℃. A significant portion of the volatile components, roughly 94%, was eliminated during the second and third steps, primarily during the second step, which occurred between 200℃ and 490℃ and between 500℃ and 840℃, respectively. In general, each of the samples lost about 89% of its volatile components throughout the entire thermal degradation process, leaving about 11% of char behind. This is consistent with the recent investigation on the meals [303], which showed that 81.58−83.68% of a volatile component was produced at 950 ℃ in 7 minutes. It was, therefore, quite reasonable to base the pyrolysis temperatures (next section) on the temperature intervals of the second and third stages as the majority of the volatile components were released at these temperature intervals which may ultimately produce very high yields of bio-oil.

5.3.2 Pyrolysis of *B. carinata* meals

According to the prior study [308], when biomass is heated, different chemical bonds within the polymers are broken, resulting in the release of volatile compounds and rearrangement reactions within the matrix of the residue. These reactions have been referred to as primary mechanisms. After being produced, some volatile compounds are unstable and can then go through subsequent changes known as secondary reactions. This could be used to explain the various chemical reactions that occurred during the pyrolysis of the meals.

The moisture level of the meals, Yellow Dodolla and Holetta-1 was found to be 5.5% and 6.2%, respectively. Table 5.1 and Figure 5.1 depict the various product yields at the different pyrolysis temperatures, with the oil yield being the highest at the highest temperature (550 ℃) while the char and gas yields were the lowest at the highest temperature but highest at the lowest (350 ℃). The increase in oil yields as the temperature rises is well-congruent with the results of the prior study outlined below. The extent of biomass breakdown, product distribution, and calorific values are all directly influenced by temperature, making it one of the most crucial variables. Several studies have been reported investigating the impact of temperature on the final bio-oil output, demonstrating that higher yields require temperatures between 450 and 550 ℃ [309].

Table 5.1 Pyrolysis product yields of *B. carinata* meals at various temperatures.

Sample	Product Yield (wt. %)		
	350 ℃	**450 ℃**	**550 ℃**
Yellow Dodolla			
Oil	22.81 ± 0.70	48.16 ± 0.22	55.01 ± 1.71
Char	31.36 ± 0.64	23.82 ± 0.29	23.02 ± 2.01
Gas	45.84 ± 1.34	28.03 ± 0.07	21.98 ± 0.41
Holetta-1			
Oil	29.83 ± 0.89	47.08 ± 2.47	49.73 ± 1.34
Char	34.93 ± 0.41	27.44± 0.19	25.54 ± 0.03
Gas	33.72 ± 1.98	25.48 ± 2.66	24.73 ± 1.31

The gas yield of Yellow Dodolla, which is displayed in blue (Figure 5.1), was initially quite high (i.e., 45.84%) compared to the other yields, and it gradually decreased and became the lowest at the highest temperature whereas the oil yield of this sample shown in black (Figure 5.1) was the smallest at the smallest temperature. However, this yield gradually increased and became the highest at the highest temperature. In general, *B. carinata* meals, especially the Yellow Dodolla have the potential to provide very high yields of high-value bio-oil and gas products.

The discrepancy between the high bio-oil yield and the expected low char yield in the current slow pyrolysis can be attributed to several factors a few of which can be discussed as follows: The composition of the feedstock can play a crucial role. If the feedstock contains a high proportion of volatile components, it's more likely to produce a higher amount of bio-oil. While slow pyrolysis is generally conducted at lower temperatures, a slightly higher temperature within the optimal range could have favoured bio-oil formation.

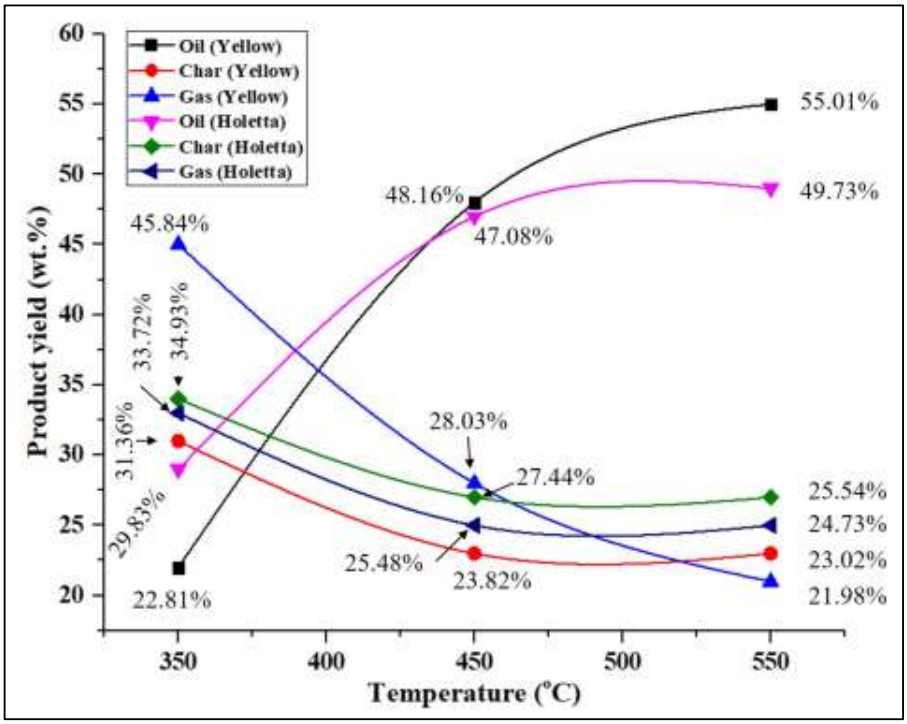

Figure 5.1 Effects of temperature (°C) on pyrolysis product yields (wt.%) of *B. carinata* meals. Yellow stands for Yellow Dodolla whereas Holetta stands for Holetta-1.

5.3.3 Bio-oil characterization

5.3.3.1 Physicochemical characterization

Table 5.2 shows the physicochemical properties of the bio-oils. The moisture content of the oils varied from 35.38 ± 1.37 to 48.64 ± 0.20 (in wt.%) derived from Yellow Dodolla and Holetta-1, respectively. When the oils' moisture content was compared to previous results, including Raw bio-oil [310] (Table 5.2), Yellow Dodolla was determined to have a significantly lower moisture content, while Holetta-1's was found to be nearly identical. According to [311], a wide range of processes, including dehydration, heterogeneous, and aromatization reactions, can produce water during the biomass pyrolysis process. Taking all of these potential reactions into account, higher oxygen concentrations may be influenced by increasing the overall moisture content of bio-oils because increased moisture content has its own set of negative impacts.

Although some earlier works such as [310] indicated that the pH of a bio-oil produced from Rice husk ash waste biomass was acidic (i.e., 3), the oils were shown to have a weak basic pH value.

The pH values of the oils, however, do not differ considerably from those reported for cow hoof pyrolysis oil (6.75) [312]. The viscosities of the oils are greater than 1.40 cSt of waste raw bio-oil [310] (Table 5.2). Yellow Dodolla has a lower density than a waste Raw bio-oil (1030 kg/m^3) [310], although Holetta-1 has a density that is rather close to this reported value. The ash contents of the oils (Table 5.2) were found to be almost within the reported ash content (0−0.2%) [294]. The lower ash content of the oils may be an indication of the lower metals' concentration discussed in the later sections.

The physicochemical properties of the oils were also compared to an upgraded bio-oil (i.e., bio-jet fuel) [150] (Table 5.2) that is produced via two-step hydroprocessing, comprising of hydrodeoxygenation and hydrocracking processes, to examine how comparable the oils are to such fuels. The oils were compared to this kind of aviation fuel because they could also be upgraded through this approach. As a result, according to the comparison made (Table 5.2), variations in the properties of the oils and the reported hydroprocessed oil are to be expected because the hydroprocessed oil has been subjected to severe hydrogen pressure and other hydroprocessing conditions. The oils' density and viscosity values, for example, are higher than those of the upgraded fuel since hydrotreating and hydrocracking reactions significantly reduce these properties.

Table 5.2 Physicochemical properties of *B. carinata* bio-oils.

Property	**Experimental Value (%)**		**Literature Value (%)**	
	Yellow Dodolla	**Holetta-1**	**Raw Bio-oil**[310]	**Hydroprocessed**[150]
Moisture content (%)	35.38 ± 1.37	48.64 ± 0.20	52.3	0
pH	8.50 ± 0.28	8.50 ± 0.14	3, 6.75[312]	-
Refractive index @ 20 °C	1.41 ± 0.00	1.40 ± 0.00	-	-
Kinematic viscosity (cSt) @ 40 °C	14.10 ± 0.13	16.05 ± 0.16	1.40	1.6
Density (kg/m3) @ 20 °C	993 ± 0.00	1024 ± 0.00	1030	840
Total ash content (%)	0.170 ± 0.00	0.208 ± 0.01	0–0.2[294]	< 0.001

Raw Bio-oil: Represents a bio-oil obtained from Rice husk ash.

5.3.3.2 Chemical composition analysis, and determination of atomic ratios

Table 5.3 shows the chemical composition of the bio-oil samples. These concentrations are also shown in Figure 5.2 to compare the concentrations of each of the chemical contents. These results indicated that pyrolysis raised the carbon content, slightly improved hydrogen content, lowered sulfur and oxygen contents, and virtually unchanged nitrogen content, relative to their values in the meals [303]. This is substantiated by a prior study [313], which proved that higher pyrolysis temperatures enhance the reduction of oxygen content while increasing carbon and hydrogen. In addition, previous studies proved that [314], thermal treatment of lignocellulosic biomass leads to the formation of H_2-rich gas. The concentration of C and H were compared to previous results in which their contents were determined to be considerably higher than those of the wood pyrolysis bio-oil, which had values of C (54−58%), H (5.5−7.0%), respectively, [294].

Table 5.3 Chemical composition and atomic ratios of *B. carinata* bio-oils.

Property	**Experimental Value (%)**		**Literature Value (%)**	
	Yellow Dodolla	**Holetta-1**	**Wood Pyrolysis Bio-Oil**[294]	**Hydroprocessed**[150]
C	62.3	55.4	54−58	88.0
H	9.29	9.02	5.5−7.0	11.5
N	6.08	6.2	8.9 ± 0.4[315]	0.5
S	0.69	0.61	0.70[316]	< 0.10
AC	0.170 ± 0.00	0.208 ± 0.01	-	< 0.001
O	21.47	28.56	35–40	0
H/C	1.79	1.95	1.37[317]	1.56
O/C	0.26	0.39	0.78[317]	< 0.001
C/N	11.95	10.42	-	-

C−carbon. H−hydrogen. N−nitrogen. S−sulfur. AC−ash content. O−oxygen. Hydroprocessed−Upgraded sewage sludge thermo-catalytic reforming (TCR) crude oil.

Furthermore, the enrichment of hydrogen in pyrolysis oil derived from oilseed meals can be better explained and is primarily due to the deoxygenation process that occurs during pyrolysis. Oilseed meals are naturally rich in oxygen-containing functional groups, such as carboxylic acids, esters, and alcohols. These oxygen-containing compounds contribute to the oxygen content of the original biomass. During pyrolysis, these oxygen-containing functional groups undergo deoxygenation

reactions. This involves the removal of oxygen atoms from the molecular structure, often in the form of water or carbon monoxide. As a result, as oxygen is removed, the remaining carbon atoms form new bonds with hydrogen atoms, leading to an increase in the hydrogen-to-carbon ratio of the pyrolysis oil. This increase in hydrogen content is a characteristic feature of pyrolysis oils derived from biomass.

The oils' oxygen levels (Table 5.3) were found to be significantly lower than that of the reported value of a wood pyrolysis oil having an oxygen content of 35–40% [294]. For nitrogen concentrations, comparisons with earlier studies were done. As a result, the oils` nitrogen contents are lower than those reported for bio-oils derived from de-oiled canola meal, which is 8.9 ± 0.4 (pyrolyzed at 500 °C) [315]. Furthermore, the sulfur level of the oils is comparable to that of a previously reported grain husk bio-oil produced through fast pyrolysis [316] (Table 5.3).

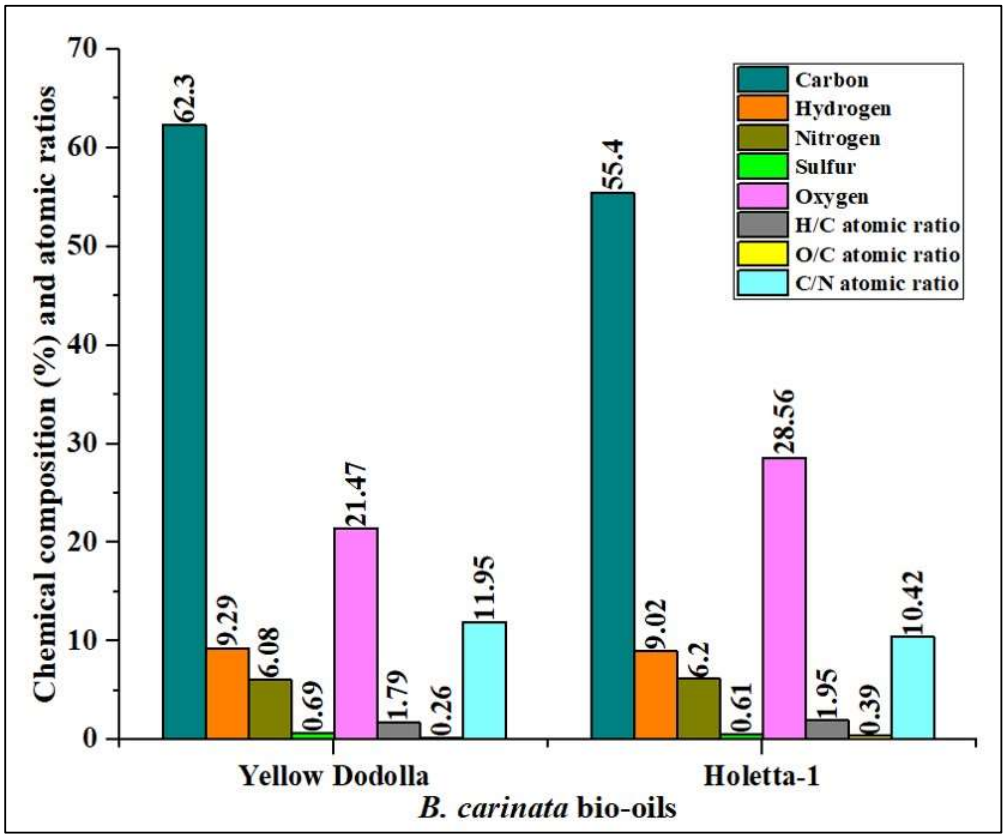

Figure 5.2 Chemical composition and atomic ratios of Brassica carinata bio-oils.

Due to the high level of hazardous substances and materials such as S-compounds, metals, N-compounds, high content of oxygenated compounds, and unique features of bio-oil as compared to fuel oil, upgrading of bio-oil produced through the pyrolysis process is essential [318]. Upgrading the oils is required since similar issues, such as nitrogenated and oxygenated compounds, are observed in the present oils (Table 5.3). As a result, upgrading processes such as hydrodenitrogenation (HDN) for nitrogen removal and hydrodeoxygenation (HDO) for oxygen removal are required. The removal of oxygen includes the breaking of many bonds and advances through a variety of deoxygenation reactions, including hydrogenolysis of C─O bonds and hydrogenation reactions. On the other hand, significant coke formation and reactor obstruction are the major challenges in bio-oil hydroprocessing, whereby a diverse spectrum of bio-oil species generate coke in the aqueous phase [319].

Comparisons of the oils to an earlier study on hydroprocessed oil [150] (Table 5.3) revealed that there are variations between the chemical composition of the oils and the reported results. Even though the C and H values of the oils appear to be lower when compared to the hydroprocessed oil (Table 5.3), following upgrading, their values may be considerably improved. The O and N concentration of the oils is substantially higher than that of the hydroprocessed oil (Table 5.3), and this higher concentration of O and N has to be removed through hydrotreatment. Thus, it was discovered that the H/C atomic ratio of the oils was bigger than that of the hardwood pyrolysis oil and hydroprocessed oil. The oils' O/C atomic ratios, on the other hand, were found to be significantly higher than that of the hydroprocessed oil (Table 5.3), indicating that the oils have lower energy densities than the upgraded oil; yet, their H/C atomic ratios were observed to be practically identical. However, when compared to a bio-oil derived from red algal biomass oil, the H/C of the oils appeared to be only slightly greater, while the O/C atomic ratio was found to be a little lower [317].

5.3.3.3 Estimation of energy densities using atomic ratios

The atomic ratios (H/C and O/C) shown in Table 5.3 and Figure 5.2 can be used to evaluate the energy densities of the bio-oils, with [245] stating that the higher the energy content of fuel sources, the lower the atomic ratio values. The greater the percentage of oxygen and hydrogen compared to carbon in biomass, the lower the energy value, because C─O and C─H bonds have reduced energy contents than C─C bonds [247]. The O/C atomic ratio of the bio-oils (Table 5.3) is less than the

corresponding value of their feedstocks, whose reported values are 0.4931 for Yellow Dodolla and 0.4914 for Holetta-1 [303]. This could also be attributed to the bio-oils' increased carbon and decreased oxygen contents when compared to their values in the feedstock [303]. The results (Table 5.3), show that Yellow Dodolla oil has lower O/C and H/C atomic ratios than Holetta-1. The fact that Yellow Dodolla has a greater calorific value (discussed below) than Holetta-1 could be due to these lower atomic ratios. This demonstrates that the greater calorific values correspond to the lower O/C and H/C values, which ultimately confirms that Yellow Dodolla oil has more C─C and less C─O and C─H bonds than Holetta-1.

5.3.3.4 Analysis of heating values

The HHV of the oils, Yellow Dodolla and Holetta-1 were found to be 30.449 and 26.979 MJ/kg, respectively. According to [320], when a bio-oil is compared to its feedstock, it has a higher calorific value, and when burned, it may produce less greenhouse gas than fossil fuels. This is consistent with the results that the HHV of the bio-oils is higher than that of their corresponding feedstock meals, which had MJ/kg values of 20.15 ± 0.07 and 23.10 ± 0.14 for Yellow Dodolla and Holetta-1, respectively, [303]. This is particularly noticeable in Yellow Dodolla bio-oil, which has an HHV that is 10 MJ/kg greater than that of its meal. The HHV of the bio-oils is also compared to results from earlier studies, such as Wood pyrolysis bio-oil [294], and based on these comparisons, the experimental bio-oils possess greater calorific values than these reported values.

5.3.3.5 Inductively coupled plasma optical emission spectroscopy measurements

The elements K, Ca, Mg, Al, Ni, Pb, and P were not detected in both bio-oils; however, Holetta-1 had Na with a concentration of 18.9 mg/kg, whereas Yellow Dodolla did not. This could indicate that the elements are completely absent from the oils or that their concentration is too low to be detected. This might additionally suggest that they were retained in the biochar during the pyrolysis process. Both oils contained Fe, with concentrations of 694 mg/kg for Yellow Dodolla and 1080 mg/kg for Holetta-1. Furthermore, the oils contain Zn at a concentration of 2.81 mg/kg from Yellow Dodolla, and 2.5 mg/kg from Holetta-1. As stated in [321], one of the primary concerns with catalysts during hydrodeoxygenation of bio-oils is their stability, which is influenced by the presence of alkali metals, sulfur, chlorine, phosphorus, and other contaminants, and the tendency

to develop coke. One of the biggest advantages of the current bio-oils is, then, the absence (i.e., extremely low concentration) of metal and non-metal impurities.

5.3.3.6 Gas chromatography-mass spectroscopy characterization

Tables 5.4, and 5.5, illustrate the GC-MS results of the bio-oils. The results showed that the oils contained a diversity of complex mixtures of organic compounds, some of which may be of significant industrial importance. Following the GC-MS analysis, the Yellow Dodolla and Holetta-1 bio-oils, however, were found to have 40 and 42 compounds, respectively. The area peaks of the compositions of these compounds are shown in Figures 5.3 and 5.4. In the majority of the peaks, as shown in Figure 5.3, Yellow Dodolla's peaks are bigger, and as a result, the concentrations of the subsequent constituents of this oil are greater; however, Holetta-1's peaks were clearly shown to be smaller than those of Yellow Dodolla. Figure 5.4 clearly illustrates the variations in concentrations of each of the compounds of the oils.

It was a bit challenging to determine the concentrations of each component in its respective chromatogram. The primary cause of the chromatograms' overlap could have been because these components were eluted concurrently. In light of this, only the major components were assigned as shown in Figure 5.4. Although the peaks of several of the components appeared to have merged for a while and coeluted because of their extremely close elution times, the peaks stood out clearly and indicated that they eluted separately. As a result, most of the components, especially, the main components were presented in the chromatograms.

The last component eluted after 22.8365 minutes retention time in Yellow Dodolla was erucic acid, methyl ester (13-Docosenoic acid, methyl ester, (Z)-), whereas the last component eluted after 24.1009 minutes in Holetta-1 was oleic acid amide (9-Octadecenamide, (Z)-). The least carbon length in the previous work [24] on the non-edible vegetable *B. carinata* oils was 17 (C16:0, palmitic, a fatty acid), while the highest was 23 (C22:1, erucic acid, a fatty acid). However, the smallest carbon length in the bio-oils of the same species and the same cultivars is 8 (an aromatic) and 14 (an unsaturated aliphatic compound), and the largest was 23 (C22:1, erucic acid, a fatty acid).

Table 5.4 GC-MS results of Yellow Dodolla bio-oil.

Peak No.	Retention Time (min)	Systematic Name	Cas Number	Molecular Formula	Saturation/ Unsaturation	Common/ Another Name	Area %	Qual
1	6.6437	1-Tetradecene	001120-36-1	$C_{14}H_{28}$	Mono	Tetradecene	1.5841	96
2	7.5037	Pentadecane	000629-62-9	$C_{15}H_{32}$	Saturated	n-Pentadecane	3.1375	96
3	7.9766	Indole	000120-72-9	C_8H_7N	-	2,3-Benzopyrrole	1.6718	97
4	8.268	3-Hexadecene, (Z)-	034303-81-6	$C_{16}H_{32}$	Mono	(Z)-3-Hexadecene	0.9662	98
5	8.3186	Hexadecane	000544-76-3	$C_{16}H_{34}$	Saturated	Cetane	1.7805	96
6	8.6197	1H-Indole, 4-methyl-	016096-32-5	C_9H_9N	-	Indole, 4-methyl-	0.8511	95
7	8.7306	Undecanenitrile	002244-07-7	$C_{11}H_{21}N$	-	Decyl Cyanide	0.467	93
8	9.0495	8-Heptadecene	002579-04-6	$C_{17}H_{34}$	Mono	Heptadecen-(8)	4.8984	99
9	9.1165	Heptadecane	000629-78-7	$C_{17}H_{36}$	Saturated	N-heptadecane	2.7456	96
10	9.6031	1H-Indole, 1,2-dimethyl-	000875-79-6	$C_{10}H_{11}N$	-	Dimethylindole	0.7201	80
11	9.6887	4-methyl phenylacetic acid, 2,2,2-trifluoroethyl ester	1000376-55-2	$C_{36}H_{42}N_4O_{12}S$	-	-	0.544	46
12	9.7643	2-Methylbenzylamine, N,N-diheptyl-	1000310-39-9	-	-	-	0.951	47
13	9.9094	9-Octadecene, (E)-	007206-25-9	$C_{18}H_{36}$	Mono	(E)-9-Octadecene	2.6525	99
14	9.9936	Octadecane	000593-45-3	$C_{18}H_{38}$	Saturated	Octadecane	0.8574	98
15	10.0376	1-Octadecene	000112-88-9	$C_{18}H_{36}$	Mono	1-Octadecene	0.5301	96
16	10.8981	9-Nonadecene	031035-07-1	$C_{19}H_{38}$	Mono	9-Nonadecene	4.7344	99
17	11.004	Nonadecane	000629-92-5	$C_{19}H_{40}$	Saturated	Nonadecane	1.5727	96
18	11.059	E-14-Hexadecenal	330207-53-9	$C_{16}H_{30}O$	Poly	E-14-Hexadecenal	0.5406	95
19	12.0507	9-Eicosene, (E)-	074685-29-3	$C_{20}H_{40}$	Mono	9-eicosene	3.5283	99
20	12.1188	1,9-Tetradecadiene	112929-06-3	$C_{14}H_{26}$	Poly	(9Z)-1,9-Tetradecadiene	0.9548	96
21	12.1835	Eicosane	000112-95-8	$C_{20}H_{42}$	Saturated	Eicosane	1.2435	98
22	12.2273	Hexadecanoic acid, methyl ester	000112-39-0	$C_{17}H_{34}O_2$	Saturated	Palmitic acid	1.5854	97
23	13.0588	10-Heneicosene (c,t)	095008-11-0	$C_{21}H_{42}$	Mono	10-Heneicosene	0.7567	99
24	13.1432	Hexadecanenitrile	000629-79-8	$C_{16}H_{31}N$	-	Palmitic acid, nitrile	3.2311	99
25	13.3508	Henicos-1-ene	001599-68-4	$C_{21}H_{42}$	Mono	1-Heneicosene	5.4638	99
26	13.4024	Henicos-1-ene	001599-68-4	$C_{21}H_{42}$	Mono	1-Heneicosene	9.5093	95
27	13.5555	Heneicosane	000629-94-7	$C_{21}H_{44}$	Saturated	Henicosane	2.5125	99
28	14.9845	11-Octadecenoic acid, methyl ester	052380-33-3	$C_{19}H_{36}O_2$	Mono	Vaccenic acid	2.8751	97
29	15.0757	9,12-Octadecadienoic acid (Z,Z)-	000060-33-3	$C_{18}H_{32}O_2$	Poly	Linoleic acid	0.8701	97
30	15.2228	Methyl stearate	000112-61-8	$C_{19}H_{38}O_2$	Saturated	Methyl stearate	0.7458	95
31	16.3027	Oleanitrile	1000308-88-1	$C_{18}H_{33}N$	Poly	-	11.3841	99
32	16.497	Heptadecanenitrile	005399-02-0	$C_{17}H_{33}N$	-	Heptadecanenitrile	2.8723	99
33	16.868	Heneicosane	000629-94-7	$C_{21}H_{44}$	Saturated	Henicosane	0.6706	95
34	18.006	Benz[f]azulene, 1,2,3,3a,4,9,10,10a-octahydro-	054798-84-4	$C_{14}H_{18}$	-	-	0.7063	37
35	18.251	Benzamide, N-[(2-hydroxyphenyl)thioxomethyl]-	1000261-60-9	-	-	-	1.6867	43
36	19.2353	2-Phenylbutyryl chloride	036854-57-6	$C_{10}H_{11}ClO$	-	-	0.7642	45
37	20.2845	Oleanitrile	1000308-88-1	$C_{18}H_{33}N$	Poly	-	10.2484	45
38	20.3944	Oleanitrile	1000308-88-1	$C_{18}H_{33}N$	Poly	-	1.3904	95
39	20.5206	Heptadecanenitrile	005399-02-0	$C_{17}H_{33}N$	Poly	Heptadecanenitrile	2.1292	99
40	22.8365	13-Docosenoic acid, methyl ester, (Z)-	001120-34-9	$C_{23}H_{44}O_2$	Mono	Erucic acid	3.6664	97

Table 5.5 GC-MS results of Holetta-1 bio-oil.

Peak No.	Retention Time (min)	Systematic Name	Cas Number	Molecular Formula	Saturation/ Unsaturation	Common/ Another Name	Area %	Qual
1	6.6519	1-Tetradecene	001120-36-1	$C_{14}H_{28}$	Mono	Tetradecene	2.1778	96
2	7.5122	Pentadecane	000629-62-9	$C_{15}H_{32}$	Saturated	n-Pentadecane	3.6003	93
3	7.9814	Indole	000120-72-9	C_8H_7N	-	2,3-Benzopyrrole	2.3318	93
4	8.2722	3-Hexadecene, (Z)-	034303-81-6	$C_{16}H_{32}$	Mono	(Z)-3-Hexadecene	1.2583	99
5	8.3244	Hexadecane	000544-76-3	$C_{16}H_{34}$	Saturated	Cetane	2.2793	95
6	8.6225	1H-Indole, 7-methyl-	000933-67-5	C_9H_9N	-	7-Methylindol	1.8323	95
7	8.7337	Undecanenitrile	002244-07-7	$C_{11}H_{21}N$	-	Decyl Cyanide	0.7669	92
8	9.0541	8-Heptadecene	002579-04-6	$C_{17}H_{34}$	Mono	Heptadecen-(8)	4.4039	98
9	9.1216	Heptadecane	000629-78-7	$C_{17}H_{36}$	Saturated	N-heptadecane	1.9852	97
10	9.1578	8-Heptadecene	002579-04-6	$C_{17}H_{34}$	Mono	Heptadecen-(8)	0.8505	97
11	9.6074	Indolizine, 2,5-dimethyl-	000769-83-5	-	-	-	1.0535	60
12	9.6939	4-methyl phenylacetic acid, 2,2,2-trifluoromethyl ester	1000376-55-2	-	-	-	0.6538	46
13	9.7695	4-methyl phenylacetic acid, 2,2,2-trifluoromethyl ester	1000376-55-2	-	-	-	1.1673	49
14	9.9153	9-Octadecene, (E)-	007206-25-9	$C_{18}H_{36}$	Mono	(E)-9-Octadecene	2.965	99
15	10.0001	Octadecane	000593-45-3	$C_{18}H_{38}$	Saturated	Octadecane	1.0605	98
16	10.0443	Cetene	000629-73-2	$C_{16}H_{32}$	Mono	1-Hexadecene	0.7256	96
17	10.6132	Tetradecanenitrile	000629-63-0	$C_{14}H_{27}N$	Poly	myristonitriles	0.4191	94
18	10.9064	Z-5-Nonadecene	1000131-11-8	$C_{19}H_{38}$	Mono	Z-5-Nonadecene	3.8441	99
19	11.0116	Nonadecane	000629-92-5	$C_{19}H_{40}$	Saturated	Nonadecane	1.4121	95
20	11.0648	E-14-Hexadecenal	330207-53-9	$C_{16}H_{30}O$	Mono	14-Hexadecenal, (E)-	0.5314	97
21	12.0619	9-Eicosene, (E)-	074685-29-3	$C_{20}H_{40}$	Mono	9-eicosene	3.175	99
22	12.1282	11-Hexadecen-1-ol, acetate, (Z)-	034010-21-4	$C_{18}H_{34}O_2$	Mono	(11Z)-11-Hexadecen-1-ol 1-Acetate	0.8527	99
23	12.1943	Eicosane	000112-95-8	$C_{20}H_{42}$	Saturated	Eicosane	1.1712	98
24	12.2366	Hexadecanoic acid, methyl ester	000112-39-0	$C_{17}H_{34}O_2$	Saturated	Palmitic acid	2.5437	98
25	13.1536	Pentadecanenitrile	018300-91-9	$C_{15}H_{29}N$	-	Pentadecannitril	3.5187	98
26	13.3622	Henicos-1-ene	001599-68-4	$C_{21}H_{42}$	Mono	1-Heneicosene	4.0401	99
27	13.4162	Henicos-1-ene	001599-68-4	$C_{21}H_{42}$	Mono	1-Heneicosene	6.8435	98
28	13.5677	Heneicosane	000629-94-7	$C_{21}H_{44}$	Saturated	Henicosane	2.0491	96
29	14.9993	9-Octadecenoic acid, methyl ester, (E)-	001937-62-8	$C_{19}H_{36}O_2$	Mono	Elaidic acid	2.9933	99
30	15.0885	10,13-Octadecadienoic acid, methyl ester	056554-62-2	$C_{19}H_{34}O_2$	Poly	10,13-Octadecadienoic acid	2.8161	99
31	15.237	Methyl stearate	000112-61-8	$C_{19}H_{38}O_2$	Saturated	Methyl stearate	1.1295	95
32	16.3222	Oleanitrile	1000308-88-1	$C_{18}H_{33}N$	Poly	-	8.8531	99
33	16.5127	Octadecanenitrile	000638-65-3	$C_{18}H_{35}N$	Poly	Octadecanonitrile	2.9296	99
34	18.0194	Diethylmalonic acid, 3-methylbenzyl	1000369-30-7	-	-	-	0.6951	25
35	18.2692	5-Chloro-2-[2-phenylethoxy]benzonitrile	038711-11-4	$C_{15}H_{12}ClNO$	-	-	1.6006	37
36	18.6676	cis-11-Eicosenoic acid, methyl ester	1000333-63-8				0.4397	99
37	19.6704	Dodecanamide	001120-16-7	$C_{12}H_{25}NO$	-	Dodecamide	0.975	93
38	20.3003	3,4-Piperidinediol, 1-[(4-nitrophenyl)methyl]-, (3R,4R)-	1000362-12-5	-	-	-	7.0286	56
39	20.4119	Oleanitrile	1000308-88-1	$C_{18}H_{33}N$	Poly	-	1.363	95
30	20.5364	Heptadecanenitrile	005399-02-0	$C_{17}H_{33}N$	-	Heptadecanenitrile	2.0149	99
41	22.8626	13-Docosenoic acid, methyl ester, (Z)-	001120-34-9	$C_{23}H_{44}O_2$	Mono	Erucic acid	6.8551	99
42	24.1009	9-Octadecenamide, (Z)-	000301-02-0	$C_{18}H_{35}NO$	-	Oleic acid amide	0.7937	64

The primary constituents of the bio-oils are saturated (e.g., alkanes) and unsaturated (e.g., alkenes and alkynes) aliphatic compounds, aliphatic fatty acids, and heterocyclic compounds (i.e., aromatic compounds containing mainly N, O, and S), where among the heteroatoms, nitrogen was abundantly found in the aromatic compounds. More than 43.84 and 50.81% of the total concentration of the constituents, as determined from Holetta-1 and Yellow Dodolla, respectively, are straight-chain hydrocarbons, which are discussed in more detail at the end of this section. The remaining classes of compounds constitute the various nitrogenated and oxygenated compounds. These compounds' relative peak areas for Yellow Dodolla and Holetta-1 varied from 0.467 to 11.3841% and from 0.4191 to 8.8531%, respectively. Accordingly, the most abundant compounds in the former oil are heterocyclic (Oleanitrile, $C_{18}H_{33}N$), monounsaturated 21-carbon hydrocarbon (Henicos-1-ene, $C_{21}H_{42}$), and monounsaturated 17-carbon hydrocarbon (8-Heptadecene, $C_{17}H_{34}$) compounds, which accounted for >23%, ca.15%, and ca. 5%, respectively. On the other hand, in the Holetta-1 oil, Oleanitrile (>10%), 3,4-Piperidinediol, 1-[(4-nitrophenyl) methyl]-, (3R,4R)- (>7%), and erucic acid (ca. 7%) are the most prevalently found components; the presence of higher erucic acid concentration is a further benefit of this oil.

It was determined that the erucic acid contents of the oils (i.e., Yellow Dodolla and Holetta-1) were 3.6664 and 6.8551%, respectively. This erucic acid is more advantageous for many value-added industrial products. This idea can be verified by the following earlier study which claimed that *B. carinata* can be exploited as a significant raw material for the production of commercial products such as bio-jet fuel, plasticizers, detergents, surfactants, and polyesters among others [302], [322]. Erucic acid is, therefore, an added advantage to the current *B. carinata* bio-oils, which can be substantiated by the following previous investigation. Each erucic acid molecule can provide twice as much fuel by the possibility of splitting its 22-carbon chain into two biofuel hydrocarbons [25]. Because of its higher erucic acid content, Holetta-1 oil is thus superior to Yellow Dodolla and becomes more desirable in this regard.

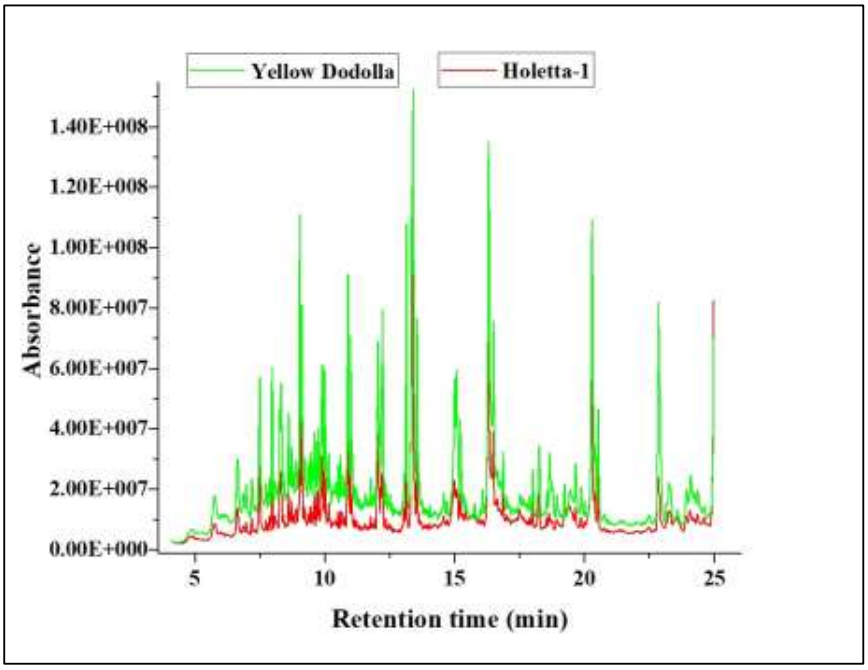

Figure 5.3 GC-MS spectra of the chemical composition of *B. carinata* bio-oils. (a) Yellow Dodolla, (b) Holetta-1.

The different kinds of compounds in the bio-oils have been classified into the following primary categories: saturated hydrocarbons (SHC), saturated fatty acids (SFA), monounsaturated hydrocarbons (MUHC), monounsaturated fatty acids (MUFA), polyunsaturated fatty acids (PUFA), and Others as indicated in Figure 5.5. The Others are classes of compounds that consist primarily of nitrogenated, nitrogenated, and oxygenated, and other compounds, the majority of which contain only nitrogen. The highest concentration of compounds is found in the Others category, with Yellow Dodolla having the highest concentration (39.62%) and Holetta-1 coming in second (38.44%); however, the next highest abundant compounds in the category are MUHC, SHC, MUFA, SFA, and PUFA, in descending order. The results showed that the compounds with only C and H, such as SHC and MUHC, consist of C_{15}–C_{21} for SHC, and C_{14}, C_{16}–C_{19}, and C_{21}, for MUHC. This demonstrated that compounds with only C and H are obtained from Yellow Dodolla, accounting for 49.14% of the compounds, and Holetta-1, accounting for 43.84% of the compounds. In general, it was possible to produce a very large concentration of compounds with straight-chain hydrocarbons (C and H) and fatty acids of oxygenated compounds (C, H, and O) with a concentration of more than 58%. As a result, the oils are the most significant choice of feedstocks for the production of advanced fuels such as bio-jet fuels.

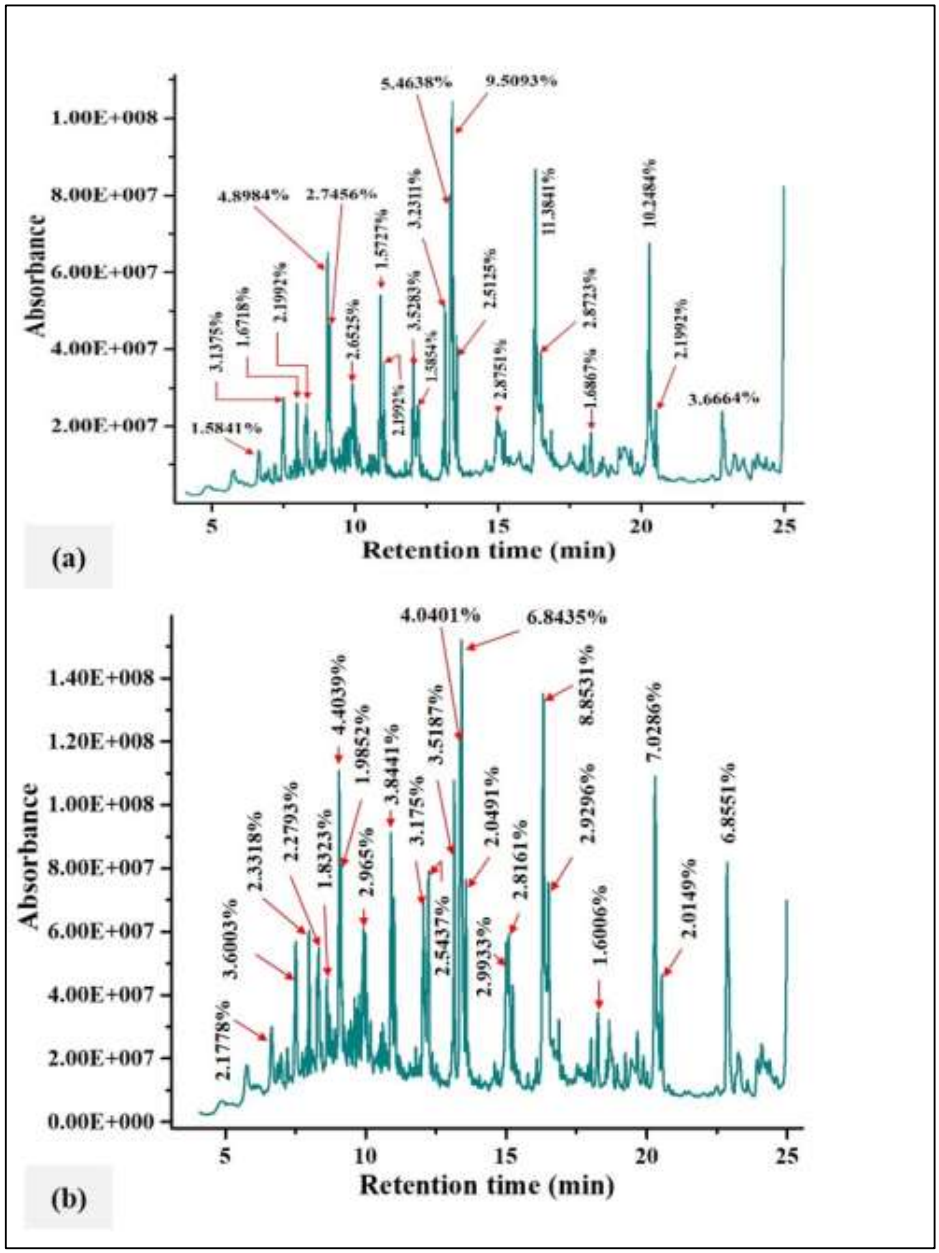

Figure 5.4 GC-MS spectra of the chemical composition of *B. carinata* bio-oils with areas of peaks (a) Yellow Dodolla, (b) Holetta-1.

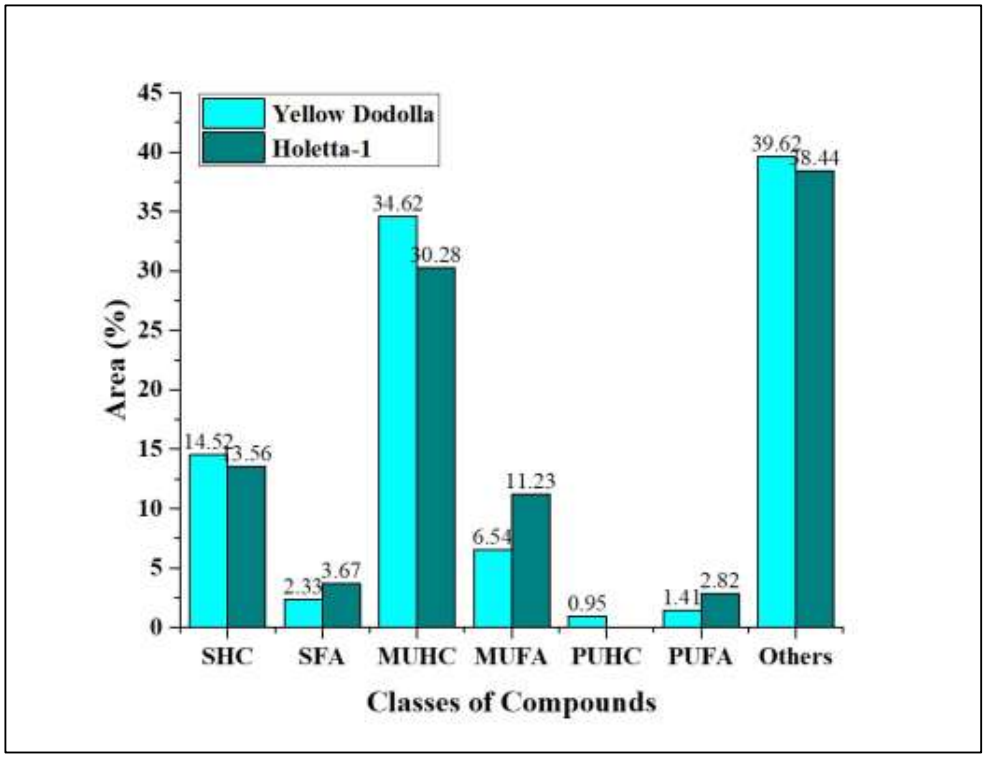

Figure 5.5 GC-MS results of the various classes of compounds of *B. carinata* bio-oils.

5.3.3.7 Fourier transform infrared spectroscopy characterization

Table 5.6 presents the frequencies of the infrared spectra observed in the bio-oils. The principal peaks identified in the IR spectra of the major functional groups are also shown in Figure 5.6. The presence of alkanes, alkenes, alkynes, phenols, alcohols, water, carboxylic acids, amines (e.g., aromatic and aliphatic amines), and amides cause the various types of peaks to appear, as this was also validated by GC-MS analysis differently. Based on Figure 5.6, the major functional groups identified in the oils were in the wavenumber ranges of 3650–3300, 3000–2850, and 1680–1395 cm^{-1}, with those found in the second position (i.e., 3000–2850) the most prevalent. These wavenumbers confirmed the presence of the bonds C=O, C≡C, C=C, C-O, C-H, O-H, C-N, N-O, and N-H. Except for very slight variations among each peak, the peaks of the oils are quite similar, indicating that their properties are identical. This is further supported by the other characterization results, which indicated that the oils have nearly identical properties.

As a result of the stretching vibration of a bond between O and H, the strong but broader wavenumbers 3371.76 cm^{-1} (Yellow Dodolla) and 3348.26 cm^{-1} (Holetta-1), suggest the presence

of alcohols, phenols, and carboxylic acids. The very short and weak intensity at 2955 cm^{-1} results from the presence of a C-H stretching medium vibration that is responsible for an alkane. In addition, the alkanes had the strongest and sharpest peaks, as evidenced by the presence of C-H stretching medium vibration at the 2923 and 2853 cm^{-1} peaks in both samples. The very weak to medium vibration caused by 1649.56 cm^{-1} is due to the presence of a C=C stretching.

There are also aromatic components (C≡C aromatic stretching) at 1549 cm^{-1}, and the vibration of methyl (-CH_3-) is what causes the peak to appear at 1456 cm^{-1} [323]. In addition, there are carboxylic acids (O–H bending) at 1406 cm^{-1}, phenols (O–H bending) at 1378 cm^{-1}, aromatic amines (C–N stretching) at 1309 and 1271 cm^{-1}, aliphatic amines (C–N stretching) at 1108, 1116, and 1022 cm^{-1}, alkenes (=C–H bending) at 966 cm^{-1}. Furthermore, the rocking vibration (C-H rocking methyl) is responsible for the alkane to occur peak at 721 cm^{-1} [216].

The so-called "fingerprint region" which encompasses a wavelength range of approximately 1500–500 cm^{-1} contains complex features of absorption bands that are specific to chemical compounds or molecules [221]. The two bio-oils have identical spectral bands and functional groups between 2955.47 and the fingerprint region such as 1309.31 cm^{-1} (Yellow Dodolla) and 1271.84 cm^{-1} (Holetta-1), and 694 cm^{-1} (Figure 4.6). As a result, it came to light that both oils were slightly different in some of the bands in the fingerprint region. It could be generally due to the fingerprint region that the oils have distinctive characterization properties addressed in the preceding sections.

Table 5.6 FT-IR spectra of *B. carinata* bio-oils.

Frequency Range (cm^{-1})	Frequency of Samples (cm^{-1})		Functional Group	Intensity of Signal	Class of Compound
	Yellow Dodolla	Holetta-1			
3650-3300	3371.76	3348.26	O-H	-	alcohols, phenols, carboxylic acids
3000-2850	2955.47	2955.54	C-H stretching	medium	alkanes
3000-2850	2923.52	2923.59	C-H stretching	medium	alkanes
	2853.53	2853.55	C-H stretching	medium	alkanes
1680-1620	1649.56	1648.71	C=C stretching	very weak to medium	alkenes
1600–1475	1549.06	1549.67	C≡C aromatic stretching	weak to medium	aromatics
1470–1450	1456.09	1456.03	C–H bending/ scissoring	medium	alkanes
1440–1395	1406.59	1405.83	O–H bending	strong	carboxylic acids
1390-1310	1378.78	1378.82	O–H bending	medium	phenols
1335–1250	1309.31	1271.84	C–N stretching	strong	aromatic amines
1250–1020	1108.15	1116.66	C–N stretching	medium	aliphatic amines
	-	1022.02	C–N stretching	medium	aliphatic amines
1000–650	966.28	966.48	=C–H bending	strong	alkenes
725-720	720.43	720.94	C–H rocking methyl	medium	alkanes
700–610	694.77	695.06	–C≡C–H: C–H bending	strong	alkynes

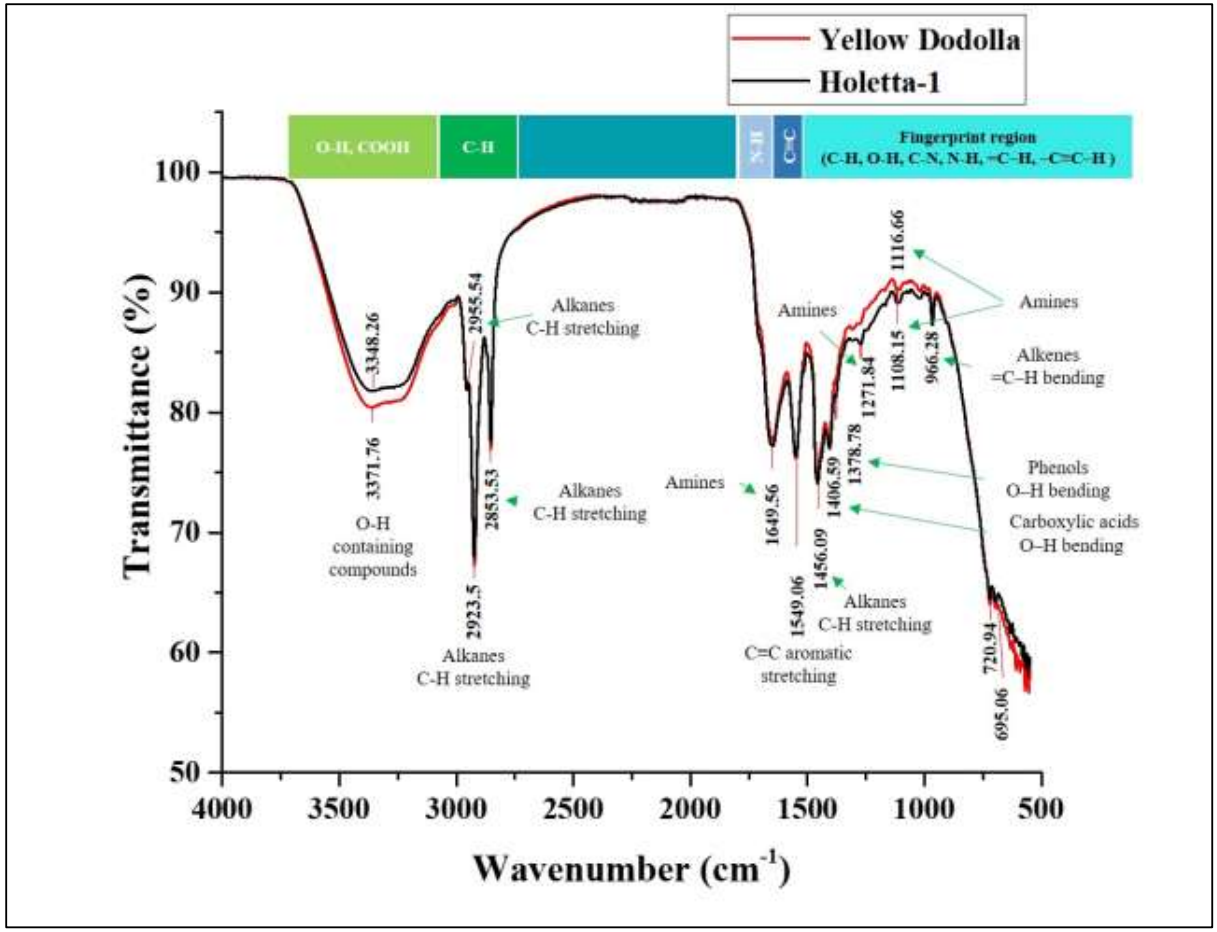

Figure 5.6 FT-IR spectra of *B. carinata* bio-oils.

According to the GC-MS results (described above), the saturated hydrocarbons (C-H), which only contained the elements C and H, are the most significant constituents of the oils. To emphasize the relevance of the other components, on the other hand, it may be presented in descending sequence of saturated fatty acids (C-O), monounsaturated hydrocarbons (C=C), monounsaturated fatty acids (C=O), polyunsaturated fatty acids, and Others (C-N, N-O, and N-H). The fact that these components, except for Others, do not consist of the heteroatom N (i.e., amine and amide functional groups) is a significant advantage for oils. Thus, the functional groups containing O (C=O, C-O, O-H, N-O) and N (C-N, N-O, and N-H) generally negatively impact the suitability of the oils since these heteroatoms are impurities that must be removed using upgrading processes such as hydrodeoxygenation, and hydrodenitrogenation, respectively.

5.3.4 Characterization of gaseous products

In addition to producing bio-oil, the slow pyrolysis also produced a mixture of gases, where the concentration of CO_2 was found to be the highest in both samples, with Holetta-1 having the greatest value, and CH_4 having the second-highest concentration. For Yellow Dodolla, the gases have a concentration of H_2 (0.0046), CH_4 (0.1345), CO_2 (4.2831), and H_2O (0.0305), while for Holetta-1, the concentrations are H_2 (0.004), CH_4 (0.0219), CO_2 (13.4707), and H_2 (0.0213).

The concentration of each of the gases may be influenced by the following significant factors. The type of feedstock, sample size (e.g., 30 g in the present study), pyrolysis type (slow, fast, flash), operating pyrolysis parameters, sampling technique, diffusion properties of the gases, and the temperature at which gases diffuse in the GC can all have a significant impact on the concentration of gases. Furthermore, gas leakage through valves, the material of construction of the sampling material, and the pressure of the gases inside the sampling bag can be considered to have significant effects on gas concentration. Taking all of these parameters into account, the slow pyrolysis experiment using *B.carinata* meals demonstrated the proof of principle for producing hydrogen and other important industrial gases. As a result, the gas mixture may be upgraded into liquid fuels (i.e., gas to liquid) using proper conversion processes.

5.4 Conclusions

In the present study, thermochemical conversion of hexane-defatted *Brassica carinata* oilseed meals via slow pyrolysis (350−550 °C) was applied and resulted in maximum bio-oil yield at the

highest temperature. The bio-oils produced at this temperature were subjected to a comprehensive characterization, including physicochemical analysis, ultimate analysis, atomic ratio determination (H/C, O/C), heating value analysis, ICP-OES elemental analysis, GC-MS analysis, and FT-IR analysis. These analyses collectively demonstrated that the oils exhibited significantly improved properties, making them promising candidates as alternative feedstocks for advanced fuel production in the aviation industry. Their characteristics align closely with those of conventional aviation fuels. Even though the oils' oxygen levels were significantly lower than the reported values discussed in the previous sections, the oxygen content remains very high and must be eliminated. Upgrading methods such as hydrodeoxygenation can be used to treat the oxygen concentration. Moreover, although the nitrogen concentration in the oils is less pronounced than their oxygen content, it still warrants removal through appropriate techniques, such as hydrodenitrogenation

CHAPTER SIX

Synthesis and Characterization of Thermally Stable $AlPO_4$-18 Supported Mesoporous β-Mo_2C, Ni_3C, and WC Nanoparticles for Bio-Jet Fuel Production Using Yellow Dodolla Oil

6.1 Introduction

The first main heterogeneous catalysts with excellent yields reported in the literature are those based on noble metals that are supported by oxides or zeolites [55]. Even though noble metals such as platinum (Pt), ruthenium (Ru), rhodium (Rh), iridium (Ir), and palladium (Pd) are highly active catalytic materials, and are more stable resisting rapid deactivation, their high costs and limited availability make them unsuitable for commercial upscaling applications [54], [55]. Over the past three decades, a great deal of research has been done on transition metal carbides (TMCs), a class of solid-state materials with exceptional mechanical hardness, excellent thermal stability, high melting point, good conductivity, and particularly catalytic activity [57], [58]. Moreover, interest in the catalytic properties of the TMCs has been inspired by their "Pt-like" properties [324], relatively inexpensive [325], and abundance [326]. The catalytic performances of the TMCs are on par with or superior to Pt-group metals in processes involving the transformation of C–H bonds of hydrocarbons, such as hydrogenation and dehydrogenation [324]. Furthermore, in reactions involving oxygen-containing compounds, TMC surfaces are more active than Pt-group metal surfaces [327]. Their catalytic characteristics are usually superior to noble metal catalysts in terms of selectivity, stability, and poison resistance. Consequently, they are being explored as potential alternatives for noble metal-based catalysts [57].

Transition metals are frequently utilized in heterogeneous catalysis due to their characteristic empty d-bands [328]. Most transition-metal elements in Groups III B to II B of the periodic table of elements can react with carbon to produce stable carbides [58]. When C is incorporated into the lattice of an early-transition metal, ensemble, and ligand effects change the system's chemical reactivity [329]. The total number of metal atoms that can be present on the surface of a metal carbide after the complex has formed is limited by the carbon atoms in the lattice (ensemble effect). Moreover, the development of bonds between metals and carbons perturbs the metal's electronic

features, causing a reduction in its density of states close to the Fermi level and a net transfer of charge from the metal to the carbon [329], lowering its chemical activity (ligand effect) and improving its catalytic properties in accordance with Sabatier's principle [329]. The hybridization of metal d-orbitals and carbon s- and p-orbitals broadens the d-band structure of metal carbides, making them possess an identical d-band structure as Pt [325]. Nevertheless, as the smaller carbon atoms tend to reside at the parent metals' interstitial locations preferably occupying the largest sites available for parent metals, the TMCs have the same crystal structures as their parent metals [330], [42]. The general reaction to the diffusion of carbon into the metal structure from any carbon source can be represented in equations 6.1 and 6.2 [331].

$$M_{(s)} + C_{(s)} \rightarrow MC_{x(s)} \quad (6.1)$$

$$M_{(s)} + C_mH_{n(g)} \rightarrow MC_{x(s)} + H_{2(g)} \quad (6.2)$$

The catalytic activity of transition metal carbides, such as molybdenum and tungsten carbides, are comparable to or superior to those of noble metals, in addition to their being less costly and more resistant to poisons [332]. Furthermore, the following previously presented investigation helps to clarify this further. Because of their unique d-band electronic structures, the molybdenum carbides have long been considered prominent heterogeneous catalysts; they demonstrated similar or comparable catalytic activities to platinum group metals in hydrogenolysis of hydrocarbons, hydrodesulfurization and hydrodenitrogenation of fuels, and ammonia synthesis/decomposition [333]. They were also shown to be more selective than noble metals in the hydrodeoxygenation of biomass-derived oxygenates to alkenes and the hydrogenation of naphthalene to tetralin [333]. The conventional approach to synthesizing carbide catalysts uses temperature-programmed reactions (TPRe), in which gas hydrocarbons and carbon monoxide are employed as carbon sources, flowing over various precursors at a slow heating rate (0.5–5 K min^{-1}) [57], at a high carburization temperature (≥800 °C) [326], to facilitate atomic diffusion of C [334].

The temperature-programmed reduction (TPR) process has been widely utilized to synthesize high surface area-supported transition metal carbide catalysts with non-carbon supports, among others [42]. Moreover, this strategy provides greater advantages than others due to its flexible, and low-cost method that is widely used to prepare various transition-metal carbides in bulk and supported forms, where the synthesis of materials with a high surface area is required for the appropriate application of carbides as a catalyst [150]. The carburization phase involves several factors,

including the carbon source, metal loading, maximum carburization temperature, heating rate, and carburization time, and all of these variables are interrelated [37].

The temperature-programmed reduction (TPR) method can be used to produce, for example, molybdenum carbide by reacting molybdenum oxide with a combination of hydrogen and carbon-containing gases such as CH_4, C_2H_6, C_3H_8, C_4H_{10}, or aromatic compounds [335]. The synthesis of this molybdenum carbide catalyst involves the preparation of one of the molybdenum precursors (such as MoO_3, MoO_2, $NiMoO_4$) and further annealing under hydrogen and carbon-containing gases [117]. Using an activated carbon (AC) as a catalytic support, Wang et al. [336] investigated the effects of the carburization temperature between 650 and 800 °C. According to their investigation, it was discovered that as the temperature of carbothermal hydrogen reduction (CHR) rose, so did the degree of Mo_2C crystallization and the Mo loading. However, at temperatures exceeding 650 °C, there was a considerable drop in BET surface area [336].

Longer times to reach the desired temperature are implied by lower heating rates, which makes carburization more efficient and results in the formation of bigger β-Mo_2C. As a result, carburization at 1 °C min^{-1} produced larger β-Mo_2C crystals (10.9 nm) than that at 10 °C min^{-1} (6.5 nm). Similar patterns and crystal sizes were produced when the catalysts were carburized at faster heating rates (10 and 5 °C min^{-1}) [37]. Guil-Lopez et al. also demonstrated that reducing the heating rate from 10 to 1 °C min^{-1} favored the carburization stage, resulting in bigger Mo_2C crystallite sizes [337]. They stated that the longer exposure to the carburization gas resulting from the lower heating rate and the rather high maximum carburization temperature (840 °C), was the primary cause of sintering of the carbide phase.

Selecting the right type of catalyst support is of the utmost significance since it is attached to the surface of the active material and improves the performance of several active materials in varying amounts [338]. To maximize active phase dispersion, the support, or carrier, is crucial in giving the catalyst mechanical strength and a large surface area [339]. As a result, one of the most important aspects in determining hydrodeoxygenation (HDO) activity and hydrocarbon selectivity with various supported catalysts is the support. Several supports, including metal oxides (TiO_2, Al_2O_3, SiO_2, CeO_2, ZrO_2) [338], zeolites (ZSM-5, HY, H-Beta) [340], [341], [342], mesoporous material (MCM-41, SAPO-11, SBA- 15, Al-SBA-15, Al-MCM-41) [338] and activated carbon (AC) [343], were investigated for HDO processes. Because only the metal's surface catalyses the

reaction, it is usually more desirable to maximize the metal surface area for a given weight of metal. As a result, small metal crystallites, typically less than 1–10 nm in size, tethered to a thermally stable, high-surface-area support are often required [344]. Even though the supported transition metal carbides discussed above have been evaluated for an array of reactions using various catalyst supports, there is still much interest as well as space for development in the potential applications of these carbide catalysts. One such application is the synthesis of thermally stable and efficient aluminophosphate-supported transition metal carbide catalysts for the production of bio-jet fuel.

To date, to the best of the authors' knowledge, no earlier research has been investigated employing $AlPO_4$-18 supported mesoporous β-Mo_2C, Ni_3C, and WC nanoparticles to produce bio-jet fuel from Yellow Dodolla vegetable oil. The objective of the present study was to synthesize these supported transition metal carbide catalysts using incipient wetness impregnation (IWI) followed by temperature programmed reduction carburization (TPRC) method. The most important parameters utilized for the synthesis were a 15 wt. % metal loading, a reductive-carburizing gas stream of 20 mL min^{-1} propane and 140 mL min^{-1} hydrogen gases, a carburization temperature of 800 °C ramping-up at a heating rate of 10 °C min^{-1}, a 2-hour holding time, followed by holding it in hydrogen environment for 1 hour. Following synthesis, different state-of-the-art technologies were applied to characterize the various properties of the carbides. Performance tests of catalysts were performed on a vegetable oil derived from *Brassica carinata* (i.e., Yellow Dodolla oil) to produce bio-jet fuel using hydroprocessing technology.

6.2 Materials and Methods

6.2.1 Raw materials

Ammonium molybdate (para) tetrahydrate ($(NH_4)_6Mo_7O_{24}\cdot 4H_2O$, 99%, ThermoFisher (Kandel) GmbH, Germany), nickel nitrate hexahydrate ($Ni(NO_3)_2.6H_2O$, ≥98%, Carl Roth GmbH, Germany), ammonium metatungstate hydrate ($(NH_4)_6W_{12}O_{39}\cdot xH_2O$, ThermoFisher (Kandel) GmbH, Germany), hydrogen gas (H_2, 99.999%, Air Liquide, French), propane gas (C_3H_8, 99.95 %, Westfalen Group, Germany), nitrogen gas (N_2, 99.999%, Air Liquide, France), and argon gas (Ar, 99.999 %, Air Liquide, France) are the most important chemicals and materials utilized in the present study. For the sake of convenience, the precursor salts ammonium heptamolybdate tetrahydrate, nickel nitrate hexahydrate, and ammonium metatungstate hydrate are referred to as

AHM, NiNH, and AMT, respectively. Furthermore, the catalyst support—aluminophosphate ($AlPO_4$-18), which was obtained from Faculty 1, University of Applied Sciences (HTW) Berlin, was used as received.

6.2.2 Synthesis of catalysts

In the current investigation, three distinct $AlPO_4$-18 supported transition metal carbide catalysts—β-$Mo_2C/AlPO_4$-18, $Ni_3C/AlPO_4$-18, and $WC/AlPO_4$-18—were synthesized by incipient wetness impregnation and then passed through a temperature-programmed reduction-carburization (TPRC) reaction [37]. Material screening is one of the most significant activities that need to be completed before synthesis; an analogous method was meticulously performed while selecting the right type of support material. Given the critical importance of hydrophobicity and thermal stability for this application, $AlPO_4$-18 was selected over zeolites like NaX and NaY based on preliminary hydrophobicity, sonication, and thermogravimetry mass spectroscopy coupled temperature programmed oxidation (TPO TG-MS) tests. The detailed synthesis procedures of catalysts were covered in the subsequent sections.

6.2.2.1 Incipient wetness impregnation (IWI)

A 15 wt. % metal loading was used as a compromise between the high density of active sites (i.e., high metal loading) and the cost of the catalysts as a result of this high metal loading [345]. As a result, the precursor salts AHM, NiNH, and AMT were used in 5, 11.5, and 3.5 g quantities to synthesize 20, 20, and 15 g of catalyst, respectively. To just fill the pore volume of the support [346], aqueous solutions of the aforesaid precursor salts were prepared, respectively, using 12 mL, 7 mL, and 10 mL of deionized water (solvent), as determined by trial and error. These aqueous solutions were then gently and cautiously sprayed onto the catalyst support, which weighed 18 g for the first two precursor salts and 13.5 g for the later precursor salt.

6.2.2.2 Drying

Drying can eliminate the solvent without resulting in a chemical change [347]**.** Thus, after impregnation, the supported impregnated precursor salts were dried in an oven utilizing AOAC 925.10 (Memmert GmbH + Co.KG, Schwabach, Germany) for the whole night at 120 °C in static air.

6.2.2.3 Calcination

To produce the final catalysts with the zero-valent metal particles fixed onto the support, dried impregnated samples were thermally treated in a calcining and/or reducing environment [344]. Based on [344], the dried impregnated samples were thermally treated in a calcining environment. As a result, the calcination of samples was performed using a programmable high-temperature electrically heated chamber Nabertherm furnace (L5/S, Nabertherm GmbH, Germany). At a rate of 2 °C min^{-1} and holding it for 5 hours in the air, the temperature was raised to 500 °C for $AlPO_4$-18 supported Mo and W catalysts and to 450 °C for $AlPO_4$-18 supported Ni catalyst. The analysis was done in the Inorganic Chemistry Department, at the Fritz-Haber-Institute of the Max-Planck-Society in Berlin, Germany.

6.2.2.4 Temperature-programmed reduction-carburization

As shown in Figure 6.1, the *ex-situ* temperature-programmed reduction-carburization (TPRC) experiment was conducted on the metal oxides (calcined) using hydrogen for reduction and propane for carburization as a carbon source. For this, approximately 1 g of each sample was introduced into the quartz glass reactor which was fitted into a three-zone horizontal split carbolite tube furnace (EVA 12/450 B, Carbolite Gero, UK). Samples were subsequently treated with a reductive-carburizing gas stream of 20 mL min^{-1} propane and 140 mL min^{-1} hydrogen (1/7 v/v C_3H_8/H_2), which were regulated by mass flow controllers (MFC) (F-201CV, Bronkhorst, Netherlands). To facilitate atomic diffusion of carbon [334], the temperature was raised at a linear rate of 10 °C min^{-1} ramping from ambient to the desired maximum temperature, 800 °C. A heating rate of 10 °C min^{-1} was chosen to minimize carbide sintering, as slower heating can lead to prolonged exposure to carburization gas at high temperatures (e.g., 840 °C) [337]**.** Once this desired carburization temperature was reached, it was then maintained for 2 hours in the reactor.

The TPRC reactor was then switched to a pure H_2 environment, with the flow rate remaining constant at 140 mL min^{-1} for 1 hour. Following this, the sample was cooled in this pure hydrogen reductive environment. To make sure that any residual remnants of gas were removed, argon gas was used to flush the whole system after the reduction-carburization process was finished. The analysis was carried out in the Inorganic Chemistry Department, at the Fritz-Haber-Institute of the Max-Planck-Society in Berlin, Germany.

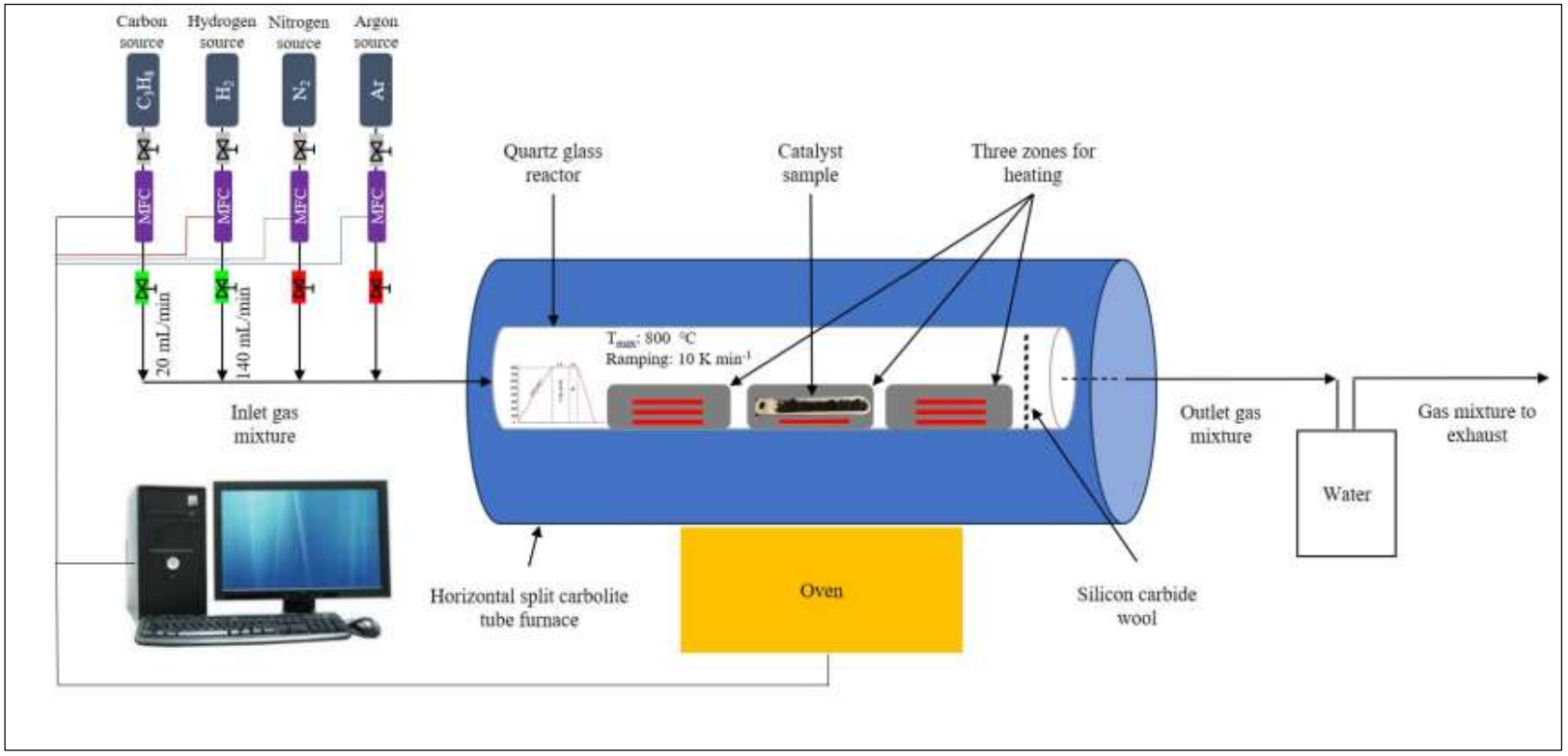

Figure 6.1 Schematic representation of the temperature-programmed reduction-carburization catalysts synthesis setup.

6.2.3 Characterization of catalysts

An in-depth characterization investigation was carried out on the oxide, and carbide catalysts, allowing the different properties of the catalysts to be studied at each stage of the catalyst synthesis steps. Moreover, a detailed study was performed on the as-received catalyst support to get a more thorough understanding of its properties. As a result, thermogravimetry mass spectroscopy coupled with temperature-programmed oxidation, BET model, BJH model, t-plot calculation, and X-ray diffraction methods were applied to investigate the thermal, textural, and structural properties of the catalysts. To further investigate a deep insight into the nominal metal loading, surface morphology, and structural properties of the catalysts, they were also characterized by energy-dispersive X-ray spectroscopy coupled with scanning transmission electron microscopy.

6.2.3.1 Temperature programmed oxidation - thermogravimetric and mass spectroscopy analysis

This is a thermogravimetric and mass spectroscopy (TG-MS) analysis after heating from room temperature to 1000 °C in an O_2 environment at a rate of 5 °C min^{-1} and holding it for 1 hour. The TG analysis (TG 209 F1 Libra, Netzsch, Germany) was utilized to investigate the thermal degradation (mass loss (%)) of the catalysts. However, a mass spectrometer (GSD301 O2, Pfeiffer Vacuum Technology AG, Germany) integrated with the TG analyzer was used to record the signal intensities of gases such as H_2O (m/z = 18), CO (m/z = 28), and CO_2 (m/z = 44) in the effluent stream. The analysis was done in the Inorganic Chemistry Department, at the Fritz-Haber-Institute of the Max-Planck-Society in Berlin, Germany.

6.2.3.2 N_2- physisorption analysis

Nitrogen sorption (adsorbate) at 77 Kelvin was used to characterize the oxide and carbide catalyst samples (adsorbents). The most important structural properties, such as the specific surface area, were determined using Brunauer-Emmett-Teller (BET) (m^2 g^{-1}); the BJH adsorption pore volume (cm^3 g^{-1}) and the BJH adsorption pore diameter (nm) were determined using Barrett-Joyner-Halenda (BJH); and the t-plot was utilized to calculate the micropore area (m^2 g^{-1}), micropore volume (m^3 g^{-1}), and external surface area (m^2 g^{-1}). Surface area analyzers (Autosorb 6, Quantachrome Instruments, USA) and (ASAP 2020, Micromeritics Instrument Corporation, USA) were used for the support material, calcined, and carbide catalysts, respectively.

Before analysis, the samples were degassed for 24 hours at room temperature to ensure that nitrogen could adsorb efficiently on the surfaces of the catalyst samples or fill the pores. The degassed samples were analyzed at the liquid nitrogen temperature of 77 Kelvin and the adsorption/desorption isotherms were measured with an equilibrium time interval of 20 seconds. Sample weights of 0.5907 g, 0.6668 g, and 0.0939 g were used to analyze the calcined oxides (α-MoO_3/$AlPO_4$-18, NiO/$AlPO_4$-18, γ-WO_3/$AlPO_4$-18), respectively. 0.0587 g of $AlPO_4$-18 was used. Sample weights of 0.3007 g, 0.3200 g, and 0.2767 g were used for β-Mo_2C/$AlPO_4$-18, Ni_3C/$AlPO_4$-18, and WC/$AlPO_4$-18, respectively. The carbide catalysts were analyzed in the Structural Analysis Department of the Federal Institute for Materials Research and Testing (BAM), Berlin, Germany. The support material and calcined samples were, on the other hand, analyzed in the Inorganic Chemistry Department of the Fritz-Haber-Institute of the Max-Planck-Society, Berlin, Germany.

6.2.3.3 X-ray diffraction analysis

With a rotating anode STOE theta-theta X-ray powder diffractometer coupled with a CuKα1+2 radiation, secondary graphite monochromator, scintillation counter radiation source (λ = 1.54184 Å), an XRD analysis was carried out to investigate phase composition, type of crystallite structures, and structural properties including average crystallite sizes and lattice constants of the catalysts. The average crystallite size was calculated using the Debye-Scherrer method, which is one of the simplest techniques that make use of peak broadening investigation that is based on the full-width half maximum (FWHM) values [348]. With a scan rate of 4° min^{-1}, it was utilized to record XRD patterns in the range 2θ = 5–100°. The analysis was done at the Helmholtz Center Berlin for Materials and Energy in Berlin, Germany.

6.2.3.4 Transmission electron microscopy-energy-dispersive X-ray spectroscopy analysis

An *ex-situ* high-resolution transmission electron microscopy/scanning transmission electron microscopy (HR TEM/STEM) analysis was used to study the morphology and structural properties (e.g., average crystallite sizes, and interplanar spacing) of the carbide catalysts. The TEM measurements were carried out using a Talos F200S Microscope (Thermo Fisher Scientific) with an acceleration voltage of 200 kV. For the EDS spectra, 2 Silicon drift detectors (SDD) were used and the results were quantified with the Velox software. Different ranges of collecting angles such as bright field scanning TEM (BF-STEM) and high angle annular dark field scanning TEM (HAADF-STEM) were used to capture BF-STEM and HAADF-STEM images, respectively.

Typically, the beam was spread out across an appropriate portion of the sample, and acquisition intervals of 5 to 10 minutes were used for analysis. A sample weighing approximately 10 mg of very fine powder was mixed with 1 mL of deionized water, and roughly 10 μL of the solution was taken to a sample carrier of the copper grid (Lacey Carbon Film). The qualitative and quantitative contents of the main elements in the catalysts were subsequently determined using the energy-dispersive X-ray spectroscopy (EDS) analyzer. The analysis was carried out in the Structural Analysis Department, at the Federal Institute for Materials Research and Testing (BAM), Berlin, Germany.

6.3 Results and Discussion

6.3.1 Synthesis of catalysts

Figure 6.S1 displays the precursor salts, support, and calcined, along with the carbide catalysts synthesized in the high-temperature TPRC system depicted in Figure 6.1. The color changes that happened during air calcination of the supported precursors and H_2-TPRC of the calcined catalysts are clearly visible as shown in Figure 6.S1. Even though the characterization of the oxides and carbides is covered in more detail in the sections below, this section discusses how they are generated through the synthesis processes. Before calcination, the impregnated catalysts were subjected to a drying phase in which the solute might redistribute via desorption and re-adsorption, and the solution kept in place by the porous support could migrate via capillary flow or diffusion. However, as the solvent evaporates, the solute precipitates out of the solution, making it supersaturated and causing the precursors to crystallize in the pores and outer surface of the carrier. As a result, drying helps to distribute catalysts within the support [349]. After the distribution of active metals over the support via drying, air calcination was carried out, which involved several processes such as the loss of chemically bonded water or carbon dioxide, texture modification via sintering (the growth of small crystals or particles into larger ones), structure modification, the formation of active phases, and mechanical property stabilization [350]. More importantly, precursor ligands are eliminated via the breakdown or reaction with air producing gaseous molecules [344].

As described in the subsequent sections, during calcination of the supported ammonium molybdate tetrahydrate catalyst, a single phase α-MoO_3 was produced at 500 °C. In the process of synthesizing

the carbide nanoparticles (e.g., β-Mo_2C), the precursor salt (ammonium molybdate) is first broken down into MoO_3(Mo^{6+}), which subsequently continually reduces to MoO_2 (Mo^{4+}). At high carburization temperatures, this Mo^{4+} is further reduced to metallic molybdenum and then converted into molybdenum carbide [351]. It was put forward that the emphasis is on the characterization of the catalysts covered in the sections below, given there is hardly any reported literature data on the synthesis of Ni_3C and WC using IWI followed by H_2-TPRC in the literature. However, the synthesis of WO_3 at 500 ℃ can be represented by equations 6.3–6.6, as stated in [352], to study the thermal behavior of ammonium metatungstate. The temperature ranges utilized in each equation are 28–135, 136–200, 250–390, and 391–500 ℃, respectively.

$$(NH_4)_6H_2W_{12}O_{40}.4H_2O \rightarrow (NH_4)_6H_2W_{12}O_{40}.H_2O + 3H_2O \quad (6.3)$$

$$(NH_4)_6H_2W_{12}O_{40}.H_2O \rightarrow (NH_4)_6H_2W_{12}O_{40} + H_2O \quad (6.4)$$

$$(NH_4)_6H_2W_{12}O_{40} \rightarrow NH_4HW_{12}O_{37} + 5NH_3 + 3H_2O \quad (6.5)$$

$$NH_4HW_{12}O_{37} \rightarrow 12WO_3 + NH_3 + H_2O \quad (6.6)$$

6.3.2 *Ex-situ* characterization of catalysts

Understanding the relationship between the catalysts' physical, chemical, and catalytic properties is the primary objective of catalyst characterization. Consequently, the catalysts' thermal, structural, and microscopic analyses are described in detail in the sections below.

6.3.2.1 Temperature programmed oxidation - thermogravimetric and mass spectroscopy analysis

Even though transition metal carbides (TMCs) have remarkable thermal stability [117], a thermal stability analysis was carried out on both the catalyst support and synthesized carbide catalysts because thermal sintering of supports and catalysts is the main cause of irreversible catalytic deactivation phenomena [353]. As a result, to better understand the nature of the support, and carbide catalysts exposed to thermal treatments in air, Figure 6.2 and Figure 6.S2 display *ex-situ* TG-MS followed by O_2-TPO results. The thermal degradation behavior of the support confirmed that it showed only a single-stage weight loss during heating from approximately 37.5 ℃ to around 200 ℃, which could be attributed to surface water sorption. This is in perfect harmony with the results of the earlier study [354], which demonstrated that the removal of physisorbed water

molecules within the zeolite AlPO-18 pores caused it to undergo a single-stage decomposition process in the temperature range of 30 to 200 ℃. When the temperature rises further up to 1000℃, the weight loss rises as well, although only slightly, with 88.84% of the residual catalyst support remaining unaffected, and the majority of the weight loss presumably caused by the evaporation of water. As a result, the $AlPO_4$-18 catalyst support can be considered a thermally stable porous material.

The thermal behaviors of the catalysts revealed significant variations between Mo and Ni-based catalysts, with the former exhibiting three zones of mass losses (Figure 6.S2) and the latter exhibiting only two zones (Figure 6.2 (b)). The first peak of the H_2O signal (m/z=18) was identified for β-Mo_2C/$AlPO_4$-18 at lower temperatures (i.e., a temperature range of room temperature to 320 ℃), indicating a weight loss of 1.94%, which could be attributed to the desorption of surface H_2O from the catalyst. In the second zone, it starts to gain weight (3.20%) at 360 °C and keeps increasing until it reaches a temperature of 800 °C. After the weight gain, its weight remains virtually constant at 800 ℃ for about 70 min, and then, after 800 ℃, in the third zone, it progressively declines its weight with a weight loss of 14.36% to achieve the residual catalyst weight of 86.91% at 1000 ℃. This weight loss might be attributed to the detection of a CO_2 signal (m/z=44), which could be related to the presence of amorphous, graphitic carbon (or free carbon), coke, and other aggregates of carbon [355], [356], or carbon from the surface of the carbide catalyst itself.

A similar phenomenon, which could also be related to H_2O desorption, was also observed in Ni_3C/$AlPO_4$-18 in the first temperature zone (room temperature to 200 ℃). However, after 200 ℃, it became constant for about 60 minutes before sharply decreasing, and after it reached a temperature of approximately 700 ℃, it obtained its final residual catalyst weight of 77.11%. The noteworthy decline in the weight of Ni_3C/$AlPO_4$-18 could potentially be attributed to the CO signal (m/z=28) and the identification of a CO_2 signal (m/z=44), with the CO_2 peak being identified as exceptionally robust contributing to a much higher drop in weight. The evolution of the CO and CO_2 signals can be explained for similar reasons as described for β-Mo_2C/$AlPO_4$-18. As a result, the generation of these gases could indicate the presence of a carbonaceous deposit, although it could effortlessly be eliminated by hydrogen during catalyst activation before catalytic activity testing.

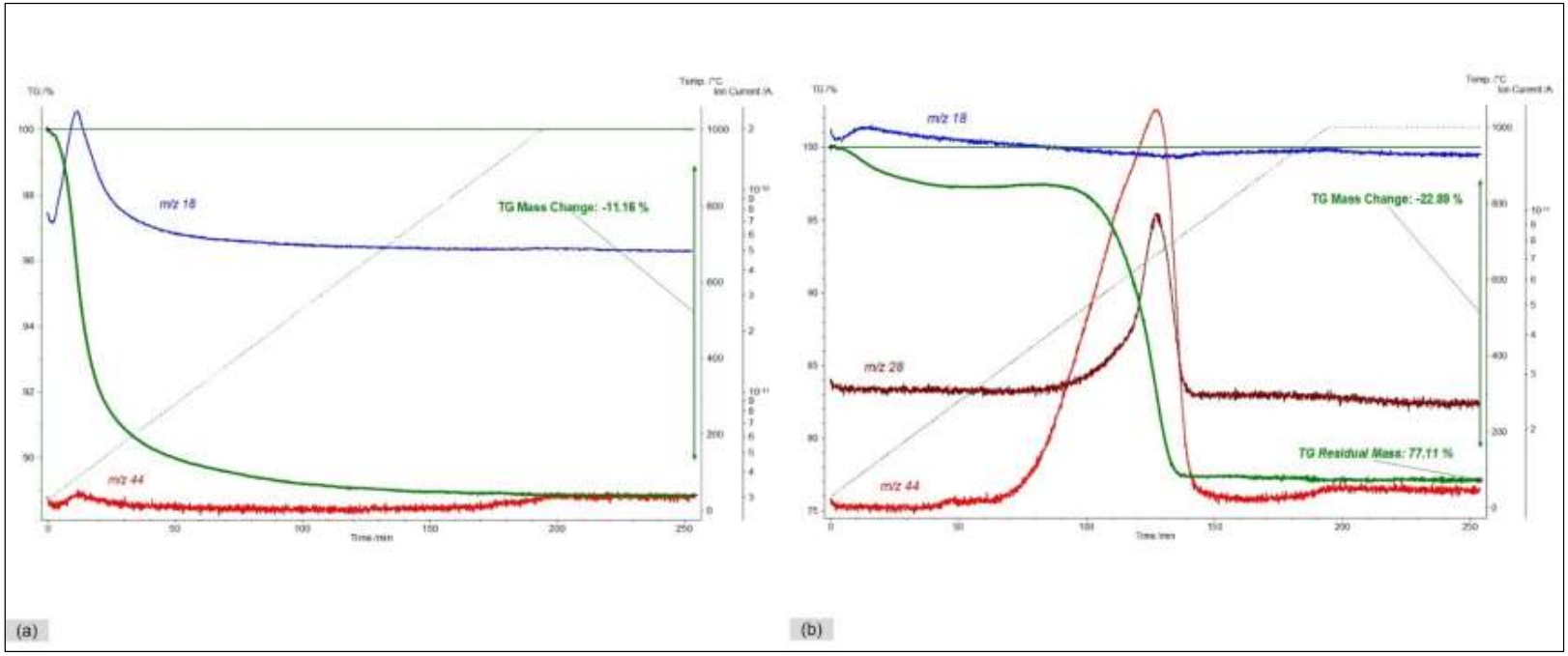

Figure 6.2 *Ex-situ* TG-MS coupled with temperature-programmed oxidation (TPO) for investigation of mass spectra of evolved gases, and mass loss (%). (a) Support material, (b) $Ni_3C/AlPO_4$-18 catalyst.

6.3.2.2 N_2- physisorption analysis

According to the N_2-physisorption analysis, Table 6.1 shows the detailed textural properties of support, calcined, and carbide catalysts. Figure 6.3, and Figure 6.S3 also display the various N_2 physisorption isotherms of the carbide and oxide samples, respectively. According to the classification of adsorption isotherms made by IUPAC in its most recent technical report [357], it appears that the isotherms of all samples—aside from the support—can be classified as type IV materials. A significant portion of N_2 gas is adsorbed at high relative pressure (P/P0), which is attributed to the presence of mesopore properties. Furthermore, it is commonly acknowledged that the texture (such as., pore size distribution, pore geometry, and connectivity) of a mesoporous material is correlated with the shape of the hysteresis loops, notably adsorption hysteresis of types IV and V isotherms [358]. Based on IUPAC classification [358], the hysteresis characteristics of both oxide and carbide samples can be categorized as an H3-type hysteresis loop, normally attributed to porous materials made up of slit-shaped pores with non-rigid aggregates of plate-like particles. Indeed, the average crystallite sizes determined by XRD and TEM measurements can further provide additional evidence for the samples' mesoporous material composition.

The results except for molybdenum confirmed that the catalysts (both calcined and carbide), which have the lowest adsorption capacities, all of the other catalysts had the greatest adsorption capacities and are nearly identical. The N_2 gas physisorption results verified that the parent support was found to possess a very high surface area, which may potentially increase the number of active catalytic sites of the catalysts. Even though the surface area of the supported catalysts declined after synthesis (i.e., after calcination and reduction-carburization) using the 15% metal loading, their surface areas are still deemed quite large. The decrease in the textural properties (such as surface area) remains by far the most noticeable following reduction-carburization compared to calcination, and it could have been triggered by any of the carburization conditions, such as higher carburization temperature for structural distortions, atomic diffusion of carbon, and so on. The earlier study [37] on carbon nanofiber supported Mo_2C reported that BET surface area dropped dramatically at temperatures above 650 °C. Furthermore, based on [359], it was determined that the surface area reduced sharply at high carburization temperatures, attributing primarily to carbon deposition during MoO_3 carburization. The earlier report [117], likewise, stated that molybdenum carbide catalyst has a low surface area supporting the present investigation's finding that molybdenum carbide catalyst has a low surface area. However, the decrease of surface areas during

reduction-carburization in all of the catalysts is in line with results reported in [332], where pore blocking occurs by metal-carbides. In a similar vein, the experimental samples—particularly the carbide catalyst samples—may confirm the superb incorporation of the bigger metal ions into the catalyst support framework.

Table 6.1 Textural properties of catalyst support, calcined, and carbide catalysts analyzed by N_2-physisorption.

Sample	BET method	t-Plot calculation		BJH adsorption	
	Surface area ($m^2 g^{-1}$)	Micropore area ($m^2 g^{-1}$)	Micropore volume ($m^3 g^{-1}$)	Volume ($cm^3 g^{-1}$)	Pore diameter (nm)
$AlPO_4$-18	257.83	213.68	0.09	0.22	4.02
Oxide					
α-$MoO_3/AlPO_4$-18	63.98	38.99	0.02	3.57	13.62
$NiO/AlPO_4$-18	210.59	181.62	0.09	0.23	1.97
γ-$WO_3/AlPO_4$-18	248.27	214.12	0.08	0.21	6.40
	BET method		**t-Plot calculation**		
	Surface area ($m^2 g^{-1}$)	**Total adsorbed surface area ($m^2 g^{-1}$)**	**Micropore area ($m^2 g^{-1}$)**	**External surface area ($m^2 g^{-1}$)**	**Micropore volume ($m^3 g^{-1}$)**
Carbide					
β-$Mo_2C/AlPO_4$-18	66.57	20.02	38.54	28.03	0.02
$Ni_3C/AlPO_4$-18	169.05	54.10	122.99	46.06	0.05
$WC/AlPO_4$-18	193.79	53.62	168.43	25.36	0.06

Although the surface area of the $WC/AlPO_4$-18 catalyst decreased after reduction-carburization, W-based catalysts (both oxide and carbide) show the greatest values, followed by Ni- and Mo-based catalysts. In decreasing order, the surface areas of the catalysts are ranked as $WC/AlPO_4$-18 > $Ni_3C/AlPO_4$-18 > β-$Mo_2C/AlPO_4$-18. The same scenario is also valid for the t-plot calculations of carbide catalysts' micropore volume ($m^3 g^{-1}$) and micropore area ($m^2 g^{-1}$), in which the $WC/AlPO_4$-18 catalyst outperformed the Mo and Ni catalysts' results. Even though the smallest surface areas are observed in Mo-based catalysts, the surface area of their carbide is slightly increased as opposed to others.

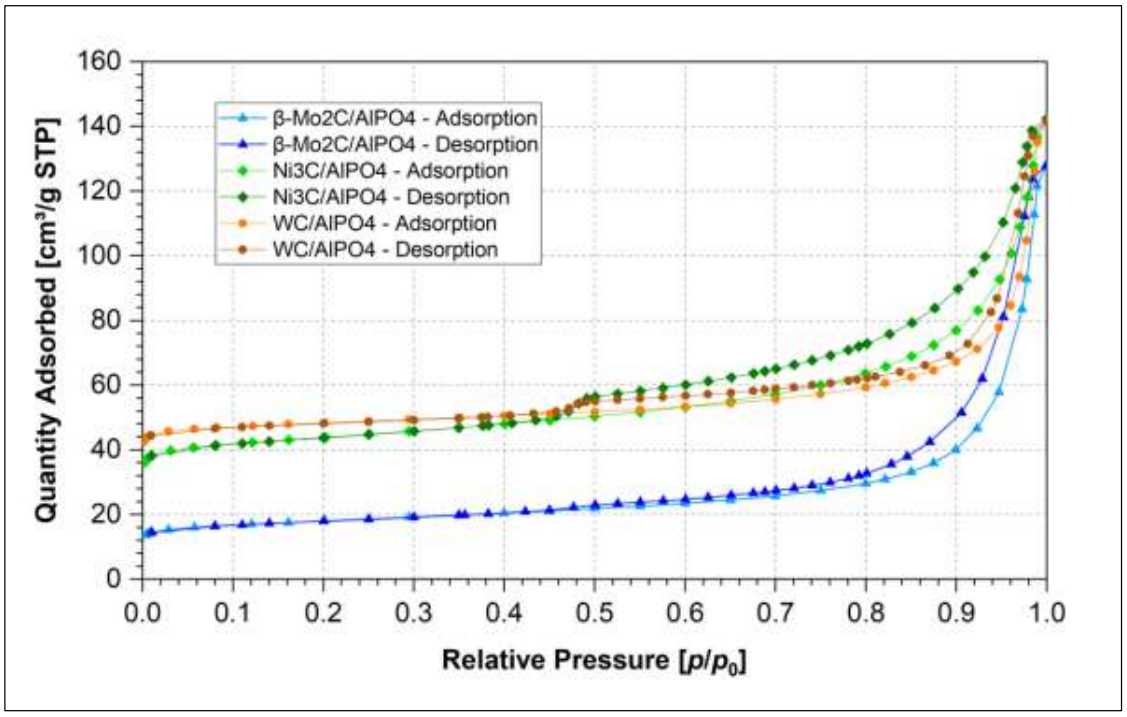

Figure 6.3 Nitrogen gas adsorption-desorption curves of $AlPO_4$ supported metal carbide catalysts. β-$Mo_2C/AlPO_4$ stands for β-$Mo_2C/AlPO_4$-18. $Ni_3C/AlPO_4$ stands for $Ni_3C/AlPO_4$-18. $WC/AlPO_4$ stands for $WC/AlPO_4$-18.

6.3.2.3 X-ray diffraction analysis

As the catalytic properties of catalysts rely on their key parameters, such as crystallite size, structure, and morphology [360], the nature of the oxide and carbide phases, average crystallite sizes, average lattice constant, and structures developed during air calcination and *ex-situ* reduction-carburization conditions are all investigated using XRD analysis, the details of which are discussed below.

A. Catalyst support

The catalyst support ($AlPO_4$-18) is a molecular sieve with a unique framework structure (AEI) [361]. The diffraction peaks of this as-received molecular sieve are shown in Figures 6.4−6.6, with its peaks located at 2θ = 7.4º, 9.4º, 20.4º, 21.7º, 26.6º, 35.5º, 59.9º (PDF 11-0500). The support exhibits strong peaks at 2θ = 7.4º, 9.4º, 21.7º, 26.6º, with its peak at 2θ = 9.4º being the strongest among all the peaks. The support is additionally distinguished by its average crystallite sizes of 0.15 nm, and an orthorhombic crystal structure.

B. Oxide catalysts

Figures 6.4−6.6 demonstrate the phases formed during calcination of $AlPO_4$ supported ammonium molybdate (para) tetrahydrate ($(NH_4)_6Mo_7O_{24}\cdot 4H_2O$), nickel nitrate hexahydrate ($Ni(NO_3)_2.6H_2O$), and ammonium metatungstate hydrate ($((NH_4)_6W_{12}O_{39}\cdot xH_2O$), respectively. The XRD results showed that the phases α-MoO_3, NiO, γ-WO_3, and α-WO_3 (detailed below), formed under the appropriate calcination conditions, were identified by forming several diffraction peaks.

(i) Molybdenum oxide. The precursor salt was first decomposed into MoO_3, NH_3, and H_2O based on [362]. Among the various typical crystal forms of MoO_3, the well-known thermodynamically stable orthorhombic MoO_3 (α-MoO_3) was developed at the calcination temperature of 500 ℃. This is in line with the results of the earlier study [363], which claimed that at 400 °C, the orthorhombic and hexagonal phases of MoO_3 were formed; but at 500 ℃, these phases became a single phase of orthorhombic α-MoO_3. The strong primary α-MoO_3 diffraction peaks (Figure 6.4) are thus located at 2θ = 23.4º, and 27.9º (PDF 47-1320), with their well-matched Miller indexes, are (111), and (200), respectively. Also, the α-MoO_3 phase's face-centered orthorhombic lattice structure exhibits an average crystal size of 0.16 nm and an average lattice constant of 0.62 nm. There was also a small peak that appeared at 2θ = 30.75º, which is hard to assign.

(ii) Nickel oxide. The XRD results presented in Figure 6.5 demonstrated that only a single phase of nickel oxide (NiO) nanoparticles was determined at the calcination temperature. With peak positions at 2θ = 37.2º, 43.3º, 62.8º, 75.4º, and 79.4º (PDF 44-1159), the single NiO phase is characterized by a cubic crystal structure that may be indexed with crystal planes (111), (200), (220), (311), and (222), respectively, as reported by the (*JCPDS*, No. 04-0835). It has been determined that the NiO phase has an average crystallite size of 0.14 nm and an average lattice constant of 0.42 nm.

(iii) Tungsten oxide. Figure 6.6 shows the phase structure of $AlPO_4$-supported ammonium metatungstate hydrate ($((NH_4)_6W_{12}O_{39}\cdot xH_2O$) at 500 ℃ air calcination. Based on the XRD results (Figure 6.6), the two WO_3 structures—monoclinic (γ-WO_3) (*JCPDS 43-1035)* and tetragonal (α-WO_3) (*JCPDS* No. 71- 0292) —were formed at this calcination temperature, which is in line with the reported study [352]. According to [364], and [365], the monoclinic type is more stable than the tetragonal one. Several diffraction peaks have been observed, some of which are sharp and

intense, and some of which are small. The most intense peaks displayed by the face-centered monoclinic WO_3 at 2θ are represented by the diffraction peaks at 2θ = 23.5º, 26.6º and 33.5º with their corresponding planes (111), (220), and (200), respectively. It was found that the average lattice constant and average crystallite sizes were, respectively, 0.39 nm and 0.13 nm. However, the planes (110), (200), and (211) with their equivalent peaks at 2θ = 35.7º, 49.8º, and 50.1º appeared to be responsible for the tetragonal α-WO_3 phase with a body-centered structure. This tetragonal phase has a slightly smaller average lattice constant (0.39 nm) than the monoclinic phase but identical average crystallite sizes.

C. Carbide catalysts

Figures 6.4–6.6 show the XRD measurements of the supported metal oxides that are reduced in a flux of hydrogen at 800 ℃ and carburized with propane into their respective carbide catalysts. The XRD analysis, which is described in more detail below, verified that carbon was successfully incorporated into the lattice of each metal and developed phases containing metal carbides at the reduction-carburization conditions.

(i) Molybdenum carbide. Among the five different crystal structures of molybdenum carbide nanoparticles (i.e., α-MoC_{1-x}, α-Mo_2C, β-Mo_2C, γ-MoC, and η-MoC) [366], which arise from different preparation methods as well as carburizing agents [367], the more stable β-Mo_2C phase [368], was identified using XRD analysis as shown in Figure 6.4. The following equations reported by [366] can better explain how the development of the β-Mo_2C phase can be formed from its oxide form:

$$(NH_4)_6Mo_7O_{24}.H_2O\ (130\ ℃)\ \rightarrow\ 7\alpha\text{-}MoO_3 + 6NH_3 + 4H_2O \tag{6.7}$$

$$2\alpha\text{-}MoO_3 + 7C\ (800\ ℃)\ \rightarrow\ \beta\text{-}Mo_2C + 6CO \tag{6.8}$$

The developed β-Mo_2C phase (*JCPDS* No. 65-8766) is characterized by its hexagonal close-packed (HCP) structure, which is consistent with the work reported by [333], and diffraction peaks at 2θ = 39.5º, 61.6º, and 74.1º, with corresponding planes (100), (110), and (111), respectively. The average crystallite sizes, average lattice constant, and lattice strain of this phase were determined to be 3.68 nm, 0.22 nm, and 0.05, respectively (Table 6.2). In addition to the β-Mo_2C phase, a single peak that is less strong and small was identified at 2θ = 32.0º, which could be a characteristic property of the MoO_2 phase. The existence of this molybdenum oxide (MoO_2) phase could be an

indication of partial carburization of the orthorhombic α-MoO_3 phase. The primary cause of the development of the β-Mo_2C phase, which resulted in smaller peaks as illustrated in Figure 6.4, could also suggest incomplete carburization of this molybdenum oxide phase.

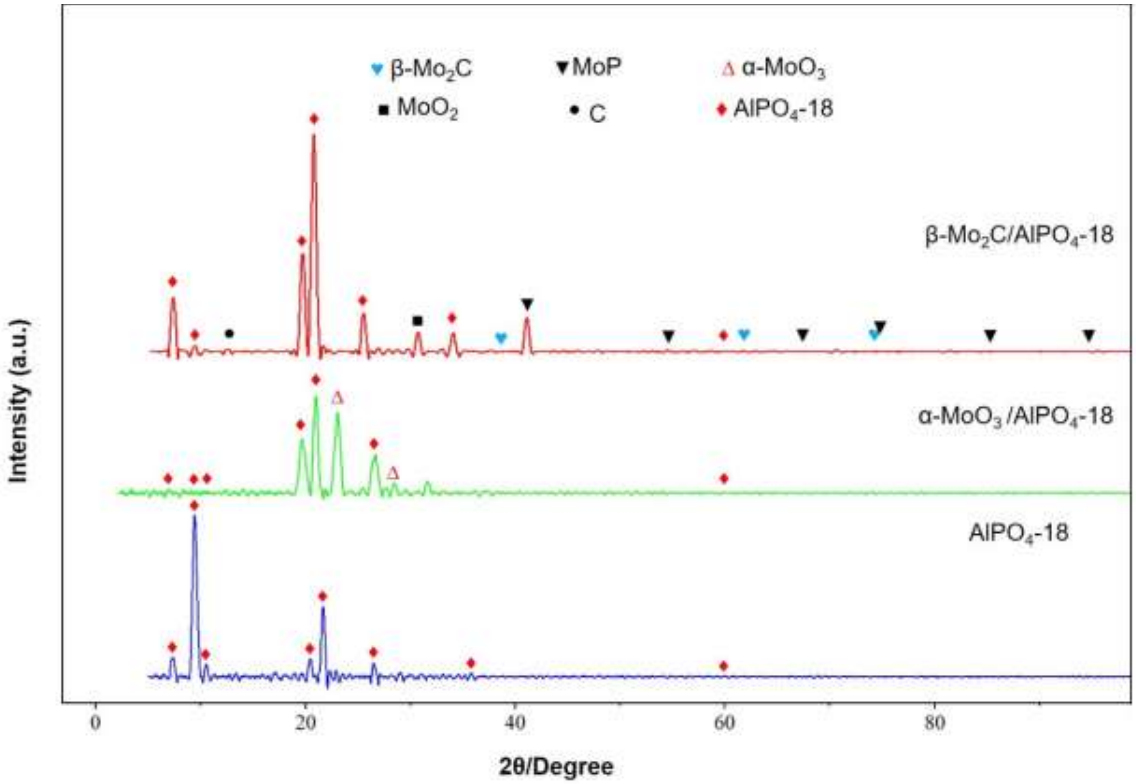

Figure 6.4 X-ray diffraction patterns of α-MoO_3/$AlPO_4$-18, and β-Mo_2C/$AlPO_4$-18 catalysts.

The peak at 2θ = 12.8º, which appears in all of the diffraction peaks of the Mo-, Ni-, and W-based catalysts, could be attributed to unreacted deposited carbon (*JCPDS No. 00-058-1638)* on the surfaces of the catalysts. This peak was not observed in either the catalyst support or the oxide catalysts, providing validity to the assignment of this diffraction to free carbon species. The use of hydrogen alone in the post-carburization process and holding it for a few hours (e.g., 1 h in the present work) may have greatly reduced the possibility of the existence of this free carbon species on the surface of the catalysts. This notion could be corroborated by the results of [369], who claimed that hydrogenation can convert deposited carbon species into gas hydrocarbons.

The XRD results (Figure 6.4) also confirmed that multiple diffraction peaks were found at 2θ = 43.0º, 57.1º, 67.7º, 74.3º, 85.7º, and 94.3º, with their corresponding planes at (110), (200), (220),

(310), (222), and (321). These peaks may represent entirely new phase, phosphorous-coated nano molybdenum phosphide (MoP) particles (*JCPDS* No. 24-0771), which could be the result of the strong interaction between the active metal molybdenum and the support ($AlPO_4$). With a relatively bigger average lattice constant of 0.36 nm, compared to its carbide phase (β-Mo_2C), these MoP crystallites have a hexagonal crystallite structure with average crystallite sizes and lattice strains identical to the β-Mo_2C phase (Table 6.2). The following previously published study helps to further clarify the phenomena of this active metal-support interaction (MSI). It is widely recognized that the interaction of metal nanoparticles (NPs) with support in the vast majority of cases results in entirely novel properties, depending on the nature of the metal-support interaction (MSI). A broad spectrum of such interactions is described, ranging from extremely weak ones (metal coordination via physical adsorption) to very strong ones associated with the formation of new surface compounds [370]. More importantly, the MSI can lead both to the improvement in and deterioration of catalytic activity. The development of new catalytic sites or phases on the interface boundary, electronic effects, the ability to anchor metal particles to prevent agglomeration and sintering of metal particles, and metal particle ornamentation, are all very important points [370].

The catalytic activity of the synthesized catalysts may be influenced as a result of the development of this new MoP phase during the active metal-support interaction during its synthesis (i.e., drying, calcination, and H_2-TPR carburization). As opposed to the metal-support interaction of the samples, the previously reported work underlines the drawback of incipient wetness impregnation. Because there is no interaction between the metal precursor and the support surface, which causes the metal precursors to agglomerate in the liquid phase during drying [345], Mehrabadi et al. [344] asserted that IWI produces relatively big metal particles with wide particle size distributions. The IWI of the present study, however, used judicious spraying of the aqueous precursor solutions on the support. This, in turn, followed by TPRC, produced metal carbide nanoparticles, which varied in average crystallite sizes from 0.85 to 3.68 nm and demonstrated an interaction between each of the active metals and the support. This phenomenon is also observed in nickel and tungsten-based phosphides, as discussed in the subsequent sections. The XRD study confirmed that samples taken from the first and last heating zones of the TPRC reactor (Figure 6.1) did not differ in the types and intensities of the phases produced during the reduction-carburization process. This could imply that samples within the reactor have been heated uniformly and that the concentrations of atomic carbon and hydrogen have been distributed evenly across the reactor.

(ii) Nickel carbide. The XRD results of the study, which are presented in Figure 6.5, demonstrate that Ni_3C (*JCPDS* No. 72-1467) and NiC (*JCPDS* No. 14–0020), two of the prevalent nickel carbide phases, have been identified. The Ni_3C phase is recognized by its hexagonal crystallite structure, which includes planes (110), (200), (211), (220), (310), and (222), and its corresponding diffraction peaks at 2θ = 31.1º, 35.7º, 44.4º, 51.7º, 59.7º, and 98.5º, respectively, with the peak at 44.4º being the most intense and long. As can be seen in Table 6.2, this phase has significantly smaller crystallite sizes but a fairly comparable average lattice constant and lattice strain values compared to that of the β-Mo_2C phase. Because of its extraordinary chemical stability, magnetic, and catalytic properties [371], the Ni_3C phase, having a strong intensity in the present investigation, has gained increased interest. The NiC phase, with a relatively short and broad peak, however, appeared at the diffraction peak of 2θ = 76.2º. The XRD results also showed the existence of metallic nickel (Ni) with a very short diffraction peak at 2θ = 92.8º, but no nickel oxides, implying that the oxides were completely reduced.

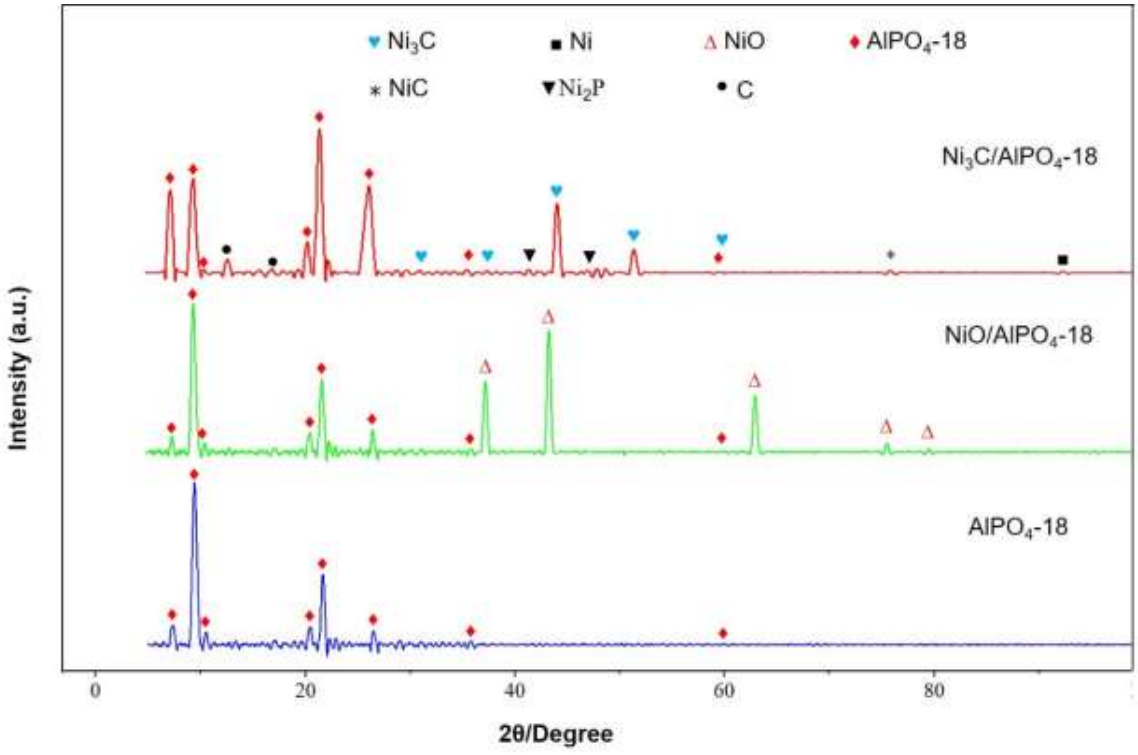

Figure 6.5 X-ray diffraction patterns of NiO/$AlPO_4$-18, and Ni_3C/$AlPO_4$-18 catalysts.

The nickel phosphide (Ni_2P) phase (*JCPDS* No. 03-0953), which has diffraction peaks at 2θ = 41.7º and 47.3º and associated planes (111), (200), respectively, is another type of phase with a hexagonal

crystal structure recognized by the XRD study. The average crystallite sizes of the Ni_2P phase (Table 6.2) turned out to be considerably smaller than those of the MoP phase, yet its average lattice constant and lattice strain were found to be virtually similar to those of the MoP phase. The active metal-support interaction, as was detailed in the above section for MoP, resulted in this new Ni_2P phase and perhaps new active sites, which may affect the catalytic activity of the catalyst. The diffraction peak at $2\theta = 12.8^{o}$ (100), which is responsible for the free carbon species, also appeared during the carburization of Ni_3C. Another diffraction peak at $2\theta = 16.9^{o}$ (110), that is identified on both Ni and W may similarly reflect an unreacted carbon. It was determined that the average lattice constant of this unreacted free carbon species was 0.72 nm.

(iii) Tungsten carbide. Figure 6.6 illustrates that the carburization conditions (i.e., H_2-TPR, C_3H_8, and 800 °C carburization temperature) predominantly formed the tungsten carbide phase (WC) (PDF 00-051-0939), despite the fact that the W_2C (PDF 89–2371) exhibits very few and very small diffraction peaks. The planes (110), (200), (211), (220), (310), (222) and their corresponding diffraction peaks located at $2\theta = 31.1^{o}$, 35.7^{o}, 43.2^{o}, 48.2^{o}, 64.4^{o}, and 73.2^{o} characterize the existence of hexagonal crystalline structure of WC phase. Nonetheless, the W_2C phase was distinguished by diffraction peaks at $2\theta = 39.4^{o}$, and 75.9^{o} along with its corresponding planes (110), and (220), respectively. Both phases had the same average crystallite sizes and lattice strains, but slightly similar average lattice constants (Table 6.2). The tungsten oxides (γ-WO_3 and α-WO_3) were not detected, suggesting that they had been completely carburized into tungsten carbides. Moreover, the XRD measurements did not reveal any metallic tungsten (W). However, as with the synthesis of molybdenum and nickel carbides, the formation of an orthorhombic crystal structure of tungsten phosphide (WP) (*JCPDS* No. 29-1364), has been observed during the H_2-TPR carburization of the tungsten oxides. This WP product is characterized by diffraction peaks at 2θ angles of 44.6°, 56.6°, 68.9°, and 85.8°, corresponding to the (110), (200), and (211) crystal planes, respectively. The peak at 44.6° is the most prominent. The emergence of this new phase, which may influence the catalytic activity of the tungsten carbide catalyst, as detailed for the other catalysts, Indicates an interaction between the active metal (W) and the support. Furthermore, the average crystallite size of this new WP phase appears to be 1.05 nm, which is slightly larger than NiP but far smaller than MoP.

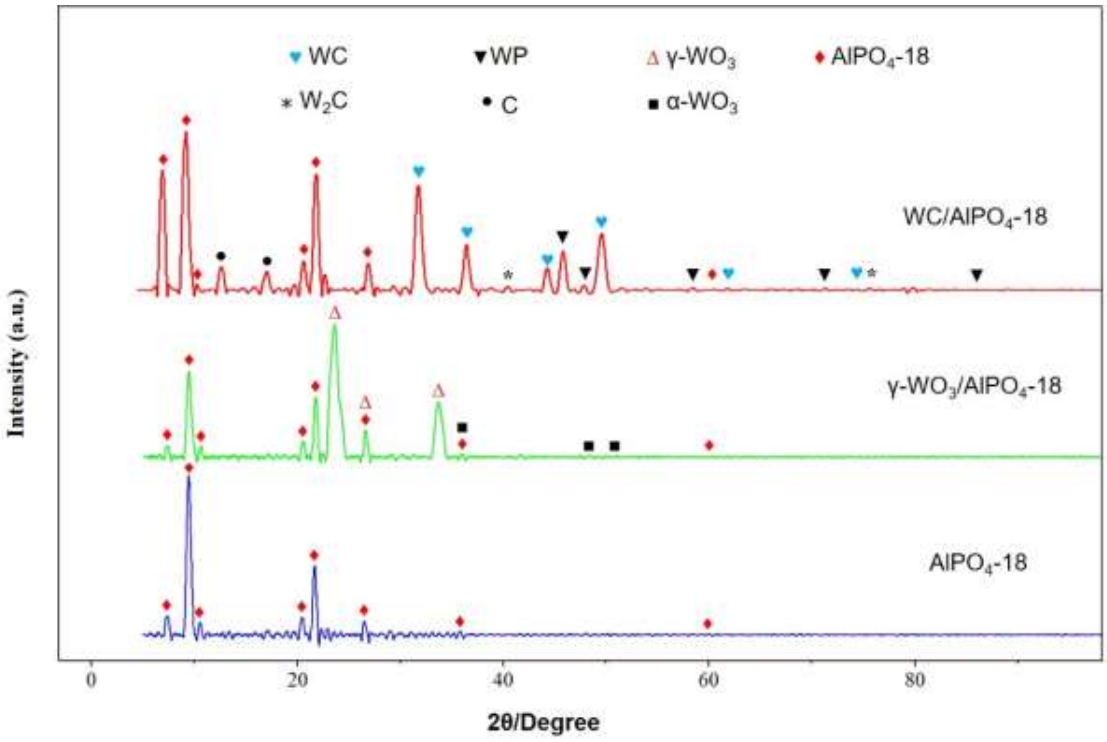

Figure 6.6 X-ray diffraction patterns of γ-WO_3/$AlPO_4$-18, and WC/$AlPO_4$-18 catalysts.

In general, except for the nickel-based catalyst, TPO TG-MS findings showed that there were no appreciable variations in the residual catalyst weights of the non-carbide catalyst support, and the carbide catalysts such as β-Mo_2C, suggesting that the introduction of these new phases has not resulted in the loss of thermal stability for the carbide phases. This may subsequently signify that even after carburization and thus the appearance of phosphides did not impair the thermal stability of the carbide catalysts.

The synthesis of carbide catalysts was greatly influenced by the incipient wetness impregnation followed by the reductive-carburizing gas stream of propane and hydrogen gas mixture, which resulted in the complete carburization of Ni and W-based catalysts. However, a residual uncarburized molybdenum oxide was found, implying that this catalyst's carburization was incomplete. Except for metallic nickel, whose diffraction peak is quite small, metallic tungsten and molybdenum were not recognized in the XRD study. This is particularly advantageous for Mo- and W-based catalysts since metallic phases are easier to sinter than carbides due to the lower melting temperatures of metallic nanoparticles [355].

Table 6.2 Summary of XRD results of $AlPO_4$-18 supported metal carbide catalysts.

Sample	Identified phase	Average crystallite size (D) (nm)	Average lattice constant (nm)	Lattice strain (ε)
$AlPO_4$-18	$AlPO_4$-18	0.15	-	-
β-Mo_2C/$AlPO_4$-18	β-Mo_2C	3.68	0.22	0.05
	MoP	3.68	0.36	0.05
	MoO_2	-	-	-
	C	-	0.72	-
Ni_3C/$AlPO_4$-18	Ni_3C	0.85	0.46	0.21
	NiC	0.85	-	0.21
	Ni	-	-	-
	Ni_2P	0.85	0.38	0.21
	C	-	0.72	-
WC/$AlPO_4$-18	WC	1.05	0.48	0.73
	W_2C	1.05	0.35	0.73
	WP	1.05	0.32	0.73
	C	-	0.72	-

6.3.2.4 Transmission electron microscopy-energy-dispersive X-ray spectroscopy analysis

The representative surface morphology and elemental composition images of the carbide catalysts that were formed during the TPRC process were analyzed using TEM/STEM-EDS as shown in Figures 6.7–6.8 and Figures 6.S4–6.S6. Figure 6.S4 shows the high-resolution TEM (HR-TEM) micrographs of the three carbide catalysts at four different magnifications (i.e., 500 nm, 200 nm, 100 nm, and 50 nm). The carbide nanoparticles' surface morphology showed that most of each of the nanoparticles (i.e., β-Mo_2C, Ni_3C, and WC) supported on the support material appeared as hexagonal, hexagonal, and square plate-like particles, respectively, as shown in Figures 6.S1, and 5.S4, and Figure 6.7. Figure 6.S1((d), (h), and (l)) provides a more detailed description of the surface morphology of individual metal carbide particles. These representative single particles help to better understand the surface morphology of the metal carbides. Metal particle size is an important characteristic to consider while designing an appropriate catalyst for various reactions since particle size not only influences activity but also plays a vital role in determining selectivity

[372]. As a result, the average crystallite sizes of the metal-containing particles were found to be 8.2–9.22 nm, 6.64–8.50 nm, and 6.03–7.56 nm for β-Mo_2C/$AlPO_4$-18, Ni_3C/$AlPO_4$-18, and WC/$AlPO_4$-18, respectively. The samples' average crystallite sizes, especially the β-Mo_2C/$AlPO_4$-18 sample, do not significantly deviate from the results of the prior study [335], which showed that the average Mo_2C particle size increased with temperature from 700 °C to 750 °C, yielding at 7.9 nm and 9.4 nm, respectively.

The nanoparticles are clearly visible as bright spots on the $AlPO_4$-18 support in the HAADF-STEM image (Figure 6.7) and as sharp and dark spots on the support (Figure 6.S4). These nanoparticles are not uniform in size, with some appearing larger and others appearing smaller (Figure 6.7, and Figure 6.S4). The fact that the particles varied in size can be more clearly articulated by the following key concept. Even though well-dispersed metal precursor may result in well-dispersed metal nanoparticles [372], an in-depth study into the structure-function relationships of heterogeneous catalysts increasingly suggests that catalysts are not only of static surface and bulk structures, they are dynamic entities that can change their structure in response to the specific reaction conditions within the reactor [373].

The results demonstrated that the crystallite sizes of the molybdenum-based nanoparticles are a little bigger than those of the nickel- and tungsten-based particles. This is in line with the crystallite sizes determined by XRD results. Moreover, the molybdenum catalyst had the smallest BET of the two catalysts based on the N_2-physisorption (previous section); this result can be correlated to the catalysts' highest TEM crystal sizes. Though the difference is not so significant, the crystallite sizes obtained by TEM/STEM study tend to be larger than those obtained using XRD analysis. In addition to the crystallite sizes, TEM analysis with the aid of ImageJ and the Fourier transforms HR TEM images shown as insets in (c), (f), and (i), enlarged view of the dashed boxes of (b), (e), and (h) of Figure 6.7, respectively, was performed to estimate the interplanar spacing (d) of the nanoparticles. The results indicated that the supported tungsten carbide had the smallest d value (0.05 nm); however, the supported molybdenum carbide had the next smallest d value of 0.13 nm, and that of the nickel carbide had the largest d value of 0.25 nm of all the catalysts studied. A summary of the TEM/STEM results is shown in Table 6.3.

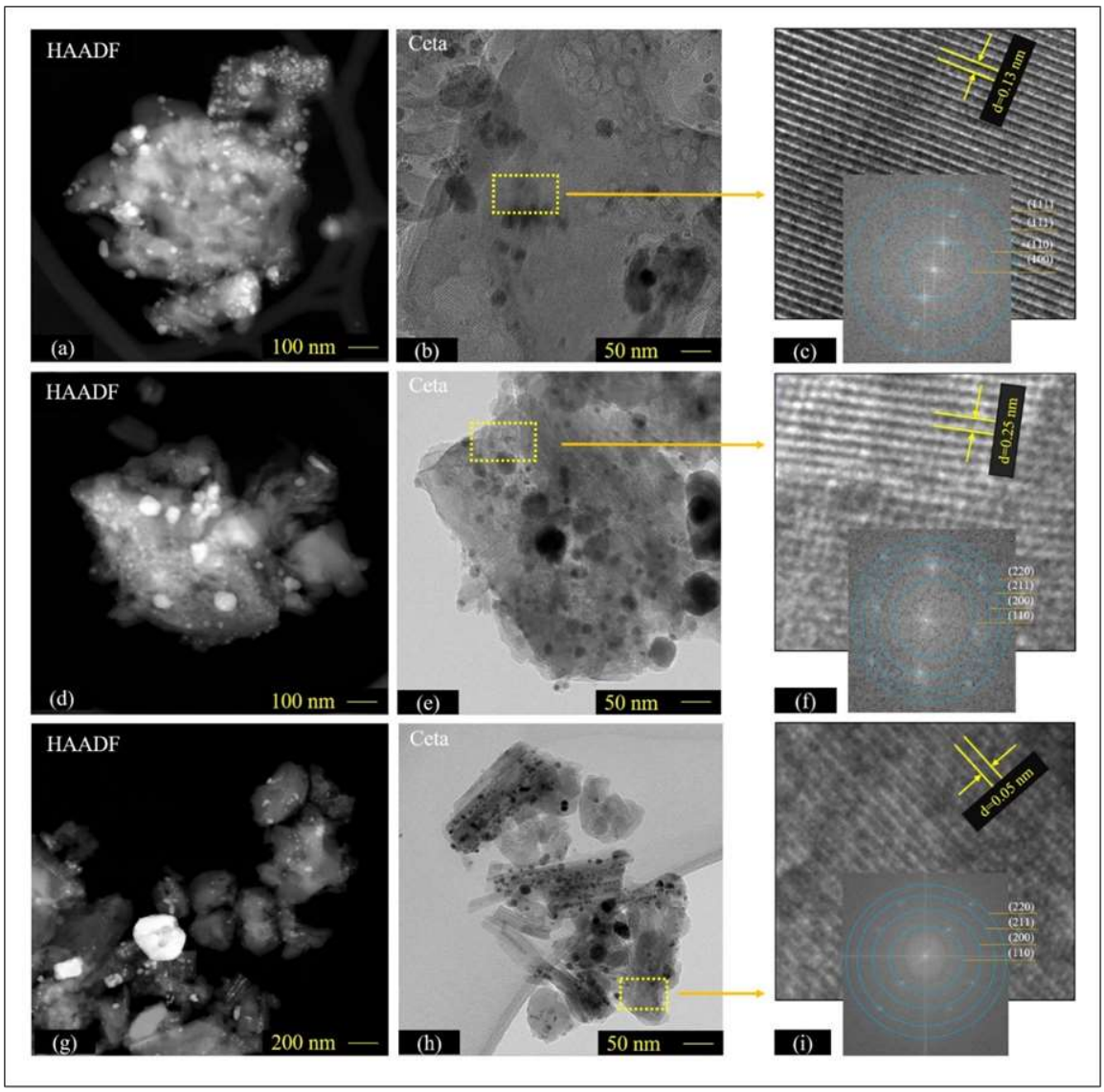

Figure 6.7 HAADF-TEM and Ceta-TEM images of $AlPO_4$-18 supported β-Mo_2C (a−c), Ni_3C (d−f), and WC (g−i) nanoparticles, with (c), (f), and (i) are enlarged TEM images from the dashed boxes in (b), (e), and (h), respectively.

The qualitative and quantitative elemental mapping of elements performed with STEM-EDX is shown in Figure 6.8 and Figures 6.S5–6.S6. The results showed the existence of the active metals Mo, Ni, and W, as well as the other elements including C, O, Al, P, and Si, with their atomic and mass fractions presented in Figure 6.S6. The C is derived from the carburizing C_3H_8 gas, while the O, Al, P, and traces of Si come from the support, with the possibility of some residual O species

due to the absence of passivation. These metal-containing nanoparticles, with special attention paid to the distribution of Mo-C, Ni-C, and W-C, are vividly depicted as magnified TEM images for better clarity in (c), (f), and (i), respectively, of Figure 6.8. This further emphasizes how well dispersed the active metals Mo, Ni, and W are over the support. This observation could suggest that these carbon-coated nanoparticle carbides have been successfully produced via the H_2-TPR carburization process. The nominal (theoretical) metal loading that was applied during the catalysts' incipient wetness impregnation is compared to the actual composition of each of the catalysts (Table 6.4), as ascertained by elemental mapping (Figure 6.S6). The results showed an excellent correlation between the nominal and actual compositions of the catalysts, validating the deposition of metal nanoparticles on the support. The tungsten-based nanoparticles, on the other hand, exhibit a discrepancy between nominal and actual metal loadings, for which we provided the following observation recorded during the reduction-carburization experiment. In contrast to the synthesis of the other carbide nanoparticles, a white-colored gaseous stream was observed during the synthesis of tungsten carbide, and the following prior study provides evidence to substantiate the experimental observation. According to [374], tungsten is shown to evaporate in steam at temperatures higher than 800 °C, and the vapor immediately condensed to a fine white aerosol as it left the metal surface and was convected away in the steam boundary layer.

Table 6.3 Morphological and structural characterization of $AlPO_4$-18 supported metal carbide catalysts using TEM/STEM, as well as comparisons of XRD average crystallite sizes to TEM data.

Catalyst	**TEM analysis**			**XRD analysis**
	Surface morphology	**Average crystallite size (nm)**	**Interplanar spacing (d) (nm)**	**Average crystallite size (nm)**
β-Mo_2C/$AlPO_4$-18	Hexagonal plates	8.20–9.22	0.13	3.68
Ni_3C/$AlPO_4$-18	Hexagonal plates	6.64–8.50	0.25	0.85
WC/$AlPO_4$-18	Square plates	6.03–7.56	0.05	1.05

Even though the presence of free surface carbon was assessed by TPO TG-MS in the prior section, the carbon-to-metal ratios (i.e., C/Mo, C/Ni, and C/W) were also determined from EDS analysis, as indicated in Table 6.4. Although the synthesis conditions and catalysts differ from the current samples, the following reported study could serve as a general framework for evaluating the nature

of surface-free carbon present in the catalysts. Based on [375], the range of C/Mo ratios (i.e., 0.556, 0.588, and 0.667, respectively, from Mo_2C, Au/Mo_2C, and Mo_2C/Al_2O_3) that they found suggests that the samples have fully carburized, and the extra carbon present may be the result of free surface carbon. Furthermore, [355] stated that C/Mo close to 0.5 indicated complete carburization because this ratio is close to the optimal stoichiometry of Mo_2C [C/Mo = 0.5], whereas the C/Mo ratios of the present investigation (Table 6.4) showed a little higher value. This modest deviation from the reported results above may indicate the existence of free surface carbon on the surface of the Mo-based catalyst. This might then be supported by the XRD results stated in the earlier section. To further emphasize the XRD analysis detailed earlier, which showed the presence of metal phosphide phases in addition to metal carbides, the representative nanoparticles of which are shown in Figure 6.S5 as P-Mo, P-Ni, and P-W.

Table 6.4 Nominal and actual metal compositions, and carbon-to-metal ratios of metal carbide catalysts.

Catalyst	Nominal loading (%)	Actual loading (%)	Carbon-to-metal ratio
β-$Mo_2C/AlPO_4$-18	15	14.73	1.20
$Ni_3C/AlPO_4$-18	15	16.68	1.74
$WC/AlPO_4$-18	15	7.36	0.79

The XRD investigation showed that, except for molybdenum carbide, all two catalysts underwent complete carburization, signaling that the final carburized catalyst is free of metal oxide phases. This is best illustrated by the earlier reported work on molybdenum carbide catalysts, which states that complete carburization of the oxide-type precursor plays an essential role in increasing the catalytic activity of the catalyst in hydrogenation reactions even at the expense of the final material's specific surface area [376]. As a result, considering the complete carburization of the carbide catalysts, the actual oxygen content determined by the EDS analysis (Figure 6.S6) might be attributed to residual O species on the catalysts' surface (particularly the Ni- and W-based ones) and oxygen from the support ($AlPO_4$-18). The presence of residual O species on the surface of the catalysts could, in turn, be attributed to the fact that the final metal carbide catalysts were not passivated. These nanoparticles with very small average crystallite sizes (i.e., less than 10 nm) and well-dispersed carbon-coated metal carbides may have enhanced catalytic performances. This

finding is further strengthened by the following reported investigation, which stated that decreasing particle size can improve the catalytic activity of supported metal nanoparticles by enhancing dispersion or metal utilization on the particles' surfaces [372].

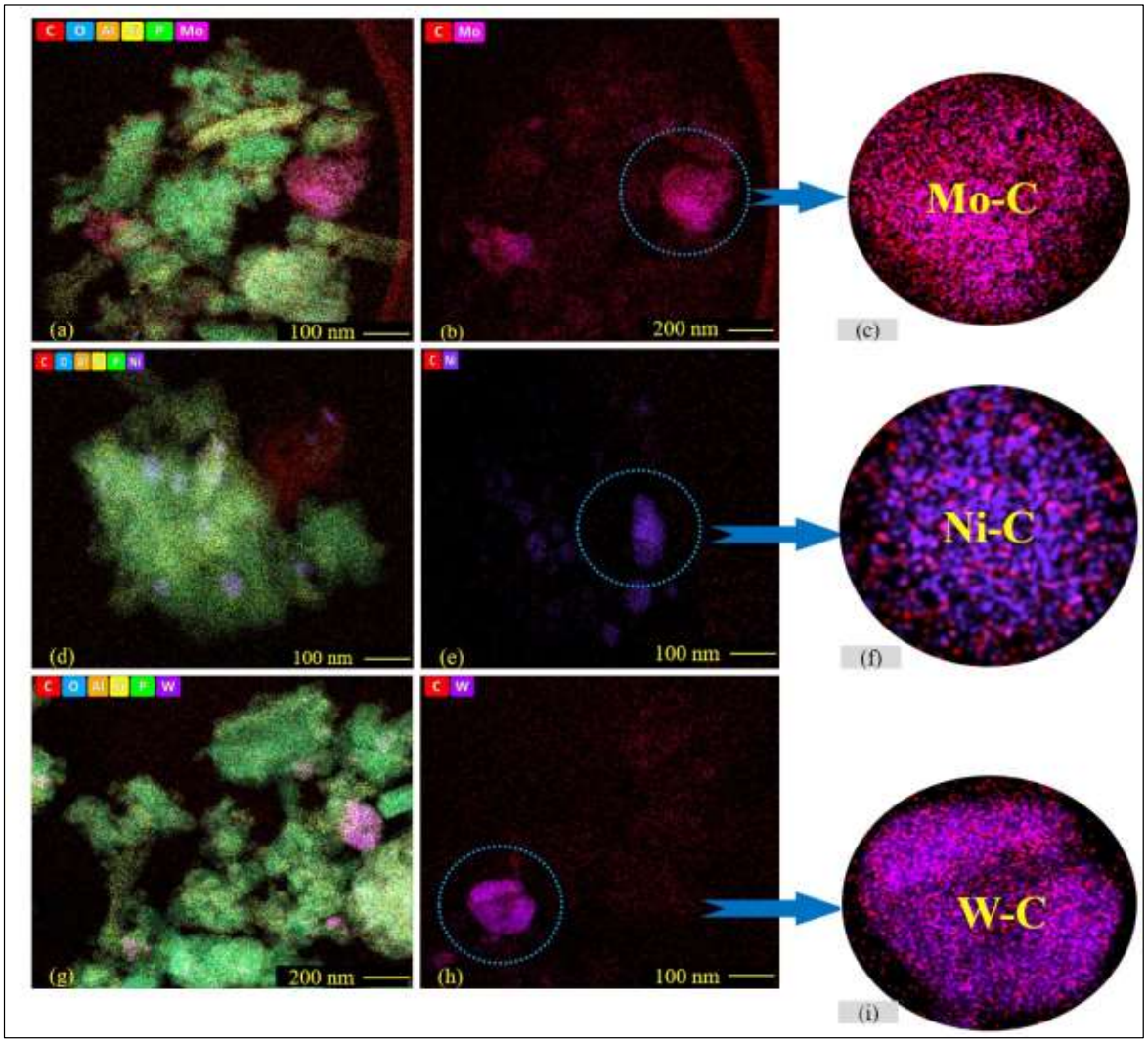

Figure 6.8 HAADF-STEM image with EDS mapping of $AlPO_4$-18 supported β-Mo_2C (a−c); Ni_3C (d−f); and WC (g−i) nanoparticles with (c), (f), and (i) are enlarged TEM images from the dashed circles in (b), (e), and (h), respectively.

6.5 Conclusions

The present study used propane-hydrogen gas mixture for the incipient wetness impregnation (IWI) followed by temperature-programmed reduction-carburization synthesis method, with XRD

characterization showing the formation of the most prominent carbide phases (i.e., β-Mo_2C, Ni_3C, and WC) on the catalyst support, and traces of other phases (such as MoO_2, NiC, Ni, W_2C, and C). The absence of diffraction peaks of nickel and tungsten oxides in their corresponding carbides shows that the carbide catalysts underwent complete carburization. The molybdenum carbide catalyst, on the other hand, experienced incomplete carburization, as evidenced by the appearance of a less intense and very small diffraction peak at $2\theta = 32.0^{o}$, which could be a distinguishing property of MoO_2. In comparison to β-$Mo_2C/AlPO_4$-18, and $Ni_3C/AlPO_4$-18 catalysts, TEM results confirmed that $WC/AlPO_4$-18 had the smallest average crystallite sizes, varying from 6.03 to 7.56 nm, and the smallest interplanar spacing, measuring 0.05 nm. Characterization of the carbide catalysts by TPO TG-MS, XRD, and carbon-to-metal ratios (from EDX) proved the presence of unreacted free surface carbon species on the surface of the nanoparticles. The catalyst support's BET surface area considerably decreased after air calcination when generating the precursor-dopped metal oxides and carburization forming metal nano carbides, with the metal carbides having smaller BETs than their analogous oxides. The TPO TG-MS results also confirmed that the catalyst support was determined to be thermally stable when exposed to severe temperatures reaching up to 1000 °C.

The most significant supporting figures including Figures 6.S1–6.S6 for this chapter are presented in Appendix B.

CHAPTER SEVEN

Catalytic Hydroprocessing of Yellow Dodolla Oil Using Thermally Stable and Mesoporous $AlPO_4$-18 Supported β-Mo_2C, Ni_3C, and WC Catalysts to Produce Bio-Jet Fuel

7.1 Introduction

In the early days of the jet era, speed and luxury were the two primary factors behind transcontinental travel. Since then, efficiency has been an enormous stimulant in the development of air travel and transportation as fundamental elements of modern society. Indeed, contemporary airliners are lighter and more aerodynamic than ever before, and engines are operating at the highest possible level of efficiency. We are significantly enhancing the effectiveness of air traffic management, and aircraft operation, and the development of less environmentally harmful airport practices. However, we continue to use the same kind of fuel for the great majority of our flights [377]. Today, civil aviation depends almost entirely on Jet A-1 (kerosene) derived from crude oil [378]. Despite this, rapid global trade and people-to-destination transportation are rendered possible to a significant extent by the industry [32]. Notwithstanding all of these advantages, the biggest downside of air travel is its enormous contribution to greenhouse gas (GHG) emissions [379]. The industry consumes around 2 billion barrels of petroleum each year, which is responsible for a substantial amount of GHG emissions into the atmosphere contributing a significant portion of global CO_2 emissions, emitting 669 million tons of CO_2 yearly [284].

Bio-jet fuel is one of the most significant forms of renewable and green energy, predicted to gradually take the place of fossil fuels with higher blending ratios in the near future [380]. It has been accentuated as a short- to medium-term approach to lowering the industry's total GHG emissions [8]. These environmentally friendly aviation fuels can significantly reduce the adverse environmental effects of the aviation sector since they can lower CO_2 emissions by up to 80% over the course of their lifecycle [60]. Recent research from the US Department of Energy (USDOE) states that jet fuel derived from crude oil is composed of a variety of hydrocarbons, such as *n*-alkanes (straight-chain paraffin), iso-alkanes (branched paraffin), cycloalkanes, and aromatics in the carbon range of C_8 to C_{16} [381], with olefin content being generally limited to less than 1% in

the jet fuel [382]. Bio-jet fuel, also known as bio-kerosene, is a mixture of hydrocarbons with boiling points ranging from C_8 to C_{16} that has the same properties as conventional jet fuel as defined by ASTM D1655 and contains the same components [380], [383].

Many bio-jet fuel conversion technologies, whether in the research and development, demonstration, or commercial stages, are described in the literature. An in-depth understanding of all upgrading technologies—approved and pending—from laboratory to commercial scale is required for accurately evaluating the current state of progress for biomass-to-jet fuel development [100]. The American Society for Testing and Materials (ASTM) is the regulating organization responsible for defining the specifications for aviation fuels in ASTM D1655 Standard Specification for Aviation Turbine Fuels [384]. This Standard Specification has recognized various technological approaches for producing bio-jet fuels [385] including hydroprocessed esters and fatty acids synthesis derived from oil & fat [386], biomass gasification Fischer – Tropsch (FT) synthesis [387], direct sugars to hydrocarbon via fermentation derived from sugar-rich feedstock and alcohol. Other pathways are still under the research and development stages, such as catalytic hydro-thermolysis [388], and hydrothermal liquefaction [389] of cellulosic biomass.

During hydroprocessing, two distinct processes, hydrotreating, and hydrocracking, may occur concurrently [390]. Triglyceride conversions over hydrotreating catalysts in the presence of hydrogen have complex reaction pathways and consist of parallel and/or consecutive reaction steps, such as saturation, cracking, decarboxylation, decarbonylation, and/or hydrodeoxygenation [130]. The decarbonylation/decarboxylation (DCO) reactions cleave the C–C bond associated with the carbonyl group or carboxyl group, resulting in loss of carbon and decreasing the energy content of the molecule. On the other hand, the hydrodeoxygenation (HDO) reaction selectively cleaves the C–O/C=O bond while preserving the carbon chain length. Moreover, under sufficient H_2 partial pressure, the HDO reaction removes oxygen in the form of H_2O instead of CO_2 and is therefore more environmentally friendly than DCO regarding CO_2 emission [391]. In general, as stated in [392], the three strategies that have been adopted to remove oxygen from fatty acids can be demonstrated as shown in Scheme 7.1. According to Scheme 7.1, the degree of H_2 consumption varies as follows: decarboxylation ($deCO_2$) < decarbonylation (deCO) < hydrodeoxygenation (HDO). An efficient HDO catalyst should effectively remove oxygen with low hydrogen consumption and suppress the coke formation that leads to catalyst deactivation [393].

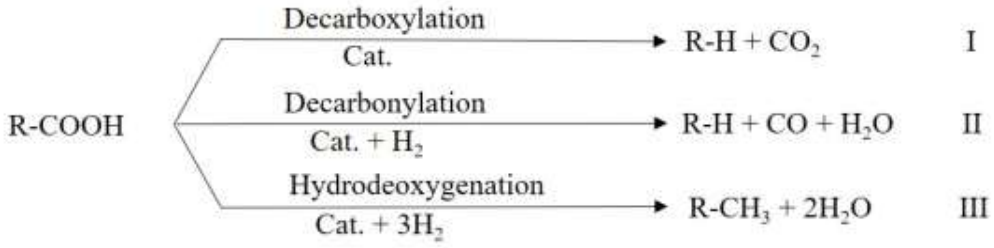

Scheme 7.1 Three proposed mechanisms for the deoxygenation of fatty acids into hydrocarbons: $deCO_2$ (I), deCO (II), and HDO (III).

In the present work, a novel feedstock known as Yellow Dodolla oil—one of the most promising and potential alternative feedstocks for the aviation industry—was upgraded into bio-jet fuel using supported mesoporous transition metal carbide catalysts (i.e., β-$Mo_2C/AlPO_4$-18, $Ni_3C/AlPO_4$-18, and $WC/AlPO_4$-18). The bio-jet fuel was produced using a single pot oil-to-jet catalytic hydroprocessing method in a laboratory-scale designed three-phase continuous fixed-bed reactor system at different temperatures (i.e., 300 and 500 °C) and an elevated hydrogen pressure of 21 bar. All other variables, including volumetric flow rate of oil feedstock (0.30 mL min^{-1}), volumetric flow rate of hydrogen gas (350 mL min^{-1}), hydrogen gas-to-oil ratio (1,667 mL H_2 gas per mL oil), catalyst-to-oil ratio (0.14 g catalyst per g oil), liquid hourly space velocity (LHSV) (2.41 h^{-1}), weight hourly space velocity (WHSV) (2.78 h^{-1}), and residence time (2.5 h), were maintained constant in all experiments. After a comprehensive analysis aimed at evaluating the catalysts' catalytic performances, a detailed characterization of the liquid products was carried out.

7.2 Materials and Methods

7.2.1 Chemicals and materials

Ultra-high purity grade gases such as hydrogen gas (H_2, 99.999%) (Air Liquide, French), and nitrogen gas (N_2, 99.999%) (Air Liquide, French), crystalline and mesoporous synthesized β-$Mo_2C/AlPO_4$-18, $Ni_3C/AlPO_4$-18, and $WC/AlPO_4$-18 catalysts, and hexane-extracted inedible Yellow Dodolla vegetable oil are the most significant chemicals and materials used throughout this investigation. In addition, chemically inert and non-porous aluminum oxide ceramic balls were obtained from Faculty 1, University of Applied Sciences (HTW) Berlin. Glass-type gas mouse, copper wire, pipes made of stainless steel with varying internal diameters, and various types of

valves, were also the most important materials utilized in the study. To keep things simple, the catalysts β-$Mo_2C/AlPO_4$-18, $Ni_3C/AlPO_4$-18, and $WC/AlPO_4$-18 can be referred to as molybdenum, nickel, and tungsten catalysts, respectively.

7.2.2 Analytical methods

7.2.2.1 Preparation of feedstock

The quality of feedstock is of the utmost importance because it affects not only the quality of the product but also the rate of hydrogenation [394]. As a result, among the numerous *Brassica carinata* oils that were thoroughly studied in our earlier investigation [24], Yellow Dodolla is one of the most prominent *Brassica carinata* cultivars growing in Ethiopia, and its hexane-extracted vegetable oil was consequently used for the present study. The oil is characterized by having very high oil content (45.25%), and its notable properties including pH, refractive index (at 20 ℃), density (at 15 ℃), acid value, iodine value, ash content, saponification value, with values of 5.33 ± 0.01, 1.473 ± 0.00, 907.75 ± 0.00 kg/m^3, 0.45 mg KOH/g, 95.15 g I2/100 g oil, 0.02 ± 0.00 wt.%, and 171.73 mg KOH/g, respectively [24]. Furthermore, the oil has kinematic viscosities of 109.39 ± 0.00, 69.46 ± 0.08, and 12.89 ± 0.00 mm^2 s^{-1}, at 25, 40, and 100 ℃, respectively. The aforesaid earlier study also contains comprehensive characterization findings on the oil's chemical composition (i.e., C, H, N, S, and O), H/C and O/C atomic ratios, metals and phosphorus contents, gross and net calorific values, fatty acid profiles, degrees of saturation and unsaturation of fatty acids, and functional group analysis. Before being used, the feedstock was, however, air-dried using an oven drying (Memmert GmbH + Co.KG, Schwabach, Germany) to remove any residual moisture, and its total moisture content was determined to be 0.01 weight percent based on (AOAC 925.10).

7.2.2.2 Hydroprocessing catalysts

The bio-jet fuel was produced utilizing catalysts synthesized at 800 ℃ carburization temperature by incipient wetness impregnation (IWI) followed by temperature-programmed reduction-carburization in a propane-hydrogen reductive-carburization gas mixture, as described in our previous work [395]. According to the study, the supported carbon-coated metal carbide nanoparticles (i.e., β-$Mo_2C/AlPO_4$-18, $Ni_3C/AlPO_4$-18, and $WC/AlPO_4$-18) possess notable characterization properties including high surface areas (66.57, 169.05, and 193.79 m^2 g$^{-1,}$

respectively) and high thermal stability. The mesoporous crystalline structures and average crystallite sizes of 8.2–9.22 nm, 6.64–8.50 nm, and 6.03–7.56 nm for β-Mo_2C/$AlPO_4$-18, Ni_3C/$AlPO_4$-18, and WC/$AlPO_4$-18, respectively, are additional distinguishing properties of the metal-containing nanoparticles. In addition, the aforementioned article has additional significant features of the catalysts.

7.2.2.3 Catalytic hydroprocessing of Yellow Dodolla oil

A. Design of a fixed-bed reactor system

Temperature, reaction rate, residence time, heat transfer rate, catalyst type, product selectivity, and yield are all significant process control parameters that are influenced by the type of reactor [396], [397], [398]. As a result, selecting the appropriate reactor is of the utmost importance for hydrocracking and deoxygenation of triglyceride (TG)-based feedstocks for jet fuel production. Laboratory-scale reactors are used in the majority of reported studies on catalytic cracking of biofuel production. Glass types, fixed bed reactors, and fixed fluidized bed reactors are among the laboratory reactors utilized for catalytic activity studies [399]. The fixed-bed reactor is the most prevalent type of reactor used for catalytic cracking of plant oils. This reactor configuration provides good mass and heat transfer distributions of the oil feed to avoid clogging, entrainment, and channeling, which are among the primary challenges in catalytic cracking reactions [400]. To better explain why fixed-bed reactors are superior to other reactors include the following critical reasons why fixed-bed reactors enhanced mass transfer (improved contact and reduced mass transfer resistance), temperature control (effective heat exchange and reduced hot spots), and flexibility (scalability and operational flexibility) for hydroprocessing.

Figure 7.1 and Figure 7.S1 demonstrate the lab-scale constructed three-phase continuous fixed-bed reactor system. Figure 7.1 presents a clear view of the reactor's internal components, with the actual ceramic balls, perforated mesh, and carbide catalyst photos ensembled into it, which could then serve as a model for the real reactor. The cylindrical hydroprocessing reactor was designed and constructed from a stainless-steel pipe with an internal diameter (I.D.), external diameter (O.D.), and length of 10, 12, and 216 mm, respectively, with its volume being 7.46 cm^3 (i.e., 0.00746 L). The primary components of the fixed-bed reactor system (Figure 7.1 (b), Figure 7.S1 (a), and Figure 7.S2) consist of the feed system, the reactor system, the cooling system, and the product separation system. The reactor is outfitted with an electrical heating system that consists of the

following major components: a glass fiber insulated heating tape (KM-HT-BS30, SAF Wärmetechnik), an RFT variable transformer (TST280/1, RFT, Germany), a voltmeter, Almemo data acquisition module (8590-9), and an N-type thermocouple (Nicrsil-Nisil). A high-pressure hose (Hy Lok Corporation, South Korea) was put to use for hydrogen and nitrogen gas flows and can manage up to 24 bars of pressure, while a pressure gauge (Wika, Germany) was used to read the pressure and can handle up to 25 bar of pressure. A microcomputer running AMR Win Control 7 software controls the temperature change over time.

Catalyst loading was carried out based on Figure 7.1, which depicts the step-wise loading of 7.3 g of inert and non-porous Al_2O_3 ceramic balls, and 5.87 g of catalyst, with extreme caution taken not to cause any damage to the catalysts. The ceramic balls are added to the reactor during catalyst loading to provide a stable and supportive structure for the catalyst particles. They also help prevent the catalyst from crushing or breaking under the weight of the overlying material, ensuring its integrity throughout the reaction process. Moreover, the addition of ceramic balls can help to improve the distribution of reactants and products within the reactor bed. By creating a more open structure, the ceramic balls can reduce channeling and dead zones, ensuring that the reactants come into contact with the catalyst more effectively. They can help to protect the catalyst particles from abrasion and attrition, which can occur during the reaction process. This can extend the catalyst's lifespan and reduce the need for frequent replacements. By providing a more open structure, the ceramic balls can facilitate the flow of heat, ensuring that the catalyst is evenly heated and cooled during the reaction.

The perforated mesh (I.D.=1 mm), which serves as a fixed-bed for the catalysts, was properly put into the reactor before the ceramic balls and catalysts were loaded. Once the catalyst was loaded, the entire system was flushed with nitrogen gas for approximately 5 min to remove air, and an *in-situ* activation of the catalyst was performed using H_2. The catalyst reduction/activation, which helps the catalyst to be in its desired state, was carried out using H_2 flowing at 340 mL min^{-1} which is regulated using a Drum-type gas meter (TG3-PVC-PVC, Germany), 21 bar pressure, at a temperature of 550 °C ramped-up at a heating rate of 3–5 °C min^{-1} which was maintained for about 1 h. The online microcomputer running AMR Win Control 7 software that was connected to the reactor was also used to regulate the quantity of water vapor generated during the catalyst reduction process.

B. Single-pot bio-jet fuel production

One of the most significant variables affecting the hydrogenation of TGs, the conversion of TG-based oils, the distribution of products, and their selectivity is temperature. The reaction temperature is also crucial for maximizing catalyst activation and minimizing catalyst sintering [401]. Since one of the most significant factors in determining the end products' quality and selectivity in hydroprocessing is the type of catalyst system employed [402], the type of catalyst is considered one of the significant variables during catalytic hydroprocessing of Yellow Dodolla oil. As a result, to gain a broader understanding of the impact of the carbide catalysts on deoxygenation and cracking reactions, a study of their performance was conducted at two distinct temperatures (300 and 500 °C).

This evaluation was based on the findings of [72], [141] which reported that catalytic cracking of vegetable oils generally transpired at reaction temperatures ranging from 380 to 525 °C. Even though two temperature points may provide some initial insights, it is often recommended to conduct experiments at a wider range of temperatures to obtain a more comprehensive understanding of the reaction kinetics and to ensure that the reactor design is robust and can accommodate potential variations in operating conditions. Following loading and catalyst activation, the reactor was slowly pressurized to an elevated H_2 pressure (21 bars) at a flow rate of 350 mL min^{-1} and was heated up to 300, and 500 °C, respectively, for deoxygenation and cracking reactions, at 3.5 °C min^{-1} heating rate. The reactor's temperatures were adjusted by varying the voltage levels using the voltmeter and variable transformer (as mentioned above), with values of 73 V and 0.5 A for the lower temperature and 110 V and 0.72 A for the higher temperature.

Achieving the intended selectivity of hydroprocessing distillates and the conversion percentage depends on the hydrogen-to-oil ratio, with hydrocarbons generally breaking and converting more readily at higher hydrogen-to-oil ratios [403]. Once the temperature and pressure stabilized, Yellow Dodolla oil (42 g) was introduced into the reactor in downflow mode at a flow rate of 0.30 mL min^{-1} using a Hitachi L-6200A HPLC pump (Hitachi L-6200A Intelligent Pump) capable of pumping pressures of up to 400 bar. The oil was supplied with hydrogen gas at a ratio of 1667:1 (mL H_2/mL oil), ensuring uniform reactant distribution and simplified temperature control.

The oil delivered to the reactor required a pressure bigger than the reactor's internal pressure (21 bar), and thus 30 bar was utilized to pump the oil feed. Furthermore, the catalyst-to-oil ratio was

0.14 g catalyst per g oil feed. Equations 6.1 and 6.2 below are used to determine the other variables, including liquid hourly space velocity (LHSV), and weight hourly space velocity (WHSV), with values of 2.41 h^{-1}, and 2.78 h^{-1}, respectively. These variables show that the reactor can process a liquid feed equivalent to 2.41 times the reactor volume and 2.78 times the catalyst mass per hour, respectively. Even though the pumping pressure of the feed was greater than the reactor's pressure, purging was mandatory and was performed at 9.99 bar before each experimental run to ensure that no gas bubbles or oil droplets remained in the HPLC pump's dosing line. Following 2.5 h of residence time for each of the cracking and deoxygenation reactions, liquid phase products were recovered from the bottom of the reactor.

$$\text{LHSV } (\text{h}^{-1}) = \frac{\text{Volume of liquid feed per hour}}{\text{Volume of reactor}} \tag{7.1}$$

$$\text{WHSV } (\text{h}^{-1}) = \frac{Weight\ of\ feed\ per\ hour}{\text{Weight of catalyst}} \tag{7.2}$$

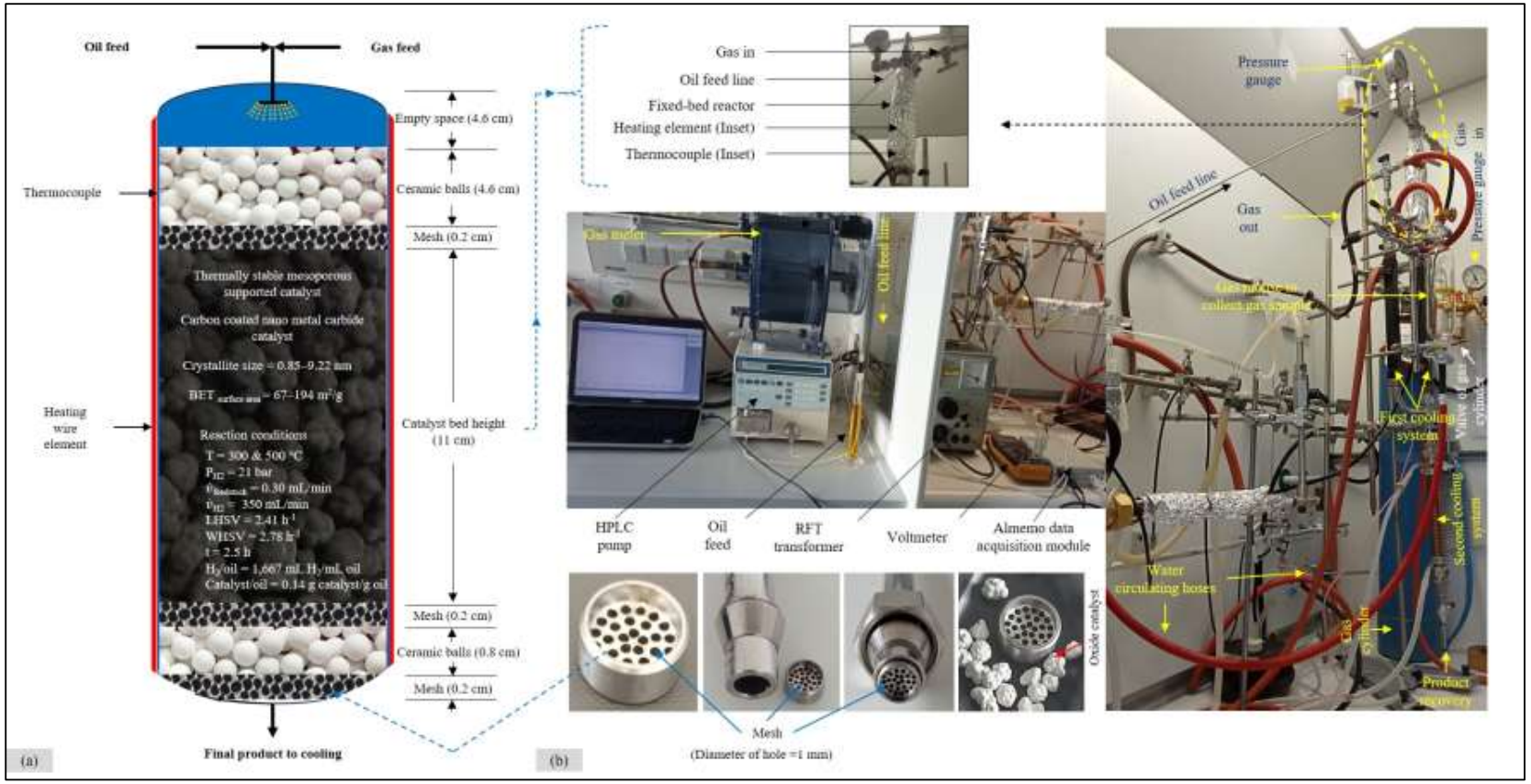

Figure 7.1 Laboratory-scale three-phase continuous fixed-bed reactor system. (a) Schematic representation of reactor system loaded with Al_2O_3 inert ceramic balls and catalyst, (b) Experimental setup of fixed-bed reactor system.

7.2.2.4 Catalytic performance evaluation

A. Qualitative and quantitative analysis of liquid organic products

To gain a deeper understanding of the composition and characteristics of the weight percentages of each class of hydrocarbon fuels, and to evaluate the catalytic performance of catalysts, an offline gas chromatography-mass spectrometry system (GC-MS, Agilent 7820A GC) equipped with a capillary column mass selective detector (60 m, 0.25 mm ID, 1.4 μm thickness, HP 5977) was used. Helium was employed as the carrier gas at a constant flow rate of 1 mL min^{-1} and a volume injection of 1 L. The injector and detector had respective temperatures of 250 and 280 ℃. The oven temperature was adjusted to 50 ℃ (isothermal for 4 minutes), 280 ℃ at 30 ℃ min^{-1} for 10 minutes, and 280 ℃ (isothermal), with the mass scan range being set to 29–800 amu. The analysis was conducted at Addis Ababa University (AAU), Addis Ababa, Ethiopia, at the Instrument Laboratory, Department of Chemistry.

B. Evaluation of conversion, yield, and selectivity of liquid phase products

After quantifying the chemical constituents of the liquid phase products resulting from the deoxygenation and hydrocracking reactions, the conversion, yield, selectivity, and rate of deoxygenation percentages are determined using the following equations (i.e., equations 7.3−7.14).

$$Conversion\ at\ 300\ ℃\ (wt.\%) = \frac{Feed_{(FA+TG)\ at\ 300\ ℃} - Product_{(FA+TG)\ at\ 300\ ℃}}{Feed_{(FA+TG)\ at\ 300\ ℃}} * 100 \quad (7.3)$$

$$Conversion\ at\ 500\ ℃\ (wt.\%) = \frac{Feed_{(FA+TG)at\ 500\ ℃} - Product_{(FA+TG)\ at\ 500\ ℃}}{Feed_{(FA+TG)at\ 500\ ℃}} * 100 \quad (7.4)$$

where Feed $_{FA+TG}$ is the weight percentage of fatty acids (FA) and triglycerides (TG) in feed, and Product $_{FA+TG}$ is the weight percent of FA and TG in the product.

$$Gasoline\ selectivity\ (wt.\%) = \frac{\mathrm{Product}_{(C4-C12)} - \mathrm{Feed}_{(C4-C12)}}{\mathrm{Feed}_{(FA+TG)} - \mathrm{Product}_{(FA+TG)}} * 100 \quad (7.5)$$

$$Jet\ fuel\ selectivity\ \ (wt.\%) = \frac{Product_{(C8-C16)} - Feed_{(C8-C16)}}{Feed_{(FA+TG)} - Product_{(FA+TG)}} * 100 \quad (7.6)$$

$$\mathrm{Diesel\ selectivity\ (wt.\%)} = \frac{\mathrm{Product}_{C12-C20} - \mathrm{Feed}_{C12-C20}}{\mathrm{Feed}_{FA+TG} - \mathrm{Product}_{FA+TG}} * 100 \quad (7.7)$$

where $Feed_{C4\text{-}C12}$ and $Product_{C4\text{-}C12}$ are the weight percentages of n-paraffins, olefins, and aromatics that are responsible for the gasoline range (C_4–C_{12}) hydrocarbons in the feed and product, respectively. The $Feed_{C8\text{-}C16}$ and $Product_{C8\text{-}C16}$ are the weight percentages of n-paraffins, iso-paraffins, cycloparaffins, aromatics, and olefins that are responsible for the jet fuel range (C_8–C_{16}) hydrocarbons in the feed and product, respectively. The $Feed_{C12\text{-}C20}$ and $Product_{C12\text{-}C20}$ are the weight percentages of n-paraffins, naphthenes, and aromatics that are responsible for the diesel range (C_{12}–C_{20}) hydrocarbons in the feed and product, respectively.

The liquid and gas fractions can be calculated by equations 7.8 and 7.9, respectively.

$$\text{Liquid fraction } (-) = \frac{\text{Weight of liquid product}}{\text{Weight of liquid feed}} \tag{7.8}$$

$$\text{Gas fraction } (-) = 1 - \frac{\text{Weight of liquid product}}{\text{Weight of liquid feed}} \tag{7.9}$$

Yields of fuels (i.e., gasoline, jet, diesel, and hydrocarbon) can be determined using equations 7.10−7.12.

$$Gasoline\ yield\ (wt.\%) = liquid\ fraction\ \times conversion\ \times gasoline\ selectivity \tag{7.10}$$

$$Jet\ fuel\ yield\ (wt.\%) = liquid\ fraction\ \times conversion\ \times jet\ fuel\ selectivity \tag{7.11}$$

$$Diesel\ yield\ (wt.\%) = liquid\ fraction\ \times conversion\ \times diesel\ selectivity \tag{7.12}$$

$$Yield\ of\ hydrocarbon\ fuel\ (wt.\%) = gasoline\ yield\ + jet\ fuel\ yield\ + diesel\ yield \tag{7.13}$$

The rate of deoxygenation (DO, wt. %) can be determined using equation 6.14.

$$DO\ (wt.\%) = \frac{(O_1 - O_2)}{O_1} * 100 \tag{7.14}$$

where O_1 and O_2 are the oxygen content of oil feedstock and product, respectively.

7.2.2.5 Characterization of liquid phase products

The liquid organic fractions were first recovered and then subjected to physicochemical characterization, elemental composition analysis, atomic ratios of hydrogen to carbon (H/C) and oxygen to carbon (O/C), heating value analysis, and analysis of functional groups.

A. Physicochemical and rheological characterization

Moisture content must be quantified since its existence is undesirable. With a digital automatic Metrohm Karl Fischer titration (*870 KF Titrino plus)*, the moisture content was determined following the E DIN 51777 (2016-08) standard method using a 10 g sample. The pH values were determined with a standard pH meter (WTW inoLab pH 7110, Xylem). Given that fuel is often measured by volume, fuel density is of utmost importance for determining an aircraft's weight. Using the EN ISO 12185:1996 standard technique, the density was measured using a density balance (Kern 152/13, Gottl. Kern & Sohn GmbH, Germany) at the standard temperature (15.6 °C). The specific gravity of samples was estimated from the densities recorded at the given temperature by dividing it by the density of water. A refractometer (RFM960, Bellingham Stanley) was used to measure the samples' refractive index (RI) at 20 °C following AOAC 921.08. Using HAAKE VT 550 from Thermo Fisher Scientific, the dynamic viscosity (η) of the liquid phase products was measured at room temperature (23–26 °C) using 9 mL of a sample.

In an electrically heated chamber Nabertherm furnace (L5/C6, Nabertherm GmbH, Germany), the total ash content of samples was ascertained using the ASTM D 482 standard testing technique, with approximately 5 mL of a sample used for analysis. The flash point is related to volatility, and so influences the fuel's combustibility. Determining fuel handling fire safety is essential. A minimum flash point of 38 °C is established by ASTM D1655 (2004). Based on the ASTM D92 standard (ASTM, 1995a through 1995d), this procedure was performed utilizing the open-cup flash point Apparatus. In addition, measurements of pour point, and cloud point were made in compliance with the relevant ASTM D97, and ASTM D2500, respectively, standard procedures from the American Society for Testing and Materials (ASTM, 1995a through 1995d). The liquid phase products' boiling points were determined using the Standard Test Method ASTM D2887.

B. Elemental composition, atomic ratio, and calorific value analysis

The weight percentage concentrations of total carbon (C), total hydrogen (H), total nitrogen (N), and total sulfur (S) were determined according to the following European standards: DIN 51732

(2014-07) for C and H, DIN 51732 mod. (2014-07) for N, and DIN EN ISO 16948:2015–09 for S content employing a CHNS analyzer (vario EL Cube, elementar, Langenselbold, Germany). The concentration of oxygen, on the other hand, was obtained by difference [i.e., 100 − (C + H + N + S + ash content)], following DIN 51733 (2016-04). The entire system was thoroughly flushed out using helium gas (He) before samples were injected for analysis. A sample was injected and combusted, and the resulting gases were detected as N_2 (first) with a thermal conductivity detector (TCD), CO_2 with a column carbon (second), H_2O with a column H (third), and SO_2 with a column S (finally detected). About 5 mg of a sample was used for each test, which was carried out in four replications to determine an average result. The analysis was carried out at the Technical University of Berlin, Germany.

After performing the CHNSO analysis, the atomic ratios H/C and O/C were estimated using equations 7.15 and 7.16.

$$\frac{\mathrm{H}}{\mathrm{C}} = \frac{\%\text{Hydrogen}/\text{Atomic weight of hydrogen}}{\%\text{Carbon}/\text{Atomic weight of carbon}} \tag{7.15}$$

$$\frac{\mathrm{O}}{\mathrm{C}} = \frac{\%\text{Oxygen}/\text{Atomic weight of oxygen}}{\%\text{Carbon}/\text{Atomic weight of carbon}} \tag{7.16}$$

The higher heating values (HHV), or the gross heating values (GHV) of the liquid fuels were estimated using equation 7.17 which was based on Channiwala and Parikh's unified equation [307] for solid, liquid, and gaseous fuels.

$$\mathrm{HHV\ (MJ/kg)} = 0.3491 * \mathrm{C} + 1.1783 * \mathrm{H} + 0.1005 * \mathrm{S} - 0.1034 * \mathrm{O} - 0.0151 * \mathrm{N} - 0.0211 * \mathrm{AC} \tag{7.17}$$

where C-carbon. H-hydrogen. S-sulphur. N-nitrogen. AC-ash content.

The low or net heat of combustion is determined based on the quantity of water formed, which can be obtained by the hydrogen content of the fuel, as two moles of hydrogen are required to form one mole of water (2 grams of H generates 18 grams of water) indicated as in equation 7.18 [404].

$$\mathrm{LHV\ (MJ/kg)} = \mathrm{HHV} - \left(\frac{\%\mathrm{H} \times 9}{100} \times \Delta \mathrm{H_v}\right) \tag{7.18}$$

where LHV-lower heating value. %H refers to the hydrogen concentration in fuel, and ΔH_v is the (latent) heat of vaporization of water, equal to 2.44 kJ/g.

C. Characterization of functional groups

With an FT-IR spectrometer (Spectrum 100, PerkinElmer, UK) equipped with built-in 6.1.1.0045 version Spectrum software for instrument monitoring and data input, the various functional groups of the liquid phase products hydroprocessed using the two different temperatures were analyzed using the attenuated total reflectance (ATR) sample method. The infrared spectra of the samples were obtained using the FT-IR, which was equipped with a deuterated triglycine sulfate (DTGS) detector and scanned the frequency range of 4000 to 550 cm^{-1} at a resolution of 2 cm^{-1} in transmission mode. A drop of the sample was applied to the surface of a diamond, a crystal with a high refractive index. At the Berlin University of Technology (BHT), in Berlin, Germany, the analysis was carried out in the Organic Chemistry Laboratory, Pharmaceutical, and Chemical Engineering Department.

7.3 Results and Discussion

7.3.1 Catalytic performance evaluation

The catalytic performance evaluation of the synthesized $AlPO_4$-18 supported transition metal carbide nanoparticles was performed for Yellow Dodolla oil conversion under the reaction conditions described earlier. The section that follows provides a detailed analysis of the influence of temperature and catalyst type on conversion, yield, selectivity, and liquid product distribution.

7.3.1.1 Effect of reaction conditions and catalyst type on conversion, yield, selectivity, and distribution of liquid products

With hydrocarbons (C_7 and higher), as well as multiple other compounds including oxygen and other traces of impurities, the liquid organic fractions were the most significant components compared to the gaseous and aqueous fraction contents. Given the large changes in liquid product proportions produced by conducting the reactions with the different catalysts at varying temperatures, the reaction paths were mainly investigated from three points of interest: hydrogenation (C=C saturation)/dehydrogenation (C-H dissociation), deoxygenation (C-O cracking or C-CO cracking), and cracking (C-C cracking)/polymerization (C-C chain growth). First, unsaturated triglycerides were hydrogenated, a process that converted unsaturated carbon–carbon double bonds into saturated carbon–carbon single bonds. The newly saturated triglycerides

were subsequently broken down to form oxygen-containing intermediates (including glycerides and fatty acids) as well as gas hydrocarbon products. This is an irrevocable procedure that happened very rapidly [405]. At 300 ℃, the rate of deoxygenation varied from 8.08 to 11.67 wt.%, with nickel catalyst achieving the highest rate and molybdenum having the lowest. Yet, the rate of deoxygenation rose sharply to 96.67, 62.44, and 57.31 weight percent, respectively, via molybdenum, nickel, and tungsten catalysts as the temperature rose to 500 ℃.

As a result, the oil feedstock—which contains nearly 100% weight percentage of SAF, MUFA, and PUFA, with carbon numbers of C_{17}, C_{19}, C_{21}, and C_{23}, as reported in the earlier sections of the study—was converted into fatty acids and triglycerides, saturated, unsaturated, and fatty alcohols, aldehydes, ketones, and several mixtures of hydrocarbons. This is evidenced by the GC-MS analysis, which is presented in Tables 7.S4–7.S6. The previous study [406], which explained how oxygen-containing oxygenates, such as carboxylic acids, alcohols, and esters, are typically formed under mild reaction conditions when the feedstock's conversion to hydrocarbons is incomplete, provides further evidence for the presence of oxygen-containing compounds in the final products of the present study. The influence of temperature and catalyst type on the hydrocracking reactions was evaluated by studying the conversion, yield, and selectivity percentages of products produced. Figure 7.2 (a–d) and Table 7.1 show the effects of temperature and catalyst type on the conversion, yield, and selectivity of liquid phase products. The conversion was significantly affected by temperature and catalyst type, with temperature having an even greater effect than catalyst type.

As indicated in Figure 7.2 (a), the W-based catalyst yielded the lowest conversion at 300 ℃ when compared to the Mo- and Ni-based catalysts, the latter of which attained the highest value. When the reaction temperature was increased from 300 to 500 ℃, the conversion was dramatically increased, elevating the rate of conversion by more than 60% for each catalyst. This could be the result of the cracking severity being significantly boosted by the greater reaction temperature. $Ni_3C/AlPO_4$-18 presented the biggest conversion at the highest temperature, with β-$Mo_2C/AlPO_4$-18 coming in second. The results showed that at the highest temperature, tungsten carbide catalyst excelled over nickel and molybdenum catalysts in terms of yields and selectivity, with jet fuel (C_9–C_{16}) exceeding gasoline and diesel distillate hydrocarbons in all catalysts. The yield of jet fuel obtained by the catalysts can be ranked as $jet_{WC/AlPO4\text{-}18} > jet_{Ni3C/AlPO4\text{-}18} > jet_{\beta\text{-}Mo2C/AlPO4\text{-}18}$. This suggests that the molybdenum-based catalyst is least selective for bio-jet fuel hydrocarbons under the given reaction conditions.

The higher hydrocracking performance towards light molecule hydrocarbons as a bio-jet fuel fraction could be because the tungsten carbide catalyst has the biggest surface area (193.79 g m^{-2}) compared to the nickel (169.05 g m^{-2}) and molybdenum-based (66.57 g m^{-2}) catalysts described earlier in the study. Even though the specific surface areas can indeed play a significant role in catalytic selectivity, it's not the sole determining factor. The specific function groups present on the catalyst's surface are often more critical. This is because catalytic reactions occur at specific sites on the catalyst surface, known as active sites. These sites are often associated with particular functional groups (e.g., metal centers, acidic or basic groups). In addition, the nature of these functional groups determines the type of chemical reaction that is favored. While specific surface areas can increase the number of active sites available, it's the specific nature of these sites that ultimately controls selectivity. A high specific surface area without the right functional groups might lead to increased conversion but not necessarily improved selectivity.

Furthermore, when compared to the other two catalysts, since the tungsten carbide catalyst has the smallest average crystallite sizes and interplanar spacing, this feature can be advantageous to greatly boost the yield and selectivity of jet fuel. This can be explained better with the help of the following explanation. Smaller crystallites have a larger surface area per unit mass. This increased surface area provides more active sites for the catalytic reaction to occur, potentially leading to higher yields. Moreover, the smaller interplanar spacing can create unique electronic and geometric properties at the catalyst surface, which can improve the reactivity of the catalyst towards specific reactions. However, it's important to note that the relationship between crystallite size, interplanar spacing, and catalytic performance is complex and can vary depending on the specific reaction and catalyst system. Factors such as the nature of the active sites, the reaction conditions, and the presence of impurities can also influence the overall performance.

The next highest yields and selectivity of jet fuel were achieved by the nickel catalyst. In a similar trend, the tungsten catalyst yielded the maximum yields and selectivity of gasoline-like hydrocarbons, with molybdenum emerging as the next most efficient catalyst. Nonetheless, the catalyst based on nickel showed a preference for diesel-like hydrocarbons. Even though there is a permissible limit for heteroatom contaminants such as N, S, and O, hydrocarbons containing these heteroatoms were excluded from the measurement of jet fuel yields.

In addition, the yield of total hydrocarbons (i.e., gasoline, jet, and diesel) was also compared with the yield of cracked non-hydrocarbon products (i.e., Others) including oxygenated, and heteroatom-containing molecules such as aldehydes (fatty and unsaturated aldehydes), ethers, ketones (cyclic and non-cyclic), alcohols (saturated, monounsaturated, polyunsaturated, aromatic, cyclic), and with the yields of unconverted fatty acids (saturated, monounsaturated, and polyunsaturated). As a result, the catalyst $WC/AlPO_4$ exhibits the greatest hydrocarbon yield while producing the least amount of unconverted fatty acids and Others while β-$Mo_2C/AlPO_4$-18 and $Ni_3C/AlPO_4$-18 have greater yields of these non-hydrocarbons and fatty acids as shown Figure 7.2 (d), and Figure 7.3 (a). Table 7.1 summarizes the conversion, yields, and selectivity of the various cracked products generated under the specified reaction conditions using the different catalysts. In general, during the hydrocracking of the oil feedstock, the temperature was found to be the most significant operating parameter affecting the product conversion, yield, and distribution; the highest temperature resulted in the highest possible product yields, conversion, and better product distribution. Considerable enhancements in the yields of products were also achieved by the $AlPO_4$-18 supported transition metal carbides, which, more significantly, proved to be more selective to the bio-jet fuel range hydrocarbons.

The study's catalytic performances in producing bio-jet fuel, measured in terms of yield, selectivity, and conversion, was benchmarked against previous research, considering the diversity of feedstocks, reaction conditions, type of catalysts (conventional), and reactor systems employed. The conversion of the catalysts in this study (72-80 wt. %, Table 6.1) was relatively lower than the 98 wt. % conversion reported by [149] for palm oil using a 3 wt. % catalyst ratio, $Ni\text{-}Mo/SiO_2$, 400 ℃, 30-50 bar, and a 2 h reaction time. Despite a lower yield of 23-27 wt. % (Table 6.1) compared to the 45 wt. % yield reported in the aforesaid study, the selectivity of the current catalysts (45 wt. %) remained consistent with the selectivity reported in the previous study. The yield of 25 wt. % reported by [150] using a mini-bench top high-pressure batch reactor and sewage sludge bio-oil with a $Ni\text{-}W/SiO_2\text{-}Al_2O_3$ conventional catalyst is in line with the kerosine yield of 23-27 wt. % obtained in our study.

Li et al. [152] reported a higher conversion of 97 wt. % for palm oil using 10 wt. % Ni/SAPO-34 at 390 ℃, 52 bar H_2, and 8 h compared to the conversion of our catalysts (72-80 wt. %). Furthermore, the yield of our catalysts (23-27 wt. %) was slightly lower than the yield reported by the above study (41 wt. %). X. Li et al. [154] presented a higher conversion of 100 wt. % for

Jatropha oil using a 2 wt. % Pt/SAPO-11 catalyst at 410 °C, 50 bar H_2, LHSV = 1.2 h^{-1}, and an H_2/oil ratio of 1000 mL/mL compared to the conversion achieved in our study. However, the selectivity of 59 wt. % reported in the study did not significantly deviate from the present study. Our study obtained a yield that is slightly smaller than the 43 wt. % yield determined by [155] for palm oil using a 0.5 wt. % Pd/Al_2O_3 catalyst at 400 °C, 60 bar H_2, and a 2 h reaction time.

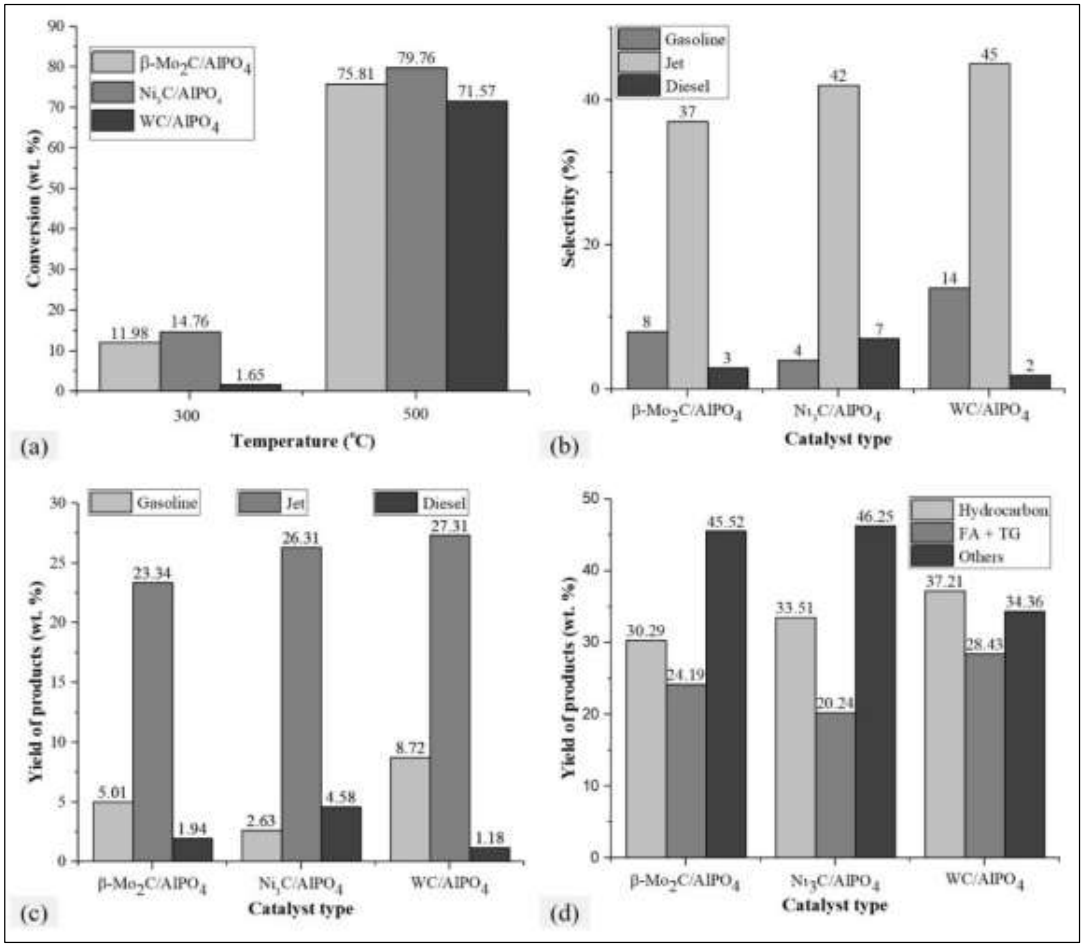

Figure 7.2 Catalytic performance evaluation of catalysts through conversion, yield, and selectivity of liquid products catalysed by β-$Mo_2C/AlPO_4$, $Ni_3C/AlPO_4$, and $WC/AlPO_4$ catalysts under reaction conditions of T = 300 and 500 °C, P = 21 bar H_2 pressure, t =2.5 h. (a) Effect of temperature on conversion, (b) Effect of catalysts type on the selectivity of middle distillate hydrocarbons, (c) Effect of catalysts type on yield of middle distillate hydrocarbons, (d) Effect of catalysts type on yield of various products.

Table 7.1 Catalytic performance evaluation of catalysts through rate of deoxygenation, conversion, yield, and selectivity of liquid products under 300 and 500 °C, 21 bar H_2 pressure, and 2.5 h reaction conditions.

Temp	Catalyst	Rate of Deoxygenation	Conversion	Yield (wt. %)			Selectivity (wt.%)		
(°C)		(wt. %)	(wt. %)	Gasoline	Jet	Diesel	Gasoline	Jet	Diesel
300	β-Mo_2C/$AlPO_4$-18	8.08	11.98	-	-	-	-	-	-
300	Ni_3C/$AlPO_4$-18	11.67	14.76	-	-	-	-	-	-
300	WC/$AlPO_4$-18	9.74	1.65	-	-	-	-	-	-
500	β-Mo_2C/$AlPO_4$-18	96.67	75.81	5.01	23.34	1.94	8	37	3
500	Ni_3C/$AlPO_4$-18	62.44	79.76	2.63	26.31	4.58	4	42	7
500	WC/$AlPO_4$-18	57.31	71.57	8.72	27.31	1.18	14	45	2

Figure 7.3 (b-d) illustrates the main constituents of jet fuel, including normal paraffins (n-paraffins), iso-paraffins, cycloparaffins (naphthene), aromatics, and olefins, that were produced during the catalytic deoxygenation, cracking and polymerization of the oil feedstock. These principal jet fuel hydrocarbons are the result of the various chemical reactions that occurred at 21 bar H_2 pressure and 500 ℃, not 300 ℃, as indicated in Table 7.1 and Tables 7.S4–7.S6. Since the feedstock only comprised C_{17}, C_{19}, C_{21}, and C_{23} fatty acids, the generation of the various complex mixtures of hydrocarbons, such as gasoline (C_4–C_{12}), bio-jet (C_8–C_{16}), and diesel hydrocarbons (C_{12}–C_{20}), validates the occurrence of hydrocracking (C–C cracking). In addition, even though the feedstock had a maximum carbon number of C_{23}, after hydrocracking, plenty of hydrocarbons and other components with carbon numbers higher than C_{23}, and as high as 30 came to light, suggesting that a polymerization reaction (C–C chain growth) had occurred. As a result, the hydrocarbons with carbon numbers C_{24}, C_{25}, C_{26}, C_{27}, C_{28}, C_{29}, and C_{30} presented in Tables 7.S4–7.S6 could be the results of the C-C chain growth of the polymerization reactions. With the supported metal carbide catalysts, it appears that the reaction temperature played an integral part in the cracking/polymerization of Yellow Dodolla oil, producing complex hydrocarbon and non-hydrocarbon compounds mentioned above. It was a remarkable accomplishment of the present study that lower liquid alkanes outside of the jet fuel range, and gasoline and diesel range hydrocarbons were not favored, despite the appearance of uncontrollably occurring cracking reactions.

As a result of deoxygenation and hydrocracking, there are only a limited number of typical n-paraffins (such as C_{11}, C_{17}, C_{18}, and C_{23}), but only one of them—the C_{11}—is a straight-chain saturated hydrocarbon that is in the jet fuel range. This could be related to the applied lower H_2 pressure of the present study where the earlier study reported [407] further explains this by explaining that a low H_2 pressure (<60 bar) could stimulate C-C cleavage during the hydrodeoxygenation of triglycerides, which would result in the formation of unsaturated intermediates and a decrease in the n-alkane proportion. These alkanes and the types of carbon numbers of the feedstock can be used to study which deoxygenation pathway—hydrodeoxygenation (HDO), decarbonylation (DCO), or decarboxylation (DCO_2)—was possibly responsible for the synthesis of these alkanes. The formation of the C_{17} and C_{23} alkanes could have occurred via C-O bond cleavage, as HDO, the main pathway for consuming H_2, yielded alkanes with the same number of carbon atoms along with water as a byproduct [408]. Nevertheless, the

least H_2-consuming DCO and the non-H_2-consuming DCO_2, respectively, produced alkanes through C-C bond cleavage that resulted in the loss of one carbon atom to CO gas and water (DCO) and CO_2 gas (DCO_2), [408], potentially producing the C_{18} from the C_{19} of the feedstock. The hydrocracking reaction, on the other hand, could have produced the C_{11}. Given that the nickel catalyst was used to produce these alkanes, it performs better in terms of HDO, DCO, and DCO_2 when it comes to producing n-paraffins under the given reaction conditions. Despite having a higher energy density, iso-paraffins are primarily added to jet fuel to enhance its cold flow characteristics since their freezing temperatures are significantly lower than those of their linear counterparts [10], with hardly these hydrocarbons generated under the specified catalytic reaction conditions.

Cyclic alkanes, with a mass percentage of 20–50 weight percent, are the second largest components required in commercial and military jet fuels [409]. According to [410], these jet fuel constituents were found to have very similar H/C molar ratio and specific gravity to Jet A-1, as well as a higher heat of combustion (46.5 vs. 43.3 MJ kg^{-1}). The most significant of these hydrocarbons that were produced in relatively larger concentrations as shown in Tables 7.S4–7.S6 include cyclopropane, 1-methyl-2-pentyl- (C_9H_{18}), cyclodecane ($C_{10}H_{20}$), cyclopropane, nonyl- ($C_{12}H_{24}$), cyclohexane, (cyclopentylmethyl)- ($C_{12}H_{22}$), cyclododecane ($C_{12}H_{24}$), n-Nonylcyclohexane ($C_{15}H_{30}$), cyclopentadecane ($C_{15}H_{30}$), cyclohexadecane ($C_{16}H_{32}$). The weight % concentrations of the cycloparaffin hydrocarbons that the $Ni_3C/AlPO_4$ generated are indicated in Table 7.S5, with the most abundantly produced hydrocarbon being C_{12} (3.1626), followed by C_9 (2.17), C_{10} (2.26), C_{15} (1.09), and C_{16} (0.81), all in wt. %. Aside from C_{16}, these paraffinic hydrocarbons, are also produced by tungsten-based catalysts, having values of C_9 (2.42 wt. %), C_{10} (2.43), C_{12} (0.81), and C_{15} (1.07), confirming that they have comparatively identical concentrations to those produced by nickel catalyst. The molybdenum catalyst, on the other hand, produced only C_9 (0.74 wt.%), C_{12} (1.27 wt. %), and C_{15} (2.07 wt.%). Also, the tungsten catalyst similarly produced these paraffinic hydrocarbons, except for C_{16}, at a concentration that is equivalent to that produced by nickel catalyst. Under the given reaction conditions, these findings substantiate the claim that $Ni_3C/AlPO_4$-18 is a more efficient catalyst at selectively producing cycloparaffins than the β-$Mo_2C/AlPO_4$-18 and $WC/AlPO_4$-18 catalysts, with $WC/AlPO_4$-18 demonstrating the second-highest level of performance.

Because it affects how well the fuel burns, the aromatic concentration of jet fuels is a significant characteristic. As a constituent of the fuel, aromatics aid in lubricity—the fuel's capacity to lower friction—and function effectively as seal swell agents [410]. As indicated in Tables 7.S4–7.S6, the high-temperature catalytic hydrocracking resulted in a variety of aromatic hydrocarbons that are in the jet fuel range hydrocarbons with carbon numbers of C_9, C_{10}, C_{11}, C_{12}, C_{13}, C_{14}. These aromatic compounds include benzene, 2-propenyl- (C_9H_{10}), benzene, (2-methyl-1-propenyl)- ($C_{10}H_{12}$), benzene, 2-ethenyl-1,4-dimethyl-($C_{10}H_{12}$), naphthalene, 1,2,3,4-tetrahydro- ($C_{10}H_{12}$), benzene, (1-ethyl-1-propenyl)-($C_{11}H_{14}$), naphthalene, 1-methyl- ($C_{11}H_{10}$), benzene, (1-methyl-1-butenyl)-($C_{11}H_{14}$), benzene, hexyl- ($C_{12}H_{18}$), benzene, 1-methyl-2-(1-ethylpropyl)- ($C_{12}H_{18}$), naphthalene, 1,2,3,4-tetrahydro-1,4-dimethyl- ($C_{12}H_{16}$), naphthalene, decahydro-1,5-dimethyl- ($C_{12}H_{22}$), 1-Phenyl-1-heptyne ($C_{13}H_{16}$), and naphthalene, 2-methyl-1-propyl- ($C_{14}H_{16}$). As illustrated in Figure 6.3, the majority of the aromatic jet fuel hydrocarbons, such as C_9 (1.75), C_{10} (1.78), C_{11} (1.68), C_{12} (1.57), and C_{14} (1.51), were produced by the nickel catalyst. Tungsten, on the other hand, produced C_{10} (1.50), C_{11} (0.56), C_{13} (2.21), and molybdenum, C_{11} (0.48), and C_{12} (0.51), all expressed in weight percentage. The complex mixtures of liquid phase products that are subjected to GC-MS analysis are also depicted in Figures 7.4–7.6.

The other class of hydrocarbons, the olefins, which are components of jet fuels but required at lower quantities are also produced by the catalytic hydrocracking of the Yellow Dodolla oil feedstock. Olefins are the most prevalent products of the catalytic hydrocracking of Yellow Dodolla oil, which produced all of the C_9-C_{16} hydrocarbons in concentrations ranging from 0.13 to 6.41 weight percent. Figure 7.3 and Tables 7.S4–7.S6 display an array of the most prevalent olefinic hydrocarbons, including 3,4-Octadiene, 7-methyl- (C_9H_{16}), 4-decene ($C_{10}H_{20}$), cyclohexene, 4-methyl-1-(1-methylethyl)- ($C_{10}H_{18}$), cyclopentene, 1-pentyl- ($C_{10}H_{18}$), 1-Undecene ($C_{11}H_{22}$), 3-undecene, (Z)- ($C_{11}H_{22}$), 1,3-cyclopentadiene, 5-(trans-2-ethyl-3-methylcyclopropylidene)- ($C_{11}H_{14}$), cyclododecene, (E)- ($C_{12}H_{22}$), 1-dodecene ($C_{12}H_{24}$), 2-dodecene, (Z)- ($C_{12}H_{24}$), 3-tridecene, (Z)- ($C_{13}H_{26}$), 2-tridecene, (E)- ($C_{13}H_{26}$), 1-tetradecene ($C_{14}H_{28}$), 3-tetradecene, (Z)- ($C_{14}H_{28}$), 1,9-tetradecadiene ($C_{14}H_{26}$), 1-pentadecene ($C_{15}H_{30}$), cetene ($C_{16}H_{32}$), and 1,7-hexadecadiene ($C_{16}H_{30}$). It was shown that molybdenum, with weight percent values of C_9 (0.13), C_{10} (2.20), C_{11} (2.88), C_{12} (5.66), C_{13} (1.37), C_{14} (6.42), C_{15} (1.67), and C_{16} (1.04), where the most dominant olefinic hydrocarbons being C_{12} and C_{14}, produced the highest proportion of olefinic jet fuel hydrocarbons when compared to the nickel and tungsten catalysts.

The tungsten catalyst achieved the second highest degree of performance, producing C_9 (0.27), C_{10} (4.10), C_{11} (2.61), C_{12} (4.97), C_{13} (2.95), C_{14} (3.37), C_{15} (1.03), and C_{16} (0.46); however, nickel produced C_9 (0.28), C_{10} (2.16), C_{11} (1.26), C_{12} (0.19), C_{13} (1.86), C_{14} (1.25), and C_{16} (3.40), all in weight percentages. When it comes to the concentration of olefin, molybdenum has the lowest degree of hydrogenation, and nickel has the highest degree, indicating that the dehydrogenation of n-paraffins could have contributed to the high olefin concentration [411]. In simple terms, this could be written as $\beta\text{-}Mo_2C/AlPO_4\text{-}18_{olefin} > WC/AlPO_4\text{-}18_{olefin} > Ni_3C/AlPO_4\text{-}18_{olefin}$.

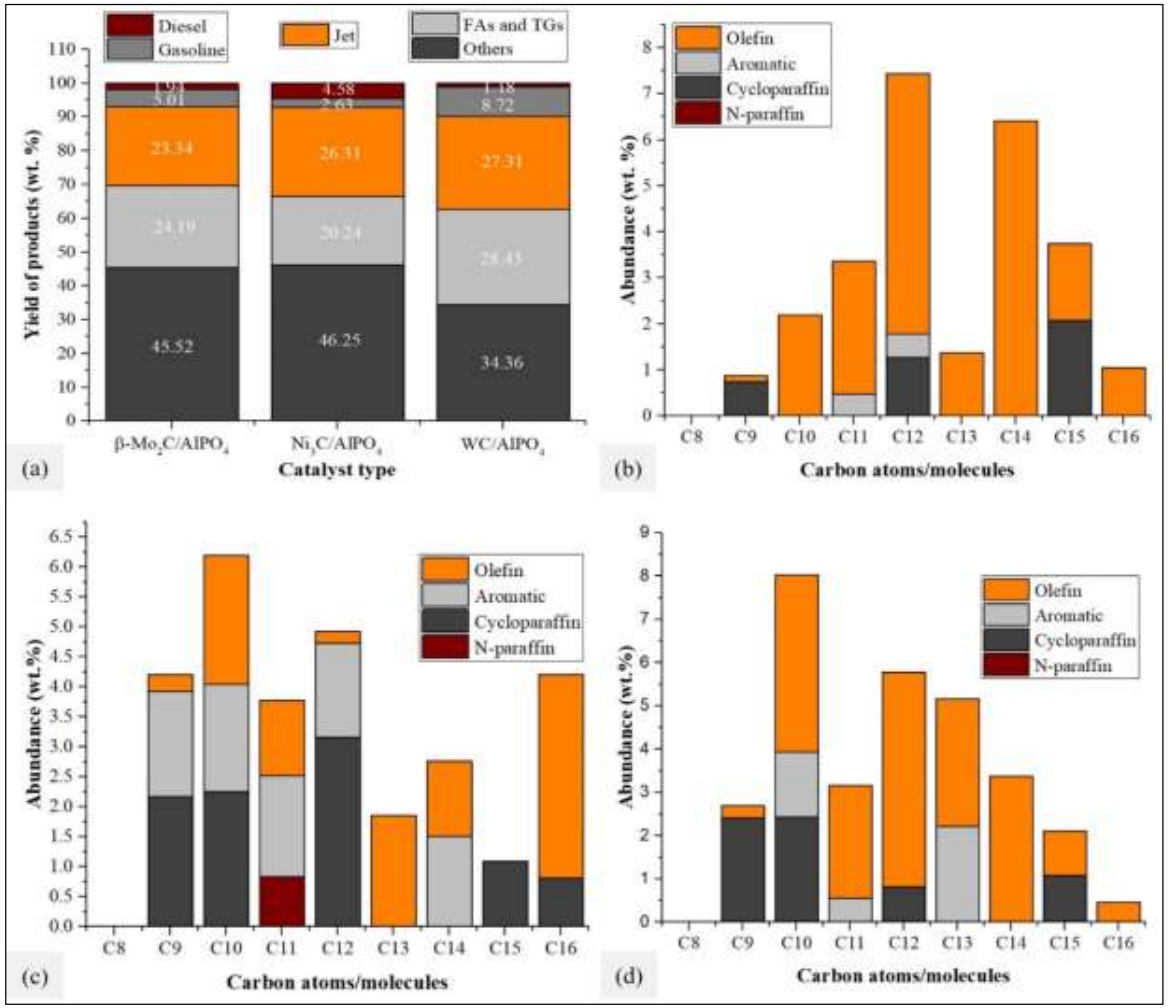

Figure 7.3 Weight percentages (i.e., chain length distribution) of each class of hydrocarbons identified in the bio-jet fuel using GC-MS. (a) Effect of type of catalyst on yield of product. The hydrocarbon chain length distributions catalyzed by (b) β-$Mo_2C/AlPO_4$, (c) $Ni_3C/AlPO_4$, and (d) $WC/AlPO_4$.

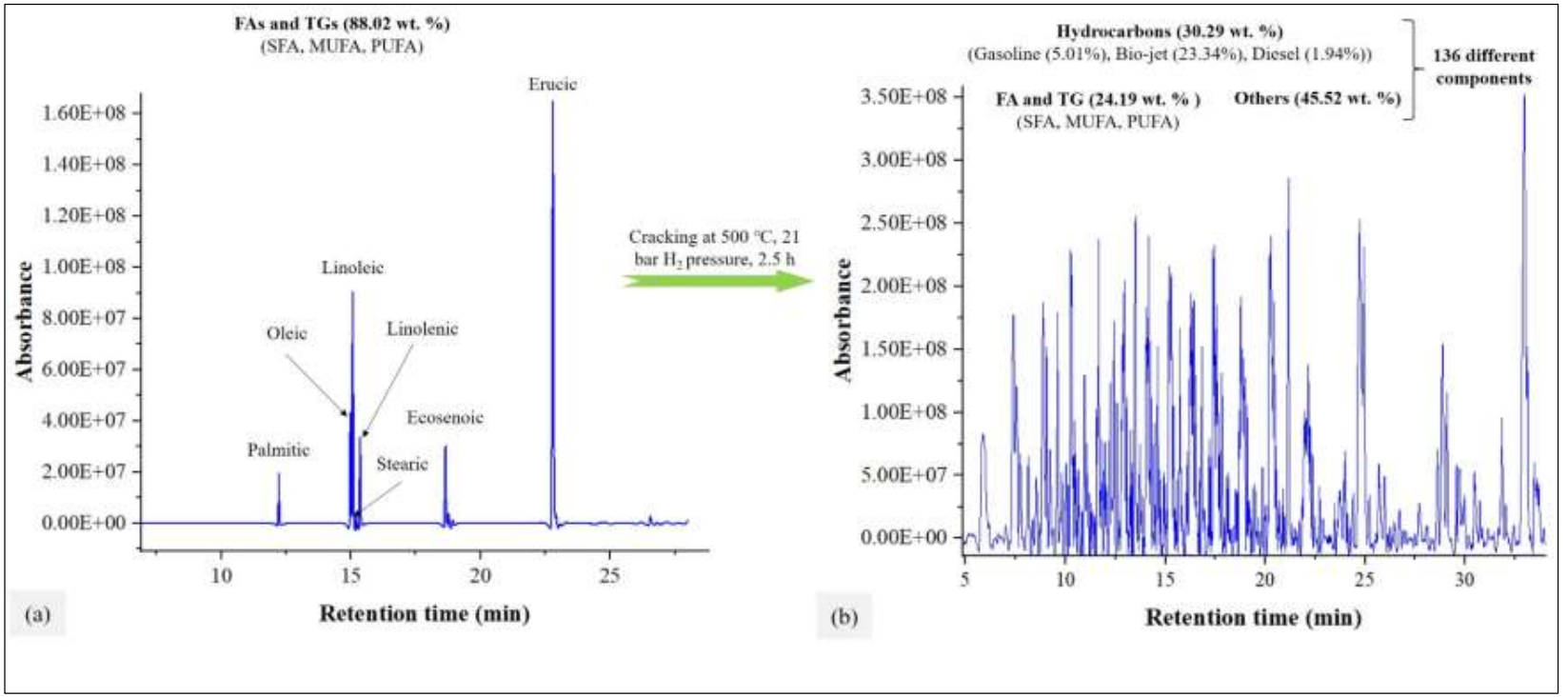

Figure 7.4 Chromatograms of Yellow Dodolla oil hydroprocessed using β-Mo_2C/$AlPO_4$-18 at which operating temperatures were varied to (a) 300 °C, and (b) 500 °C.

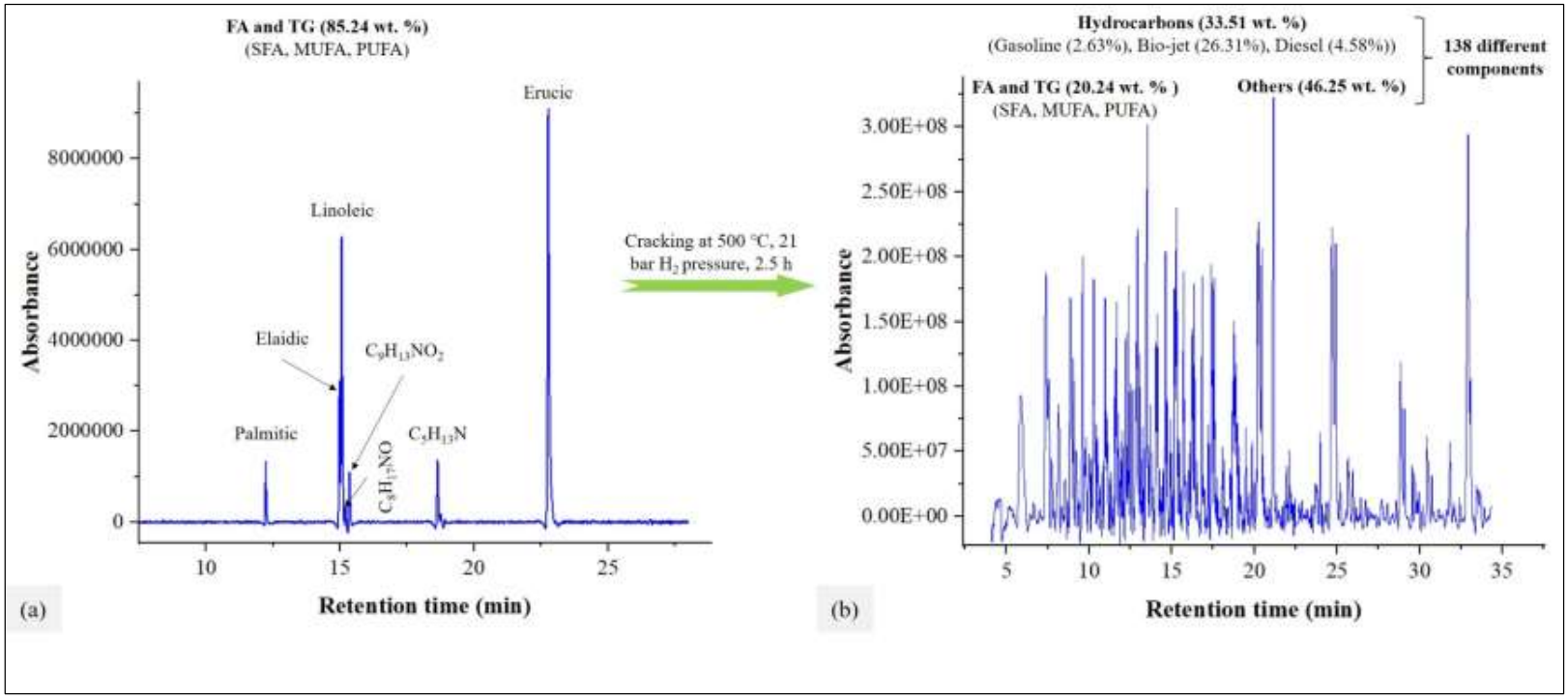

Figure 7.5 Chromatograms of Yellow Dodolla oil hydroprocessed using $Ni_3C/AlPO_4$-18 at which operating temperatures were varied to (a) 300 °C, and (b) 500 °C.

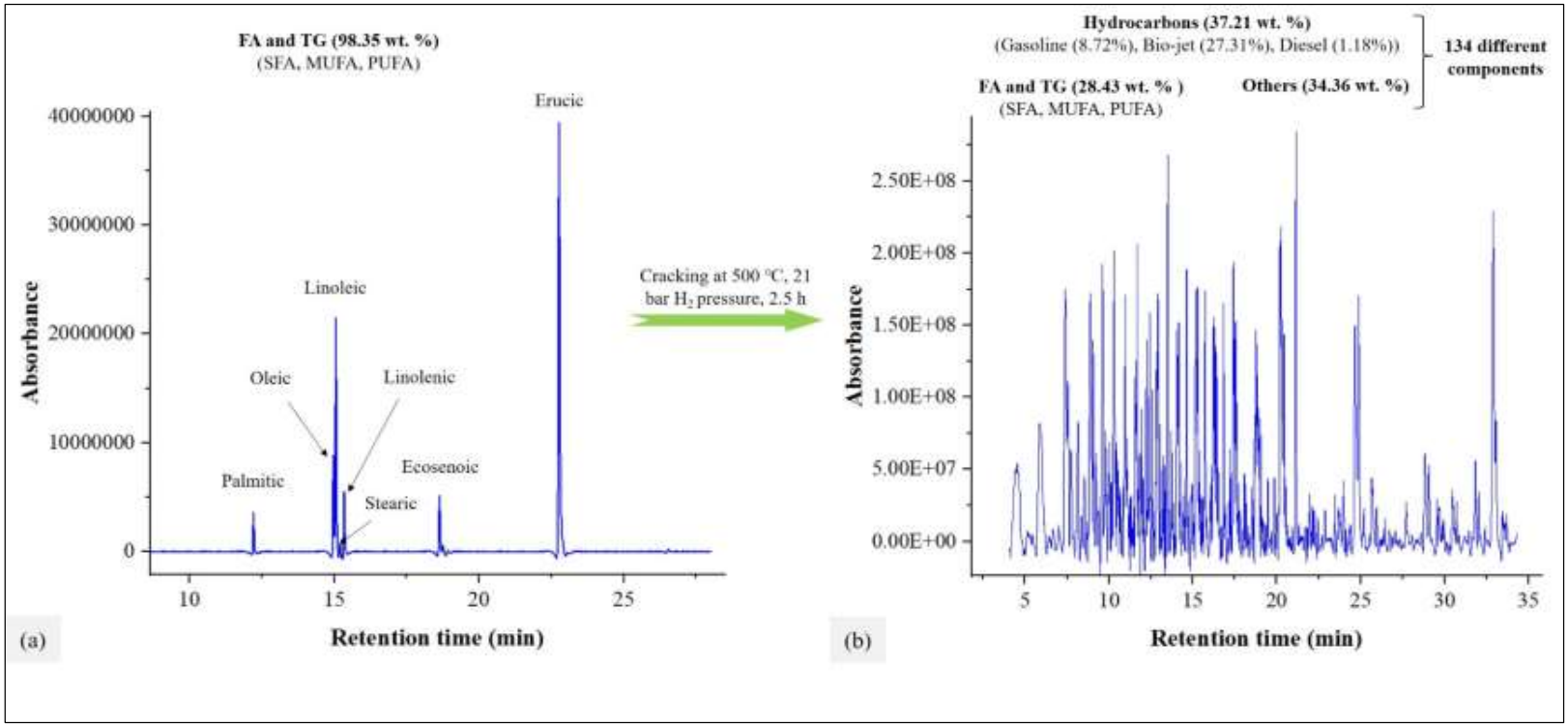

Figure 7.6 Chromatograms of Yellow Dodolla oil hydroprocessed using WC/$AlPO_4$-18 at which operating temperatures were varied to (a) 300 ℃, and (b) 500 ℃.

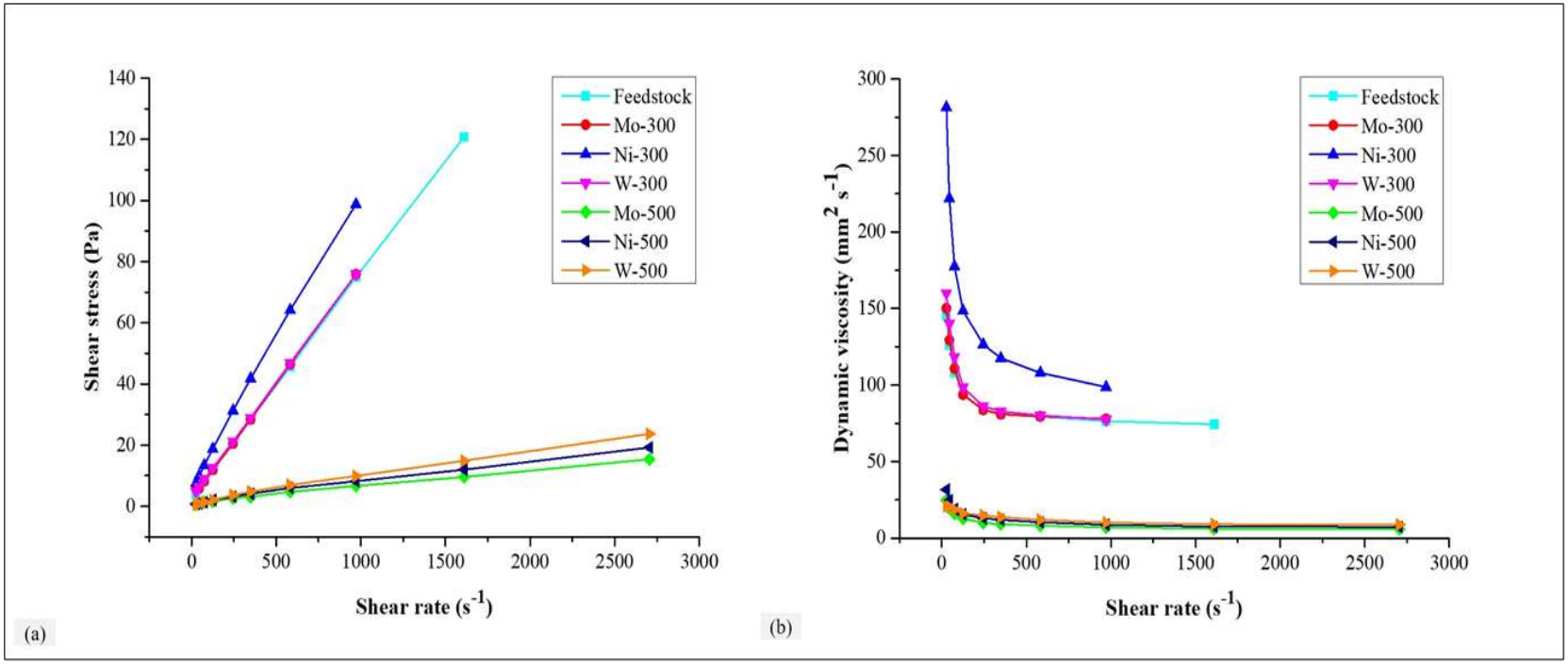

Figure 7.7 Analysis of the fluid nature of liquid phase products. (a) Shear rate (S^{-1}) vs. shear stress (Pa), (b) Shear rate (S^{-1}) vs. dynamic viscosity ($mm^2 S^{-1}$).

7.3.2 Characterization of liquid phase products

7.3.2.1 Physicochemical and rheological characterization

Below is an in-depth discussion of the most significant physicochemical properties and rheological studies, along with a summary of the results provided in Table 7.2. As reported in [412], the moisture levels should be low enough to prevent microbial development and limit corrosivity. Even small amounts of water can cause filter blockage at high elevations, where the low temperature causes water to freeze. The solubility of water in commercial jet fuel typically ranges from 40 to 80 ppm at 21 °C [413], with the moisture levels of the liquid fuels shown in Table 7.2 determined to be considerably higher compared to this reported value. Water is produced as the primary byproduct during the hydrodeoxygenation process, which is beneficial in terms of environmental pollution but may impair catalyst activity [414]. In the molybdenum-catalyzed sample at 500 °C, the high rate of deoxygenation at which the rate of oxygen removal was highest (96.67 weight percent) could account for the appearance of the maximum level of moisture (0.035 wt. %). The moisture content of the fuels at maximum temperature does not differ significantly from that of a blend of 20% coconut biokerosene and 80% conventional kerosene [415], which has a moisture content of 0.028%.

As it appears in Table 7.2, the liquid products were determined to be acidic in all catalyzed reactions, regardless of temperature. Because the hydrocarbons gasoline, jet fuel, and diesel were not produced at 300 °C and because hydrogenation may have accounted for the majority of the hydroprocessing reactions, it is expected that the density of the products synthesized at this temperature would increase significantly. The density of the fuels generated at 500 °C is relatively higher than the standard values of Jet A/Jet A-1 kerosene (775 to 840 kg m^{-3}) described in [416], [417]. These enhanced density values may be due in part to the fuels' aromatic content, which can be correlated to the findings reported in [404]. The appearance of changes in specific gravities between the smallest and maximum temperature-catalyzed samples is apparent due to the observation of density differences between these samples. Thus, hydrocracking has resulted in products having specific gravities that are considerably lower than that of the parent oil feedstock (0.914 ± 00) [24], yet nearly equivalent to that of JP-8/Jet A-1 (0.81) (Table 7.2), and the jet fuel standard (0.775–0.840) [409]. Furthermore, as per the study reported by [418], lower specific

gravity is crucial due to apprehensions regarding the total weight of the aircraft, energy efficiency, and flight autonomy.

An essential physical characteristic required for the operation of many industrial processes, such as fluid flow units, heat exchangers, and pumping machines, is the dynamic viscosity of industrial fluids. A physical property that relates directly to the applied shear stress and velocity gradient is fluid viscosity. Viscosity influences the physical properties of fuels [419]. Figure 7.7 demonstrates the rheogram behavior (i.e., dynamic viscosity and shear stress) of the liquid organic fractions against shear rates of 27.05–2705 s^{-1}. As a result, it became apparent that the oil feedstock indicated in Figure 7.7 (a) follows a straight line as Newtonian fluids do. This finding is consistent with the previous study on Yellow Dodolla oil [24], in which the fluid nature of the oil was not taken into account when evaluating its kinematic viscosity, thus verifying its Newtonian fluid nature, proving that direct determination of its kinematic viscosity was correct.

Newtonian fluid properties were similarly evidenced by the liquid phase products catalyzed by the Mo and W catalysts at 300 ℃ (Figure 7.7 (a)), with the Ni-catalyzed sample marginally deviating from this phenomenon. The divergence from the Newtonian fluid characteristic becomes more apparent for the liquid products catalyzed at 500 ℃ as shown in Figure 7.7. The results presented in Figure 7.7 (b) and Table 7.S9 show that the nickel-catalyzed product (Ni-300) had the highest dynamic viscosity value, while the feedstock's and the other two products' (Mo-300 and W-300) values remained identical. The hydrocracked liquid products (i.e., Mo-500, Ni-500, and W-500) resulted in significant reductions in dynamic viscosities when compared to their corresponding values, implying that hydrocracking of the oil feedstock significantly reduced viscosity. Furthermore, compared to products hydroprocessed at a lower temperature, the cracked products are less affected by the shear rate. The shear rate values (27.05–2705 s^{-1}) shown in Tables 7.S11–7.S13 were utilized to estimate the average dynamic viscosity values summarized in Table 7.2. It was determined that the dynamic viscosities of these cracked liquid products were found to be much greater than those of a fully formulated synthetic jet fuel analyzed at 15 ℃ (Table 7.2) and coconut HEFA evaluated at -20 ℃ (6.458 mm^2 s^{-1}) [7].

As a byproduct of combustion, ash content is a crucial metric for fuel since it indicates the quantity of non-combustible components the fuel contains. It was found that the total ash concentration of the liquid products—particularly those generated at 500 ℃ and displayed in Table 7.2—was

extremely negligible, indicating that the fuels' inorganic contaminants were exceptionally insignificant compared to their organic volatile constituents. As indicated in Table 7.2, the total ash levels of the cracked products were approximately the same as the reported values of cracked bio-crude oil of sewage sludge at 60 bar H_2 pressure. The analysis generated the following results about the cloud points of the samples: Table 7.2 indicates that the fuels produced at the maximum temperature generated their initial clouds earlier than their corresponding ones. As jet fuel's flash point is measured to determine the flammability risk during transportation and storage, the flash points of fuel samples are shown in Table 7.2. As already stated in the study, because the hydroprocessed liquids at the lowest temperature had no hydrocarbon fuels, they appear to have flash points that are significantly higher than those of the cracked products. The flash points of these cracked products, particularly, the nickel and tungsten catalyzed samples (Table 7.2), however, remain smaller than the ASTM D7566-18 minimum flash standards of 38 ℃ for various kinds of bio-jet fuels, including FT-SPK, HEFA, FT-SPK/A, and ATJ-SPK [7]. The analysis revealed that the flash points of the cracked liquid products exceeded the claimed flash point of a blended fuel that was composed of 20% palm kernel biokerosene and 80% conventional kerosene, with a temperature of 21.0 ℃ [415].

The temperature at which fuel stops flowing, or the pour point, is another important fuel property that must be taken into account when evaluating flow characteristics at low temperatures. Table 7.2 shows the pour points of the cracked and hydrogenated products. The samples produced at the maximum temperature cease to flow earlier than their corresponding ones. The samples were analysed for boiling points, as indicated in Table 7.2, and it was discovered that the non-fuel products had higher boiling temperatures, ranging from 194.5 to 208.3 ℃, with the nickel-catalyzed sample having relatively the highest value. Nevertheless, after hydrocracking, the nickel and tungsten-catalyzed samples' boiling points were dropped, falling between 150 and 250 ℃, which is the typical boiling point of jet A-1. This is marginally higher than that of coconut HEFA, which has an initial boiling point of 141 ℃ [7], but it isn't markedly different from the value of 162 ℃ [420] for the fully synthetic jet fuel. It became apparent that the dark color of the liquid fuel products could be pertaining to the color of the metal carbide catalysts and possibly the coke generated during the catalytic cracking process.

Table 7.2 A summary of the physicochemical properties of liquid products hydroprocessed at 21 bar H_2 pressure, various temperatures, and 2.5 hours with different catalysts.

Property	**Experimental Value**						**Literature value**
	300 °C			**500 °C**			
	β-Mo_2C/$AlPO_4$-18	**Ni_3C/$AlPO_4$-18**	**WC/$AlPO_4$-18**	**β-Mo_2C/$AlPO_4$-18**	**Ni_3C/$AlPO_4$-18**	**WC/$AlPO_4$-18**	
Total moisture content (wt. %)	0.011	0.012	0.011	0.035	0.024	0.022	0.008[413]
pH	3.06	2.99	2.87	3.06	2.87	2.67	–
Density (kg/m^3) at 15 °C	923.5	925.4	924.6	852.4	863.3	865.4	867[415]
Specific gravity at 15 °C	0.92	0.93	0.93	0.85	0.86	0.87	0.81[421]
Dynamic viscosity (mm^2 s^{-1})	100.73	160.02	105.41	11.90	14.94	14.47	1.8[420]
Total ash content (wt. %)	0.011	0.011	0.011	0.006	0.008	0.009	< 0.001[150]
Cloud point (°C)	−10	−12	−15	−25	−25	−32	-
Flash point (°C)	220	210	135	50	32	30	38[7]
Pour point (°C)	−26	−16	−24	−32	−35	−45	-
Boiling point (°C)	195.6	208.3	194.5	124.8	173.4	177.1	162[420]

7.3.2.2 Elemental composition, atomic ratio, and calorific value analysis

In Table 7.3, the elemental composition of the liquid phase products—including the amounts of carbon, hydrogen, nitrogen, sulfur, and oxygen—as well as an atomic ratio of oxygen to carbon (O/C) and hydrogen to oxygen (H/O), and the heating values are displayed. After hydroprocessing, carbon and hydrogen contents showed no noticeable spike at 300 °C compared to their corresponding values in the vegetable oil (C=79.8, H=12.3 wt. %) [24], but they did show an appreciable boost at 500 °C, with the β-Mo_2C/$AlPO_4$-18 catalyzed sample having the greatest carbon and hydrogen contents. Compared to earlier research (Table 7.3), the total nitrogen concentration of the liquid phase products was in agreement with the cracked bio-crude oil of sewage sludge at 60 bar H_2 pressure. This could potentially be attributed to the highest rate of deoxygenation experienced by this catalyst, which resulted in the lowest total oxygen concentration as shown in Table 7.3. The significant decrease in total oxygen concentrations might have been caused by any of the hydrotreatment processes, specifically HDO, HDCO, and DCO_2, each with pros and cons. According to the results of the analysis, the liquid fuels produced at the maximum temperature had a total oxygen content that was found to be marginally lower than that of a blend of 20% coconut biokerosene and 80% conventional kerosene [415] but far bigger than jet A [422] (Table 7.3).

Based on [410], introducing oxygen in a fuel molecule often lowers its energy density. Because combustion is an exothermic oxidation of a fuel, including oxygen in its molecular structure results in less useful work per unit mass than a pure hydrocarbon equivalent. In addition, the complete removal of oxygen from oil feedstocks is what gives a hydrocarbon fuel its high lubricity [414]. Reducing the O/C ratio and concurrently raising the H/C ratio is the primary objective of the hydrodeoxygenation process [423]. According to [424], the molar ratio of oxygen to carbon (O/C) in the fuel molecule indicates how linearly the energy density of biofuels and biomass processing intermediates declines as the oxygen concentration rises. In comparison to the data previously presented, as indicated in Table 7.3, the O/C atomic ratios of the fuels produced at 500 °C had extremely low concentrations. Table 7.3 shows that the concentration of heteroatom impurities, such as S, is within the acceptable range as mentioned in [425], where the value is quoted as ≤ 0.3 for conventional jet A or jet A-1 (ASTM D1655-13).

Table 7.3 Elemental composition (wt. %), atomic ratios, and calorific values (MJ kg^{-1}) of liquid fuel products evaluated at different temperatures and catalysts.

Property	Experimental value						Literature value	
	300 °C			500 °C				
	β-Mo_2C/$AlPO_4$-18	Ni_3C/$AlPO_4$-18	WC/$AlPO_4$-18	β-Mo_2C/$AlPO_4$-18	Ni_3C/$AlPO_4$-18	WC/$AlPO_4$-18		
C	79.91	79.87	79.89	85.44	83.01	82.84	86.4[426]	86.3[426]
H	12.53	12.68	12.73	13.64	13.41	13.32	13.8[427]	13.5[422]
N	0.24	0.36	0.24	0.42	0.35	0.38	1.8[150]	0.5[150]
S	0.14	0.18	0.09	0.23	0.29	0.12	<0.3[426]	0.04[426]
O	7.17	6.89	7.04	0.26	2.93	3.33	0.0044[422]	4.40[415]
H/C	1.87	1.89	1.90	1.90	1.92	1.92	1.90[428]	1.92[7]
O/C	0.067	0.065	0.066	0.002	0.026	0.030	0.077[410]	-
GCV	41.93	42.12	42.17	45.89	44.50	44.28	44.1[429]	43.7[7]
NHC	39.18	39.34	39.37	42.89	41.56	41.35	42.48[430]	43.3[7]

C-carbon, H-hydrogen, N-nitrogen, S-sulphur, O-oxygen. GCV-gross calorific value (MJ kg^{-1}). NHC-net heat of combustion (MJ kg^{-1}).

When comparing different fossil feedstocks for energy density and hydrogen content, the petroleum and coal industries employ the hydrogen-to-carbon ratio (H/C ratio) as a convenient measurement. Bringing the biomass feedstock's low H/C ratio up to the level of diesel, jet, and gasoline fuels—which have H/C ratios closer to two—is one of the primary objectives of producing drop-in biofuels [424]. This is because a fuel with a greater H/C ratio has a higher energy efficiency and produces less CO_2 as it burns [431]. This is because, during hydrocarbon combustion, the primary energy release stems from breaking carbon-carbon and carbon-hydrogen bonds. Complete combustion of fuels with higher H/C ratios yields more water and less carbon dioxide, enhancing energy efficiency. While carbon-carbon bonds contribute significantly to energy content, carbon-hydrogen bonds also play a role. The increased number of carbon-hydrogen bonds in fuels with higher H/C ratios leads to higher energy content and lower CO_2 emissions.

After deoxygenation and cracking reactions yielded 30.29−37.21 wt. % total hydrocarbon yields, the H/C atomic ratio of the liquid phase products, which is one of the most pertinent combustion-related fuel properties, rose, as shown in Table 7.3, with those generated at the highest temperature surpassing the best results. In addition, Table 7.3 provides a comparison between these findings and prior researched results of conventional jet fuels, and it shows that the experimental results are perfectly in line with the findings from the literature.

The atomic ratios, H/C and O/C, mentioned thus far offer a better understanding of the combustion properties, with the former ratio providing vital insights into the heating values of fuels. Table 7.3 illustrates the calorific values of the liquid phase products (MJ/kg), with cracked products at the highest temperature having the highest values as compared to those hydroprocessed samples at the lowest temperature. The liquid products generated at 500 °C had gravimetric energy densities (net heat of combustion) that are quite similar to those of conventional fuels such as a Jet A-1 (43.3 MJ kg^{-1}) [7] and an isomerization-free coconut HEFA bio-jet fuel that comprises 87.2 wt. % of n-paraffins (42.48 MJ kg^{-1}) [430]. In addition, it was claimed that because of concerns about overall aircraft weight, energy economy, and flight autonomy, aviation kerosene needs to have a higher gravimetric energy density of >42.8 MJ kg^{-1}, a volumetric energy density of > 33.2 MJ L^{-1}, and a low specific gravity (0.775–0.820) [414], [425]. The gravimetric energy densities of the liquid phase products have also been compared with other bio-jet fuels such as an 80 vol.% isomerization-free coconut HEFA bio-jet fuel that comprises 87.2 wt. % of n-paraffins/Jet A-1 (42.8 MJ kg^{-1}) [7], 20 vol.% palm biokerosene/Jet A-1 (41.19 MJ kg^{-1}) [7], HEFA from camelina oil (43.7 MJ kg^{-1})

[432], indicating that the experimental results do not significantly deviate from the literature values. The higher heating values of the samples were also in line with prior research studies, such as those that reported 100% Fischer-Tropsh- synthetic paraffinic kerosine (FT-SPK) (44.1 MJ kg^{-1}) [429] and 50% vol.% FT-SPK/Jet A-1 (43.7 MJ kg^{-1}) [7] with the sample catalyzed by β-Mo_2C/$AlPO_4$-18 appeared to be slightly larger than these reported values.

7.3.2.4 Analysis of functional groups

The FT-IR analysis results, illustrated in Figures 7.8 and 7.9 and Tables 7.S14−7.S16, reveal the various functional groups attributed to every band wavelength identified in the liquid phase product samples. It has been determined that the principal vibration bands identified in the IR spectra of the major functional groups are presented in Figures 7.8 and 7.9. These distinguishing absorption peaks in the infrared spectrum indicate the existence of several functional groups. It turned out that the cracked products have no distinctive bands detected at the wavenumber greater than 3000 cm^{-1}, in contrast to the samples at the lower temperature, implying that there are no =C–H stretching vibrations of alkenes in the former samples at this absorption band, yet this is still valid for the later samples. The highest absorption intensities in the samples were found to be in the region 3000−2800 cm^{-1}, which corresponds to bands of 2922 and 2853 cm^{-1}, which reflect the symmetrical and asymmetrical C–H stretching vibrations of cycloalkanes at 300 °C. The greatest absorption intensities were also observed in samples Mo-300, Ni-300, and W-300 in the bands 1744 and 1710 cm^{-1}, which are located in the 1730–1700 cm^{-1} region and correspond to the C=O stretching vibrations of carboxylic acids. This continues to be evident for the cracked products where after the feedstock was hydrocracked and deoxygenated at the highest temperature, the intensity of the absorption band at 1744 cm^{-1} of a carbonyl group sharply decreased to 1710 cm^{-1} of a carbonyl group. This is in line with the rate of deoxygenation detailed in the preceding sections, with the carbonyl C=O bond cleavage triggering the peak intensity to decline during the removal of the heteroatom oxygen.

The existence of olefinic hydrocarbons is evidenced by the bands at 1656 and 1641 cm^{-1}, which are attributed to the weak C=C stretching vibrations. However, all samples presented weak aromatic C-C stretching in the 1500-1400 cm^{-1} band region. A relatively medium band, 1464 cm^{-1}, emerged for Mo-300, Ni-300, and W-300 based on the methylene vibration, which typically appears in the range of 1465–1430 cm^{-1}. However, a slightly lower value, 1456 cm^{-1}, is identified

for the cracked samples. A weak aromatic C–C stretching vibration was observed in the 1500–1400 cm^{-1} band region, with the Mo-300, Ni-300, and W-300 samples showing a band of 1418 cm^{-1} and the cracked products presenting a band of 1413 cm^{-1}. At 1377 cm^{-1}, a C–H bending vibration of methylene CH_2 was identified for all samples. Nonetheless, the C–O stretching of a carboxylic acid is brought about by the weak band that was found at (1284, 1285, and 1286 cm^{-1}) of the cracked samples. The presence of alcohols caused the peak band at 1238 cm^{-1} to slightly fall to 1236 cm^{-1} when the reaction temperature increased for all of the cracked products. This could also be due to the loss of oxygen via deoxygenation. It is apparent that a small peak has emerged at 1165 cm^{-1}, and this peak is an indication of the appearance of an ester in the cracked products. Only the Mo-300, Ni-300, and W-300 samples exhibited a relatively significant peak (1160 cm^{-1}) in the region 1300–1160 cm^{-1}, which is indicative of a C–O stretching that is emerged because of the presence of α, β-unsaturated esters.

The samples generated at lower and higher temperatures exhibited the existence of secondary alcohols, as indicated by the bands at (1118, 1119, 1119) and (1116, 1113, 1119 cm^{-1}), which were attributed to C–O stretching. Mo-300, Ni-300, and W-300 samples exhibit C-O-C stretching vibrations at 1105 and 1098 cm^{-1}, indicating the presence of aliphatic ethers. However, these ethers also emerged on 1098 cm^{-1} by Mo-500, Ni-500, and W-500 samples. All samples exhibited shoulder trans = C-H out-of-plane bending in the 970–920 cm^{-1} region; however, the cracked samples further displayed O–H bending for carboxylic acid in the 950–910 cm^{-1} region. Other bands such as aromatic –C–H out of plane bending are also visible in the cracked products at (813, 813, 814 cm^{-1}) and a terminal wag of ethers at 909 cm^{-1}. C-H rocking methyl of n-alkanes/cycloalkanes is evident at 725-720 cm^{-1}.

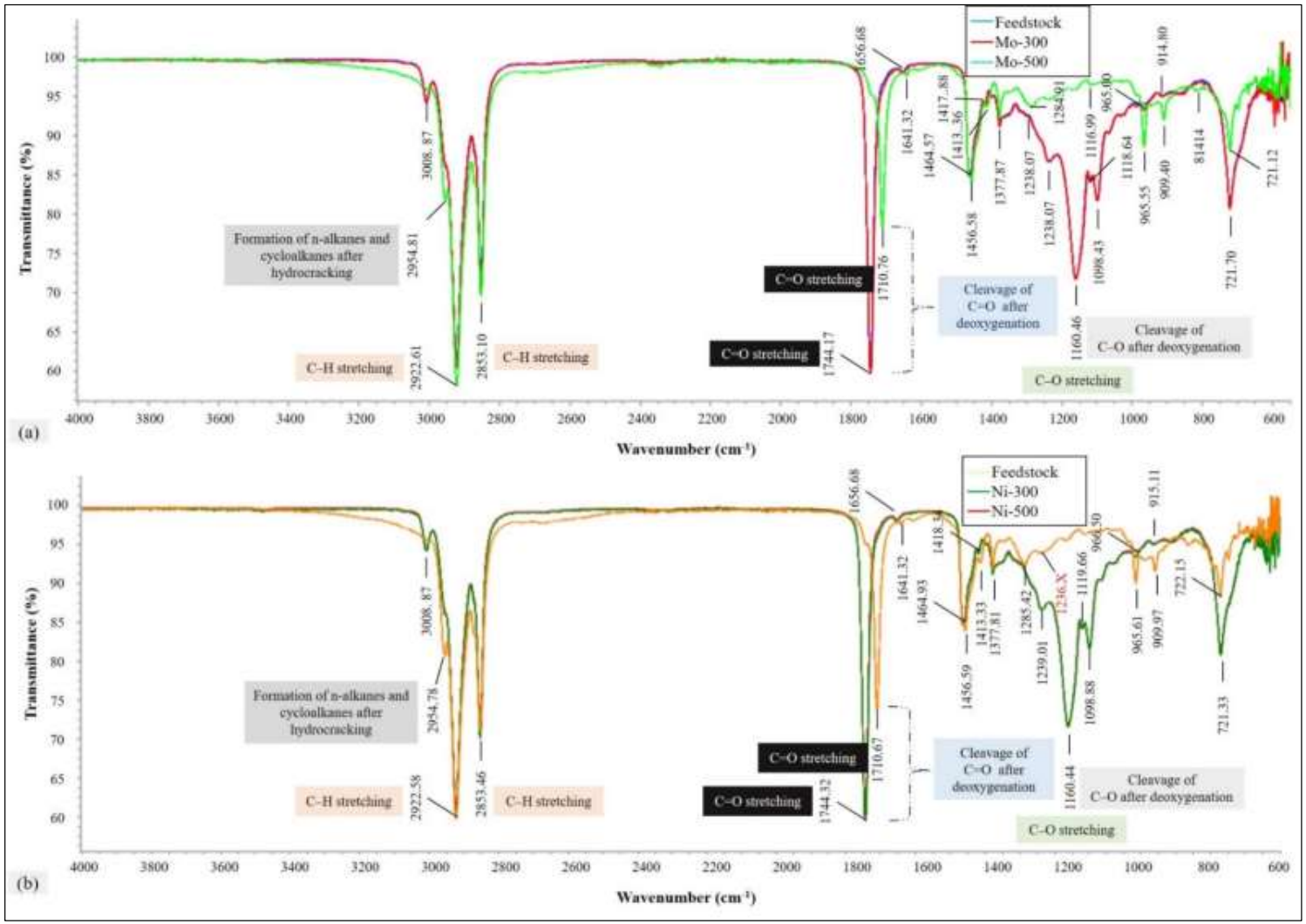

Figure 7.8 FT-IR spectra of samples. (a) Feedstock and β-Mo_2C/$AlPO_4$-18 catalyzed products, (b) Feedstock and Ni_3C/$AlPO_4$-18 catalyzed products.

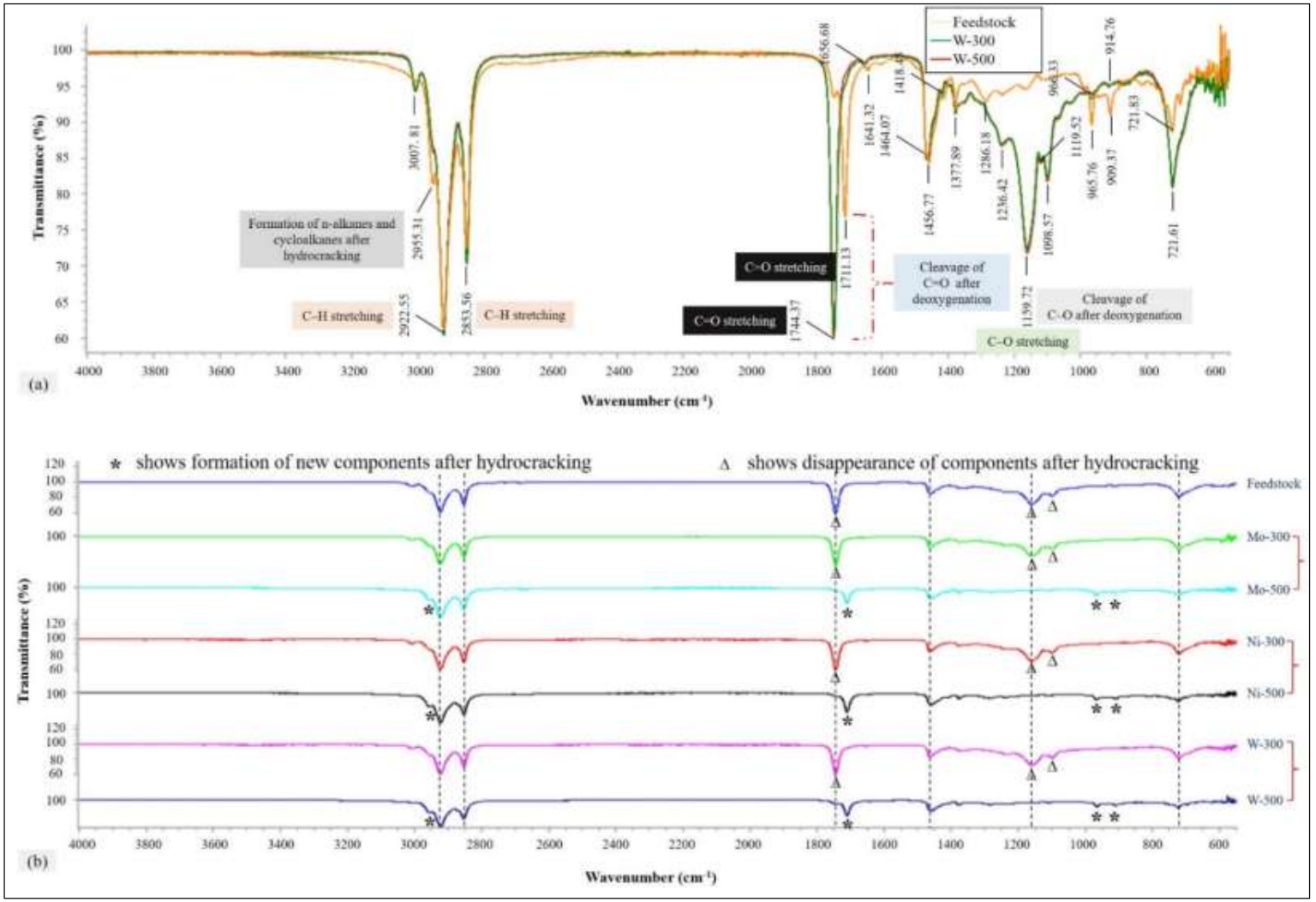

Figure 7.9 FT-IR spectra of samples. (a) feedstock and WC/$AlPO_4$-18 catalyzed products, and (b) Feedstock and β-Mo_2C/$AlPO_4$-18, Ni_3C/$AlPO_4$-18, and WC/$AlPO_4$-18 catalyzed products.

7.3.3 Deactivation and regeneration of catalysts

Catalyst lifetime is one of the most significant economic variables in most industrial catalytic processes, due to expensive shutdowns, catalyst replacements, and efficient disposal of used materials [433]. One of the most notable deactivation mechanisms is catalyst coking; after the metal carbide is formed, inactive carbon accumulates on the catalyst, coking the surface and blocking access to active sites [434]. While the metal carbide is catalytically active, further carbon accumulating results in the formation of unreactive graphitic carbon, deactivating the catalyst [434]. This type of deactivation is a complicated process involving a series of physical and chemical interactions. Coke formation in catalytic systems using hydrocarbon feedstock often begins with strong chemisorption as a monolayer of coke precursor or physisorption in multilayers over active sites [435].

In a similar vein, given that the feedstock used in the current study was a liquid hydrocarbon, there was an opportunity for mechanical deactivation—such as fouling—and chemical deactivation—such as poisoning (strong chemisorption of species) to occur. Furthermore, even though the TPO TG-MS results (described in Chapter 6), which showed the presence of free carbon graphite species on the catalyst surfaces, the hydrogenation reaction that occurred during catalyst activation before catalytic activity testing could have removed it. Furthermore, an efficient regeneration approach for the aforementioned sort of deactivated catalyst could consist of the inclusion of certain oxidants in the regeneration gas stream, including steam, O_2, or CO_2, yet the same oxidants can produce overoxidation [434]. In the current work, an attempt has been made to rejuvenate the used catalysts if the complex catalytic reactions on the liquid feedstock caused them to become deactivated. Nonetheless, overoxidation might have happened, which would have eliminated all the carbide carbon species that had been present in the metal carbide catalyst's interstitial regions. As a result, the regenerated catalyst became a metal oxide catalyst rather than a metal carbide catalyst, emphasizing that highly appropriate reaction conditions must be defined to avoid overoxidation. The most significant supporting materials including Tables 7.S1–7.S16 and Figures 7.S1–7.S2 and for this chapter are presented in Appendix A and Appendix B, respectively.

7.4 Challenges and Considerations for Scaling Up

7.4.1 Synthesis of supported metal carbide catalysts

Supported carbon-coated transition metal carbides (TMCs) have gained significant prominence due to their exceptional catalytic performances across various applications. By carefully addressing the challenges and considerations detailed below, it is possible to successfully scale up the synthesis of the supported TMC catalysts, paving the way for their widespread application in various energy-related and environmental technologies.

- **Uniformity and reproducibility.** Maintaining a uniform particle size distribution is crucial for achieving consistent catalytic activity and selectivity. Inconsistent particle sizes can lead to variations in the surface area and active site density, affecting the overall performance. The thickness and quality of the carbon coating are critical factors influencing the catalyst's stability and interaction with the active metal carbide core. Controlling these parameters during the scaling-up process is essential.
- **Phase competition and coexistence.** Because metal-carbon systems can have multiple stable phases under different synthesis conditions, competition can cause the development of undesirable phases or phase combinations. The formation of specific phases can be influenced by kinetic factors, such as heating rate, reaction time, and the presence of impurities. This can make it difficult to control the phase composition. In general, the primary challenges in phase control during catalyst synthesis are thermodynamic competition, synthesis conditions, support interactions, characterization difficulties, and catalyst deactivation (including phase transformation and sintering).
- **Carbon content and carbide formation.** Ensuring a uniform distribution of carbon within the support material is essential for the formation of pure metal carbides. Agglomeration or segregation of carbon can lead to the formation of mixed phases or carbon-rich regions.
- **Support material interactions.** The interaction between the support material and the metal precursor can influence the formation of metal carbide phases. Strong interactions may hinder the formation of desired phases or promote the formation of undesired compounds. The support material can also interact with the carbon source, affecting the carbon distribution and carbide formation. This can lead to phase competition or the formation of support-carbon complexes.

7.4.2 Production of SAF using catalytic hydroprocessing

Brassica carinata, a promising oilseed crop for the aviation industry, offers a viable path toward producing SAF and reduces the environmental impact of air travel. Some of its most significant

advantages include high oil yield, multiple uses, adaptability, reduced greenhouse gas emissions, improved soil health, biodiversity support, economic benefits, job creation, market diversification, renewable resources, and a contribution to a more sustainable future.

However, catalytic hydroprocessing, a crucial method for producing sustainable aviation fuel (SAF), faces several significant challenges. The challenges outlined below require a concerted effort from industry, academia, and governments through ongoing research, development, and collaboration. By addressing these obstacles, catalytic hydroprocessing can significantly contribute to the decarbonization of aviation.

- **Land availability and competition.** Expanding *Brassica carinata* cultivation may compete with other food crops or require the conversion of natural habitats, leading to environmental concerns and potential conflicts with land-use interests. While *Brassica carinata* can grow on marginal lands, the productivity and yield may be lower compared to more fertile areas, limiting the overall scale of production.
- **Infrastructure and logistics.** Establishing and scaling up processing facilities to extract oil from *Brassica carinata* and convert it into sustainable aviation fuel (SAF) may require substantial investments and infrastructure development. Building a robust supply chain, including transportation and storage networks, to efficiently deliver the oilseed crops to processing facilities can be challenging, especially in remote or less developed regions.
- **Economic viability.** The cost of producing SAF from *Brassica carinata* may be higher than that of conventional fossil jet fuel, especially in the early stages of commercialization. The market demand for sustainable aviation fuel (SAF) and its pricing structure may significantly influence the economic feasibility of *Brassica carinata*-based SAF production. SAF must be produced at a competitive cost compared to traditional fossil jet fuel to gain widespread adoption.
- **Regulatory and policy challenges**. Ensuring that SAF meets stringent aviation fuel standards and regulations is essential for its acceptance by the aviation industry. Establishing a robust system for carbon credits and incentives to support SAF production can be complex and challenging.

7.5 Conclusions

The following significant conclusions were drawn after the catalytic hydroprocessing was applied to transform the vegetable oil into an advanced jet fuel. The current study has made a significant contribution to the aviation industry's decarbonization agenda by introducing a unique and low-carbon fuel alternative feedstock, Yellow Dodolla oil, which is one of the most prominent *Brassica carinata* vegetable oils indigenous to Ethiopia. A catalytic hydroprocessing method was used to upgrade inedible vegetable oil into a sustainable aviation fuel in a continuous fixed-bed reactor system employing very high temperatures and elevated hydrogen pressure, producing a tremendous and complex mixture of hydrocarbons and other trace residuals. With the supported metal carbide catalysts, it appears that the reaction temperature played an integral part in the deoxygenation, and hydrocracking/polymerization of oil feedstock, yielding a very complex mixture of pure hydrocarbon compounds, and oxygenated hydrocarbon compounds (i.e., alcohols, aldehydes, ketones, carboxylic acids, esters, triglycerides, etc.). After hydrocracking and deoxygenation reactions, a smaller quantity of straight-chain (n-paraffin) hydrocarbons was produced. This could be attributed to the applied hydrogen pressure being smaller, which stimulated C-C cleavage and resulted in the formation of unsaturated intermediates, leaving it an olefinic hydrocarbon and thus decreasing the n-alkane proportion.

Cycloalkanes, the second most abundant component of commercial and military jet fuels, are produced in significantly higher quantities, with an excellent product distribution of C_9, C_{10}, C_{12}, C_{15}, and C_{16} achieved in the nickel catalyzed sample at the highest temperature. Although the study showed signs of uncontrolled cracking reactions as it is expected, it was a remarkable accomplishment that the production of gasoline and diesel range hydrocarbons and lower liquid alkanes outside of the jet fuel range was not favored. Aromatics are other major components of jet fuels generated with a better product distribution of C_9, C_{10}, C_{11}, C_{12}, and C_{14} produced by nickel, with tungsten catalyst coming in second at the highest temperature. Even though the feedstock had a maximum carbon number of C_{23}, after hydrocracking, plenty of hydrocarbons and other components with carbon numbers higher than C_{23}, and as high as 30 came to light such as C_{24}, C_{25}, C_{26}, C_{27}, C_{28}, C_{29}, and C_{30}, suggesting that a C-C chain growth polymerization reactions had occurred. The absence of wax formation during the hydrocracking reactions was noticed; which could be attributed to the slowly occurring hydrogenation of large triglyceride molecules. This is an enormous advance for the current upgrading process because the product's early development could prevent further cracking and deoxygenation reactions.

CHAPTER EIGHT

CONCLUSIONS AND RECOMMENDATIONS

8.1 Conclusions

In the present study, four distinct and novel *Brassica carinata* oilseed crops—Yellow Dodolla, Holetta-1, Derash, and Tesfa—that are indigenous to Ethiopia were investigated to study their promising industrial applications. The various coproducts derived from these oilseed crops—such as inedible hexane-extracted vegetable oils, hexane-defatted oilseed meals, and bio-oils produced by slow pyrolysis—were the primary emphasis of the study.

Solvent extraction using n-hexane was carried out using Response surface methodology (RSM) with three levels of Box-Behnken Design (BBD) in an isothermal batch reactor. The application of heat energy and continuous mixing of the extraction process in the reactor may have substantially lowered the potential mass transfer resistances (i.e., solid-solid, solid-liquid, and liquid-liquid), and enhanced the rate of extraction. As a result, it was practical to obtain maximum and optimum oil yields (35.93–45.25%) with very short extraction times (30.00–39.38 min) and lower temperatures slightly higher than room temperature (35.52–38.94 °C).

The following noteworthy advantages may arise from the use of this extraction technique: (a) The solvent's boiling point does not need to be raised; (b) It shortens the time required to boil, condense, and reach the surface of the sample; (c) It prevents the possible loss of solvent while boiling; (d) There is no evaporation, no solvent loss, and hence, no potential reduction in extraction yield; (e) It saves energy for boiling; (f) It may also be applied for the extraction of heat-sensitive components at temperatures slightly higher than room temperature. Furthermore, although recovery of products by vacuum filtration is a disadvantage when compared to the Soxhlet extraction method, it is also easy to use and doesn't require thimbles.

Due to their distinctive characteristics, solvent-defatted meals can be valorized into a range of valuable industrial products, with the aviation and feed industries being two of the potential areas that stand to gain greatly from this. The results of the pyrolysis studies showed that the maximum yield of bio-oil (55.01%) was generated at the highest temperature of 550 °C, while the maximum

yields of bio-char (34.93%) and gas (45.84%) were produced at the lowest temperature of 350 ℃. The bio-oils' characterization findings indicated that they had substantially enhanced qualities, making them promising alternative feedstocks for advanced fuel production in the aviation industry. They can be upgraded into high-quality bio-jet fuels via hydrotreatment (deoxygenation, hydrodenitrogenation), and hydrocracking upgrading processes. Thus, it came to light that the various carinata derived coproducts were found to be highly relevant for a wide range of industrial applications.

Using a propane-hydrogen gas mixture, $AlPO_4$-18 supported catalysts were synthesized, with XRD characterization findings showing that the most prominent carbide phases (i.e., β-Mo_2C, Ni_3C, and WC), and traces of other phases (such as MoO_2, NiC, Ni, W_2C, and C) were identified. TEM results verified that WC/$AlPO_4$-18 had the smallest average crystallite sizes, ranging from 6.03 to 7.56 nm, and the smallest interplanar spacing, measuring 0.05 nm, when compared to β-Mo_2C/$AlPO_4$-18 and Ni_3C/$AlPO_4$-18 catalysts. The existence of unreacted free surface carbon species on the surface of the nanoparticles has been verified by TPO TG-MS, XRD, and carbon-to-metal ratios (from EDX) characterization methods. While generating the precursor-dopped metal oxides and carburization to form the metal carbide nanoparticles, the catalyst support's BET surface area was considerably lowered after air calcination. The catalyst support was shown to be thermally stable even when exposed to extreme temperatures of up to 1000 ℃, as the TPO TG-MS data further verified.

Following the successful synthesis of supported metal carbide nanocatalysts, a catalytic hydroprocessing approach was applied to transform the non-food Yellow Dodolla vegetable oil into a sustainable aviation fuel. As a result, the following key conclusions came about after the catalytic hydrocracking of the oil feedstock.

It appears that the reaction temperature played an integral part in the deoxygenation, and hydrocracking/polymerization of feedstock, producing a very complex mixture of pure hydrocarbon compounds, and oxygenated hydrocarbon compounds (i.e., alcohols, aldehydes, ketones, carboxylic acids, esters, triglycerides, etc.). Straight-chain (n-paraffin) hydrocarbons were generated in a lower concentration following the hydrocracking and deoxygenation reactions. The observed decrease in the n- paraffin fraction may be explained by the fact that the applied hydrogen pressure was lower, which induced C-C cleavage and led to the production of unsaturated

intermediates, resulting in an olefinic hydrocarbon. The production of cycloalkanes—the second most abundant component of both commercial and military jet fuels—is substantially higher. The nickel-catalysed sample at the maximum temperature yielded a superior cycloalkanic product distribution of C_9, C_{10}, C_{12}, C_{15}, and C_{16} compared to the other catalysts.

Although the study showed signs of uncontrolled cracking reactions, it was a remarkable accomplishment that the production of gasoline and diesel range hydrocarbons and lower liquid alkanes outside of the jet fuel range was not favored. Aromatics are another key component of jet fuels, with nickel yielding a greater product distribution of C_9, C_{10}, C_{11}, C_{12}, and C_{14}, with tungsten catalyst ranking second at the highest temperature. Notwithstanding the feedstock's maximum carbon number of C_{23}, hydrocracking proved a variety of hydrocarbons and other components with carbon numbers higher than C_{23}—up to 30—such as C_{24}, C_{25}, C_{26}, C_{27}, C_{28}, C_{29}, and C_{30}, in smaller concentration were generated. This confirms that a C-C chain growth polymerization reaction had taken place.

Catalyst performance evaluations demonstrated that WC/$AlPO_4$-18 exhibited superior selectivity and yield, indicating its effectiveness in producing the desired product while minimizing byproducts. Although Ni_3C/$AlPO_4$-18 achieved high conversion, the overall process efficiency must be considered. A high conversion rate may be less valuable if the desired product is not formed with sufficient yield or selectivity. Therefore, based on the available data, WC/$AlPO_4$-18 emerges as the preferred catalyst due to its superior selectivity and yield. However, further evaluation of its cost, long-term stability, and scalability should be considered.

In general, the production of SAF from *Brassica carinata* oils significantly diversifies fuel sources, enabling the aviation industry to reduce its reliance on fossil fuels and enhance energy security. Furthermore, the cultivation of *Brassica carinata* for SAF production can stimulate sustainable agriculture practices and contribute to rural economic development.

8.2 Recommendations and Future Outlooks

The following topics deemed critical to the advancement of this study, are included in this section. They represent key areas that remain unexplored but offer significant potential for future research. To further elucidate the impact of feedstock composition on the process, future studies could

investigate the effects of varying *Brassica carinata* oil varieties (e.g., Holetta-1, Derash, Tesfa) and those cultivated in diverse geographic regions, on catalyst performance and process optimization. To facilitate informed decision-making, future studies should conduct comprehensive economic analysis including cost-benefit analyses comparing the production costs of bio-jet fuel derived from *Brassica carinata* oil to those of other feedstocks and conventional jet fuel. This section could also address policy issues like land use and competition. Although *Brassica carinata* is not a food crop, its cultivation can still impact land use and biodiversity.

Additionally, an economic feasibility study of SAF production from *Brassica carinata* could inform investment decisions and policy development. The same goes for a more comprehensive environmental impact assessment, which must promote the use of a life cycle assessment (LCA) to quantify the environmental impacts related to the entire production process, from cultivation to final fuel production, with a main focus on quantifying SAF's carbon footprint and identifying potential areas for improvement.

Despite the exploration of potential practical applications in the present study, it remains imperative to maintain catalyst properties, including activity, selectivity, and stability, mitigate catalyst deactivation mechanisms, and ensure long-term catalyst stability under industrial conditions. Despite extensive research, the reaction kinetics and mechanisms underlying hydroprocessing processes remain inadequately explored, necessitating further mechanistic studies to enhance a better understanding of the field. Consequently, future research efforts should be directed toward elucidating these fundamental aspects and establishing robust methodologies for their consistent application. Although an in-depth study of the fixed-bed reactor system has been conducted, future research should encompass a comprehensive investigation of its hydrodynamic profile, including flow regime, hold-up, pressure drop, and flow maldistribution, to fully understand its performance characteristics. Catalytic processes, including performance tests, must be optimized through research to enhance SAF production, reduce byproducts, and improve energy efficiency

Further investigations into $AlPO_4$-18 supported carbon-coated metal carbide catalytic materials could be undertaken using alternative TPRC synthesis conditions to those employed in the present study. This is attributable to the susceptibility of nanoparticle thermal, structural, microscopic, textural, and catalytic properties to modification through variations in reduction-carburization

conditions, such as carbon source, hydrocarbon/hydrogen gas mixture composition, maximum carburization temperature, heating rate, and holding time.

The catalysts demonstrated substantially superior performance in the production of bio-jet fuel relative to other middle distillate hydrocarbon fractions. To further augment catalyst performance by accelerating deoxygenation and hydrocracking rates, the imposition of substantially elevated hydrogen pressures beyond that utilized in this study could be explored. Such conditions are anticipated to suppress the formation of unsaturated products. Consequently, researchers are strongly urged to conduct further investigations to accelerate the rate of deoxygenation and hydrocracking reactions, thereby achieving higher conversion, yield, and selectivity rates.

BIBLIOGRAPHY

[1] O. Ogunkunle and N. A. Ahmed, "Overview of biodiesel combustion in mitigating the adverse impacts of engine emissions on the sustainable human–environment scenario," *Sustainability*, vol. 13, no. 10, p. 5465, 2021, doi: 10.3390/su13105465.

[2] IEA, "World energy outlook," *OECD/IEA*, pp. 1–601, 2006, doi: 10.1787/20725302.

[3] A. Demirbas and M. F. Demirbas, *Green energy and technology*. London: Springer London, 2010.

[4] N. Lior, "Energy resources and use: The present situation and possible paths to the future," *Energy*, vol. 33, no. 6, pp. 842–857, 2008, doi: 10.1016/j.energy.2007.09.009.

[5] S. Lestari, P. Mäki-Arvela, J. Beltramini, G. Q. M. Lu, and D. Y. Murzin, "Transforming triglycerides and fatty acids into biofuels," *ChemSusChem*, vol. 2, no. 12, pp. 1109–1119, 2009, doi: 10.1002/cssc.200900107.

[6] N. E. Benti *et al.*, "Biodiesel production in Ethiopia: Current status and future prospects," *Sci. African*, vol. 19, p. e01531, 2023, doi: 10.1016/j.sciaf.2022.e01531.

[7] J. Yang, Z. Xin, K. Corscadden, and H. Niu, "An overview on performance characteristics of bio-jet fuels," *Fuel*, vol. 237, no. 1 February 2019, pp. 916–936, 2019, doi: 10.1016/j.fuel.2018.10.079.

[8] S. S. Doliente, A. Narayan, J. F. D. Tapia, N. J. Samsatli, Y. Zhao, and S. Samsatli, "Bio-aviation Fuel: A Comprehensive Review and Analysis of the Supply Chain Components," *Front. Energy Res.*, vol. 8, no. July, pp. 1–38, 2020, doi: 10.3389/fenrg.2020.00110.

[9] A. Almena, R. Siu, K. Chong, P. Thornley, and M. Röder, "Reducing the environmental impact of international aviation through sustainable aviation fuel with integrated carbon capture and storage," *Energy Convers. Manag.*, vol. 303, p. 118186, 2024, doi: 10.1016/j.enconman.2024.118186.

[10] M. A. Díaz-Pérez and J. C. Serrano-Ruiz, "Catalytic production of jet fuels from biomass," *Molecules*, vol. 25, no. 4, p. 802, 2020, doi: 10.3390%2Fmolecules25040802.

[11] IATA, "An Airline bandbook on CORSIA," no. April, pp. 1–54, 2018, [Online]. Available: http://www.iata.org/pages/search.aspx?k=emissions.

[12] A. Bittner, W. E. Tyner, and X. Zhao, "Field to flight: A techno-economic analysis of the corn stover to aviation biofuels supply chain," *Biofuels, Bioprod. Biorefining*, vol. 9, no. 2, pp. 201–210, 2015, doi: 10.1002/bbb.1536.

[13] W. Moonsrikaew *et al.*, "Bio-jet fuel production from crude palm kernel oil under hydrogen-nitrogen atmosphere in a fixed-bed reactor by using Pt/C as catalyst," *Energy Convers. Manag. X*, vol. 20, p. 100471, 2023, doi: 10.1016/j.ecmx.2023.100471.

[14] N. R. Baral *et al.*, "Techno-economic analysis and life-cycle greenhouse gas mitigation cost of five routes to bio-jet fuel blendstocks," *Energy Environ. Sci.*, vol. 12, no. 3, pp. 807–824, 2019, doi: 10.1039/C8EE03266A.

[15] D. Klein-Marcuschamer *et al.*, "Technoeconomic analysis of renewable aviation fuel from microalgae, Pongamia pinnata, and sugarcane," *Biofuels, Bioprod. Biorefining*, vol. 7, no. 4, pp. 416–428, 2013, doi: 10.1002/bbb.1404.

[16] E. Mupondwa, X. Li, L. Tabil, K. Falk, and R. Gugel, "Technoeconomic analysis of camelina oil extraction as feedstock for biojet fuel in the Canadian Prairies," *Biomass and Bioenergy*, vol. 95, pp. 221–234, 2016, doi: 10.1016/j.biombioe.2016.10.014.

[17] L. Tao, Z. Lin, J. Chen, Y. Wu, and X. Liu, "Mid-infrared and near-infrared spectroscopy for rapid detection of Gardeniae Fructus by a liquid-liquid extraction process," *J. Pharm. Biomed. Anal.*, vol. 145, pp. 1–9, 2017, doi: 10.1016/j.jpba.2017.06.021.

[18] N. None, "Alternative Aviation Fuels: Overview of Challenges, Opportunities, and Next Steps. United States," 2017. doi: 10.2172/1358063.

[19] A. Milbrandt, C. Kinchin, and R. McCormick, "The Feasibility of producing and using biomass-based diesel and jet fuel in the United States," Golden, CO: National Renewable Energy Lab.(NREL). NREL/TP6A20-5805., 2013. doi: 10.2172/1260324.

[20] L. Tao, A. Milbrandt, Y. Zhang, and W.-C. C. Wang, "Techno-economic and resource analysis of hydroprocessed renewable jet fuel," *Biotechnol. Biofuels*, vol. 10, no. 1, p. 16, 2017, doi: 10.1186/s13068-017-0945-3.

[21] R. Seepaul *et al.*, "Brassica carinata: Biology and agronomy as a biofuel crop," *GCB Bioenergy*, vol. 13, no. 4, pp. 582–599, 2021, doi: 10.1111/gcbb.12804.

[22] A. Alam, M. F. H. Masum, and P. Dwivedi, "Break-even price and carbon emissions of carinata-based sustainable aviation fuel production in the Southeastern United States," *GCB Bioenergy*, vol. 13, no. 11, pp. 1800–1813, 2021, doi: 10.1111/gcbb.12888.

[23] M. Wang *et al.*, "Summary of Expansions and Updates in GREET® 2018," Argonne National Lab.(ANL), Argonne, IL (United States), 2018. doi: 10.2172/1483843.

[24] Z. T. Redda, A. Laß-Seyoum, A. Yimam, M. Barz, and S. A. Jabasingh, "Solvent extraction and characterization of Brassica carinata oils as promising alternative feedstock for bio-jet

fuel production," *Biomass Conv. and Bioref.*, 2022, doi: 10.1007/s13399-022-03343-x.

[25] R. Seepaul *et al.*, "Carinata, the Sustainable Crop for a Bio-Based Economy : 2018–2019 Production Recommendations for the Southeastern United States," *Univ. Florida, IFAS Ext.*, pp. 1–12, 2019, [Online]. Available: http://edis.ifas.ufl.edu/pdffiles/AG/AG38900.pdf.

[26] M. Basili and M. A. Rossi, "Brassica carinata-derived biodiesel production: economics, sustainability and policies. The Italian case," *J. Clean. Prod.*, vol. 191, pp. 40–47, 2018, doi: 10.1016/j.jclepro.2018.03.306.

[27] B. Lal *et al.*, "Biomass, yield, quality and moisture use of Brassica carinata as influenced by intercropping with chickpea under semiarid tropics," *J. Saudi Soc. Agric. Sci.*, vol. 18, no. 1, pp. 61–71, 2019, doi: 10.1016/j.jssas.2017.01.001.

[28] W. Zegada-Lizarazu and A. Monti, "Energy crops in rotation. A review," *Biomass and bioenergy*, vol. 35, no. 1, pp. 12–25, 2011, doi: 10.1016/j.biombioe.2010.08.001.

[29] S. Kumar *et al.*, "Brassica carinata genotypes demonstrate potential as a winter biofuel crop in South East United States," *Ind. Crops Prod.*, vol. 150, no. October 2019, pp. 1–10, 2020, [Online]. Available: https://doi.org/10.1016/j.indcrop.2020.112353.

[30] S. George *et al.*, "A Regional Inter-Disciplinary Partnership Focusing on the Development of a carinata-Centered Bioeconomy," *GCB Bioenergy*, vol. 13, no. 7, pp. 1018–1029, 2021, doi: 10.1111/gcbb.12828.

[31] R. R. C. Monteiro *et al.*, "Production of jet biofuels by catalytic hydroprocessing of esters and fatty acids: a review," *Catalysts*, vol. 12, no. 2, p. 237, 2022, doi: 10.3390/catal12020237.

[32] J. A. Okolie *et al.*, "Multi criteria decision analysis for the evaluation and screening of sustainable aviation fuel production pathways," *Iscience*, 2023, doi: 10.1016%2Fj.isci.2023.106944.

[33] G. R. Wilson III, T. Edwards, E. Corporan, and R. L. Freerks, "Certification of alternative aviation fuels and blend components," *Energy & Fuels*, vol. 27, no. 2, pp. 962–966, 2013, doi: 10.1021/ef301888b.

[34] P. L. Chu, C. Vanderghem, H. L. MacLean, and B. A. Saville, "Process modeling of hydrodeoxygenation to produce renewable jet fuel and other hydrocarbon fuels," *Fuel*, vol. 196, pp. 298–305, 2017, doi: 10.1016/j.fuel.2017.01.097.

[35] J. K. Satyarthi, T. Chiranjeevi, D. T. Gokak, and P. S. Viswanathan, "An overview of catalytic conversion of vegetable oils/fats into middle distillates," *Catal. Sci. Technol.*, vol.

3, no. 1, pp. 70–80, 2013, doi: 10.1039/c2cy20415k.

[36] B. Chan and L. Radom, “Design of effective zeolite catalysts for the complete hydrogenation of CO2,” *J. Am. Chem. Soc.*, vol. 128, no. 16, pp. 5322–5323, 2006, doi: 10.1021/ja0602492.

[37] E. Ochoa, D. Torres, R. Moreira, J. L. Pinilla, and I. Suelves, “Carbon nanofiber supported Mo2C catalysts for hydrodeoxygenation of guaiacol: The importance of the carburization process,” *Appl. Catal. B Environ.*, vol. 239, pp. 463–474, 2018, doi: 10.1016/j.apcatb.2018.08.043.

[38] D. A. Ruddy, J. A. Schaidle, J. R. Ferrell, J. Wang, L. Moens, and J. E. Hensley, “Recent advances in heterogeneous catalysts for bio-oil upgrading via ‘ex situ catalytic fast pyrolysis’: Catalyst development through the study of model compounds,” *Green Chem.*, vol. 16, no. 2, pp. 454–490, 2014, doi: 10.1039/c3gc41354c.

[39] L. Chen, H. Li, J. Fu, C. Miao, P. Lv, and Z. Yuan, “Catalytic hydroprocessing of fatty acid methyl esters to renewable alkane fuels over Ni/HZSM-5 catalyst,” *Catal. today*, vol. 259, pp. 266–276, 2016, doi: 10.1016/j.cattod.2015.08.023.

[40] H. Prats, J. J. Piñero, F. Viñes, S. T. Bromley, R. Sayós, and F. Illas, “Assessing the usefulness of transition metal carbides for hydrogenation reactions,” *Chem. Commun.*, vol. 55, no. 85, pp. 12797–12800, 2019, doi: 10.1039/C9CC06084G.

[41] H. H. Hwu and J. G. Chen, “Surface chemistry of transition metal carbides,” *Chem. Rev.*, vol. 105, no. 1, pp. 185–212, 2005, doi: 10.1021/cr0204606.

[42] J. Pang, J. Sun, M. Zheng, H. Li, Y. Wang, and T. Zhang, “Transition metal carbide catalysts for biomass conversion: A review,” *Appl. Catal. B Environ.*, vol. 254, pp. 510–522, 2019, doi: 10.1016/j.apcatb.2019.05.034.

[43] J. I. Hileman and R. W. Stratton, “Alternative jet fuel feasibility,” *Transp. Policy*, vol. 34, pp. 52–62, 2014, doi: 10.1016/j.tranpol.2014.02.018.

[44] M. Lim, M. K. (Marty. Luckert, and F. Qiu, “Economic opportunities and challenges in biojet production: A literature review and analysis,” *Biomass and Bioenergy*, vol. 170, p. 106727, 2023, doi: 10.1016/j.biombioe.2023.106727.

[45] C. Bergero, G. Gosnell, D. Gielen, S. Kang, M. Bazilian, and S. J. Davis, “Pathways to net-zero emissions from aviation,” *Nat. Sustain.*, vol. 6, no. 4, pp. 404–414, 2023, doi: 10.1038/s41893-022-01046-9.

[46] K. Ericsson, “Potential for the integrated production of biojet fuel in swedish plant infrastructures,” *Energies*, vol. 14, no. 20, p. 6531, 2021, doi: 10.3390/en14206531.

[47] N. Pavlenko and A. Kharina, “Policy and environmental implications of using HEFA+ for aviation,” *Int Counc Clean Transp*, vol. 9, pp. 1–9, 2018.

[48] M. Wang, M. Chen, Y. Fang, and T. Tan, “Highly efficient conversion of plant oil to bio-aviation fuel and valuable chemicals by combination of enzymatic transesterification, olefin cross-metathesis, and hydrotreating,” *Biotechnol. Biofuels*, vol. 11, no. 1, pp. 1–9, 2018, doi: 10.1186/s13068-018-1020-4.

[49] D. Chiaramonti, M. Prussi, M. Buffi, and D. Tacconi, “Sustainable bio kerosene: Process routes and industrial demonstration activities in aviation biofuels,” *Appl. Energy*, vol. 136, pp. 767–774, 2014, doi: 10.1016/j.apenergy.2014.08.065.

[50] T. D. Hong, T. H. Soerawidjaja, I. K. Reksowardojo, O. Fujita, Z. Duniani, and M. X. Pham, “A study on developing aviation biofuel for the tropics: Production process - experimental and theoretical evaluation of their blends with fossil kerosene,” *Chem. Eng. Process. Process Intensif.*, vol. 74, pp. 124–130, 2013, doi: 10.1016/j.cep.2013.09.013.

[51] K. Crawford, “International environmental agreements on climate change,” in *International Environmental Agreements on Climate Change*, vol. 6, no. 1, Morris: Springer, Dordrecht, 2013, pp. 1–8.

[52] M. Cardone *et al.*, “Brassica carinata as an alternative oil crop for the production of biodiesel in Italy: Agronomic evaluation, fuel production by transesterification and characterization,” *Biomass and Bioenergy*, vol. 25, no. 6, pp. 623–636, 2003, doi: 10.1016/S0961-9534(03)00058-8.

[53] M. Bashyal *et al.*, “Brassica carinata biomass, yield, and seed chemical composition response to nitrogen rates and timing on southern Coastal Plain soils in the United States,” *GCB Bioenergy*, vol. 13, no. 8, pp. 1275–1289, 2021, doi: 10.1111/gcbb.12846.

[54] S. Saconsint *et al.*, “Development of Ni–Mo carbide catalyst for production of syngas and CNTs by dry reforming of biogas,” *Sci. Rep.*, vol. 13, no. 1, p. 12928, 2023, doi: 10.1038/s41598-023-38436-8.

[55] I. Kubičková, M. Snåre, K. Eränen, P. Mäki-Arvela, and D. Y. Murzin, “Hydrocarbons for diesel fuel via decarboxylation of vegetable oils,” *Catal. Today*, vol. 106, no. 1–4, pp. 197–200, 2005, doi: 10.1016/j.cattod.2005.07.188.

[56] P. A. Alaba, A. Abbas, J. Huang, and W. M. A. W. Daud, “Molybdenum carbide nanoparticle: Understanding the surface properties and reaction mechanism for energy production towards a sustainable future,” *Renew. Sustain. Energy Rev.*, vol. 91, pp. 287–

300, 2018, doi: 10.1016/j.rser.2018.03.106.

[57] X.-H. Wang, H.-L. Hao, M.-H. Zhang, W. Li, and K.-Y. Tao, “Synthesis and characterization of molybdenum carbides using propane as carbon source,” *J. Solid State Chem.*, vol. 179, no. 2, pp. 538–543, 2006, doi: 10.1016/j.jssc.2005.11.009.

[58] K.-H. Wu, Y. Jiang, S. Jiao, K.-C. Chou, and G.-H. Zhang, “Synthesis of high purity nano-sized transition-metal carbides,” *J. Mater. Res. Technol.*, vol. 9, no. 5, pp. 11778–11790, 2020, doi: 10.1016/j.jmrt.2020.08.053.

[59] H. M. Noh, A. Benito, and G. Alonso, “Study of the current incentive rules and mechanisms to promote biofuel use in the EU and their possible application to the civil aviation sector,” *Transp. Res. Part D*, vol. 46, no. 2016, pp. 298–316, 2016, doi: 10.1016/j.trd.2016.04.007.

[60] IATA, “Carbon offsetting for international aviation,” pp. 1–4, 2019, [Online]. Available: https://www.iata.org/policy/environment/Documents/paper-offsetting-for-aviation.pdf.

[61] J. Remón *et al.*, “Sustainable production of liquid biofuels and value-added platform chemicals by hydrodeoxygenation of lignocellulosic bio-oil over a carbon–neutral Mo2C/CNF catalyst,” *Chem. Eng. J.*, vol. 405, pp. 1–36, 2021, doi: 10.1016/j.cej.2020.126705.

[62] J. Remón *et al.*, “Bio-oil upgrading in supercritical water using Ni-Co catalysts supported on carbon nanofibres,” *Fuel Process. Technol.*, vol. 154, pp. 178–187, 2016, doi: 10.1016/j.fuproc.2016.08.030.

[63] S. Cheng, “Development of Heterogeneous Catalysts for Upgrading Biomass Pyrolysis Bio-Oils into Advanced Biofuels,” 2017.

[64] K. Rambabu *et al.*, “Sustainable production of bio-jet fuel and green gasoline from date palm seed oil via hydroprocessing over tantalum phosphate,” *Fuel*, vol. 331, p. 125688, 2023, doi: 10.1016/j.fuel.2022.125688.

[65] B. K. Barnwal and M. P. Sharma, “Prospects of biodiesel production from vegetable oils in India,” *Renew. Sustain. Energy Rev.*, vol. 9, pp. 363–378, 2005, doi: 10.1016/j.rser.2004.05.007.

[66] G. Toscano, G. Riva, E. Foppa Pedretti, and D. Duca, “Vegetable oil and fat viscosity forecast models based on iodine number and saponification number,” *Biomass and Bioenergy*, vol. 46, pp. 511–516, 2012, doi: 10.1016/j.biombioe.2012.07.009.

[67] R. Sotelo-Boyas, F. Trejo-Zarraga, and F. de Jesus Hernandez-Loyo, “Hydroconversion of triglycerides into green liquid fuels,” in *Hydrogenation*, México D.F.: IntechOpen, 2012,

pp. 187–216.

[68] H. Wang, “Biofuels production from hydrotreating of vegetable oil using supported noble metals, and transition metal carbide and nitride,” Wayne State University, 2012.

[69] F. Cherubini, “The biorefinery concept: Using biomass instead of oil for producing energy and chemicals,” *Energy Convers. Manag.*, vol. 51, no. 7, pp. 1412–1421, 2010, doi: 10.1016/j.enconman.2010.01.015.

[70] E. Yara-Varón, Y. Li, M. Balcells, R. Canela-Garayoa, A. S. Fabiano-Tixier, and F. Chemat, “Vegetable oils as alternative solvents for green oleo-extraction, purification and formulation of food and natural products,” *Molecules*, vol. 22, no. 9, pp. 1–24, 2017, doi: 10.3390/molecules22091474.

[71] V. G. Gude and G. Grant, “Sustainable biodiesel production,” in *2nd World Sustainability Forum*, 2012, pp. 1–14, doi: 10.3390/wsf2-00889.

[72] M. Al-Sabawi, J. Chen, and S. Ng, “Fluid catalytic cracking of biomass-derived oils and their blends with petroleum feedstocks: A review,” *Energy and Fuels*, vol. 26, no. 9, pp. 5355–5372, 2012, doi: 10.1021/ef3006417.

[73] E. M. Kondili and J. K. Kaldellis, “Biofuel implementation in East Europe: Current status and future prospects,” *Renew. Sustain. Energy Rev.*, vol. 11, no. 9, pp. 2137–2151, 2007, doi: 10.1016/j.rser.2006.05.001.

[74] M. M. Gui, K. T. Lee, and S. Bhatia, “Feasibility of edible oil vs. non-edible oil vs. waste edible oil as biodiesel feedstock,” *Energy*, vol. 33, no. 11, pp. 1646–1653, 2008, doi: 10.1016/j.energy.2008.06.002.

[75] T. V. M. Rao, M. M. Clavero, and M. Makkee, “Effective gasoline production strategies by catalytic cracking of Rapeseed vegetable oil in refinery conditions,” *ChemSusChem*, vol. 3, pp. 807–810, 2010, doi: 10.1002/cssc.201000128.

[76] A. H. Demirbas and I. Demirbas, “Importance of rural bioenergy for developing countries,” *Energy Convers. Manag.*, vol. 48, pp. 2386–2398, 2007, doi: 10.1016/j.enconman.2007.03.005.

[77] F. Pinto, F. T. Varela, M. Gonçalves, R. Neto André, P. Costa, and B. Mendes, “Production of bio-hydrocarbons by hydrotreating of pomace oil,” *Fuel*, vol. 116, pp. 84–93, 2014, doi: 10.1016/j.fuel.2013.07.116.

[78] B. Kindo, “Carinata FAME production process and biofuel oxidation,” 2016.

[79] M. Ionescu and Z. S. Petrović, “Phenolation of vegetable oils,” *J. Serbian Chem. Soc.*, vol.

76, no. 4, pp. 591–606, 2011, doi: 10.2298/JSC100820050I.

[80] R. W. Gosselink *et al.*, "Reaction pathways for the deoxygenation of vegetable oils and related model compounds," *ChemSusChem*, vol. 6, no. 9, pp. 1576–1594, 2013, doi: 10.1002/cssc.201300370.

[81] J. E. Iboyi *et al.*, "Tillage system and seeding rate effects on the performance of Brassica carinata," *GCB Bioenergy*, vol. 13, no. 4, pp. 600–617, 2021, doi: 10.1111/gcbb.12809.

[82] E. M. Ammar, J. Martin, and G. P. Philippidis, "Biochemical conversion of Brassica carinata biomass to organic acids," *GCB Bioenergy*, vol. 13, no. 4, pp. 618–626, 2021, doi: 10.1111/gcbb.12812.

[83] S. George *et al.*, "A regional inter-disciplinary partnership focusing on the development of a carinata-centered bioeconomy. GCB Bioenergy, 13 (7), 1018–1029." 2021, doi: 10.1111/gcbb.12828.

[84] P. Dwivedi, "Sustainable aviation fuel production from Brassica carinata in the Southern United States," *Glob. Change Biol. Bioenergy*, vol. 13, no. 12, pp. 1854–1858, 2021.

[85] N. Hoghooghi, D. D. Bosch, and B. P. Bledsoe, "Assessing hydrologic and water quality effects of land use conversion to Brassica carinata as a winter biofuel crop in the southeastern coastal plain of Georgia, USA using the SWAT model," *Gcb Bioenergy*, vol. 13, no. 3, pp. 473–492, 2021, doi: 10.1111/gcbb.12792.

[86] R. Seepaul, S. George, and D. L. Wright, "Comparative response of Brassica carinata and B. napus vegetative growth, development and photosynthesis to nitrogen nutrition," *Ind. Crops Prod.*, vol. 94, pp. 872–883, 2016, doi: 10.1016/j.indcrop.2016.09.054.

[87] J. M. Baldwin, S. V Paula-Moraes, M. J. Mulvaney, and R. L. Meagher, "Occurrence of arthropod pests associated with Brassica carinata and impact of defoliation on yield," *GCB Bioenergy*, vol. 13, no. 4, pp. 570–581, 2021, doi: 10.1111/gcbb.12801.

[88] P. Gegg, L. Budd, and S. Ison, "The market development of aviation biofuel: Drivers and constraints," *J. Air Transp. Manag.*, vol. 39, pp. 34–40, 2014, doi: 10.1016/j.jairtraman.2014.03.003.

[89] S. Kumar *et al.*, "Brassica carinata genotypes demonstrate potential as a winter biofuel crop in South East United States," *Ind. Crops Prod.*, vol. 150, p. 112353, 2020, doi: 10.1016/j.indcrop.2020.112353.

[90] B. Brem *et al.*, "Effects of fuel aromatic content on non-volatile particulate emissions of an in-production aircraft gas turbine," *Environ. Sci. Technol.*, vol. 49, no. 22, pp. 13149–13157,

2015, doi: 10.1021/acs.est.5b04167.

[91] R. L. J. Coetzer, T. S. Joubert, C. L. Viljoen, R. J. J. Nel, and C. A. Strydom, "Response surface models for synthetic jet fuel properties," *Appl. Petrochemical Res.*, vol. 8, no. 1, pp. 39–53, 2018, doi: 10.1007/s13203-018-0196-7.

[92] G. Liu, B. Yan, and G. Chen, "Technical review on jet fuel production," *Renew. Sustain. Energy Rev.*, vol. 25, pp. 59–70, 2013, doi: 10.1016/j.rser.2013.03.025.

[93] S. Liu, Q. Zhu, Q. Guan, L. He, and W. Li, "Bio-aviation fuel production from hydroprocessing castor oil promoted by the nickel-based bifunctional catalysts," *Bioresour. Technol.*, vol. 183, pp. 93–100, 2015, doi: 10.1016/j.biortech.2015.02.056.

[94] J. I. Hileman *et al.*, "Near-term feasibility of alternative jet fuels -Technical report," Santa Monica, Arlington, Pittsburgh, 2009. [Online]. Available: https://www.rand.org/pubs/technical_reports/TR554.html.

[95] R. Berger, "Sustainable aviation fuels: The best solution to large sustainable aircraft?," London, UK, 2020.

[96] E. I. Fitriasari, W. Won, and J. J. Liu, "Sustainability assessment of biojet fuel produced from pyrolysis oil of woody biomass," *Sustain. Energy Fuels*, vol. 7, no. 15, pp. 3625–3636, 2023, doi: 10.1039/D3SE00468F.

[97] A. Demirbas, "Biofuels sources, biofuel policy, biofuel economy and global biofuel projections," *Energy Convers. Manag.*, vol. 49, no. 8, pp. 2106–2116, 2008, doi: 10.1016/j.enconman.2008.02.020.

[98] M. Mofijur, M. A. Hazrat, M. G. Rasul, and H. M. Mahmudul, "Comparative evaluation of edible and non-edible oil methyl ester performance in a vehicular engine," *Energy procedia*, vol. 75, pp. 37–43, 2015, doi: 10.1016/j.egypro.2015.07.134.

[99] C. Zhang, L. Luo, W. Chen, F. Yang, G. Luo, and J. Xu, "Experimental Investigation on the Performance of an Aviation Piston Engine Fueled with Bio-Jet Fuel Prepared via Thermochemical Conversion of Triglyceride," *Energies*, vol. 15, no. 9, 2022, doi: 10.3390/en15093246.

[100] W. Wang and L. Tao, "Bio-Jet Fuel Conversion Technologies," *Renew. Sustain. Energy Rev.*, vol. 53, no. 1, pp. 1–37, 2016, doi: 10.1016/j.rser.2015.09.016.

[101] R. D. Brandão, A. M. de Freitas Júnior, S. C. Oliveira, P. A. Z. Suarez, and M. J. Prauchner, "The conversion of coconut oil into hydrocarbons within the chain length range of jet fuel," *Biomass Convers. biorefinery*, vol. 11, pp. 837–847, 2021, doi: 10.1007/s13399-020-01046-

9.

[102] W. Kiatkittipong *et al.*, “Bioresources and biofuels—From classical to perspectives and trends,” *AZ Biorefinery*, pp. 165–220, 2022, doi: 1016/B978-0-12-819248-1.00004-X.

[103] X. Zhang and T. Jia, “Development history and basics of aerospace fuels,” in *High-Energy-Density Fuels for Advanced Propulsion: Design and Synthesis*, L. P. Ji-Jun Zou, Xiangwen Zhang, Ed. Wiley Online Library, 2020, pp. 5–38.

[104] I. E. A. B. Task, “Progress in commercialization of biojet/Sustainable Aviation Fuels (SAF): Technologies, potential and challenges,” 2021.

[105] R. Yang *et al.*, “Transformation of jatropha oil into high-quality biofuel over Ni–W bimetallic catalysts,” *ACS omega*, vol. 4, no. 6, pp. 10580–10592, 2019, doi: 10.1021/acsomega.9b00375.

[106] J. Pechstein, U. Neuling, J. Gebauer, and M. Kaltschmitt, “Alcohol-to-Jet (AtJ),” *Biokerosene Status Prospect.*, pp. 543–574, 2018, doi: 10.1007/978-3-662-53065-8_21.

[107] M. Elkelawy, H. A.-E. Bastawissi, A. M. Radwan, M. T. Ismail, and M. El-Sheekh, “Biojet fuels production from algae: conversion technologies, characteristics, performance, and process simulation,” in *Handbook of Algal Biofuels*, Elsevier, 2022, pp. 331–361.

[108] E. Emmanouilidou, S. Mitkidou, A. Agapiou, and N. C. Kokkinos, “Solid waste biomass as a potential feedstock for producing sustainable aviation fuel: a systematic review,” *Renew. Energy*, vol. 206, 2023, doi: 10.1016/j.renene.2023.02.113.

[109] L. Tao, J. N. Markham, Z. Haq, and M. J. Biddy, “Techno-economic analysis for upgrading the biomass-derived ethanol-to-jet blendstocks,” *Green Chem.*, vol. 19, no. 4, pp. 1082–1101, 2017, doi: 10.1039/C6GC02800D.

[110] P. Foster, “Version of Record: https://www.sciencedirect.com/science/article/pii/S0034425719300781,” no. x, pp. 1–37, 2019.

[111] T. V. Choudhary and C. B. Phillips, “Renewable fuels via catalytic hydrodeoxygenation,” *Appl. Catal. A Gen.*, vol. 397, no. 1–2, pp. 1–12, 2011, doi: 10.1016/j.apcata.2011.02.025.

[112] H. Topsøe, B. S. Clausen, and F. E. Massoth, “Hydrotreating catalysis,” in *Catalysis: Science and Technology*, Vol 11., J. R. Anderson and M. Boudart, Eds. Berlin, Heidelberg: Springer Berlin Heidelberg, 1996, pp. 1–269.

[113] I. E. Maxwell, “Zeolite catalysis in hydroprocessing technology,” *Catal. Today*, vol. 1, no. 4, pp. 385–413, 1987, doi: 10.1016/0920-5861(87)80006-8.

[114] N. Arun, R. V. Sharma, and A. K. Dalai, “Green diesel synthesis by hydrodeoxygenation of bio-based feedstocks: Strategies for catalyst design and development,” *Renew. Sustain. Energy Rev.*, vol. 48, pp. 240–255, 2015, doi: 10.1016/j.rser.2015.03.074.

[115] S. Carenco, D. Portehault, C. Boissière, N. Mézailles, and C. Sanchez, “Nanoscaled metal borides and phosphides : Recent developments and perspectives,” *Chem. Rev.*, vol. 113, p. 7981−8065, 2013, doi: 10.1021/cr400020d.

[116] S. Meng *et al.*, “Synthesis and characterization of molybdenum carbide catalysts on different carbon supports,” *Catal. Today*, vol. 402, pp. 266–275, 2022, doi: 10.1016/j.cattod.2022.04.020.

[117] N. Czaplicka, A. Rogala, and I. Wysocka, “Metal (Mo, W, Ti) carbide catalysts: Synthesis and application as alternative catalysts for dry reforming of hydrocarbons—A review,” *Int. J. Mol. Sci.*, vol. 22, no. 22, p. 12337, 2021, doi: 10.3390/ijms222212337.

[118] D. Akmach, S. Bathla, C.-C. Tran, S. Kaliaguine, and S. H. Mushrif, “Transition metal carbide catalysts for Upgrading lignocellulosic biomass-derived oxygenates: A review of the experimental and computational investigations into structure-property relationships,” *Catal. Today*, vol. 423, p. 114285, 2023, doi: 10.1016/j.cattod.2023.114285.

[119] X. Wang, M. Zhang, W. Li, and K. Tao, “Synthesis and characterization of cobalt – molybdenum bimetallic carbides catalysts,” *Catal. Today*, vol. 131, pp. 111–117, 2008, doi: 10.1016/j.cattod.2007.10.070.

[120] J. S. Lee, S. T. Oyama, and M. Boudart, “Molybdenum carbide catalysts,” *J. Catal.*, vol. 133, pp. 125–133, 1987, doi: 10.1016/0021-9517(87)90218-1.

[121] J. Vakros, C. Papadopoulou, G. A. Voyiatzis, A. Lycourghiotis, and C. Kordulis, “Modification of the preparation procedure for increasing the hydrodesulfurisation activity of the CoMo/γ-alumina catalysts,” *Catal. Today*, vol. 127, no. 1–4, pp. 85–91, 2007, doi: 10.1016/j.cattod.2007.02.028.

[122] P. Salerno, S. Mendioroz, and A. López Agudo, “Al-pillared montmorillonite-based NiMo catalysts for HDS and HDN of gas oil: Influence of the method and order of Mo and Ni impregnation,” *Appl. Catal. A Gen.*, vol. 259, no. 1, pp. 17–28, 2004, doi: 10.1016/j.apcata.2003.09.019.

[123] R. L. Austermann *et al.*, “Catalyst characterization,” *Anal. Chem.*, vol. 59, no. 12, pp. 68–102, 1987, doi: 10.1021/ac00139a005.

[124] G. Leofanti, G. Tozzola, M. Padovan, G. Petrini, S. Bordiga, and A. Zecchina, “Catalyst

characterization: Applications," *Catal. Today*, vol. 34, no. 3–4, pp. 329–352, 1997, doi: 10.1016/S0920-5861(97)86089-0.

[125] E. Furimsky, "Hydroprocessing challenges in biofuels production," *Catal. Today*, vol. 217, pp. 13–56, 2013, doi: 10.1016/j.cattod.2012.11.008.

[126] S. Bezergianni, "Catalytic hydroprocessing of liquid biomass for biofuels production.," in *Advanced Biofuels: Using Catalytic Routes for the Conversion of Biomass Platform Molecules. Berghahn Books*, 2015, pp. 47–82.

[127] L. Tao, A. Milbrandt, Y. Zhang, and W.-C. Wang, "Techno-economic and resource analysis of hydroprocessed renewable jet fuel," *Biotechnol. Biofuels*, vol. 10, no. 261, 2017, doi: 10.1186/s13068-017-0945-3.

[128] C. S. Hsu and P. R. Robinson, *Practical advances in petroleum processing*, vol. 1. Baton Rouge, Louisiana, USA: Springer, 2006.

[129] V. Verma, A. Mishra, M. Anand, S. A. Farooqui, and A. K. Sinha, "Catalytic hydroprocessing of waste cooking oil for the production of drop-in aviation fuel and optimization for improving jet biofuel quality in a fixed bed reactor," *Fuel*, vol. 333, p. 126348, 2023, doi: 10.1016/j.fuel.2022.126348.

[130] B. Veriansyah *et al.*, "Production of renewable diesel by hydroprocessing of soybean oil: Effect of catalysts," *Fuel*, vol. 94, pp. 578–585, 2012, doi: 10.1016/j.fuel.2011.10.057.

[131] M. Nasikin, B. H. Susanto, M. A. Hirsaman, and A. Wijanarko, "Biogasoline from palm oil by simultaneous cracking and hydrogenation reaction over nimo/zeolite catalyst," *World Appl. Sci. J.*, vol. 5, pp. 74–79, 2009, [Online]. Available: http://www.idosi.org/wasj/wasj5(s)/11.pdf.

[132] M. Patel and A. Kumar, "Production of renewable diesel through the hydroprocessing of lignocellulosic biomass-derived bio-oil: A review," *Renew. Sustain. Energy Rev.*, vol. 58, pp. 1293–1307, 2016, doi: 10.1016/j.rser.2015.12.146.

[133] S. Wan *et al.*, "Decoupling HZSM-5 catalyst activity from deactivation during upgrading of pyrolysis oil vapors," *ChemSusChem*, pp. 1–9, 2014, doi: 10.1002/cssc.201402861.

[134] M. Guisnet and P. Magnoux, "Coking and deactivation of zeolites: Influence of the pore structure," *Appl. Catal.*, vol. 54, no. 1, pp. 1–27, 1989, doi: 10.1016/S0166-9834(00)82350-7.

[135] C. H. Bartholomew, "Mechanisms of catalyst deactivation," *Appl. Catal. A Gen.*, vol. 212, no. 1–2, pp. 17–60, 2001, doi: 10.1016/S0926-860X(00)00843-7.

[136] S. Brunet, D. Mey, G. Perota, C. Bouchy, and F. Diehl, “On the hydrodesulfurization of FCC gasoline : A review,” *Appl. Catal. A Gen.*, vol. 278, no. 2, pp. 143–172, 2005, doi: 10.1016/j.apcata.2004.10.012.

[137] E. Furimsky and F. E. Massoth, “Deactivation of hydroprocessing catalysts,” *Catal. Today*, vol. 52, no. 4, pp. 381–495, 1999, doi: 10.1016/S0920-5861(99)00096-6.

[138] T. L. Cable and F. E. Massth, “A Basic study of catalyst aging in the H-coal process,” *Fuel Process. Technol.*, vol. 10, no. 2, pp. 105–120, 1985, doi: 10.1016/0378-3820(85)90040-2.

[139] X. Zhao, L. Wei, S. Cheng, and J. Julson, “Review of heterogeneous catalysts for catalytically upgrading vegetable oils into hydrocarbon biofuels,” *Catalysts*, vol. 7, no. 3, 2017, doi: 10.3390/catal7030083.

[140] H. Jahromi *et al.*, “Production of green transportation fuels from Brassica carinata oil: A comparative study of noble and transition metal catalysts,” *Fuel Process. Technol.*, vol. 215, p. 106737, 2021, doi: 10.1016/j.fuproc.2021.106737.

[141] X. Zhao *et al.*, “Development of hydrocarbon biofuel from sunflower seed and sunflower meat oils over ZSM-5,” *J. Renew. Sustain. Energy*, vol. 8, no. 1, pp. 1–18, 2016, doi: 10.1063/1.4941911.

[142] H. Wang, S. Yan, S. O. Salley, and K. Y. S. Ng, “Hydrocarbon fuels production from hydrocracking of soybean oil using transition metal carbides and nitrides supported on ZSM-5,” *Ind. Eng. Chem. Res.*, vol. 51, no. 30, pp. 10066–10073, 2012, doi: 10.1021/ie3000776.

[143] L. S. Macedo, R. R. Oliveira Jr, T. van Haasterecht, V. T. da Silva, and H. Bitter, “Influence of synthesis method on molybdenum carbide crystal structure and catalytic performance in stearic acid hydrodeoxygenation,” *Appl. Catal. B Environ.*, vol. 241, pp. 81–88, 2019, doi: 10.1016/j.apcatb.2018.09.020.

[144] J. D. Adjaye and N. N. Bakhshi, “Catalytic conversion of a biomass-derived oil to fuels and chemicals I: Model compound studies and reaction pathways,” *Biomass and Bioenergy*, vol. 8, no. 3, pp. 131–149, 1995, doi: 10.1016/0961-9534(95)00018-3.

[145] T. Li, J. Cheng, R. Huang, J. Zhou, and K. Cen, “Conversion pathways of palm oil into jet biofuel catalyzed by mesoporous zeolites,” *RSC Adv.*, vol. 6, no. 106, pp. 103965–103972, 2016, doi: 10.1039/C6RA22500D.

[146] T. Li, J. Cheng, R. Huang, J. Zhou, and K. Cen, “Conversion of waste cooking oil to jet biofuel with nickel-based mesoporous zeolite Y catalyst,” *Bioresour. Technol.*, vol. 197, pp. 289–294, 2015, doi: 10.1016/j.biortech.2015.08.115.

[147] S. Bezergianni, S. Voutetakis, and A. Kalogianni, “Catalytic hydrocracking of fresh and used cooking oil,” *Ind. Eng. Chem. Res.*, vol. 48, no. 18, pp. 8402–8406, 2009, doi: 10.1021/ie900445m.

[148] J. Han, J. Duan, P. Chen, H. Lou, X. Zheng, and H. Hong, “Nanostructured molybdenum carbides supported on carbon nanotubes as efficient catalysts for one-step hydrodeoxygenation and isomerization of vegetable oils,” *Green Chem.*, vol. 13, no. 9, pp. 2561–2568, 2011, doi: 10.1039/C1GC15421D.

[149] M. Zanata, S. Tri Wulan Amelia, M. R. Mumtazy, F. Kurniawansyah, and A. Roesyadi, “Synthesis of bio jet fuel from crude palm oil by hefa (Hydroprocessed esters and fatty acids) using ni-mo catalyst supported by rice husk ash-based sio2,” in *Materials Science Forum*, 2019, vol. 964, pp. 193–198, doi: 10.4028/www.scientific.net/MSF.964.193.

[150] M. A. Bashir *et al.*, “A step change towards sustainable aviation fuel from sewage sludge,” *J. Anal. Appl. Pyrolysis*, vol. 163, p. 105498, 2022, doi: 10.1016/j.jaap.2022.105498.

[151] C. Wang *et al.*, “High quality diesel-range alkanes production via a single-step hydrotreatment of vegetable oil over Ni/zeolite catalyst,” *Catal. Today*, vol. 234, pp. 153–160, 2014, doi: 10.1016/j.cattod.2014.02.011.

[152] T. Li, J. Cheng, R. Huang, W. Yang, J. Zhou, and K. Cen, “Hydrocracking of palm oil to jet biofuel over different zeolites,” *Int. J. Hydrogen Energy*, vol. 41, no. 47, pp. 21883–21887, 2016, doi: 10.1016/j.ijhydene.2016.09.013.

[153] J. Cheng, Z. Zhang, X. Zhang, J. Liu, J. Zhou, and K. Cen, “Hydrodeoxygenation and hydrocracking of microalgae biodiesel to produce jet biofuel over H3PW12O40-Ni/hierarchical mesoporous zeolite Y catalyst,” *Fuel*, vol. 245, pp. 384–391, 2019, doi: 10.1016/j.fuel.2019.02.062.

[154] X. Li, Y. Chen, Y. Hao, X. Zhang, J. Du, and A. Zhang, “Optimization of aviation kerosene from one-step hydrotreatment of catalytic Jatropha oil over SDBS-Pt/SAPO-11 by response surface methodology,” *Renew. energy*, vol. 139, pp. 551–559, 2019, doi: 10.1016/j.renene.2019.01.085.

[155] N. Srihanun, P. Dujjanutat, P. Muanruksa, and P. Kaewkannetra, “Biofuels of green diesel–kerosene–gasoline production from palm oil: effect of palladium cooperated with second metal on hydrocracking reaction,” *Catalysts*, vol. 10, no. 2, p. 241, 2020, doi: 10.3390/catal10020241.

[156] M. Anand *et al.*, “Optimizing renewable oil hydrocracking conditions for aviation bio-

kerosene production," *Fuel Process. Technol.*, vol. 151, pp. 50–58, 2016, doi: 10.1016/j.fuproc.2016.05.028.

[157] H. Wang, S. Yan, S. O. Salley, and K. Y. S. Ng, "Hydrocarbon fuels production from hydrocracking of soybean oil using transition metal carbides and nitrides supported on ZSM-5," *Ind. Eng. Chem. Res.*, vol. 51, no. 30, pp. 10066–10073, 2012, doi: 10.1021/ie3000776.

[158] IEA, "Renewables 2021," *Int. Energy Agency Publ. Int.*, p. 167, 2021, [Online]. Available: www.iea.org/t&c/%0Ahttps://webstore.iea.org/download/direct/4329.

[159] IRENA, "Reaching Zero with Renewables: Bio-jet fuels," Abu Dhabi, 2021.

[160] S. Bezergianni, V. Dagonikou, and S. Sklari, "The suspending role of H2O and CO on catalytic hydrotreatment of gas-oil; myth or reality?," *Fuel Process. Technol.*, vol. 144, pp. 20–26, 2016, doi: 10.1016/j.fuproc.2015.12.007.

[161] G. Ionescu, *Transportation and the environment: Assessments and sustainability*, 1st ed. Apple Academic Press., 2016.

[162] S. Pinzi, L. M. Gandía, G. Arzamendi, J. J. Ruiz, and M. P. Dorado, "Influence of vegetable oils fatty acid composition on reaction temperature and glycerides conversion to biodiesel during transesterification," *Bioresour. Technol.*, vol. 102, no. 2, pp. 1044–1050, 2011, doi: 10.1016/j.biortech.2010.08.029.

[163] S. Bezergianni, S. Voutetakis, and A. Kalogianni, "Catalytic hydrocracking of fresh and used cooking oil," *Ind. Eng. Chem. Res.*, vol. 48, no. 18, pp. 8402–8406, 2009, doi: 10.1021/ie900445m.

[164] X. Zhao, L. Wei, and J. Julson, "First stage of bio-jet fuel production: non-food sunflower oil extraction using cold press method," *AIMS Energy*, vol. 2, no. 2, pp. 193–209, 2014, doi: https://doi.org/10.3934/energy.2014.2.193.

[165] T. Oecd, "Brassica crops (Brassica species)," *Saf. Assess. transgenic Org. Environ.*, vol. 5, pp. 151–291, 2016.

[166] A. Getinet, G. Rakow, J. P. Raney, and R. K. Downey, "Development of zero erucic acid Ethiopian mustard through an interspecific cross with zero erucic acid Oriental mustard," *Can. J. plant Sci.*, vol. 74, no. 4, pp. 793–795, 1994, doi: 10.4141/cjps94-141.

[167] M. Tesfaye, B. Weyessa, and T. Debele, "Breeding for Yellow Seeded Ethiopian Mustard (Brassica Carinata) With High Seed Yield and Oil Content at Holetta Agricultural Research Center, Ethiopia," *Int. J. Res. Stud. Agric. Sci.*, vol. 5, no. 3, pp. 1–7, 2019, doi: 10.20431/2454-6224.0503001.

[168] H. Xin, K. Theodoridou, and P. Yu, “Implication of modified molecular structure of lipid through heat-related process to fatty acids supply in Brassica carinata seed,” *Ind. Crops Prod.*, vol. 62, pp. 204–211, 2014, doi: 10.1016/j.indcrop.2014.08.025.

[169] D. C. Taylor *et al.*, “Brassica carinata – A new molecular farming platform for delivering bio-industrial oil feedstocks: case studies of genetic modifi cations to improve very long-chain fatty acid and oil content in seeds,” *Biofuels, Bioprod. Biorefining*, vol. 4, pp. 538–561, 2010, doi: 10.1002/bbb.

[170] E.-F. Marillia, T. Francis, K. C. Falk, M. Smith, and D. C. Taylor, “Palliser’s promise: Brassica carinata, an emerging western Canadian crop for delivery of new bio-industrial oil feedstocks,” *Biocatal. Agric. Biotechnol.*, vol. 3, no. 1, pp. 65–74, 2014, doi: 10.1016/j.bcab.2013.09.012.

[171] N. Alemayehu and H. C. Becker, “Variation and inheritance of erucic acid content in Brassica carinata germplasm collections from Ethiopia,” *Plant Breed.*, vol. 120, no. 4, pp. 331–335, 2001, doi: 10.1046/j.1439-0523.2001.00623.x.

[172] A. Getinet, G. Rakow, J. P. Raney, and R. K. Downey, “The inheritance of erucic acid content in Ethiopian mustard,” *Can. J. Plant Sci.*, vol. 77, no. 1, pp. 33–41, 1997, doi: 10.4141/P96-074.

[173] P. Wang, X. Xiong, X. Zhang, G. Wu, and F. Liu, “A Review of Erucic Acid Production in Brassicaceae Oilseeds: Progress and Prospects for the Genetic Engineering of High and Low-Erucic Acid Rapeseeds (Brassica napus),” *Front. Plant Sci.*, vol. 13, no. May, pp. 1–13, 2022, doi: 10.3389/fpls.2022.899076.

[174] Y. Sharafi, M. M. Majidi, S. A. H. Goli, and F. Rashidi, “Oil content and fatty acids composition in Brassica Species,” *Int. J. Food Prop.*, vol. 18, no. 10, pp. 2145–2154, 2015, doi: 10.1080/10942912.2014.968284.

[175] R. Hagos *et al.*, “Ethiopian mustard (Brassica carinata A. Braun) as an alternative energy source and sustainable crop,” *Sustainability*, vol. 12, no. 18, p. 7492, 2020.

[176] R. Seepaul *et al.*, “Carinata, the sustainable crop for a bio-based economy: 2018–2019 production recommendations for the southeastern United States,” *Univ. Florida Inst. Food Agric. Sci. Gainesville, FL, USA*, pp. 1–12, 2019.

[177] D. Kubička and J. Horáček, “Deactivation of HDS catalysts in deoxygenation of vegetable oils,” *Appl. Catal. A Gen.*, vol. 394, pp. 9–17, 2011, doi: 10.1016/j.apcata.2010.10.034.

[178] AOAC, *Oils and fats. In AOAC International (ed.) Official Methods of Analysis, 17th Ed.*

Association of Official Analytical Chemists. Gaithersburg, 2000.

[179] J. Singh, S. Paroha, and R. P. Mishra, "Factors affecting oilseed quality during storage with special reference to soybean (Glycine max) and Niger (Guizotia abyssinica) seeds," *Int. J. Curr. Microbiol. Appl. Sci.*, vol. 6, no. 10, pp. 2215–2226, 2017, doi: 10.20546/ijcmas.2017.610.262.

[180] M. P. López-Fernández, L. Moyano, M. D. Correa, F. Vasile, H. P. Burrieza, and S. Maldonado, "Deterioration of Willow seeds during storage," *Sci. Rep.*, vol. 8, no. 1, pp. 1–11, 2018, doi: 10.1038/s41598-018-35476-3.

[181] A. Koskosidis, E. M. Khah, O. I. Pavli, and D. N. Vlachostergios, "Effect of storage conditions on seed quality of soybean (Glycine max L.) germplasm," *AIMS Agric. Food*, vol. 7, no. 2, pp. 387–402, 2022, doi: 10.3934/agrfood.2022025.

[182] C. J., M. R., L. L., and D. Y., "Optimum moisture contents of seeds stored at ambient temperatures," *Seed Sci. Res.*, vol. 8, no. 1, pp. 23–28, 1998.

[183] J. E. Cacace and G. Mazza, "Mass transfer process during extraction of phenolic compounds from milled berries," *J. Food Eng.*, vol. 59, no. 4, pp. 379–389, 2003, doi: 10.1016/S0260-8774(02)00497-1.

[184] Y. Lu, L. Y. Foo, and H. Wong, "Sagecoumarin, a novel caffeic acid trimer from Salvia officinalis," *Phytochemistry*, vol. 52, no. 6, pp. 1149–1152, 1999, doi: 10.1016/S0031-9422(99)00368-4.

[185] J. Pawliszyn, *Comprehensive sampling and sample preparation: Analytical techniques for scientists*, 1st ed. New York: Academic Press, 2012.

[186] F. Javed, S. W. Ahmad, A. Rehman, S. Zafar, and S. R. Malik, "Recovery of rice Bran oil using solid-liquid extraction technique," *J. Food Process Eng.*, vol. 38, no. 4, pp. 1–6, 2014, doi: 10.1111/jfpe.12166.

[187] Z. Z. E. Sikorski and A. Kolakowska, *Chemical and functional properties of food lipids*, 1st Editio. Boca Raton: CRC press, 2002.

[188] M. U. Makeri, R. Karim, M. S. Abdulkarim, H. M. Ghazali, M. S. Miskandar, and K. Muhammad, "Comparative Analysis of the Physico-Chemical, Thermal, and Oxidative Properties of Winged Bean and Soybean Oils," *Int. J. Food Prop.*, vol. 19, no. 12, pp. 2769–2787, 2016, doi: 10.1080/10942912.2015.1031246.

[189] A. Bouaid, M. Martinez, and J. Aracil, "Production of biodiesel from bioethanol and Brassica carinata oil: Oxidation stability study," *Bioresour. Technol.*, vol. 100, no. 7, pp.

2234–2239, 2009, doi: 10.1016/j.biortech.2008.10.045.

[190] A. Bouaid, Y. Diaz, M. Martinez, and J. Aracil, "Pilot plant studies of biodiesel production using Brassica carinata as raw material," *Catal. Today*, vol. 106, no. 1–4, pp. 193–196, 2005, doi: 10.1016/j.cattod.2005.07.163.

[191] A. Serouti, M. Korichi, and O. Ben Mya, "Characterization and fatty acid profile analysis of Jatropha curcas L. oil cultivated in the Algerian desert," *Biomass Convers. Biorefinery*, 2021, doi: 10.1007/s13399-021-02013-8.

[192] M. S. Yeasmin, "Physico-chemical properties and GCMS analyses of Indigenous Rice Bran and Mustard seed oils and their blends," *Biomed. J. Sci. Tech. Res.*, vol. 34, no. 5, pp. 27167–27172, 2021, doi: 10.26717/bjstr.2021.34.005620.

[193] R. Sharif, R. Paul, D. Bhattacharjya, and K. Ahmed, "Physicochemical characters of oilseeds from selected mustard genotypes," *J. Bangladesh Agric. Univ.*, vol. 15, no. 1, pp. 27–40, 2017, doi: 10.3329/jbau.v15i1.33527.

[194] G. Toscano and E. Maldini, "Analysis of the physical and chemical characteristics of vegetable oils as fuel," *J. Agric. Eng.*, vol. 38, no. 3, p. 39, 2007, doi: 10.4081/jae.2007.3.39.

[195] D. C. Nwokonkwo, S. U. Nwaolisa, and H. A. Odo, "Comparative physicochemical study of the oils from the seeds of Cussonia Bateri (JANSA) and Brasssica Juncea (MUSTARD)," *Int. J. Appl. Chem.*, vol. 12, no. 1, pp. 51–58, 2016.

[196] A. B. Fadhil and W. S. Abdulahad, "Transesterification of Mustard (Brassica nigra) seed oil with ethanol: Purification of the crude ethyl ester with activated carbon produced from de-oiled cake," *Energy Convers. Manag.*, vol. 77, pp. 495–503, 2014, doi: 10.1016/j.enconman.2013.10.008.

[197] T. V. Choudhary and C. B. Phillips, "Renewable fuels via catalytic hydrodeoxygenation," *Appl. Catal. A Gen.*, vol. 397, no. 1–2, pp. 1–12, 2011, doi: 10.1016/j.apcata.2011.02.025.

[198] Z. Ma, L. Wei, W. Qu, J. Juson, Q. Zhu, and X. Wang, "The effect of support on the catalytic performance for bio-oil upgrading," *Adv. Mater. Res.*, vol. 608–609, pp. 350–355, 2013, doi: 10.4028/www.scientific.net/AMR.608-609.350.

[199] P. Mäki-Arvela, M. Martínez-Klimov, and D. Y. Murzin, "Hydroconversion of fatty acids and vegetable oils for production of jet fuels," *Fuel*, vol. 306, no. August, 2021, doi: 10.1016/j.fuel.2021.121673.

[200] M. Molefe, D. Nkazi, and H. E. Mukaya, "Method Selection for Biojet and Biogasoline Fuel Production from Castor Oil: A Review," *Energy and Fuels*, vol. 33, no. 7, pp. 5918–5932,

2019, doi: 10.1021/acs.energyfuels.9b00384.

[201] C. S. Osorio-González, N. Gómez-Falcon, F. Sandoval-Salas, R. Saini, S. K. Brar, and A. A. Ramírez, "Production of biodiesel from castor oil: A review," *Energies*, vol. 13, no. 10, pp. 1–22, 2020, doi: 10.3390/en13102467.

[202] S. Gharby, H. Harhar, Z. Bouzoubaa, A. Asdadi, A. El Yadini, and Z. Charrouf, "Chemical characterization and oxidative stability of castor oil grown in Morocco," *Moroccan J. Chem. [S.l.], v. 4, n. 2, p. Mor. J. Chem. 4 N°2*, vol. 4, no. 2, pp. 279–284, 2016, doi: 10.1016/j.jssas.2015.03.004.

[203] R. Seepaul, J. Marois, I. M. Small, S. George, and D. L. Wright, "Carinata dry matter accumulation and nutrient uptake responses to nitrogen fertilization," *Agron. J.*, vol. 111, no. 4, pp. 2038–2046, 2019, doi: 10.2134/agronj2018.10.0678.

[204] H. Wang, H. Farooqi, and J. Chen, "Co-hydrotreating light cycle oil-canola oil blends," *Front. Chem. Sci. Eng.*, vol. 9, no. 1, pp. 64–76, 2015, doi: 10.1007/s11705-015-1504-8.

[205] X. Zhao, L. Wei, and J. Julson, "Effects of cold press operating conditions on vegetable oil fatty acid profiles," *Int. J. Green Energy*, vol. 13, no. 10, pp. 990–999, 2016, doi: 10.1080/15435075.2016.1171226.

[206] J. Fu, S. Summers, T. J. Morgan, S. Q. Turn, and W. Kusch, "Fuel Properties of Pongamia (Milletia pinnata) Seeds and Pods Grown in Hawaii," *ACS Omega*, vol. 6, no. 13, pp. 9222–9233, 2021, doi: 10.1021/acsomega.1c00635.

[207] X. Zhao, L. Wei, S. Cheng, Y. Cao, J. Julson, and Z. Gu, "Catalytic cracking of carinata oil for hydrocarbon biofuel over fresh and regenerated Zn/Na-ZSM-5," *Appl. Catal. A Gen.*, vol. 507, pp. 44–55, 2015, doi: 10.1016/j.apcata.2015.09.031.

[208] M. Ajam, C. Woolard, and C. L. Viljoen, "Biomass pyrolysis oil as a renewable feedstock for bio-jet fuel," *13th Int. Conf. Stability, Handl. Use Liq. Fuels 2013*, no. March 2021, pp. 48–69, 2013.

[209] P. Šimáček, D. Kubička, G. Šebor, and M. Pospíšil, "Fuel properties of hydroprocessed rapeseed oil," *Fuel*, vol. 89, no. 3, pp. 611–615, 2010, doi: 10.1016/j.fuel.2009.09.017.

[210] S. Karatzos, J. S. van Dyk, J. D. McMillan, and J. Saddler, "Drop-in biofuel production via conventional (lipid/fatty acid) and advanced (biomass) routes. Part I," *Biofuels, Bioprod. Biorefining*, vol. 11, no. 2, pp. 344–362, 2017, doi: 10.1002/bbb.

[211] S. Martínez, R. Sánchez, J. Lefevre, and J. L. Todolí, "Multielemental analysis of vegetable oils and fats by means of ICP-OES following a dilution and shot methodology," *J. Anal. At.*

Spectrom., vol. 35, no. 9, pp. 1897–1909, 2020, doi: 10.1039/d0ja00112k.

[212] D. Kowalczuk and M. Pitucha, "Application of FTIR method for the assessment of immobilization of active substances in the matrix of biomedical materials," *Materials (Basel).*, vol. 12, no. 18, p. 13, 2019, doi: 10.3390/ma12182972.

[213] A. Agoston, C. Schneidhofer, N. Dörr, and B. Jakoby, "A concept of an infrared sensor system for oil condition monitoring," *Elektrotechnik und Informationstechnik*, vol. 125, no. 3, pp. 71–75, 2008, doi: 10.1007/s00502-008-0506-3.

[214] Y. Wang, Y. Ding, W. Wei, Y. Cao, D. F. Davidson, and R. K. Hanson, "On estimating physical and chemical properties of hydrocarbon fuels using mid-infrared FTIR spectra and regularized linear models," *Fuel*, vol. 255, p. 115715, 2019, doi: 10.1016/j.fuel.2019.115715.

[215] T. R. P. de Souza, L. Olenka, and W. S. Peternella, "A Study of Degradation in Vegetable Oils by Exposure to Sunlight Using Fourier Transform Infrared Spectroscopy," *Mater. Sci. Appl.*, vol. 11, no. 10, pp. 678–691, 2020, doi: 10.4236/msa.2020.1110046.

[216] Z. Wu, H. Li, and D. Tu, "Application of Fourier Transform Infrared (FT-IR) Spectroscopy Combined with Chemometrics for Analysis of Rapeseed Oil Adulterated with Refining and Purificating Waste Cooking Oil," *Food Anal. Methods*, vol. 8, no. 10, pp. 2581–2587, 2015, doi: 10.1007/s12161-015-0149-z.

[217] J. Nisar *et al.*, "Enhanced biodiesel production from Jatropha oil using calcined waste animal bones as catalyst," *Renew. Energy*, vol. 101, no. February, pp. 111–119, 2017, doi: 10.1016/j.renene.2016.08.048.

[218] M. D. Guillén and N. Cabo, "Characterization of edible oils and lard by fourier transform infrared spectroscopy. Relationships between composition and frequency of concrete bands in the fingerprint region," *JAOCS, J. Am. Oil Chem. Soc.*, vol. 74, no. 10, pp. 1281–1286, 1997, doi: 10.1007/s11746-997-0058-4.

[219] Y. Lu, C. Du, Y. Shao, and J. Zhou, "Characterization of rapeseed oil using FTIR-ATR spectroscopy," *J. Food Sci. Eng.*, vol. 4, no. May, pp. 244–249, 2014, doi: 10.17265/2159-5828/2014.05.004.

[220] M. D. Guillén and N. Cabo, "Study of the effects of smoke flavourings on the oxidative stability of the lipids of pork adipose tissue by means of Fourier transform infrared spectroscopy," *Meat Sci.*, vol. 66, no. 3, pp. 647–657, 2004, doi: 10.1016/S0309-1740(03)00185-2.

[221] H. Hu *et al.*, “Far-field nanoscale infrared spectroscopy of vibrational fingerprints of molecules with graphene plasmons,” *Nat. Commun.*, vol. 7, pp. 1–8, 2016, doi: 10.1038/ncomms12334.

[222] J. Blin *et al.*, “Characteristics of vegetable oils for use as fuel in stationary diesel engines - Towards specifications for a standard in West Africa,” *Renew. Sustain. Energy Rev.*, vol. 22, pp. 580–597, 2013, doi: 10.1016/j.rser.2013.02.018.

[223] S. Yadav, P.-Y. Teng, J. Choi, A. K. Singh, and W. K. Kim, “Nutrient profile and effects of carinata meal as alternative feed ingredient on broiler performance, tight junction gene expression and intestinal morphology,” *Poult. Sci.*, vol. 101, no. 2, p. 101411, 2022, doi: 10.1016/j.psj.2021.101411.

[224] Y. Ban, L. L. Prates, and P. Yu, “Biodegradation characteristics and nutrient availability of newly developed carinata seeds in comparison with canola seeds in dairy cattle,” *Anim. Feed Sci. Technol.*, vol. 240, pp. 88–101, 2018, doi: 10.1016/j.anifeedsci.2018.03.014.

[225] T. M. Schulmeister *et al.*, “Evaluation of Brassica carinata meal as a protein supplement for growing beef heifers,” *J. Anim. Sci.*, vol. 97, no. 10, pp. 4334–4340, 2019, doi: 10.1093/jas/skz280.

[226] D. C. Taylor *et al.*, “Brassica carinata–a new molecular farming platform for delivering bio-industrial oil feedstocks: case studies of genetic modifications to improve very long-chain fatty acid and oil content in seeds,” *Biofuels, Bioprod. Biorefining*, vol. 4, no. 5, pp. 538–561, 2010, doi: 10.1002/bbb.231.

[227] P. Serrano-Pérez, A. De Santiago, and M. del C. Rodríguez-Molina, “Biofumigation With Pellets of Defatted Seed Meal of Brassica carinata: Factors Affecting Performance Against Phytophthora nicotianae in Pepper Crops,” *Front. Sustain. Food Syst.*, vol. 5, p. 664531, 2021, doi: 10.3389/fsufs.2021.664531.

[228] P. Ancuța and A. Sonia, “Oil press-cakes and meals valorization through circular economy approaches: A review,” *Appl. Sci.*, vol. 10, no. 21, p. 7432, 2020, doi: 10.3390/app10217432.

[229] AOAC, *Association of Official Analytical Chemists, method 923.03. Ash of Flour (Direct Method). In: Official Methods of Analysis, 18th ed., AOAC International Publisher*. Gaithersburg, MD, USA, 2005.

[230] M. Egouletey and O. C. Aworh, “Production and physicochemical properties of Tempeh fortified maize based weaning food,” *Niger. Food J.*, vol. 70, pp. 92–102, 1991.

[231] P. Jayaraman, S. NesaPriya, S. Parameshwari, S. Shyamala, N. Jawahar, and H. Sekar,

"Occurrence of storage fungi in jatropha (Jatropha curcas L.) seeds," *African J. Microbiol. Res.*, vol. 5, no. 5, pp. 475–480, 2011, doi: 10.5897/AJMR10.865.

[232] M. Aboulfadl, N. El-Badry, and M. Ammar, "Nutritional and Chemical evaluation for two different varieties of Mustard Seeds," *World Appl. Sci. J.*, vol. 15, no. 9, pp. 1225–1233, 2011, [Online]. Available: http://www.idosi.org/.../5.pdf.

[233] D. Hossain, K. U. Ahmed, F. N. Chowdhury, K. M. Roksana, S. Islam, and A. Barman, "Experimental study on grain weight, moisture, ash, carbohydrates, protein, oil, total energy and minerals content of different varieties of Rapeseed and Mustard (Brassica spp.)," *Int. J. Sci. Res. Publ.*, vol. 5, no. 12, pp. 394–400, 2015, doi: 10.9790/2380-07633439.

[234] J. K. Bernard, "Oilseed and oilseed meals," *Encycl. Dairy Sci.*, vol. 1, pp. 614–619, 2022, doi: 10.1016/B978-0-12-818766-1.00103-3.

[235] A. Lomascolo, E. Uzan-Boukhris, J. C. Sigoillot, and F. Fine, "Rapeseed and sunflower meal: A review on biotechnology status and challenges," *Appl. Microbiol. Biotechnol.*, vol. 95, no. 5, pp. 1105–1114, 2012, doi: 10.1007/s00253-012-4250-6.

[236] A. M. de Castro, L. dos Reis Castilho, and D. M. G. Freire, "Characterization of babassu, canola, castor seed and sunflower residual cakes for use as raw materials for fermentation processes," *Ind. Crops Prod.*, vol. 83, pp. 140–148, 2016, doi: 10.1016/j.indcrop.2015.12.050.

[237] M. J. Mulvaney, R. G. Leon, R. Seepaul, D. L. Wright, and T. L. Hoffman, "Brassica carinata seeding rate and row spacing effects on morphology, yield, and oil," *Agron. J.*, vol. 111, no. 2, pp. 528–535, 2019, doi: 10.2134/agronj2018.05.0316.

[238] H. Cheng *et al.*, "Rapeseed Meal and Its Application in Pig Diet: A Review," *Agriculture*, vol. 12, no. 6, p. 849, 2022, doi: 10.3390/agriculture12060849.

[239] G. Mejicanos, N. Sanjayan, I. H. Kim, and C. M. Nyachoti, "Recent advances in canola meal utilization in swine nutrition," *J. Anim. Sci. Technol.*, vol. 58, no. 1, pp. 1–13, 2016, doi: 10.1186/s40781-016-0085-5.

[240] S. Şensöz, D. Angin, S. Yorgun, and Ö. M. Koçkar, "Biooil production from an oilseed crop: Fixed-bed pyrolysis of rapeseed (Brassica napus L.)," *Energy Sources*, vol. 22, no. 10, pp. 891–899, 2000, doi: 10.1080/00908310051128255.

[241] A. A. Adeleke, J. K. Odusote, P. P. Ikubanni, O. A. Lasode, M. Malathi, and D. Paswan, "Essential basics on biomass torrefaction, densification and utilization," *Int. J. Energy Res.*, vol. 45, no. 2, pp. 1375–1395, 2021.

[242] A. A. Adeleke, J. K. Odusote, D. Paswan, O. A. Lasode, and M. Malathi, “Influence of torrefaction on lignocellulosic woody biomass of Nigerian origin,” *J. Chem. Technol. Metall.*, vol. 54, pp. 274–285, 2019.

[243] S. Mehmood, B. V Reddy, and M. A. Rosen, “Energy analysis of a biomass co-firing based pulverized coal power generation system,” *Sustainability*, vol. 4, no. 4, pp. 462–490, 2012, [Online]. Available: https://doi.org/10.3390/su4040462.

[244] M. M. Maroto-Valer, G. D. Love, and C. E. Snape, “Relationship between carbon aromaticities and HC ratios for bituminous coals,” *Fuel*, vol. 73, no. 12, pp. 1926–1928, 1994, [Online]. Available: https://doi.org/10.1016/0016-2361(94)90224-0.

[245] P. Basu, “Economic issues of biomass energy conversion,” *Energy Convers. Manag*, vol. 75, pp. 25–43, 2013.

[246] K. Qian *et al.*, “Effects of biomass feedstocks and gasification conditions on the physiochemical properties of char,” *Energies*, vol. 6, no. 8, pp. 3972–3986, 2013, [Online]. Available: https://doi.org/10.3390/en6083972.

[247] P. McKendry, “Energy production from biomass (part 1): overview of biomass,” *Bioresour. Technol.*, vol. 83, no. 1, pp. 37–46, 2002, [Online]. Available: https://doi.org/10.1016/S0960-8524(01)00118-3.

[248] M. Tsarpali, J. Martin, J. Kuhn, and G. P. Philippidis, “Valorization of Brassica carinata biomass through conversion to hydrolysate and hydrochar,” *Biomass Convers. Biorefinery*, 2022, doi: 10.1007/s13399-022-02578-y.

[249] L. Yue, G. Li, G. He, Y. Guo, L. Xu, and W. Fang, “Impacts of hydrogen to carbon ratio (H/C) on fundamental properties and supercritical cracking performance of hydrocarbon fuels,” *Chem. Eng. J.*, vol. 283, pp. 1216–1223, 2016, doi: 10.1016/j.cej.2015.08.081.

[250] J. V Kumar and B. C. Pratt, “Determination of calorific values of some renewable biofuels,” *Thermochim. Acta*, vol. 279, pp. 111–120, 1996, doi: 10.1016/0040-6031(96)90070-2.

[251] K. Annamalai, S. Priyadarsan, S. Arumugam, and J. M. Sweeten, “Energy conversion: Principles for coal, animal waste, and biomass fuels,” *Encycl. Energy Eng Technol*, vol. 1, no. 1, pp. 476–497, 2007.

[252] L. Pari, A. Suardi, L. Longo, M. Carnevale, and F. Gallucci, “Jatropha curcas, L. pruning residues for energy: Characteristics of an untapped by-product,” *Energies*, vol. 11, no. 7, p. 1622, 2018, [Online]. Available: https://doi.org/10.3390/en11071622.

[253] A. Demirbaş, “Calculation of higher heating values of biomass fuels,” *Fuel*, vol. 76, no. 5,

pp. 431–434, 1997, [Online]. Available: https://doi.org/10.1016/S0016-2361(97)85520-2.

[254] Y. G. Keneni, L. A. Bahiru, and J. M. Marchetti, “Effects of different extraction solvents on oil extracted from jatropha seeds and the potential of seed residues as a heat provider,” *BioEnergy Res.*, vol. 14, no. 4, pp. 1207–1222, 2021, [Online]. Available: https://doi.org/10.1007/s12155-020-10217-5.

[255] G. Mejicanos, N. Sanjayan, I. H. Kim, and C. M. Nyachoti, “Recent advances in canola meal utilization in swine nutrition,” *J. Anim. Sci. Technol.*, vol. 58, no. 1, pp. 1–13, 2016, doi: 10.1186/s40781-016-0085-5.

[256] E. M. Paula, L. G. da Silva, V. L. N. Brandao, X. Dai, and A. P. Faciola, “Feeding canola, camelina, and carinata meals to ruminants,” *Animals*, vol. 9, no. 10, pp. 1–19, 2019, doi: 10.3390/ani9100704.

[257] E. M. Paula, L. Galoro, V. Lucia, N. Brandao, X. Dai, and A. P. Faciola, “Feeding Canola, Camelina, and Carinata Meals to Ruminants,” *Animals*, vol. 9, no. 10, pp. 1–19, 2019, doi: 10.3390/ani9100704.

[258] A. S. Brandão, A. Gonçalves, and J. M. Santos, “Circular bioeconomy strategies: From scientific research to commercially viable products,” *J. Clean. Prod.*, vol. 295, p. 126407, 2021.

[259] M. Rahman, A. Khatun, L. Liu, and B. J. Barkla, “Brassicaceae mustards: Traditional and agronomic uses in Australia and New Zealand,” *Molecules*, vol. 23, no. 1, pp. 1–18, 2018, doi: 10.3390/molecules23010231.

[260] G. Rakow and A. Getinet, “Brassica carinata an oilseed crop for Canada,” in *Acta Hortic.*, 1998, pp. 419–428, doi: 10.17660/ActaHortic.1998.459.50.

[261] S. Chen and E. Andreasson, “Update on glucosinolate metabolism and transport,” *Plant Physiol. Biochem.*, vol. 39, no. 9, pp. 743–758, 2001, doi: 10.1016/S0981-9428(01)01301-8.

[262] E. J. Rosenthal, J. A. Clapper, G. A. Perry, and D. W. Brake, “635 Effects of solvent- or mechanically extracted Brassica carinata meal on performance of cows,” *J. Anim. Sci.*, vol. 95, no. suppl_4, p. 311, Aug. 2017, doi: 10.2527/asasann.2017.635.

[263] M. K. Tripathi and A. S. Mishra, “Glucosinolates in animal nutrition: A review,” *Anim. Feed Sci. Technol.*, vol. 132, no. 1–2, pp. 1–27, 2007, doi: 10.1016/j.anifeedsci.2006.03.003.

[264] T. M. Schulmeister *et al.*, “Evaluation of Brassica carinata meal on ruminant metabolism and apparent total tract digestibility of nutrients in beef steers,” *J. Anim. Sci.*, vol. 97, no. 3,

pp. 1325–1334, 2019, doi: 10.1093/jas/skz009.

[265] S. Colombini *et al.*, "Evaluation of Camelina sativa (L.) Crantz meal as an alternative protein source in ruminant rations," *J. Sci. Food Agric.*, vol. 94, no. 4, pp. 736–743, 2014, doi: 10.1002/jsfa.6408.

[266] J. Pedroche *et al.*, "Brassica carinata protein isolates: chemical composition, protein characterization and improvement of functional properties by protein hydrolysis," *Food Chem.*, vol. 88, no. 3, pp. 337–346, 2004, doi: 10.1016/j.foodchem.2004.01.045.

[267] A. Akbari and J. Wu, "An integrated method of isolating napin and cruciferin from defatted canola meal," *LWT-Food Sci. Technol.*, vol. 64, no. 1, pp. 308–315, 2015, doi: 10.1016/j.lwt.2015.05.046.

[268] J. Wu and A. D. Muir, "Comparative structural, emulsifying, and biological properties of 2 major canola proteins, cruciferin and napin," *J. Food Sci.*, vol. 73, no. 3, pp. C210–C216, 2008, doi: 10.1111/j.1750-3841.2008.00675.x.

[269] A. Akbari, A. Lavasanifar, and J. Wu, "Interaction of cruciferin-based nanoparticles with Caco-2 cells and Caco-2/HT29-MTX co-cultures," *Acta Biomater.*, vol. 64, pp. 249–258, 2017, doi: 10.1016/j.actbio.2017.10.017.

[270] E. Monaci *et al.*, "Brassica carinata Seed Meal as Soil Amendment and Potential Biofumigant," *Crops*, vol. 2, no. 3, pp. 233–246, 2022, doi: 10.3390/crops2030017.

[271] E.-M. Meemken and M. Qaim, "Organic agriculture, food security, and the environment," *Annu. Rev. Resour. Econ.*, vol. 10, pp. 39–63, 2018, doi: 10.1146/annurev-resource-100517-023252.

[272] M. E. Popa, A. C. Mitelut, E. E. Popa, A. Stan, and V. I. Popa, "Organic foods contribution to nutritional quality and value," *Trends Food Sci. Technol.*, vol. 84, no. February 2019, pp. 15–18, 2019, doi: 10.1016/j.tifs.2018.01.003.

[273] R. Alvarez, "A review of nitrogen fertilizer and conservation tillage effects on soil organic carbon storage," *Soil Use Manag.*, vol. 21, no. 1, pp. 38–52, 2005, doi: 10.1111/j.1475-2743.2005.tb00105.x.

[274] C. Celestina, J. R. Hunt, P. W. G. Sale, and A. E. Franks, "Attribution of crop yield responses to application of organic amendments: A critical review," *Soil Tillage Res.*, vol. 186, pp. 135–145, 2019, doi: 10.1016/j.still.2018.10.002.

[275] A. Khan, M. T. Jan, M. Afzal, I. Muhammad, J. Amanullah, and Z. Shah, "An integrated approach using organic amendments under a range of tillage practices to improve wheat

productivity in a cereal based cropping system," *Int. J. Agric. Biol.*, vol. 17, no. 3, pp. 467–474, 2015, doi: 10.17957/IJAB/17.3.13.248.

[276] E. Röös *et al.*, "Risks and opportunities of increasing yields in organic farming. A review," *Agron. Sustain. Dev.*, vol. 38, no. 2, pp. 1–21, 2018, doi: 10.1007/s13593-018-0489-3.

[277] J. S. Duhan, R. Kumar, N. Kumar, P. Kaur, K. Nehra, and S. Duhan, "Nanotechnology: The new perspective in precision agriculture," *Biotechnol. Reports*, vol. 15, pp. 11–23, 2017, doi: 10.1016/j.btre.2017.03.002.

[278] M. Mazzoncini, D. Antichi, S. Tavarini, N. Silvestri, L. Lazzeri, and L. D'Avino, "Effect of defatted oilseed meals applied as organic fertilizers on vegetable crop production and environmental impact," *Ind. Crops Prod.*, vol. 75, pp. 54–64, 2015, doi: 10.1016/j.indcrop.2015.04.061.

[279] A. L. Gimsing and J. A. Kirkegaard, "Glucosinolates and biofumigation: fate of glucosinolates and their hydrolysis products in soil," *Phytochem. Rev.*, vol. 8, no. 1, pp. 299–310, 2009, doi: 10.1007/s11101-008-9105-5.

[280] M. Mazzola and L. M. Manici, "Apple replant disease: role of microbial ecology in cause and control," *Annu. Rev. Phytopathol.*, vol. 50, pp. 45–65, 2012, doi: 10.1146/annurev-phyto-081211-173005.

[281] E. Biagini, F. Barontini, and L. Tognotti, "Devolatilization of biomass fuels and biomass components studied by TG/FTIR technique," *Ind. Eng. Chem. Res.*, vol. 45, no. 13, pp. 4486–4493, 2006, [Online]. Available: https://doi.org/10.1021/ie0514049.

[282] M. Licata, S. La Bella, C. Leto, G. Bonsangue, M. C. Gennaro, and T. Tuttolomondo, "Agronomic evaluation of ethiopian mustard (Brassica carinata A. Braun) germplasm and physical-energy characterization of crop residues in a semi-arid area of sicily (Italy)," *Chem. Eng. Trans.*, vol. 58, no. 2016, pp. 535–540, 2017, doi: 10.3303/CET1758090.

[283] Y. Han *et al.*, "Hydrotreatment of pyrolysis bio-oil: A review," *Fuel Process. Technol.*, vol. 195, p. 106140, 2019, doi: 10.1016/j.fuproc.2019.106140.

[284] M. Braun-Unkhoff and U. Riedel, "Alternative fuels in aviation," *CEAS Aeronaut. J.*, vol. 6, pp. 83–93, 2015, doi: 10.1007/s13272-014-0131-2.

[285] G. M. Souza *et al.*, "The role of bioenergy in a climate-changing world," *Environ. Dev.*, vol. 23, pp. 57–64, 2017, doi: 10.1016/j.envdev.2017.02.008.

[286] IEA, "World Energy Outlook 2022," IEA, Paris, France, 2022.

[287] V. Quaschning, *Renewable Energy and Climate Change; John Wiley & Sons, Ltd.:*

Hoboken, NJ, USA, 2019. 2019.

[288] L. Singh and Z. A. Wahid, "Methods for enhancing bio-hydrogen production from biological process: A review," *J. Ind. Eng. Chem.*, vol. 21, pp. 70–80, 2015, doi: 10.1016/j.jiec.2014.05.035.

[289] C. Carriel Schmitt, M. B. Gagliardi Reolon, M. Zimmermann, K. Raffelt, J.-D. Grunwaldt, and N. Dahmen, "Synthesis and regeneration of nickel-based catalysts for hydrodeoxygenation of beech wood fast pyrolysis bio-oil," *Catalysts*, vol. 8, no. 10, p. 449, 2018, doi: 10.3390/catal8100449.

[290] M. M. Campos Fraga, B. Lacerda de Oliveira Campos, H. Hendrawidjaja, C. Carriel Schmitt, K. Raffelt, and N. Dahmen, "Fast Pyrolysis Oil Upgrading via HDO with Fe-Promoted Nb2O5-Supported Pd-Based Catalysts," *Energies*, vol. 15, no. 13, p. 4762, 2022, doi: 10.3390/en15134762.

[291] S. Ge *et al.*, "Progress in microwave pyrolysis conversion of agricultural waste to value-added biofuels: A batch to continuous approach," *Renew. Sustain. Energy Rev.*, vol. 135, 2021, doi: 10.1016/j.rser.2020.110148.

[292] N. A. Negm, A. M. Rabie, and E. A. Mohammed, "Molecular interaction of heterogeneous catalyst in catalytic cracking process of vegetable oils: chromatographic and biofuel performance investigation," *Appl. Catal. B Environ.*, vol. 239, pp. 36–45, 2018, doi: 10.1016/j.apcatb.2018.07.070.

[293] R. Dong, M. Zhao, W. Xia, X. Yi, P. Dai, and N. Tang, "Chemical and microscopic investigation of co-pyrolysis of crumb tire rubber with waste cooking oil at mild temperature," *Waste Manag.*, vol. 79, pp. 516–525, 2018, doi: 10.1016/j.wasman.2018.08.024.

[294] S. Czernik and A. V Bridgwater, "Overview of applications of biomass fast pyrolysis oil," *Energy & fuels*, vol. 18, no. 2, pp. 590–598, 2004, doi: 10.1021/ef034067u.

[295] D. S. Fardyanti, Megawati, H. Istanto, M. K. Anajib, Prayogo, and U. Habibah, "Extraction of phenol from bio-oil produced by pyrolysis of coconut shell," *J. Phys. Sci.*, vol. 29, pp. 195–202, 2018, doi: 10.21315/jps2018.29.s2.15.

[296] A. V. Bridgwater, "Review of fast pyrolysis of biomass and product upgrading," *Biomass and Bioenergy*, vol. 38, pp. 68–94, 2012, doi: 10.1016/j.biombioe.2011.01.048.

[297] Z. Si, X. Zhang, C. Wang, L. Ma, and R. Dong, "An overview on catalytic hydrodeoxygenation of pyrolysis oil and its model compounds," *Catalysts*, vol. 7, no. 6, pp.

1–22, 2017, doi: 10.3390/catal7060169.

[298] F. de Miguel Mercader, M. J. Groeneveld, S. R. A. Kersten, R. H. Venderbosch, and J. A. Hogendoorn, “Pyrolysis oil upgrading by high pressure thermal treatment,” *Fuel*, vol. 89, no. 10, pp. 2829–2837, 2010, doi: 10.1016/j.fuel.2010.01.026.

[299] W.-J. Liu and H.-Q. Yu, “Thermochemical conversion of lignocellulosic biomass into mass-producible fuels: emerging technology progress and environmental sustainability evaluation,” *ACS Environ. Au*, vol. 2, no. 2, pp. 98–114, 2021, doi: 10.1021/acsenvironau.1c00025.

[300] P. M. Mortensen *et al.*, “Deactivation of Ni-MoS2 by bio-oil impurities during hydrodeoxygenation of phenol and octanol,” *Appl. Catal. A Gen.*, vol. 523, no. 5, pp. 159–170, 2016, doi: 10.1016/j.apcata.2016.06.002.

[301] T. Oecd, “Brassica crops (Brassica species),” in *Safety Assessment of Transgenic Organisms in the Environment*, vol. 5, no. December 2012, Paris: OECD Publishing, 2016, pp. 151–291.

[302] R. Hagos *et al.*, “Ethiopian mustard (Brassica carinata A. Braun) as an alternative energy source and sustainable crop,” *Sustain.*, vol. 12, no. 18, pp. 1–12, 2020, doi: 10.3390/su12187492.

[303] Z. T. Redda, A. Laß-Seyoum, A. Yimam, M. Barz, and S. A. Jabasingh, “Characterization of Hexane-Defatted Brassica carinata Oilseed Meals to Explore Their Potential for Valorization Towards a Sustainable Circular Bioeconomy,” *Waste Biomass Valor*, 2023, doi: 10.1007/s12649-023-02248-8.

[304] R. E. Guedes, A. S. Luna, and A. R. Torres, “Operating parameters for bio-oil production in biomass pyrolysis: A review,” *J. Anal. Appl. Pyrolysis*, vol. 129, pp. 134–149, 2018, doi: 10.1016/j.jaap.2017.11.019.

[305] A. M. Gonzalez-Aguilar, V. P. Cabrera-Madera, J. R. Vera-Rozo, and J. M. Riesco-Ávila, “Effects of heating rate and temperature on the thermal pyrolysis of expanded polystyrene post-industrial waste,” *Polymers (Basel).*, vol. 14, no. 22, p. 4957, 2022, doi: 10.3390/polym14224957.

[306] Y. Lee, P. R. B. Eum, C. Ryu, Y. K. Park, J. H. Jung, and S. Hyun, “Characteristics of biochar produced from slow pyrolysis of Geodae-Uksae 1,” *Bioresour. Technol.*, vol. 130, pp. 345–350, 2013, doi: 10.1016/j.biortech.2012.12.012.

[307] S. A. Channiwala and P. P. Parikh, “A unified correlation for estimating HHV of solid, liquid

and gaseous fuels," *Fuel*, vol. 81, no. 8, pp. 1051–1063, 2002, doi: 10.1016/S0016-2361(01)00131-4.

[308] F.-X. Collard and J. Blin, "A review on pyrolysis of biomass constituents: Mechanisms and composition of the products obtained from the conversion of cellulose, hemicelluloses and lignin," *Renew. Sustain. Energy Rev.*, vol. 38, pp. 594–608, 2014, doi: 10.1016/j.rser.2014.06.013.

[309] D. Lachos-Perez *et al.*, "Review on Biomass Pyrolysis with a Focus on Bio-Oil Upgrading Techniques," *Analytica*, vol. 4, no. 2, pp. 182–205, 2023, doi: 10.3390/analytica4020015.

[310] M. Irfan *et al.*, "Response Surface Methodology for the Synthesis and Characterization of Bio-Oil Extracted from Biomass Waste and Upgradation Using the Rice Husk Ash Catalyst," *ACS Omega*, pp. 17869–17879, 2023, doi: 10.1021/acsomega.3c00868.

[311] D. Vamvuka, "Bio-oil, solid and gaseous biofuels from biomass pyrolysis processes—An overview," *Int. J. ENERGY Res.*, vol. 33, no. 4, pp. 23–40, 2011, doi: 10.1002/er.1804.

[312] J. L. Chukwuneke, J. E. Sinebe, H. O. Orugba, H. C. Olisakwe, and C. Ajike, "Production and physico-chemical characteristics of pyrolyzed bio-oil derived from cow hooves," *Arab J. Basic Appl. Sci.*, vol. 29, no. 1, pp. 363–371, 2022, doi: 10.1080/25765299.2022.2129633.

[313] J. Zhao, Z. Wang, J. Li, B. Yan, and G. Chen, "Pyrolysis of food waste and food waste solid digestate: A comparative investigation," *Bioresour. Technol.*, vol. 354, p. 127191, 2022, doi: 10.1016/j.biortech.2022.127191.

[314] J. Grams *et al.*, "Hydrogen-rich gas production by upgrading of biomass pyrolysis vapors over NiBEA catalyst: Impact of dealumination and preparation method," *Energy & Fuels*, vol. 34, no. 12, pp. 16936–16947, 2020, doi: 10.1021/acs.energyfuels.0c02958.

[315] R. Azargohar, S. Nanda, B. V. S. K. Rao, and A. K. Dalai, "Slow pyrolysis of deoiled canola meal: Product yields and characterization," *Energy and Fuels*, vol. 27, no. 9, pp. 5268–5279, 2013, doi: 10.1021/ef400941a.

[316] K. Du *et al.*, "Hydrodeoxygenation of Bio-Oil over an Enhanced Interfacial Catalysis of Microemulsions Stabilized by Amphiphilic Solid Particles," *Catalysts*, vol. 13, no. 3, p. 573, 2023, doi: 10.3390/catal13030573.

[317] H. Bouaik, A. Tabal, A. Barakat, K. El Harfi, and A. Aboulkas, "Optimal parameters and structural composition of bio-oil and biochar from intermediate pyrolysis of red algal biomass," *Comptes Rendus. Chim.*, vol. 24, no. S1, pp. 85–99, 2021, doi: 10.5802/crchim.90.

[318] M. Attia, S. Farag, and J. Chaouki, “Upgrading of oils from biomass and waste: Catalytic hydrodeoxygenation,” *Catalysts*, vol. 10, no. 12, p. 1381, 2020, doi: 10.3390/catal10121381.

[319] K. Routray, K. J. Barnett, and G. W. Huber, “Hydrodeoxygenation of Pyrolysis Oils,” *Energy Technol.*, vol. 5, no. 1, pp. 80–93, 2017, doi: 10.1002/ente.201600084.

[320] T. S. Ahamed, S. Anto, T. Mathimani, K. Brindhadevi, and A. Pugazhendhi, “Upgrading of bio-oil from thermochemical conversion of various biomass–Mechanism, challenges and opportunities,” *Fuel*, vol. 287, p. 119329, 2021, doi: 10.1016/j.fuel.2020.119329.

[321] P. M. Mortensen, J. D. Grunwaldt, P. A. Jensena, K.G. Knudsenc, and A. D. Jensena, “A review of catalytic upgrading of bio-oil to engine fuels,” *Appl. Catal. A Gen*, vol. 407, no. 4 November, pp. 1–19, 2011, doi: 10.1016/j.apcata.2011.08.046.

[322] Y. Sharafi, M. M. Majidi, S. A. H. Goli, and F. Rashidi, “Oil content and fatty acids composition in Brassica species,” *Int. J. Food Prop.*, vol. 18, no. 10, pp. 2145–2154, 2015.

[323] X. Wu, A. Kang, B. Wu, K. Lou, and Z. Fan, “Prediction of crack resistance of LFSMA-13 with and without anti-rut agent using parameters of FTIR spectrum under different aging degrees,” *Materials (Basel).*, vol. 14, no. 12, p. 3209, 2021, doi: 10.3390/ma14123209.

[324] Q. Zhang, L. Pastor-Perez, S. Gu, and T. Ramirez Reina, “Transition metal carbides (TMCS) catalysts for gas phase CO2 upgrading reactions: A comprehensive overview,” *Catalysts*, vol. 10, no. 9, p. 955, 2020, doi: 10.3390/catal10090955.

[325] P. Chen, J. Ye, H. Wang, L. Ouyang, and M. Zhu, “Recent progress of transition metal carbides/nitrides for electrocatalytic water splitting,” *J. Alloys Compd.*, vol. 883, p. 160833, 2021, doi: 10.1016/j.jallcom.2021.160833.

[326] Z. Zhou, Y. Jia, Q. Wang, Z. Jiang, J. Xiao, and L. Guo, “Recent Progress on Molybdenum Carbide-Based Catalysts for Hydrogen Evolution: A Review,” *Sustainability*, vol. 15, no. 19, p. 14556, 2023, doi: 10.3390/su151914556.

[327] A. L. Stottlemyer, T. G. Kelly, Q. Meng, and J. G. Chen, “Reactions of oxygen-containing molecules on transition metal carbides: Surface science insight into potential applications in catalysis and electrocatalysis,” *Surf. Sci. Rep.*, vol. 67, no. 9–10, pp. 201–232, 2012, doi: 10.1016/j.surfrep.2012.07.001.

[328] T. Chen, C. Foo, and S. C. E. Tsang, “Interstitial and substitutional light elements in transition metals for heterogeneous catalysis,” *Chem. Sci.*, vol. 12, no. 2, pp. 517–532, 2021, doi: 10.1039/D0SC06496C.

[329] J. A. Rodriguez, “Activation of gold on metal carbides: novel catalysts for C1 chemistry,”

Front. Chem., vol. 7, p. 875, 2020, doi: 10.3389/fchem.2019.00875.

[330] K. N. Dinh *et al.*, "Nanostructured metallic transition metal carbides, nitrides, phosphides, and borides for energy storage and conversion," *Nano Today*, vol. 25, pp. 99–121, 2019, doi: 10.1016/j.nantod.2019.02.008.

[331] S. Ahmad, I. Ashraf, M. A. Mansoor, S. Rizwan, and M. Iqbal, "An overview of recent advances in the synthesis and applications of the Transition Metal Carbide Nanomaterials," *Nanomaterials*, vol. 11, no. 3, p. 776, 2021, doi: 10.3390/nano11030776.

[332] M. Führer, T. van Haasterecht, and J. H. Bitter, "Catalytic performance of carbon-supported mixed MoW carbides for the deoxygenation of stearic acid," *Catal. today*, vol. 418, p. 114108, 2023, doi: 10.1016/j.cattod.2023.114108.

[333] Z. Li, C. Chen, E. Zhan, N. Ta, Y. Li, and W. Shen, "Crystal-phase control of molybdenum carbide nanobelts for dehydrogenation of benzyl alcohol," *Chem. Commun.*, vol. 50, no. 34, pp. 4469–4471, 2014, doi: 10.1039/C4CC00242C.

[334] T. Wakisaka *et al.*, "Rational synthesis for a noble metal carbide," *J. Am. Chem. Soc.*, vol. 142, no. 3, pp. 1247–1253, 2019, doi: 10.1021/jacs.9b09219.

[335] X. Du, R. Zhang, D. Li, C. Hu, and H. Garcia, "Molybdenum carbide as catalyst in biomass derivatives conversion," *J. Energy Chem.*, vol. 73, pp. 68–87, 2022, doi: 10.1016/j.jechem.2022.05.014.

[336] H. Wang, S. Liu, and K. J. Smith, "Synthesis and hydrodeoxygenation activity of carbon supported molybdenum carbide and oxycarbide catalysts," *Energy & Fuels*, vol. 30, no. 7, pp. 6039–6049, 2016.

[337] R. Guil-López, E. Nieto, J. A. Botas, and J. L. G. Fierro, "On the genesis of molybdenum carbide phases during reduction-carburization reactions," *J. Solid State Chem.*, vol. 190, pp. 285–295, 2012, doi: 10.1016/j.jssc.2012.02.021.

[338] S. Bagheri, N. Muhd Julkapli, and S. Bee Abd Hamid, "Titanium dioxide as a catalyst support in heterogeneous catalysis," *Sci. World J.*, vol. 2014, pp. 1–22, 2014, doi: 10.1155/2014/727496.

[339] A. Stanislaus, A. Marafi, and M. S. Rana, "Recent advances in the science and technology of ultra low sulfur diesel (ULSD) production," *Catal. Today*, vol. 153, no. 1–2, pp. 1–68, 2010, doi: 10.1016/j.cattod.2010.05.011.

[340] A. Galadima and O. Muraza, "Catalytic upgrading of vegetable oils into jet fuels range hydrocarbons using heterogeneous catalysts: A review," *J. Ind. Eng. Chem.*, vol. 29, pp. 12–

23, 2015, doi: 10.1016/j.jiec.2015.03.030.

[341] T. Li, J. Cheng, R. Huang, J. Zhou, and K. Cen, “Conversion of waste cooking oil to jet biofuel with nickel-based mesoporous zeolite Y catalyst,” *Bioresour. Technol.*, vol. 197, pp. 289–294, 2015, doi: 10.1016/j.biortech.2015.08.115.

[342] X. Zhao, L. Wei, S. Cheng, and J. Julson, “Review of heterogeneous catalysts for catalytically upgrading vegetable oils into hydrocarbon biofuels,” *Catalysts*, vol. 7, no. 3, p. 83, 2017, doi: 10.3390/catal7030083.

[343] F. P. De Sousa, C. C. Cardoso, and V. M. D. Pasa, “Producing hydrocarbons for green diesel and jet fuel formulation from palm kernel fat over Pd/C,” *Fuel Process. Technol.*, vol. 143, pp. 35–42, 2016, doi: 10.1016/j.fuproc.2015.10.024.

[344] B. A. T. Mehrabadi, S. Eskandari, U. Khan, R. D. White, and J. R. Regalbuto, “A review of preparation methods for supported metal catalysts,” *Adv. Catal.*, vol. 61, pp. 1–35, 2017, doi: 10.1016/bs.acat.2017.10.001.

[345] P. Munnik, P. E. De Jongh, and K. P. De Jong, “Recent developments in the synthesis of supported catalysts,” *Chem. Rev.*, vol. 115, no. 14, pp. 6687–6718, 2015, doi: 10.1021/cr500486u.

[346] C. J. Zhong and J. R. Regalbuto, “Metal nanoparticle synthesis,” in *Comprehensive Inorganic Chemistry II: From Elements to Applications*, Second Edi., Elsevier Ltd., 2013, pp. 75–102.

[347] J. Haber, “Manual on catalyst characterization,” *Int. Union Pure Appl. Chem.*, vol. 63, no. 9, pp. 1227–1246, 1991, doi: 10.1351/pac199163091227.

[348] S. K. Sen, T. C. Paul, M. S. Manir, S. Dutta, M. N. Hossain, and J. Podder, “Effect of Fe-doping and post annealing temperature on the structural and optical properties of MoO 3 nanosheets,” *J. Mater. Sci. Mater. Electron.*, vol. 30, pp. 14355–14367, 2019, doi: 10.1007/s10854-019-01805-z.

[349] J. Regalbuto, *Catalyst preparation science and engineering*. CRC Press, Taylor & Francis Group, 2007.

[350] C. Perego and P. Villa, “Catalyst preparation methods,” in *Catalysis Today*, vol. 34, P. V. Carlo Perego, Ed. Milano, Italy: Elsevier Science B.V., 1997, pp. 281–305.

[351] Y. Ma, G. Guan, X. Hao, J. Cao, and A. Abudula, “Molybdenum carbide as alternative catalyst for hydrogen production–A review,” *Renew. Sustain. Energy Rev.*, vol. 75, pp. 1101–1129, 2017, doi: 10.1016/j.rser.2016.11.092.

[352] A. E.-A. A. Said, M. M. M. Abd El-Wahab, and M. Abd El-Aal, “The role of acid sites in the catalytic performance of tungsten oxide during the dehydration of isopropyl and methyl alcohols,” *Chem. Mater. Eng.*, vol. 4, no. 2, pp. 17–25, 2016, doi: 10.13189/cme.2016.040202.

[353] D. L. Trimm, “Thermal stability of catalyst supports,” in *Studies in Surface Science and Catalysis*, vol. 68, Elsevier, 1991, pp. 29–51.

[354] L. D. Anbealagan, T. L. Chew, Y. F. Yeong, Z. A. Jawad, and C. D. Ho, “Synthesis and characterization of (3-aminopropyl) triethoxysilane (APTES) functionalized zeolite AlPO-18,” in *IOP Conference Series: Materials Science and Engineering*, 2021, vol. 1195, no. 1, p. 12047, doi: 10.1088/1757-899x/1195/1/012047.

[355] J. S. Lee, S. T. Oyama, and M. Boudart, “Molybdenum carbide catalysts: I. Synthesis of unsupported powders,” *J. Catal.*, vol. 106, no. 1, pp. 125–133, 1987, doi: 10.1016/0021-9517(87)90218-1.

[356] W. Wu, Z. Wu, C. Liang, X. Chen, P. Ying, and C. Li, “In situ FT-IR spectroscopic studies of CO adsorption on fresh Mo2C/Al2O3 catalyst,” *J. Phys. Chem. B*, vol. 107, no. 29, pp. 7088–7094, 2003, doi: 10.1021/jp027582m.

[357] M. Thommes *et al.*, “Physisorption of gases, with special reference to the evaluation of surface area and pore size distribution (IUPAC Technical Report),” *Pure Appl. Chem.*, vol. 87, no. 9–10, pp. 1051–1069, 2015, doi: 10.1515/pac-2014-1117.

[358] Z. A. ALOthman, “A review: fundamental aspects of silicate mesoporous materials,” *Materials (Basel).*, vol. 5, no. 12, pp. 2874–2902, 2012, doi: 10.3390/ma5122874.

[359] T. Mo, J. Xu, Y. Yang, and Y. Li, “Effect of carburization protocols on molybdenum carbide synthesis and study on its performance in CO hydrogenation,” *Catal. Today*, vol. 261, pp. 101–115, 2016, doi: 10.1016/j.cattod.2015.07.014.

[360] G. Słowik, A. Gawryszuk-Rżysko, M. Greluk, and A. Machocki, “Estimation of average crystallites size of active phase in ceria-supported cobalt-based catalysts by hydrogen chemisorption vs TEM and XRD methods,” *Catal. Letters*, vol. 146, pp. 2173–2184, 2016, doi: 10.1007/s10562-016-1843-1.

[361] Y. Huang, B. A. Demko, and C. W. Kirby, “Investigation of the evolution of intermediate phases of AlPO4-18 molecular sieve synthesis,” *Chem. Mater.*, vol. 15, no. 12, pp. 2437–2444, 2003, doi: 10.1021/cm021728c.

[362] S. Murase and Y. Yang, “Solution processed MoO3 interfacial layer for organic

photovoltaics prepared by a facile synthesis method," *Adv. Mater.*, vol. 24, no. 18, pp. 2459–2462, 2012, doi: 10.1002/adma.201104771.

[363] P. Jittiarporn, L. Sikong, K. Kooptarnond, and W. Taweepreda, "Influence of calcination temperature on the structural and photochromic properties of nanocrystalline MoO3," *Dig. J. Nanomater. Biostructures*, vol. 10, pp. 1237–1248, 2015.

[364] X. Liu, F. Wang, and Q. Wang, "Nanostructure-based WO 3 photoanodes for photoelectrochemical water splitting," *Phys. Chem. Chem. Phys.*, vol. 14, no. 22, pp. 7894–7911, 2012, doi: 10.1039/C2CP40976C.

[365] H. Zheng, J. Z. Ou, M. S. Strano, R. B. Kaner, A. Mitchell, and K. Kalantar-zadeh, "Nanostructured tungsten oxide–properties, synthesis, and applications," *Adv. Funct. Mater.*, vol. 21, no. 12, pp. 2175–2196, 2011, doi: 10.1002/adfm.201002477.

[366] Y. Zhong, X. Xia, F. Shi, J. Zhan, J. Tu, and H. J. Fan, "Transition metal carbides and nitrides in energy storage and conversion," *Adv. Sci.*, vol. 3, no. 5, p. 1500286, 2016, doi: 10.1002/advs.201500286.

[367] J. R. dos Santos Politi, F. Vines, J. A. Rodriguez, and F. Illas, "Atomic and electronic structure of molybdenum carbide phases: bulk and low Miller-index surfaces," *Phys. Chem. Chem. Phys.*, vol. 15, no. 30, pp. 12617–12625, 2013, doi: 10.1039/C3CP51389K.

[368] H. W. Hugosson, U. Jansson, B. Johansson, and O. Eriksson, "Phase stability diagrams of transition metal carbides, a theoretical study," *Chem. Phys. Lett.*, vol. 333, no. 6, pp. 444–450, 2001, doi: 10.1016/S0009-2614(00)01414-7.

[369] Y. Zhao *et al.*, "A novel approach to the synthesis of bulk and supported β-Mo 2 C using dimethyl ether as a carbon source," *New J. Chem.*, vol. 39, no. 6, pp. 4901–4908, 2015, doi: 10.1039/C5NJ00395D.

[370] E. S. Lokteva and E. V Golubina, "Metal-support interactions in the design of heterogeneous catalysts for redox processes," *Pure Appl. Chem.*, vol. 91, no. 4, pp. 609–631, 2019, doi: 10.1515/pac-2018-0715.

[371] S.-W. Kim, J. C. Ro, and S.-J. Suh, "Simple Synthesis and Characterization of Shell-Thickness-Controlled Ni/Ni3C Core-Shell Nanoparticles," *Nanomaterials*, vol. 12, no. 12, p. 1954, 2022, doi: 10.3390/nano12121954.

[372] S. Eskandari, "Design, Synthesis, and Characterization of Monometallic and Bimetallic Catalysts," 2018.

[373] R. Ahorsu, M. Constanti, and F. Medina, "Recent impacts of heterogeneous catalysis in

Biorefineries," *Ind. Eng. Chem. Res.*, vol. 60, no. 51, pp. 18612–18626, 2021, doi: 10.1021/acs.iecr.1c02789.

[374] G. A. Greene and C. C. Finfrock, "Vaporization of Tungsten-metal In Steam At High Temperatures," Brookhaven National Lab.(BNL), Upton, NY (United States), 2000. doi: 10.2172/777720.

[375] N. Perret, X. Wang, L. Delannoy, C. Potvin, C. Louis, and M. A. Keane, "Enhanced selective nitroarene hydrogenation over Au supported on β-Mo2C and β-Mo2C/Al2O3," *J. Catal.*, vol. 286, pp. 172–183, 2012, doi: 10.1016/j.jcat.2011.10.026.

[376] J.-S. Choi, J.-M. Krafft, A. Krzton, and G. Djéga-Mariadassou, "Study of residual oxygen species over molybdenum carbide prepared during in situ DRIFTS experiments," *Catal. Letters*, vol. 81, pp. 175–180, 2002, doi: 10.1023/A:1016568804706.

[377] Air Transport Action Group, "Beginner ' s guide to sustainable aviation fuel, 3rd Ed.," no. November, pp. 1–24, 2017, [Online]. Available: https://aviationbenefits.org/media/166152/beginners-guide-to-saf_web.pdf.

[378] U. Neuling and M. Kaltschmitt, "Techno-economic and environmental analysis of aviation biofuels," *Fuel Process. Technol.*, vol. 171, no. September 2017, pp. 54–69, 2018, doi: 10.1016/j.fuproc.2017.09.022.

[379] M. A. Hasan *et al.*, "Climate change mitigation pathways for the aviation sector," *Sustainability*, vol. 13, no. 7, p. 3656, 2021, doi: 10.3390/su13073656.

[380] S. H. Hassan, N. K. Attia, G. I. El Diwani, S. K. Amin, R. S. Ettouney, and M. A. El-Rifai, "Catalytic hydrocracking of jatropha oil over natural clay for bio-jet fuel production," *Sci. Rep.*, vol. 13, no. 1, p. 13419, 2023, doi: 10.1038/s41598-023-40500-2.

[381] J. Holladay, Z. Abdullah, and J. Heyne, "Sustainable aviation fuel: Review of technical pathways," DOE EERE; Pacific Northwest National Lab.(PNNL), Richland, WA (United States …, 2020. doi: 10.2172/1660415.

[382] 2022 ASTM D7566, "Standard specification for aviation turbine fuel containing synthesized hydrocarbons," 2022, doi: 10.1520/D1655-10.2.

[383] G. Contreras-Zarazúa, E. Sánchez-Ramirez, E. A. Hernández-Vargas, J. G. Segovia-Hernández, and J. J. Q. Ramírez, "Process intensification in bio-jet fuel production: Design and control of a catalytic reactive distillation column for oligomerization," *Chem. Eng. Process. Intensif.*, vol. 193, p. 109548, 2023, doi: 10.1016/j.cep.2023.109548.

[384] A. L. C. De Mestral, P. P. Fitzgerald, and M. T. Ahmad, *Introduction: Sustainable*

Development, International Aviation, and Treaty Implementation. Sustainable Development, International Aviation, and Treaty Implementation. Cambridge University Press, 2018.

[385] T. J. Morgan, A. Youkhana, S. Q. Turn, R. Ogoshi, and M. Garcia-Pérez, "Review of Biomass Resources and Conversion Technologies for Alternative Jet Fuel Production in Hawai'i and Tropical Regions," *Energy and Fuels*, vol. 33, no. 4, pp. 2699–2762, 2019, doi: 10.1021/acs.energyfuels.8b03001.

[386] H. Wei, W. Liu, X. Chen, Q. Yang, J. Li, and H. Chen, "Renewable bio-jet fuel production for aviation: A review," *Fuel*, vol. 254, p. 115599, 2019, doi: 10.1016/j.fuel.2019.06.007.

[387] M. Li *et al.*, "Comprehensive Life Cycle Evaluation of Jet Fuel from Biomass Gasification and Fischer–Tropsch Synthesis Based on Environmental and Economic Performances," *Ind. Eng. Chem. Res.*, vol. 58, no. 41, pp. 19179–19188, 2019, doi: 10.1021/acs.iecr.9b03468.

[388] J. Q. Bond *et al.*, "Production of renewable jet fuel range alkanes and commodity chemicals from integrated catalytic processing of biomass," *Energy Environ. Sci.*, vol. 7, no. 4, pp. 1500–1523, 2014, doi: 10.1039/C3EE43846E.

[389] R. Xing *et al.*, "Production of jet and diesel fuel range alkanes from waste hemicellulose-derived aqueous solutions," *Green Chem.*, vol. 12, no. 11, pp. 1933–1946, 2010, doi: 10.1039/c0gc00263a.

[390] B. S. Rana *et al.*, "Transportation fuels from co-processing of waste vegetable oil and gas oil mixtures," *Biomass and Bioenergy*, vol. 56, pp. 43–52, 2013, doi: 10.1016/j.biombioe.2013.04.029.

[391] K. Xiong, W. Yu, D. G. Vlachos, and J. G. Chen, "Reaction pathways of biomass-derived oxygenates over metals and carbides: From model surfaces to supported catalysts," *ChemCatChem*, vol. 7, no. 9, pp. 1402–1421, 2015, doi: 10.1002/cctc.201403067.

[392] D. Li, H. Xin, X. Du, X. Hao, Q. Liu, and C. Hu, "Recent advances for the production of hydrocarbon biofuel via deoxygenation progress," *Sci. Bull.*, vol. 60, no. 24, pp. 2096–2106, 2015, doi: 10.1007/s11434-015-0971-0.

[393] S. Cheng, L. Wei, X. Zhao, and J. Julson, "Application, deactivation, and regeneration of heterogeneous catalysts in bio-oil upgrading," *Catalysts*, vol. 6, no. 12, pp. 1–24, 2016, doi: 10.3390/catal6120195.

[394] J. A. Kenar, B. R. Moser, and G. R. List, "Chapter 2-Naturally occurring fatty acids : Source,chemistry, and uses," *Fat. Acids*, vol. 2600, pp. 23–82, 2017, doi: 10.1016/B978-0-

12-809521-8.00002-7.

[395] Z. T. Redda *et al.*, "Synthesis and Characterization of AlPO4-18 Supported Mesoporous and Crystalline β-Mo2C, Ni3C, and WC Nanoparticles," *Catal. Letters*, pp. 1–20, 2024, doi: 10.1007/s10562-024-04791-y.

[396] M. Ni, D. Y. C. Leung, M. K. H. Leung, and K. Sumathy, "An overview of hydrogen production from biomass," *Fuel Process. Technol.*, vol. 87, no. 5, pp. 461–472, 2006, doi: 10.1016/j.fuproc.2005.11.003.

[397] K. M. Qureshi, A. N. K. Lup, S. Khan, F. Abnisa, and W. M. A. W. Daud, "A technical review on semi-continuous and continuous pyrolysis process of biomass to bio-oil," *J. Anal. Appl. Pyrolysis*, vol. 131, pp. 52–75, 2018, doi: 10.1016/j.jaap.2018.02.010.

[398] M. J. A. Romero, A. Pizzi, G. Toscano, G. Busca, B. Bosio, and E. Arato, "Deoxygenation of waste cooking oil and non-edible oil for the production of liquid hydrocarbon biofuels," *Waste Manag.*, vol. 47, pp. 62–68, 2016, doi: 10.1016/j.wasman.2015.03.033.

[399] N. Taufiqurrahmi and S. Bhatia, "Catalytic cracking of edible and non-edible oils for the production of biofuels," *Energy Environ. Sci.*, vol. 4, no. 4, pp. 1087–1112, 2011, doi: 10.1039/c0ee00460j.

[400] J. Liu, C. Liu, G. Zhou, S. Shen, and L. Rong, "Hydrotreatment of Jatropha oil over NiMoLa/Al2O3 catalyst," *Green Chem.*, vol. 14, no. 9, pp. 2499–2505, 2012, doi: 10.1039/c2gc35450k.

[401] A. N. Lup Kay, F. Abnisa, W. M. A. Wan Daud, and M. K. Aroua, "Delayed volatiles release phenomenon at higher temperature in TGA via sample encapsulation technique," *Fuel*, vol. 234, pp. 422–429, 2018, doi: 10.1016/j.fuel.2018.06.120.

[402] M. Alherbawi, G. McKay, H. R. Mackey, and T. Al-Ansari, "Jatropha curcas for jet biofuel production: Current status and future prospects," *Renew. Sustain. Energy Rev.*, vol. 135, p. 110396, 2021, doi: 10.1016/j.rser.2020.110396.

[403] Y. Liu, R. Sotelo-Boyás, K. Murata, T. Minowa, and K. Sakanishi, "Hydrotreatment of vegetable oils to produce bio-hydrogenated diesel and liquefied petroleum gas fuel over catalysts containing sulfided Ni–Mo and solid acids," *Energy & Fuels*, vol. 25, no. 10, pp. 4675–4685, 2011, doi: 10.1021/ef200889e.

[404] A. P. P. Pires, Y. Han, J. Kramlich, and M. Garcia-Perez, "Chemical composition and fuel properties of alternative jet fuels," *BioResources*, vol. 13, no. 2, pp. 2632–2657, 2018, doi: 10.15376/biores.13.2.2632-2657.

[405] H. Zhang, H. Lin, W. Wang, Y. Zheng, and P. Hu, “Hydroprocessing of waste cooking oil over a dispersed nano catalyst: Kinetics study and temperature effect,” *Appl. Catal. B Environ.*, vol. 150, pp. 238–248, 2014, doi: 10.1016/j.apcatb.2013.12.006.

[406] P. Straka, J. Blažek, D. Toullis, T. Ihnát, and P. Šimáček, “The Effect of the Reaction Conditions on the Properties of Products from Co-hydrotreating of Rapeseed oil and Petroleum Middle Distillates,” *Catalysts*, vol. 11, no. 4, p. 442, 2021, doi: 10.3390/catal11040442.

[407] P. Chintakanan, T. Vitidsant, P. Reubroycharoen, P. Kuchonthara, T. Kida, and N. Hinchiranan, “Bio-jet fuel range in biofuels derived from hydroconversion of palm olein over Ni/zeolite catalysts and freezing point of biofuels/Jet A-1 blends,” *Fuel*, vol. 293, p. 120472, 2021, doi: 10.1016/j.fuel.2021.120472.

[408] V. Itthibenchapong, A. Srifa, R. Kaewmeesri, P. Kidkhunthod, and K. Faungnawakij, “Deoxygenation of palm kernel oil to jet fuel-like hydrocarbons using Ni-MoS2/γ-Al2O3 catalysts,” *Energy Convers. Manag.*, vol. 134, pp. 188–196, 2017, doi: 10.1016/j.enconman.2016.12.034.

[409] E. Corporan *et al.*, “Chemical, thermal stability, seal swell, and emissions studies of alternative jet fuels,” *Energy & fuels*, vol. 25, no. 3, pp. 955–966, 2011, doi: 10.1021/ef101520v.

[410] R. W. Jenkins, C. M. Moore, T. A. Semelsberger, C. J. Chuck, J. C. Gordon, and A. D. Sutton, “The Effect of Functional Groups in Bio-Derived Fuel Candidates,” *ChemSusChem*, vol. 9, no. 9, pp. 922–931, 2016, doi: 10.1002/cssc.201600159.

[411] R. Saab, K. Polychronopoulou, L. Zheng, S. Kumar, and A. Schiffer, “Synthesis and performance evaluation of hydrocracking catalysts: A review,” *J. Ind. Eng. Chem.*, vol. 89, pp. 83–103, 2020, doi: 10.1016/j.jiec.2020.06.022.

[412] C. C. Gaylarde, F. M. Bento, and J. Kelley, “Microbial contamination of stored hydrocarbon fuels and its control,” *Rev. Microbiol.*, vol. 30, pp. 1–10, 1999, doi: 10.1590/S0001-37141999000100001.

[413] G. Hemighaus *et al.*, “Aviation fuels technical review,” *Chevron Corp.*, 2006.

[414] M. Mohammad, T. K. Hari, Z. Yaakob, Y. C. Sharma, and K. Sopian, “Overview on the production of paraffin based-biofuels via catalytic hydrodeoxygenation,” *Renew. Sustain. Energy Rev.*, vol. 22, pp. 121–132, 2013, doi: 10.1016/j.rser.2013.01.026.

[415] A. Llamas, M. García-Martínez, A.-M. Al-Lal, L. Canoira, and M. Lapuerta, “Biokerosene

from coconut and palm kernel oils: Production and properties of their blends with fossil kerosene," *Fuel*, vol. 102, pp. 483–490, 2012, doi: 10.1016/j.fuel.2012.06.108.

[416] S. Zabarnick and N. Widmor, "Studies of jet fuel freezing by differential scanning calorimetry," *Energy & fuels*, vol. 15, no. 6, pp. 1447–1453, 2001, doi: 10.1021/ef010074b.

[417] M. Exxon, "World Jet Fuel Specifications. Retrieved from http://www.exxonmobil.com/AviationGlobal/Files/WorldJetFuelSpec2008_1.pdf." ExxonMobil Aviation International Leatherhead, 2005.

[418] J. Baumi, C. M. Bertosse, and C. L. B. Guedes, "Aviation fuels and biofuels," in *Renewable Energy-Resources, Challenges and Applications*, IntechOpen, 2020.

[419] M. T. Ghannam and M. Y. E. Selim, "Rheological properties of the jojoba biofuel," *Sustainability*, vol. 13, no. 11, p. 6047, 2021, doi: 10.3390/su13116047.

[420] A. de Klerk *et al.*, "Sustainable aviation fuel: Pathways to fully formulated synthetic jet fuel via Fischer–Tropsch synthesis," *Energy Sci. Eng.*, vol. 12, no. 2, pp. 394–409, 2024, doi: 10.1002/ese3.1379.

[421] T. Edwards and L. Q. Maurice, "Surrogate mixtures to represent complex aviation and rocket fuels," *J. Propuls. power*, vol. 17, no. 2, pp. 461–466, 2001, doi: 10.2514/2.5765.

[422] ASTM, *Standard specification for aviation turbine fuel containing synthesized hydrocarbons. West Conshohocken, PA: ASTM; 2009*. ASTM International, 2014.

[423] S. M. Kim, M. E. Lee, J.-W. Choi, D. J. Suh, and Y.-W. Suh, "Conversion of biomass-derived butanal into gasoline-range branched hydrocarbon over Pd-supported catalysts," *Catal. Commun.*, vol. 16, no. 1, pp. 108–113, 2011, doi: 10.1016/j.catcom.2011.09.022.

[424] S. Karatzos, J. D. McMillan, and J. N. Saddler, "The potential and challenges of drop-in biofuels," *Rep. IEA Bioenergy Task*, vol. 39, 2014.

[425] K. P. Brooks *et al.*, "Low-carbon aviation fuel through the alcohol to jet pathway," *Biofuels Aviat.*, pp. 109–150, 2016, doi: 10.1016/B978-0-12-804568-8.00006-8.

[426] P. Dagaut and M. Cathonnet, "The ignition, oxidation, and combustion of kerosene: A review of experimental and kinetic modeling," *Prog. energy Combust. Sci.*, vol. 32, no. 1, pp. 48–92, 2006, doi: 10.1016/j.pecs.2005.10.003.

[427] W.-C. Wang and L. Tao, "Bio-jet fuel conversion technologies," *Renew. Sustain. Energy Rev.*, vol. 53, pp. 801–822, 2016, doi: 10.1016/j.rser.2015.09.016.

[428] P. Bi *et al.*, "From lignin to cycloparaffins and aromatics: directional synthesis of jet and diesel fuel range biofuels using biomass," *Bioresour. Technol.*, vol. 183, pp. 10–17, 2015,

doi: 10.1016/j.biortech.2015.02.023.

[429] M. T. Timko *et al.*, "Combustion products of petroleum jet fuel, a Fischer–Tropsch synthetic fuel, and a biomass fatty acid methyl ester fuel for a gas turbine engine," *Combust. Sci. Technol.*, vol. 183, no. 10, pp. 1039–1068, 2011, doi: 10.1080/00102202.2011.581717.

[430] T. D. Hong, T. H. Soerawidjaja, I. K. Reksowardojo, O. Fujita, Z. Duniani, and M. X. Pham, "A study on developing aviation biofuel for the Tropics: Production process—Experimental and theoretical evaluation of their blends with fossil kerosene," *Chem. Eng. Process. Process Intensif.*, vol. 74, pp. 124–130, 2013, doi: 10.1016/j.cep.2013.09.013.

[431] B. Gopalakrishnan, N. Khanna, and D. Das, "Dark-fermentative biohydrogen production," in *Biohydrogen*, Elsevier, 2019, pp. 79–122.

[432] B. Gawron and T. Białecki, "Impact of a Jet A-1/HEFA blend on the performance and emission characteristics of a miniature turbojet engine," *Int. J. Environ. Sci. Technol.*, vol. 15, pp. 1501–1508, 2018, doi: 10.1007/s13762-017-1528-3.

[433] M. D. Argyle and C. H. Bartholomew, "Heterogeneous catalyst deactivation and regeneration: a review," *Catalysts*, vol. 5, no. 1, pp. 145–269, 2015, doi: 10.3390/catal5010145.

[434] M. M. Moyer, C. Karakaya, R. J. Kee, and B. G. Trewyn, "In situ formation of metal carbide catalysts," *ChemCatChem*, vol. 9, no. 16, pp. 3090–3101, 2017, doi: 10.1002/cctc.201700304.

[435] V. Daligaux, R. Richard, and M.-H. Manero, "Deactivation and regeneration of zeolite catalysts used in pyrolysis of plastic wastes—a process and analytical review," *Catalysts*, vol. 11, no. 7, p. 770, 2021, doi: 10.3390/catal11070770.

LIST OF APPENDIXES

GC-MS Results of Hydroprocessed Liquid Organic Fractions

Table 7.S1 Product distribution for hydroprocessed Yellow Dodolla oil using β-Mo_2C/$AlPO_4$-18 at 300 °C, 21 H_2 pressure, and 2.5 hours.

Peak No.	Retention time (min)	Systematic name	Cas number	Molecular formula	Shorthand notation	Type of compound	Common/ another name	Area %	Qual
1	12.2215	Hexadecanoic acid, methyl ester	000112-39-0	$C_{17}H_{34}O_2$	C16:0	SFA	Palmitic	3.0069	98
2	14.9822	9-Octadecenoic acid (Z)-, methyl ester	000112-62-9	$C_{19}H_{36}O_2$	C18:1	MUFA	Oleic	8.1442	99
3	15.0726	9,12-Octadecadienoic acid, methyl ester	002462-85-3	$C_{19}H_{34}O_2$	C18:2	PUFA	Linoleic	17.0445	99
4	15.2163	Methyl stearate	000112-61-8	$C_{19}H_{38}O_2$	C18:0	SFA	Stearic	1.6451	99
5	15.3543	9,12,15-Octadecatrienoic acid, methyl ester, (Z,Z,Z)-	000301-00-8	$C_{19}H_{32}O_2$	C18:3	PUFA	Linolenic	6.5933	99
6	18.6455	cis-11-Eicosenoic acid, methyl ester	1000333-63-8	$C_{21}H_{40}O_2$	C20:1	MUFA	Eicosenoic	7.4351	99
7	18.7708	11-Eicosenoic acid, methyl ester	003946-08-5	$C_{21}H_{40}O_2$	C20:1	MUFA	Eicosenoic	1.7944	98
8	22.7967	13-Docosenoic acid, methyl ester, (Z)-	001120-34-9	$C_{23}H_{44}O_2$	C22:1	MUFA	Erucic	42.3553	94
9	22.9143	Z,E-2,13-Octadecadien-1-ol	1000131-10-3	$C_{18}H_{34}O$	-	-	-	1.6732	93
10	24.7226	2-(Dimethylaminomethyl)-3-nitrophenol	303194-49-2	$C_9H_{12}N_2O_3$	-	-	-	9.094	60
11	26.5534	1,2-Benzenediol, 4-[2-(methylamino)ethyl]-	000501-15-5	$C_9H_{13}NO_2$	-	-	-	1.2139	38

Table 7.S2 Product distribution for hydroprocessed Yellow Dodolla oil using Ni_3C/$AlPO_4$-18 at 300 °C, 21 H_2 pressure, and 2.5 hours.

Peak No.	Retention time (min)	Systematic name	Cas number	Molecular formula	Shorthand notation	Type of compound	Common/ another name	Area %	Qual
1	12.2303	Hexadecanoic acid, methyl ester	000112-39-0	$C_{17}H_{34}O_2$	C16:0	SFA	Palmitic	4.2033	96
2	14.9802	9-Octadecenoic acid, methyl ester, (E)-	001937-62-8	$C_{19}H_{36}O_2$	C18:1	MUFA	Elaidic	9.0192	99
3	15.0682	9,12-Octadecadienoic acid, methyl ester	002462-85-3	$C_{19}H_{34}O_2$	C18:2	PUFA	Linoleic	23.1368	99
4	15.212	Cyclohexanol, 2-(methylaminomethyl)-, trans-	077612-16-9	$C_8H_{17}NO$	-	-	-	3.712	49
5	15.3556	Phenylephrine	000059-42-7	$C_9H_{13}NO_2$	-	-	-	6.4484	45
6	18.6434	1-Butanamine, N-methyl-	000110-68-9	$C_5H_{13}N$	-	-	-	4.5951	43
7	22.77	13-Docosenoic acid, methyl ester, (Z)-	001120-34-9	$C_{23}H_{44}O_2$	C22:1	MUFA	Erucic	48.8853	99

Table 7.S3 Product distribution for hydroprocessed Yellow Dodolla oil using WC/$AlPO_4$-18 at 300 °C, 21 H_2 pressure, and 2.5 hours.

Peak No.	Retention time (min)	Systematic name	Cas number	Molecular formula	Shorthand notation	Type of compound	Common/ another name	Area %	Qual
1	12.221	Hexadecanoic acid, methyl ester	000112-39-0	$C_{17}H_{34}O_2$	C16:0	SFA	Palmitic	3.4859	98
2	14.9743	9-Octadecenoic acid (Z)-, methyl ester	000112-62-9	$C_{19}H_{36}O_2$	C18:1	MUFA	Oleic	8.305	99
3	15.0618	9,12-Octadecadienoic acid, methyl ester	002462-85-3	$C_{19}H_{34}O_2$	C18:2	PUFA	Linoleic	21.4136	99
4	15.2074	Heptadecanoic acid, 16-methyl-, methyl ester	005129-61-3	$C_{19}H_{38}O_2$	C18:1	MUFA	Methyl isostearate	2.5542	97
5	15.3472	9,12,15-Octadecatrienoic acid, methyl ester, (Z,Z,Z)-	000301-00-8	$C_{19}H_{32}O_2$	C18:3	PUFA	Linolenic	7.3279	99
6	18.6379	cis-11-Eicosenoic acid, methyl ester	1000333-63-8	$C_{21}H_{40}O_2$	C20:1	MUFA	Eicosenoic	6.1997	97
7	18.7589	1-Propanamine, N,2-dimethyl-	000625-43-4	$C_5H_{13}N$	-	-	-	1.6454	47
8	22.7644	13-Docosenoic acid, methyl ester, (Z)-	001120-34-9	$C_{23}H_{44}O_2$	C22:1	MUFA	Erucic	49.0682	99

Table 7.S4 Product distribution for hydroprocessed Yellow Dodolla oil using β-Mo_2C/$AlPO_4$-18 at 500 °C, 21 bar H_2 pressure, and 2.5 hours.

Peak No.	Retention time (min)	Systematic name	Cas number	Molecular formula	Shorthand notation	Type of compound	Common/ another name	Area %	Qual
1	0.7388	Cyclopropane, 1-methyl-2-pentyl-	041977-37-1	C_9H_{18}	C8:0	Naphthene HC	-	0.7388	90
2	1.4549	4-Decene	019689-18-0	$C_{10}H_{20}$	C9:1	Olefinic HC	-	1.4549	93
3	0.2281	4-Decene	019689-18-0	$C_{10}H_{20}$	C9:1	Olefinic HC	-	0.2281	95
4	0.247	Cyclohexene, 4-methyl-1-(1-methylethyl)-	000500-00-5	$C_{10}H_{18}$	C9:1	Cycloolefin HC	-	0.247	81
5	1.4434	1-Undecene	000821-95-4	$C_{11}H_{22}$	C10:1	Olefinic HC	Undecene-1	1.4434	64
6	0.7851	5-Undecene	004941-53-1	$C_{11}H_{22}$	C10:1	Olefinic HC	-	0.7851	95
7	0.6475	3-Undecene, (Z)-	000821-97-6	$C_{11}H_{22}$	C10:1	Olefinic HC	(Z)-3-Undecene	0.6475	94
8	0.6353	Cyclohexanone, 2-methyl-5-(1-methylethenyl)-	007764-50-3	$C_{10}H_{16}O$	-	Ketone	p-Menth-8-en-2-one	0.6353	59
9	0.2664	Cyclopentene, 1-pentyl-	004291-98-9	$C_{10}H_{18}$	C9:1	Cycloolefin HC	1-Pentyl-1-cyclopentene	0.2664	58
10	0.4848	Decalin, anti-1-methyl-, cis-	1000158-89-0	$C_{11}H_{20}$	-	HC (polycyclic aromatic)	-	0.4848	95
11	0.1335	Carane, 4,5-epoxy-, trans	006909-20-2	$C_{10}H_{16}O$	-	Carbobicyclic	4,5-Epoxycarene	0.1335	49
12	1.4056	1-Dodecene	000112-41-4	$C_{12}H_{24}$	C11:1	Olefinic HC	α-Dodecene	1.4056	91
13	0.5715	2-Dodecene, (Z)-	007206-26-0	$C_{12}H_{24}$	C11:1	Olefinic HC	(2Z)-2-Dodecene	0.5715	86
14	0.4783	2-Dodecene, (Z)-	007206-26-0	$C_{12}H_{24}$	C11:1	Olefinic HC	(2Z)-2-Dodecene	0.4783	97
15	0.7157	Cyclododecene, (E)-	001486-75-5	$C_{12}H_{22}$	C11:1	Cycloolefin HC	(E)-Cyclododecene	0.7157	90
16	9.8076	Naphthalene, decahydro-1,5-dimethyl-	066552-62-3	$C_{12}H_{22}$	C11:1	Polycyclic aromatic HC	-	0.5077	46
17	10.0295	2-Isopropenyl-5-methyl-6-hepten-1-ol	013066-55-2	$C_{11}H_{20}O$	-	-	Alcohol	0.4514	64
18	10.1491	Cyclohexene,1-hexyl-	003964-66-7	$C_{12}H_{22}$	C11:1	Cycloolefin HC	1-hexyl-1-cyclohexene	0.1683	50
19	10.2751	trans-2,3-Epoxyoctane	028180-70-3	$C_8H_{16}O$	-	-	-	1.3818	42
20	10.4599	3-Tridecene, (Z)-	041446-53-1	$C_{13}H_{26}$	C12:1	Olefinic HC	(3Z)-3-Tridecene	0.4477	95
21	10.6376	2-Tridecene, (E)-	041446-58-6	$C_{13}H_{26}$	C12:1	Olefinic HC	(2E)-2-Tridecene	0.2815	96
22	10.8333	2-Propenal, 3-(4-methylphenyl)-	001504-75-2	$C_{10}H_{10}O$	-	FA (aldehyde)	-	0.1569	70
23	10.9536	Octanoic acid	000124-07-2	$C_8H_{16}O_2$	C7:0	SFA	n-Caprylic acid	0.5734	64
24	11.0645	1,19-Eicosadiene	014811-95-1	$C_{20}H_{38}$	C19:2	Olefinic HC	-	0.4805	58
25	11.235	3,4-Octadiene, 7-methyl-	037050-05-8	C_9H_{16}	C8:2	Olefinic HC	-	0.1298	70
26	11.3307	1,3-Cyclopentadiene, 5-(trans-2-ethyl-3-methylcyclopropylidene)-	079209-36-2	$C_{11}H_{14}$	-	Cycloolefin HC	-	0.2518	50
27	11.437	11-Hexadecyn-1-ol	065686-49-9	$C_{16}H_{30}O$	-	Polyunsaturated alcohol	-	0.177	64

Table 7.S4 Continued.

Peak No.	Retention time (min)	Systematic name	Cas number	Molecular formula	Shorthand notation	Type of compound	Common/ another name	Area %	Qual
28	11.6649	1-Tetradecene	001120-36-1	$C_{14}H_{28}$	C13:1	Olefinic HC	α-Tetradecene	1.279	56
29	11.7935	3-Tetradecene, (Z)-	041446-67-7	$C_{14}H_{28}$	C13:1	Olefinic HC	(3Z)-3-Tetradecene	0.4834	97
30	11.9604	Pyridine, 2,5-dimethyl-	000589-93-5	C_7H_9N	-	-	2,5-Lutidine	0.4297	25
31	12.0402	Undec-10-ynoic acid, tridec-2-yn-1-yl ester	1000406-96-9	$C_{24}H_{40}O_2$	C23:4	PUFA	-	0.302	38
32	12.2277	Cyclopentanecarboxylic acid, heptadecyl ester	1000282-77-6	$C_{23}H_{44}O_2$	C22:1	MUFA (cyclic)	-	0.4096	22
33	12.4224	1-Tetradecene	001120-36-1	$C_{14}H_{28}$	C13:1	Olefinic HC	α-Tetradecene	0.8102	97
34	12.5779	9,17-Octadecadienal, (Z)-	056554-35-9	$C_{18}H_{32}O$	-	Unsaturated aldehyde	9,17-Octadecadienal	0.4257	51
35	12.7196	9-Eicosyne	071899-38-2	$C_{20}H_{38}$	C19:2	Olefinic HC	-	0.2281	70
36	12.9485	Carbonic acid, hexadecyl 2,2,2-trichloroethyl ester	1000314-56-2	$C_{19}H_{35}Cl_3O_3$	-	Chlorinated FA	-	1.9682	68
37	13.0616	Cetene	000629-73-2	$C_{16}H_{32}$	C15:1	Olefinic HC	1-Hexadecene	0.4427	95
38	13.2379	1-Pentadecene	013360-61-7	$C_{15}H_{30}$	C14:1	Olefinic HC	Pentadecene,1-	0.6229	80
39	13.3431	1-Hexadecyne	000629-74-3	$C_{16}H_{30}$	C15:2	Alkyne HC	hexadec-1-yne	0.257	81
40	13.5065	n-Decanoic acid	000334-48-5	$C_{10}H_{20}O_2$	C9:0	SFA	Decanoic acid	1.7393	27
41	13.724	n-Nonylcyclohexane	002883-02-5	$C_{15}H_{30}$	C14:0	Naphthene HC	Nonylcyclohexane	0.7321	49
42	13.8366	(-)-trans-Pinane	033626-25-4	$C_{10}H_{18}$	-	-	E-pinane	0.2076	80
43	13.9102	7-Pentadecyne	022089-89-0	$C_{15}H_{28}$	C14:2	Alkyne HC	-	0.2558	86
44	14.0514	1,13-Tetradecadiene	021964-49-8	$C_{14}H_{26}$	C13:2	Olefinic HC	-	0.9952	89
45	14.1625	1-Piperidinamine, N-ethylidene-	075267-99-1	$C_7H_{14}N_2$	-	-	-	1.0951	50
46	14.2651	Formic acid, decyl ester	005451-52-5	$C_{11}H_{22}O_2$	C10:0	SFA	n-Decyl methanoate	0.7056	60
47	14.4463	5-Eicosene, (E)-	074685-30-6	$C_{20}H_{40}$	C19:1	Olefinic HC	(5E)-5-Icosene	0.8264	98
48	14.6191	Dodecyl nonyl ether	1000406-37-5	$C_{21}H_{44}O$	-	Ether	-	0.8258	38
49	14.6762	(R)-(-)-14-Methyl-8-hexadecyn-1-ol	064566-18-3	$C_{17}H_{34}O$	-	Unsaturated alcohol	-	0.2374	41
50	14.7448	8-Dodecen-1-ol, (Z)-	040642-40-8	$C_{12}H_{24}O$	-	Unsaturated alcohol	-	0.4947	83
51	14.9322	Hexadecanal	000629-80-1	$C_{16}H_{32}O$	-	Fatty aldehyde	-	0.7997	89
52	15.1767	n-Heptadecanol-1	001454-85-9	$C_{17}H_{36}O$	-	Alcohol	-	1.5678	60
53	15.2718	2-Butenedioic acid (Z)-, monododecyl ester	002424-61-5	$C_8H_{12}O_4$	C7:1	Fatty (dicarboxylic acid)	Maleic acid, monobutyl ester	1.3604	92
54	15.4071	3-Heptadecene, (Z)-	1000141-67-3	$C_{17}H_{34}$	C16:1	Olefinic HC	cis-3-Heptadecene	0.9723	95
55	15.5843	Cyclopentadecane	000295-48-7	$C_{15}H_{30}$	C14:0	Naphthene HC	decylcyclopentane	0.55	91
56	15.7178	Dodecanoic acid	000143-07-7	$C_{12}H_{24}O_2$	C11:0	SFA	n-Dodecanoic acid	1.6739	66
57	16.0495	(R)-(-)-14-Methyl-8-hexadecyn-1-ol	064566-18-3	$C_{17}H_{32}O$	-	Unsaturated alcohol	-	1.1299	83
58	16.2768	Cyclodecanol	001502-05-2	$C_{10}H_{20}O$	-	Cyclic alcohol	-	1.852	70

Table 7.S4 Continued.

Peak No.	Retention time (min)	Systematic name	Cas number	Molecular formula	Shorthand notation	Type of compound	Common/ another name	Area %	Qual
59	16.3713	1-Tridecene	002437-56-1	$C_{13}H_{26}$	C12:1	Olefinic HC	n-Tridec-1-ene	0.6435	95
60	16.4185	1,9-Tetradecadiene	112929-06-3	$C_{14}H_{26}$	C13:2	Olefinic HC	-	0.7211	86
61	16.5123	1,13-Tetradecadiene	021964-49-8	$C_{14}H_{26}$	C13:2	Olefinic HC	Tetradeca-1,13-diene	1.1987	81
62	16.8337	Tridecanoic acid	000638-53-9	$C_{13}H_{26}O_2$	C12:0	SFA	n-Tridecanoic acid	1.4456	64
63	16.9534	7-Hexadecyne	074685-28-2	$C_{16}H_{30}$	C15:2	Alkyne HC	-	0.5008	64
64	17.1972	1-Heptacosanol	002004-39-9	$C_{27}H_{56}O$	-	Alcohol	-	0.8743	87
65	17.2756	5-Nonadecen-1-ol	1000131-11-9	$C_{19}H_{38}O$	-	Alcohol	-	0.3787	64
66	17.445	trans-2-Dodecen-1-ol, trifluoroacetate	1000352-26-2	$C_{14}H_{23}F_3O_2$	-	--		1.9739	83
67	17.5635	Cyclopropane, nonyl-	074663-85-7	$C_{12}H_{24}$	C11:0	Naphthene HC	n-Nonyl-cyclopropane	1.2696	86
68	17.7153	1-Octadecene	000112-88-9	$C_{18}H_{36}$	C17:1	Olefinic HC	α-Octadecene	0.4331	90
69	17.8299	Hexadecanal	000629-80-1	$C_{16}H_{32}O$	-	Fatty aldehyde	-	0.6982	93
70	17.9486	2-Methyl-7-nonadecene	219750-68-2	$C_{20}H_{40}$	C19:1	Olefinic HC	-	0.4183	86
71	18.0699	Tetradecanoic acid	000544-63-8	$C_{14}H_{28}O_2$	C13:1	SFA	Myristic acid	0.4421	83
72	18.1567	p-Menth-8(10)-en-9-ol, cis-	015714-13-3	$C_{10}H_{18}O$	-	Cyclic alcohol	-	0.5485	44
73	18.5204	Linoelaidic acid	000506-21-8	$C_{18}H_{32}O_2$	C17:2	PUFA	-	0.7095	94
74	18.6032	9-Eicosyne	071899-38-2	$C_{20}H_{38}$	C19:2	Alkyne HC	-	0.3147	86
75	18.7769	Cyclodecanol	001502-05-2	$C_{10}H_{20}O$	-	Cyclic alcohol	-	1.8641	76
76	18.9128	Cyclopentadecane	000295-48-7	$C_{15}H_{30}$	C14:0	Naphthene HC	decylcyclopentane	0.7886	94
77	18.9813	Eicosen-1-ol, cis-9-	112248-30-3	$C_{20}H_{40}O$	-	Unsaturated alcohol	(Z)-Icos-9-en-1-ol	0.4788	94
78	19.0863	3-Eicosene, (E)-	074685-33-9	$C_{20}H_{40}$	C19:1	Olefinic HC	-	1.1859	97
79	19.3549	1-Octadecene	000112-88-9	$C_{18}H_{36}$	C17:1	Olefinic HC	α-Octadecene	0.4548	98
80	19.4893	D-Homoandrostane, (5.alpha.,13.alpha.)-	054482-31-4	$C_{20}H_{34}$	-	Naphthene HC	-	0.7361	92
81	19.6818	Linoelaidic acid	000506-21-8	$C_{18}H_{32}O_2$	C17:2	PUFA	-	0.3691	84
82	19.8608	1-Nonadecene	018435-45-5	$C_{19}H_{38}$	C18:1	Olefinic HC	Nonadec-1-ene	0.686	95
83	20.0068	(R)-(-)-(Z)-14-Methyl-8-hexadecen-1-ol	030689-78-2	$C_{17}H_{34}O$	-	Unsaturated alcohol	-	0.5381	53
84	20.2083	cis-7-Dodecen-1-yl acetate	014959-86-5	$C_{14}H_{26}O_2$	C13:1	MUFA	7-Dodecen-1-ol, acetate, (Z)-	1.2635	86
85	20.2811	trans-2-Dodecen-1-ol, trifluoroacetate	1000352-26-2	$C_{14}H_{23}F_3O_2$	-	Fluorinated FA	-	1.9997	70
86	20.4523	1,13-Tetradecadiene	021964-49-8	$C_{14}H_{26}$	C13:2	Olefinic HC	Tetradeca-1,13-diene	0.9276	91
87	20.5339	Z-5-Nonadecene	1000131-11-8	$C_{19}H_{38}$	C18:1	Olefinic HC	-	0.5873	98
88	20.6978	1,11-Dodecadiene	005876-87-9	$C_{12}H_{22}$	C11:2	Olefinic HC	Dodecadiene, 1,11-	0.9496	92

Table 7.S4 Continued.

Peak No.	Retention time (min)	Systematic name	Cas number	Molecular formula	Shorthand notation	Type of compound	Common/ another name	Area %	Qual
89	20.883	9-Hexadecen-1-ol, (Z)-	010378-01-5	$C_{16}H_{32}O$	-	Alcohol	-	0.9612	91
90	21.1691	Dodecanoic acid	000143-07-7	$C_{12}H_{24}O_2$	C11:0	SFA	n-Dodecanoic acid	2.2367	35
91	21.3377	13-Docosen-1-ol, (Z)-	000629-98-1	$C_{22}H_{44}O$	-	Unsaturated alcohol	-	0.3259	62
92	21.4826	Z-11-Tetradecen-1-ol trifluoroacetate	1000131-33-7	$C_{16}H_{27}F_3O_2$	-	Fluorinated FA	-	0.4306	92
93	21.7115	Linoelaidic acid	000506-21-8	$C_{18}H_{32}O_2$	C17:2	PUFA	-	0.5242	83
94	21.9777	Cycloundecene, 1-methyl-	088828-82-4	$C_{12}H_{22}$	C11:1	Cycloolefin HC	cis-Cycloundecene, 1-methyl-	1.3752	92
95	22.0474	1,14-Docosanediol	004452-45-3	$C_{22}H_{46}O_2$	-	Alcohol	-	0.6518	90
96	22.1514	E-14-Hexadecenal	330207-53-9	$C_{16}H_{30}O$	-	Unsaturated aldehyde	(14E)-14-Hexadecenal	0.9633	95
97	22.2479	1-Nonadecene	018435-45-5	$C_{19}H_{38}$	C18:1	Olefinic HC	Nonadec-1-ene	0.6266	97
98	22.3677	1-Docosanol, methyl ether	1000333-91-9	$C_{23}H_{48}O$	-	Ether	-	0.5214	96
99	22.4654	13-Tetradecen-1-ol acetate	056221-91-1	$C_{16}H_{30}O_2$	C15:1	MUFA	13-tetradecenyl acetate	0.7056	91
100	22.7192	cis-1-Chloro-9-octadecene	016507-61-2	$C_{18}H_{35}Cl$	-	-		0.405	97
101	22.8924	13-Tetradecen-1-ol acetate	056221-91-1	$C_{16}H_{30}O_2$	C15:1	MUFA	13-tetradecenyl acetate	0.4499	90
102	23.4799	1H-Indene, 2-butyl-5-hexyloctahydro-	055044-33-2	$C_{19}H_{36}$	C18:0	Naphthene HC	Bicyclo[4.3.0]nonane, 8-butyl-3-hexyl-	0.2925	62
103	23.7488	9-Tricosene, (Z)-	027519-02-4	$C_{23}H_{46}$	C22:1	Olefinic HC	(Z)-9-Tricosene	1.1732	99
104	23.9993	1-Octadecanethiol	002885-00-9	$C_{18}H_{38}S$	-	-	-	0.8215	94
105	24.1079	1-Hexacosene	018835-33-1	$C_{26}H_{52}$	C23:1	Olefinic HC	Hexacos-1-ene	0.3091	91
106	24.2419	Linoelaidic acid	000506-21-8	$C_{18}H_{32}O_2$	C17:2	PUFA	-	0.2242	92
107	24.4009	9,12-Octadecadienoic acid (Z,Z)-	000060-33-3	$C_{18}H_{32}O_2$	C17:2	PUFA	cis-9,cis-12-Octadecadienoic acid	0.621	93
108	24.7327	9-Octadecenoic acid, (E)-	000112-79-8	$C_{18}H_{34}O_2$	C17:1	MUFA	trans-δ9-Octadecenoic acid	2.7095	95
109	24.9391	Octadecanoic acid	000057-11-4	$C_{18}H_{36}O_2$	C17:0	SFA	Stearic acid	1.6863	83
110	25.2166	11,13-Dimethyl-12-tetradecen-1-ol acetate	1000130-81-0	$C_{18}H_{34}O_2$	C17:1	MUFA	-	0.7696	86
111	25.5624	11,13-Dimethyl-12-tetradecen-1-ol acetate	1000130-81-0	$C_{18}H_{34}O_2$	C17:1	MUFA	-	0.3368	87
112	25.6855	1-Tetracosene	010192-32-2	$C_{24}H_{48}$	C23:1	Olefinic HC	Tetracos-1-ene	1.0075	97
113	25.9718	Oxirane, hexadecyl-	007390-81-0	$C_{18}H_{36}O$	-	Ether	1,2-Epoxyoctadecane	0.5527	93

Table 7.S4 Continued.

Peak No.	Retention time (min)	Systematic name	Cas number	Molecular formula	Shorthand notation	Type of compound	Common/ another name	Area %	Qual
114	26.2542	Cyclotetracosane	000297-03-0	$C_{24}H_{48}$	C23:0	Naphthene HC	-	0.1763	99
115	26.4486	cis-9-Hexadecenal	056219-04-6	$C_{16}H_{30}O$	-	Aldehyde	9-Hexadecenal, (Z)-	0.3925	89
116	26.7185	9,12-Octadecadienoic acid (Z,Z)-	000060-33-3	$C_{18}H_{32}O_2$	C17:2	PUFA	cis-9,cis-12-Octadecadienoic acid	0.3414	98
117	27.5056	Z,E-3,13-Octadecadien-1-ol acetate	1000131-01-6	$C_{20}H_{36}O_2$	C19:2	PUFA	-	0.1207	81
118	27.7088	10,13-Octadecadienoic acid, methyl ester	056554-62-2	$C_{19}H_{34}O_2$	C18:2	PUFA	-	0.5887	90
119	28.069	11,13-Dimethyl-12-tetradecen-1-ol acetate	1000130-81-0	$C_{18}H_{34}O_2$	C17:1	MUFA	-	0.152	86
120	28.6214	E-14-Hexadecenal	330207-53-9	$C_{16}H_{30}O$	-	Aldehyde	-	0.4892	93
121	28.8846	1-Heptadecene	006765-39-5	$C_{24}H_{48}$	C23:0	Naphthene HC		1.4383	95
122	29.1073	1-Tricosene	018835-32-0	$C_{19}H_{34}O_2$	C18:2	PUFA	-	0.7753	96
123	29.5761	1,7-Hexadecadiene	125110-62-5	$C_{16}H_{30}$	C15:2	Olefinic HC	-	0.3008	90
124	29.7292	11-Hexacosyne	034291-69-5	$C_{26}H_{50}$	C25:1	Alkyne HC	-	0.6005	93
125	29.8853	Nonacos-1-ene	018835-35-3	$C_{29}H_{52}$	C28:1	Olefinic HC	1-Nonacosene	0.256	97
126	29.967	(R)-(-)-14-Methyl-8-hexadecyn-1-ol	064566-18-3	$C_{17}H_{34}O$	-	Alcohol	-	0.3879	95
127	30.4701	13-Tetradecen-1-ol acetate	056221-91-1	$C_{16}H_{30}O_2$	C15:1	MUFA	13-tetradecenyl acetate	0.4887	91
128	30.7412	11-Tricosene	052078-56-5	$C_{23}H_{46}$	C22:1	Olefinic HC	-	0.165	52
129	31.8548	9-Octadecen-1-ol, (Z)-	000143-28-2	$C_{18}H_{36}O$	-	Unsaturated alcohol	-	0.8349	90
130	32.039	11,13-Dimethyl-12-tetradecen-1-ol acetate	1000130-81-0	$C_{18}H_{34}O_2$	C17:1	MUFA	-	0.3697	70
131	32.4329	13-Tetradecen-1-ol acetate	056221-91-1	$C_{16}H_{30}O_2$	C15:1	MUFA	13-tetradecenyl acetate	0.1003	94
132	32.9732	Tricosanal	072934-02-2	$C_{23}H_{46}O$	-	Aldehyde	-	3.2721	56
133	33.1215	1-Tetracosene	010192-32-2	$C_{24}H_{48}$	C23:1	Olefinic HC	-	0.8265	96
134	33.4737	13-Docosen-1-ol, (Z)-	000629-98-1	$C_{22}H_{44}O$	-	Unsaturated alcohol	-	0.4125	86
135	33.606	1,14-Docosanediol	004452-45-3	$C_{22}H_{46}O_2$	-	Alcohol	-	0.2618	93
136	33.7094	1-Tricosene	018835-32-0	$C_{23}H_{46}$	C22:1	Olefinic HC	Tricosene-1	0.2441	96

Table 7.S5 Product distribution for hydroprocessed Yellow Dodolla oil using $Ni_3C/AlPO_4$-18 at 500 °C, 21 bar H_2 pressure, and 2.5 hours.

Peak No.	Retention time (min)	Systematic name	Cas number	Molecular formula	Shorthand notation	Type of compound	Common/ another name	Area %	Qual
1	4.4042	Cyclopropane, 1-methyl-2-pentyl-	041977-37-1	C_9H_{18}	C8:0	Naphthene HC	-	1.1359	55
2	4.5268	Cyclopropane, 1-methyl-2-pentyl-	041977-37-1	C_9H_{18}	C8:0	Naphthene HC	-	1.036	50
3	5.1373	4-Nonyne	020184-91-2	C_9H_{16}	C8:2	Alkyne HC	4-C9H16	0.207	41
4	5.8788	1-Decene	000872-05-9	$C_{10}H_{20}$	C9:1	Olefinic HC	n-1-Decene	1.7216	86
5	6.4487	3,6-Nonadien-1-ol, (E,Z)-	056805-23-3	$C_9H_{16}O$	-	Unsaturated alcohol	(3E,6E)-3,6-Nonadien-1-ol	0.1532	43
6	6.6421	Cyclohexanone, 2-(2-propenyl)-	000094-66-6	$C_9H_{14}O$	-	Unsaturated ketone (cyclic)	Cyclohexanone, 2-allyl-	0.5526	38
7	7.3951	Benzene, 2-propenyl-	000300-57-2	C_9H_{10}	-	Aromatic HC	Benzene, allyl-	1.7509	53
8	7.5456	3-Undecene, (E)-	001002-68-2	$C_{11}H_{22}$	C10:1	Olefinic HC	(E)-3-Undecene	0.8126	92
9	7.7376	5-Undecene	004941-53-1	$C_{11}H_{22}$	C10:1	Olefinic HC	-	0.452	96
10	7.8813	Naphth[2,3-b]oxirene, decahydro-	021399-51-9	$C_{10}H_{16}O$	-	-	-	0.159	45
11	8.152	Benzene, (2-methyl-1-propenyl)-	000768-49-0	$C_{10}H_{12}$	C9:1	Aromatic HC	Benzene, (2-methylpropenyl)-	0.958	94
12	8.342	3,4-Octadiene, 7-methyl-	037050-05-8	C_9H_{16}	C8:2	Olefinic HC	-	0.2791	52
13	8.5398	3-Cyclohexene-1-carboxaldehyde, 1,3,4-trimethyl-	040702-26-9	$C_{10}H_{16}O$	-	Aldehyde	-	0.4158	64
14	8.7065	3-Decanynoic acid	027007-78-9	$C_{10}H_{16}O_2$	-	-	-	0.1523	42
15	8.8691	Cyclodecane	000293-96-9	$C_{10}H_{20}$	C9:0	Naphthene HC	-	1.5733	78
16	9.0487	2-Propanone, phenylhydrazone	000103-02-6	$C_9H_{12}N_2$	-	Ketone	-	0.6318	70
17	9.2015	Benzene, 2-ethenyl-1,4-dimethyl-	002039-89-6	$C_{10}H_{12}$	-	Aromatic HC	Styrene, 2,5-dimethyl-	0.5751	95
18	9.396	Naphthalene, 1,2,3,4-tetrahydro-	000119-64-2	$C_{10}H_{12}$	-	HC (cyclic and aromatic)	Tetralin	0.2488	94
19	9.6154	8-Dodecen-1-ol, (Z)-	040642-40-8	$C_{12}H_{24}O$	-	Alcohol	-	1.0468	53
20	9.7429	Benzene, (1-ethyl-1-propenyl)-	004701-36-4	$C_{11}H_{14}$	-	Aromatic HC	3-Phenyl-2-pentene	0.3434	53
21	9.8089	Phenol, 2-methyl-	000095-48-7	C_7H_8O	-	Aromatic alcohol	o-Cresol	0.3935	76
22	10.0311	9-Methylbicyclo[3.3.1]nonane	025107-01-1	$C_{10}H_{18}$	C9:0	Naphthene HC	-	0.4341	64
23	10.1521	Cyclohexene,1-hexyl-	003964-66-7	$C_{12}H_{22}$	C11:1	Cycloolefin HC	1-hexyl-1-cyclohexene	0.1926	25
24	10.2932	1-Tridecene	002437-56-1	$C_{13}H_{26}$	C12:1	Olefinic HC	n-Tridec-1-ene	1.5144	94
25	10.4624	2-Tridecene, (E)-	041446-58-6	$C_{13}H_{26}$	C12:1	Olefinic HC	(2E)-2-Tridecene	0.1849	25
26	10.5122	Benzene, hexyl-	001077-16-3	$C_{12}H_{18}$	-	Aromatic HC	Hexane, 1-phenyl-	0.3092	70

Table 7.S5 Continued.

Peak No.	Retention time (min)	Systematic name	Cas number	Molecular formula	Shorthand notation	Type of compound	Common/ another name	Area %	Qual
27	10.6727	Benzene, 1-methyl-2-(1-ethylpropyl)-	054410-74-1	$C_{12}H_{18}$	-	Aromatic HC	-	0.2254	43
28	10.8335	2-(2-Hydroxyphenyl)buta-1,3-diene	038865-47-3	$C_{10}H_{10}O$	-	-	-	0.265	64
29	10.9626	Octanoic acid	000124-07-2	$C_8H_{16}O_2$	C7:0	SFA	n-Caprylic acid	0.8541	50
30	11.0632	1-Hexadecanol	036653-82-4	$C_{16}H_{34}O$	-	Alcohol	-	0.6565	55
31	11.2358	E-12-Tetradecenal	1000130-96-1	$C_{14}H_{26}O$	-	Aldehyde	12-tetradecenal, E	0.1122	64
32	11.3224	Benzene, (1-methyl-1-butenyl)-	053172-84-2	$C_{11}H_{14}$	-	Aromatic HC	2-Phenyl-2-pentene	0.2768	50
33	11.4401	1-Heptylcyclohexene	015232-86-7	$C_{13}H_{24}$	C12:1	Cycloolefin HC	Cyclohexene,1-heptyl-	0.1613	91
34	11.5595	7-Tetradecene, (E)-	041446-63-3	$C_{14}H_{28}$	C13:1	Olefinic HC	(7E)-7-Tetradecene	0.4969	68
35	11.6577	Carbonic acid, tridecyl 2,2,2-trichloroethyl ester	1000314-55-9	$C_{16}H_{29}Cl_3O_3$	-	Chlorinated FA	-	0.9171	74
36	11.7655	Naphthalene, 1-methyl-	000090-12-0	$C_{11}H_{10}$	-	Aromatic HC	α-Methylnaphthalen	0.6228	94
37	11.9115	3-(Phenylhydrazono)-2-butanone	013732-32-6	$C_{10}H_{12}N_2O$	-	-	2,3-Butanedione 2-(phenylhydrazone)	0.1933	47
38	11.9537	Naphthalene, 1,2,3,4-tetrahydro-1,4-dimethyl-	004175-54-6	$C_{12}H_{16}$	-	Aromatic and cyclic HC	1,4-Dimethyltetralin	0.2119	47
39	12.0329	Naphthalene, 2-methyl-	000091-57-6	$C_{11}H_{10}$	-	Aromatic HC	β-Methylnaphthalene	0.4405	90
40	12.2363	Pentadecafluorooctanoic acid, undecyl ester	1000406-04-1	$C_{19}H_{23}F_{15}O_2$	-	Fluorinated FA	-	0.8774	15
41	12.4224	1-Tetradecene	001120-36-1	$C_{14}H_{28}$	C13:1	Olefinic HC	n-Tetradec-1-ene	0.7561	95
42	12.5771	Bicyclo[3.1.1]heptane, 2,6,6-trimethyl-, [1R-(1.alpha.,2.alpha.,5.alpha.)]-	004863-59-6	$C_{10}H_{18}$	-	Bicyclic HC	-	0.5248	46
43	12.9141	trans-2,3-Epoxydecane	054125-39-2	$C_{10}H_{20}O$	-	-	-	2.3014	43
44	13.059	Naphthalene, 2,7-dimethyl-	000582-16-1	$C_{12}H_{12}$	-	Aromatic HC	2,7-Dimethylnaphthalene	0.5419	46
45	13.2289	Benzene, octyl-	002189-60-8	$C_{14}H_{22}$	-	Aromatic HC	Octane, 1-phenyl-	0.661	46
46	13.3429	9-Octadecyne	035365-59-4	$C_{18}H_{34}$	C17:2	Alkyne HC	Octadec-9-yne	0.2609	49
47	13.5225	2,3-Hexadiene, 2-methyl-	029212-09-7	C_7H_{12}	C6:2	Olefinic HC	2-methyl-2,3-hexadiene	2.7032	25
48	13.7254	n-Nonylcyclohexane	002883-02-5	$C_{15}H_{30}$	C14:0	Naphthene HC	Nonylcyclohexane	1.0922	46
49	13.9383	Naphthalene, 1,4-dimethyl-	000571-58-4	$C_{12}H_{12}$	-	Aromatic HC	1,4-Dimethylnaphthalene	0.2845	87

Table 7.S5 Continued.

Peak No.	Retention time (min)	Systematic name	Cas number	Molecular formula	Shorthand notation	Type of compound	Common/ another name	Area %	Qual
50	14.0506	1,7-Hexadecadiene	125110-62-5	$C_{16}H_{30}$	C15:2	Olefinic HC	-	2.1269	91
51	14.2614	Cyclohexadecane	000295-65-8	$C_{16}H_{32}$	C15:0	Naphthene HC	-	0.4433	86
52	14.476	4,4-Dimethyl-1,1a,3a,4,5,6-hexahydrocyclopropa[c]pentalene	264628-27-5	-	-	-	-	0.868	42
53	14.6246	2-Methyl-1-dimethyl(ethenyl)silyloxypropane	137307-77-8	-	-	-	-	2.1248	38
54	14.9363	Pentadecanal-	002765-11-9	$C_{15}H_{30}O$	-	Aldehyde	1-Pentadecanal	0.8696	60
55	15.0754	1,8,11-Heptadecatriene, (Z,Z)-	056134-03-3	$C_{17}H_{30}$	C16:3	Olefinic HC	Dihydro-aplotaxene	0.3689	95
56	15.1705	cis-7-Dodecen-1-yl acetate	014959-86-5	$C_{14}H_{26}O_2$	C13:1	MUFA	7-Dodecen-1-ol, acetate, (Z)-	1.2107	93
57	15.2711	Chloroacetic acid, undecyl ester	005458-29-7	$C_{14}H_{27}ClO_2$	-	Chlorinated FA	-	1.4706	55
58	15.3973	1-Nonadecene	018435-45-5	$C_{19}H_{38}$	C18:1	Olefinic HC	Nonadec-1-ene	0.622	96
59	15.4819	Naphthalene, 2-methyl-1-propyl-	054774-89-9	$C_{14}H_{16}$	-	Aromatic HC	-	0.8466	42
60	15.7215	Dodecanoic acid	000143-07-7	$C_{12}H_{24}O_2$	C11:1	MUFA	n-Dodecanoic acid	2.2039	42
61	16.0491	3-n-Hexylthiane, S,S-dioxide	061639-18-7	$C_{11}H_{22}O_2S$	-	-	-	0.9043	49
62	16.269	E-15-Heptadecenal	1000130-97-9	$C_{17}H_{32}O$	-	Aldehyde	-	1.6488	90
63	16.3649	Cyclododecane	000294-62-2	$C_{12}H_{24}$	C11:0	Naphthene HC	-	1.1803	90
64	16.5142	9-Borabicyclo[3.3.1]nonane, 9-[(methylsulfonyl)oxy]-	096532-76-2	$C_9H_{17}BO_3S$	-	-	-	1.2367	45
65	16.8346	Tridecanoic acid	000638-53-9	$C_{13}H_{26}O_2$	C12:0	SFA	n-Tridecanoic acid	1.183	60
66	16.9616	Dodecanoic acid, 10-undecen-1-yl ester	1000159-98-0	$C_{22}H_{42}O_2$	C21:1	MUFA	-	0.4873	64
67	17.195	1-Heptadecene	006765-39-5	$C_{17}H_{34}$	C16:1	Olefinic HC	Hexahydroaplotaxene	0.886	86
68	17.272	1-Nonadecene	018435-45-5	$C_{19}H_{38}$	C18:1	Olefinic HC	Nonadec-1-ene	0.4951	78
69	17.4369	E-7-Tetradecenol	037011-95-3	$C_{14}H_{28}O$	-	Alcohol	7-tetradecenol, E	1.754	93
70	17.5599	2-Butenedioic acid (Z)-, monododecyl ester	002424-61-5	$C_8H_{12}O_4$	C7:1	FA (dicarboxylic acid)	Maleic acid, monobutyl ester	1.2861	95
71	17.7141	1-Nonadecene	018435-45-5	$C_{19}H_{38}$	C18:1	Olefinic HC	Nonadec-1-ene	0.4052	91
72	17.7943	13-Oxabicyclo[10.1.0]tridecane	000286-99-7	$C_{12}H_{22}O$	-	Cyclododecane epoxide	-	0.9041	56
73	18.0692	Tetradecanoic acid	000544-63-8	$C_{14}H_{28}O_2$	C13:0	SFA	Myristic acid	0.4665	80
74	18.1527	Benzene, dodecyl-	000123-01-3	$C_{18}H_{30}$	-	Aromatic HC	Dodecane, 1-phenyl-	0.5281	46

Table 7.S5 Continued.

Peak No.	Retention time (min)	Systematic name	Cas number	Molecular formula	Shorthand notation	Type of compound	Common/ another name	Area %	Qual
75	18.4244	E-15-Heptadecenal	1000130-97-9	$C_{17}H_{32}O$	-	Aldehyde	-	0.3234	90
76	18.5248	1-Hexacosanol	000506-52-5	$C_{26}H_{54}O$	-	Alcohol	n-Hexacosanol	0.4483	90
77	18.5991	Heptadecanal	1000376-70-0	$C_{17}H_{34}O$	-	Aldehyde	n-Heptadecanal	0.2612	62
78	18.7687	3-Eicosene, (E)-	074685-33-9	$C_{20}H_{40}$	C19:1	Olefinic HC	-	1.7232	96
79	18.8997	3-Eicosene, (E)-	074685-33-9	$C_{20}H_{40}$	C19:1	Olefinic HC	-	1.0567	93
80	19.0827	5-Eicosene, (E)-	074685-30-6	$C_{20}H_{40}$	C19:1	Olefinic HC	(5E)-5-Icosene	0.408	91
81	19.1494	13-Oxabicyclo[10.1.0]tridecane	000286-99-7	$C_{12}H_{22}O$	-	Cyclododecane epoxide	-	0.5919	90
82	19.343	Cyclohexadecane	000295-65-8	$C_{16}H_{32}$	C15:0	Naphthene HC	-	0.3645	93
83	19.4857	Undecane	001120-21-4	$C_{11}H_{24}$	C10:0	n-paraffinic HC	n-Undecane	0.8317	70
84	19.6814	9,12-Octadecadienoic acid (Z,Z)-	000060-33-3	$C_{18}H_{32}O_2$	C17:2	PUFA	cis-9,cis-12-Octadecadienoic acid	0.3961	91
85	19.857	n-Tetracosanol-1	000506-51-4	$C_{24}H_{50}O$	-	Alcohol	Lignoceric alcohol	0.6526	90
86	19.9949	1-Nonadecene	018435-45-5	$C_{19}H_{38}$	C18:1	Olefinic HC	Nonadec-1-ene	0.5037	86
87	20.1976	1,7-Hexadecadiene	125110-62-5	$C_{16}H_{30}$	C15:2	Olefinic HC	-	1.2773	90
88	20.2634	trans-2-Dodecen-1-ol, trifluoroacetate	1000352-26-2	$C_{14}H_{23}F_3O_2$	-	Fluorinated FA	-	1.8184	66
89	20.4432	1,2-Oxathiane, 6-dodecyl-, 2,2-dioxide	015224-88-1	$C_{16}H_{32}O_3S$	-		δ-Hexadecanesultone	1.8064	81
90	20.8119	Cyclohexane, 1,2-dimethyl-3-pentyl-4-propyl-	062376-17-4	$C_{16}H_{32}O_3S$	-	Heterocyclic HC (organosulfur)	-	0.3551	81
91	20.9406	1-Heneicosanol	015594-90-8	$C_{21}H_{44}O$	-	Alcohol	Henicosan-1-ol	0.4721	81
92	21.1611	p-(4-Ethylcyclohexyl)benzonitrile	073592-81-1	$C_{15}H_{19}N$	-	-	-	2.2426	25
93	21.3312	Heptacosyl acetate	1000351-78-2	$C_{29}H_{58}O_2$	C28:0	SFA	-	0.4659	90
94	21.7081	1,14-Docosanediol	004452-45-3	$C_{22}H_{46}O_2$	-	Alcohol	-	0.2436	94
95	21.843	Z-11-Tetradecen-1-ol trifluoroacetate	1000131-33-7	$C_{16}H_{27}F_3O_2$	-	-	-	0.3205	91
96	21.9564	(Z)-14-Tricosenyl formate	077899-10-6	$C_{24}H_{46}O_2$	C23:1	MUFA	-	0.6928	96
97	22.1223	Heptadecane	000629-78-7	$C_{17}H_{36}$	C16:0	n-paraffinic HC	n-Heptadecane	0.4736	89
98	22.226	13-Tetradecen-1-ol acetate	056221-91-1	$C_{16}H_{30}O_2$	C15:1	MUFA	13-tetradecenyl acetate	0.401	90
99	22.4417	Linoelaidic acid	000506-21-8	$C_{18}H_{32}O_2$	C17:2	PUFA	-	0.3499	89
100	22.6996	Octacosyl acetate	018206-97-8	$C_{30}H_{60}O_2$	C29:0	SFA	n-Octacosyl acetate	0.3307	90
101	22.8864	Octacosyl acetate	018206-97-8	$C_{30}H_{60}O_2$	C29:0	SFA	n-Octacosyl acetate	0.5381	92

Table 7.S5 Continued.

Peak No.	Retention time (min)	Systematic name	Cas number	Molecular formula	Shorthand notation	Type of compound	Common/ another name	Area %	Qual
102	23.471	15-Methyl-Z-11-hexadecenal	1000130-85-9	-	-	Aldehyde	-	0.1937	78
103	23.7441	1-Tetracosene	010192-32-2	$C_{24}H_{48}$	C23:1	Olefinic HC	Tetracos-1-ene	1.0146	98
104	23.9868	Octadecane	000593-45-3	$C_{18}H_{38}$	C17:0	n-paraffinic HC	n-Octadecane	0.7855	95
105	24.0976	1-Hexacosene	018835-33-1	$C_{26}H_{52}$	C25:1	Olefinic HC	Hexacos-1-ene	0.2359	90
106	24.2323	13-Tetradecen-1-ol acetate	056221-91-1	$C_{16}H_{30}O_2$	C15:1	MUFA	13-tetradecenyl acetate	0.2109	91
107	24.3796	Oxirane, 2,2-dimethyl-3-(3,7,12,16,20-pentamethyl-3,7,11,15,19-heneicosapentaenyl)-, (all-E)-	007200-26-2	$C_{30}H_{50}O$	-	Ether (cyclic)	-	0.5095	72
108	24.7051	9-Octadecenoic acid, (E)-	000112-79-8	$C_{18}H_{34}O_2$	C17:1	MUFA	trans-δ^9-Octadecenoic acid	2.8204	99
109	24.9167	Octadecanoic acid	000057-11-4	$C_{18}H_{36}O_2$	C17:0	SFA	Stearic acid	1.9505	90
110	25.2026	9-Octadecenoic acid, (E)-	000112-79-8	$C_{18}H_{34}O_2$	C17:1	MUFA	trans-δ^9-Octadecenoic acid	0.9387	81
111	25.6702	1-Tetracosene	010192-32-2	$C_{24}H_{48}$	C23:1	MUFA	Tetracos-1-ene	0.872	99
112	25.9613	13-Oxabicyclo[10.1.0]tridecane	000286-99-7	$C_{12}H_{22}O$	-	Cyclododecane epoxide	-	0.4863	89
113	26.1487	9,12-Octadecadienoic acid (Z,Z)-	000060-33-3	$C_{18}H_{32}O_2$	C17:2	PUFA	cis-9,cis-12-Octadecadienoic acid	0.3372	97
114	26.4399	Z,Z-10,12-Hexadecadienal	1000130-86-6	$C_{16}H_{28}O$	-	Unsaturated aldehyde	-	0.2293	72
115	26.7322	9,12-Octadecadienoic acid (Z,Z)-	000060-33-3	$C_{18}H_{32}O_2$	C17:2	PUFA	cis-9,cis-12-Octadecadienoic acid	0.3322	97
116	26.8813	9,12-Octadecadienoic acid (Z,Z)-	000060-33-3	$C_{18}H_{32}O_2$	C17:2	PUFA	cis-9,cis-12-Octadecadienoic acid	0.1679	93
117	27.7189	9,12-Octadecadienoic acid (Z,Z)-, methyl ester	000112-63-0	$C_{19}H_{34}O_2$	C18:2	PUFA	-	0.5339	83
118	28.0484	Octacosanol	000557-61-9	$C_{28}H_{58}O$	-	Alcohol	-	0.1454	90
119	28.5998	1-Nonadecene	018435-45-5	$C_{19}H_{38}$	C18:1	MUFA	Nonadec-1-ene	0.1641	94

Table 7.S5 Continued.

Peak No.	Retention time (min)	Systematic name	Cas number	Molecular formula	Shorthand notation	Type of compound	Common/ another name	Area %	Qual
120	28.8501	Heptadecanolide	005637-97-8	$C_{17}H_{32}O_2$	C16:0	Cyclic FA	Heptadecanoic acid, 17-hydroxy-, π-lactone	1.1816	97
121	29.0837	Eicosanoic acid	000506-30-9	$C_{20}H_{40}O_2$	C19:0	SFA	Arachic acid	0.6615	68
122	29.5577	10,13-Octadecadienoic acid, methyl ester	056554-62-2	$C_{19}H_{34}O_2$	C18:2	PUFA	-	0.2543	91
123	29.6795	E,E,Z-1,3,12-Nonadecatriene-5,14-diol	1000131-11-4	$C_{19}H_{34}O_2$	-	Unsaturated alcohol	-	0.5066	90
124	29.8659	Heptacos-1-ene	015306-27-1	$C_{27}H_{54}$	C26:1	Olefinic HC	1-Heptacosene	0.1702	97
125	29.9496	Undec-10-ynoic acid, hexadecyl ester	1000406-16-9	$C_{27}H_{50}O_2$	C26:2	PUFA	-	0.2698	90
126	30.165	Tricosane	000638-67-5	$C_{23}H_{48}$	C22:0	n-paraffinic HC	n-Tricosane	0.1247	90
127	30.4582	13-Tetradecen-1-ol acetate	056221-91-1	$C_{16}H_{30}O_2$	C15:1	MUFA	13-tetradecenyl acetate	0.4946	70
128	30.7333	Octadecanal	000638-66-4	$C_{18}H_{36}O$	-	Aldehyde	-	0.101	64
129	31.8381	Bicyclo[10.8.0]eicosane, cis-	1000155-82-2	$C_{20}H_{38}$	C19:0	Naphthene HC	-	0.684	89
130	32.0288	7-Pentadecyne	022089-89-0	$C_{15}H_{28}$	C14:2	PUFA	-	0.137	83
131	32.12	Cyclotriacontane	000297-35-8	$C_{30}H_{60}$	C29:0	Naphthene HC	-	0.1693	95
132	32.4244	1-Hexacosene	018835-33-1	$C_{26}H_{52}$	C25:1	Olefinic HC	Hexacos-1-ene	0.1258	91
133	32.9344	Erucic acid	000112-86-7	$C_{23}H_{44}O_2$	C22:1	MUFA	ω-9; cis-13-docosenoic acid	3.0906	89
134	33.0834	1-Tetracosene	010192-32-2	$C_{24}H_{48}$	C23:1	Olefinic HC	Tetracos-1-ene	0.7118	98
135	33.4563	Oxirane, hexadecyl-	007390-81-0	$C_{18}H_{36}O$	-	-	-	0.2338	89
136	33.509	Z-14-Octadecen-1-ol acetate	1000131-07-6	$C_{20}H_{38}O_2$	C19:1	MUFA	-	0.1709	93
137	33.5867	1,14-Docosanediol	004452-45-3	$C_{22}H_{46}O_2$	-	Alcohol	-	0.2075	94
138	33.687	1-Tricosene	018835-32-0	$C_{23}H_{46}$	C22:1	MUFA	Tricosene-1	0.2357	95

Table 7.S6 Product distribution for hydroprocessed Yellow Dodolla oil using WC/$AlPO_4$-18 at 500 °C, 21 bar H_2 pressure, and 2.5 hours.

Peak No.	Retention time (min)	Systematic name	Cas number	Molecular formula	Shorthand notation	Type of compound	Common/ another name	Area %	Qual
1	4.4226	Cyclopropane, 1-methyl-2-pentyl-	041977-37-1	C_9H_{18}	C8:0	Naphthene HC	-	1.1597	92
2	4.5335	Cyclopropane, 1-methyl-2-pentyl-	041977-37-1	C_9H_{18}	C8:0	Naphthene HC	-	1.2583	91
3	5.1435	3,6-Nonadien-1-ol, (E,Z)-	056805-23-3	$C_9H_{16}O$	-	Unsaturated alcohol	(3E,6E)-3,6-Nonadien-1-ol	0.4472	47
4	5.8943	4-Decene	019689-18-0	$C_{10}H_{20}$	C9:1	Olefinic HC	-	2.4221	93
5	6.4313	(Z)6,(Z)9-Pentadecadien-1-ol	077899-11-7	$C_{15}H_{28}O$	-	Unsaturated alcohol	-	0.5033	64
6	6.6539	(S)-(-)-2-Amino-3-phenyl-1-propanol	003182-95-4	$C_9H_{13}NO$	-	-	-	0.527	27
7	7.016	Cyclodecene	003618-12-0	$C_{10}H_{18}$	C9:1	Cycloolefin HC	-	0.5741	89
8	7.3967	Acetic acid, trichloro-, nonyl ester	065611-32-7	$C_{11}H_{19}Cl_3O_2$	-	Chlorinated FA	Trichloroacetic acid, nonyl ester	2.1345	68
9	7.553	5-Undecene	004941-53-1	$C_{11}H_{22}$	C10:1	Olefinic HC	-	1.1728	91
10	7.7375	5-Undecene	004941-53-1	$C_{11}H_{22}$	C10:1	Olefinic HC	-	1.082	95
11	8.1605	1-Phenyl-1-butene	000824-90-8	$C_{10}H_{12}$	-	Aromatic HC	-	1.1302	25
12	8.3564	Cyclohexene, 1-pentyl-	015232-85-6	$C_{11}H_{20}$	C10:1	Cycloolefin HC	1-Pentyl-1-cyclohexene	0.3545	52
13	8.5368	Cyclohexanone, 2-methyl-5-(1-methylethenyl)-, trans-	005948-04-9	$C_{10}H_{16}O$	-	Ketone (cyclic)	p-Menth-8-en-2-one, trans-	0.7198	83
14	8.7049	1,E-8,Z-10-Dodecatriene	1000098-05-5	$C_{12}H_{20}$	C11:2	Olefinic HC	-	0.2268	64
15	8.8805	1-Dodecene	000112-41-4	$C_{12}H_{24}$	C11:1	Olefinic HC	α-Dodecene	2.0315	91
16	9.0544	3-Dodecene, (Z)-	007239-23-8	$C_{12}H_{24}$	C11:1	Olefinic HC	cis-3-Dodecene	0.984	64
17	9.2216	2-Dodecene, (Z)-	007206-26-0	$C_{12}H_{24}$	C11:1	Olefinic HC	(2Z)-2-Dodecene	0.7511	95
18	9.3622	Benzene, (1-methyl-2-cyclopropen-1-yl)-	065051-83-4	$C_{10}H_{10}$	-	Aromatic HC	3-Methyl-3-phenylcyclopropene	0.3705	96
19	9.6181	(R)-(-)-(Z)-14-Methyl-8-hexadecen-1-ol	030689-78-2	$C_{17}H_{34}O$	-	Unsaturated alcohol	-	1.3311	25
20	9.8087	Phenol, 2-methyl-	000095-48-7	C_7H_8O	-	Aromatic alcohol	o-Cresol	0.8511	66
21	10.0325	Cyclododecene	001501-82-2	$C_{12}H_{22}$	C11:1	Cycloolefin HC	Cyclododecene,c&t	0.7165	78
22	10.1552	Cyclohexene,1-hexyl-	003964-66-7	$C_{12}H_{22}$	C11:1	Cycloolefin HC	1-hexyl-1-cyclohexene	0.2555	35
23	10.3118	1-Tridecene	002437-56-1	$C_{13}H_{26}$	C12:1	Olefinic HC	n-Tridec-1-ene	1.816	64
24	10.4632	3-Tridecene, (Z)-	041446-53-1	$C_{13}H_{26}$	C12:1	Olefinic HC	(3Z)-3-Tridecene	0.6554	93
25	10.6415	3-Tridecene, (E)-	041446-57-5	$C_{13}H_{26}$	C12:1	Olefinic HC	(3E)-3-Tridecene	0.3525	90
26	10.8365	Naphthalene, 1,2,3,4-tetrahydro-5-methyl-	002809-64-5	$C_{11}H_{14}$	-	Aromatic and cyclic HC	5-Methyltetralin	0.2535	60
27	10.9641	Octanoic acid	000124-07-2	$C_8H_{16}O_2$	C7:0	SFA	n-Caprylic acid	0.9944	50

Table 7.S6 Continued.

Peak No.	Retention time (min)	Systematic name	Cas number	Molecular formula	Shorthand notation	Type of compound	Common/ another name	Area %	Qual
28	11.0659	Trichloroacetic acid, undec-10-enyl ester	1000280-51-3	$C_{13}H_{21}Cl_3O_2$	-	Chlorinated FA	-	0.3289	45
29	11.1099	1,4-Methanonaphthalen-9-ol, 1,2,3,4-tetrahydro-, stereoisomer	001198-20-5	$C_{11}H_{12}O$	-	Aromatic alcohol	-	0.4083	49
30	11.2373	Cyclopentene, 1-octyl-	052315-44-3	$C_{13}H_{24}$	C12:1	Cycloolefin HC	-	0.1296	74
31	11.3289	Naphthalene, 1,2,3,4-tetrahydro-5-methyl-	002809-64-5	$C_{11}H_{14}$	-	HC (cyclic and aromatic)	5-Methyltetralin	0.3039	58
32	11.5633	7-Tetradecene	010374-74-0	$C_{14}H_{28}$	C13:1	Olefinic HC	7-Tetradecene,c&t	0.8722	56
33	11.6669	Borane, 2,3-dimethyl-2-butyl- (dimer)	1000159-64-3	$C_{12}H_{30}B_2$	-	-	-	1.1687	64
34	11.7942	5-Tetradecene, (E)-	041446-66-6	$C_{14}H_{28}$	C13:1	Olefinic HC	(5E)-5-Tetradecene	0.6103	96
35	11.9588	2-Cyclopenten-1-one, 2-pentyl-	025564-22-1	$C_{10}H_{16}O$	-	Ketone (cycloalkene)	2-Pentyl-2-cyclopenten-1-one	0.6258	91
36	12.0398	Benzenamine, 3-chloro-4-methyl-	000095-74-9	C_7H_8ClN	-	-	p-Toluidine, 3-chloro-	0.3807	30
37	12.2372	Diglycolic acid	000110-99-6	$C_4H_6O_5$	-	Aliphatic dicarboxylic acid	Acetic acid, 2,2'-oxybis-	0.7193	25
38	12.4245	1-Pentadecene	013360-61-7	$C_{15}H_{30}$	C14:1	Olefinic HC	Pentadecene,1-	1.0338	92
39	12.5791	(-)-trans-Pinane	033626-25-4	$C_{10}H_{18}$	C9:1	-	E-pinane	0.5557	55
40	12.7224	9-Eicosyne	071899-38-2	$C_{20}H_{38}$	C19:2	Alkyne HC	-	0.3079	55
41	12.9131	Cyclodecane	000293-96-9	$C_{10}H_{20}$	C9:0	Naphthene HC	-	2.4276	45
42	13.0619	Dodecane, 1-cyclopentyl-4-(3-cyclopentylpropyl)-	007225-68-5	$C_{25}H_{48}$	C24:0	Naphthene HC	1,7-Dicyclopentyl-4-n-octylheptane	0.5122	59
43	13.2376	Cyclopentadecane	000295-48-7	$C_{15}H_{30}$	C14:0	Naphthene HC	decylcyclopentane	1.0749	56
44	13.5095	1-Phenyl-1-heptyne	014374-45-9	$C_{13}H_{16}$	-	Aromatic HC	Benzene, 1-heptynyl-	2.2126	41
45	13.6021	3,4-Octadiene, 7-methyl-	037050-05-8	C_9H_{16}	C8:2	Olefinic HC	-	0.2706	78
46	13.7252	1,6-Octadiene, 2,6-dimethyl-	031222-43-2	$C_{10}H_{18}$	C9:2	Olefinic HC	-	1.1072	43
47	14.0529	(E)-Dodec-2-enyl ethyl carbonate	1000373-76-9	$C_{15}H_{28}O_3$	C14:1	MUFA	-	1.4741	90
48	14.1604	9-Octadecen-1-ol, (Z)-	000143-28-2	$C_{18}H_{36}O$	-	Alcohol	cis-9-Octadecen-1-ol	1.2374	90
49	14.2634	7-Hexadecene, (Z)-	035507-09-6	$C_{16}H_{32}$	C15:1	Olefinic HC	(7Z)-7-Hexadecene	0.4591	96
50	14.3867	(Z)-14-Tricosenyl formate	077899-10-6	$C_{24}H_{46}O_2$	C23:1	MUFA	-	0.3345	91
51	14.4782	Bicyclo[3.3.1]nonan-3-one, 7-methylene-	017933-29-8	$C_{10}H_{14}O$	-	Cyclic ketone	-	0.5082	49
52	14.6214	Undecanoic acid	000112-37-8	$C_{11}H_{22}O_2$	C10:0	SFA	n-Undecanoic acid	1.3042	43

Table 7.S6 Continued.

Peak No.	Retention time (min)	Systematic name	Cas number	Molecular formula	Shorthand notation	Type of compound	Common/ another name	Area %	Qual
53	14.7433	3-Propylglutaric acid, monomethyl ester	1000254-25-9	$C_8H_{14}O_4$	C7:1	Fatty (dicarboxylic acid)	-	0.4648	51
54	14.9356	Cyclohexane, (cyclopentylmethyl)-	004431-89-4	$C_{12}H_{22}$	C11:0	Naphthene HC	Methane, cyclohexylcyclopentyl-	0.8129	53
55	15.1731	1,13-Tetradecadiene	021964-49-8	$C_{14}H_{26}$	C13:2	Olefinic HC	Tetradeca-1,13-diene	1.8908	86
56	15.269	2-Butenedioic acid (Z)-, monododecyl ester	002424-61-5	$C_8H_{12}O_4$	-	FA (dicarboxylic acid)	-	1.3518	95
57	15.4027	E-14-Hexadecenal	330207-53-9	$C_{16}H_{30}O$	-	Aldehyde	(14E)-14-Hexadecenal	0.6287	94
58	15.4814	13-Tetradece-11-yn-1-ol	1000131-00-4	$C_{14}H_{24}O$	-	Unsaturated alcohol	-	0.688	50
59	15.7202	Dodecanoic acid	000143-07-7	$C_{12}H_{24}O_2$	C11:0	SFA	n-Dodecanoic acid	1.821	83
60	16.1011	Oxirane, hexadecyl-	007390-81-0	$C_{18}H_{36}O$	-	-	1,2-Epoxyoctadecane	0.7397	83
61	16.2732	E-7-Octadecene	1000130-92-0	$C_{18}H_{36}$	C17:1	Olefinic HC	-	3.0416	91
62	16.5095	1-Octadecene	000112-88-9	$C_{18}H_{36}$	C17:1	Olefinic HC	-	0.7826	90
63	16.6967	9,12-Octadecadienoic acid (Z,Z)-	000060-33-3	$C_{18}H_{32}O_2$	C17:2	PUFA	cis-9,cis-12-Octadecadienoic acid	0.1876	91
64	16.8336	Tridecanoic acid	000638-53-9	$C_{13}H_{26}O_2$	C12:0	SFA	n-Tridecanoic acid	0.9376	78
65	16.9489	7-Pentadecyne	022089-89-0	$C_{15}H_{28}$	C14:2	Alkyne HC	-	0.3436	91
66	17.1961	Dodecane, 1-cyclopentyl-4-(3-cyclopentylpropyl)-	007225-68-5	$C_{25}H_{48}$	-	Naphthene HC	1,7-Dicyclopentyl-4-n-octylheptane	0.5794	70
67	17.2733	Dodecane, 1-cyclopentyl-4-(3-cyclopentylpropyl)-	007225-68-5	$C_{25}H_{48}$	-	Naphthene HC	1,7-Dicyclopentyl-4-n-octylheptane	0.3546	64
68	17.4387	Oleyl alcohol, acetate	1000352-67-9	$C_{20}H_{38}O_2$	C19:1	MUFA	-	1.8486	94
69	17.557	1-Pentadecene	013360-61-7	$C_{15}H_{30}$	C14:1	MUFA	Pentadecene,1-	1.1594	95
70	17.7118	Z,Z-3,13-Octadecadien-1-ol	1000131-10-9	$C_{18}H_{34}O$	-	Unsaturated alcohol	-	0.2985	44
71	17.8058	1,2-Benzisothiazole, 3-(hexahydro-1H-azepin-1-yl)-, 1,1-dioxide	309735-29-3	$C_{13}H_{16}N_2O_2S$	-	-	-	0.3974	91
72	17.9468	Cyclotetracosane	000297-03-0	$C_{24}H_{48}$	C23:0	Naphthene HC	-	0.1364	95
73	18.0684	Tetradecanoic acid	000544-63-8	$C_{14}H_{28}O_2$	C13:0	SFA	Myristic acid	0.279	83
74	18.1549	p-Menth-8(10)-en-9-ol, cis-	015714-13-3	$C_{10}H_{18}O$	-	Cyclic alcohol	-	0.2683	45
75	18.293	Bicyclo[3.3.2]decan-9-one	028054-91-3	$C_{10}H_{16}O$	-	Ketone	-	0.1233	89

Table 7.S6 Continued.

Peak No.	Retention time (min)	Systematic name	Cas number	Molecular formula	Shorthand notation	Type of compound	Common/ another name	Area %	Qual
76	18.4286	1-Docosene	001599-67-3	$C_{22}H_{44}$	C21:1	Olefinic HC	Docos-1-ene	0.0967	95
77	18.5223	9-Eicosyne	071899-38-2	$C_{20}H_{38}$	C19:1	Alkyne HC	-	0.2415	89
78	18.6025	Heptacosyl acetate	1000351-78-2	$C_{29}H_{58}O_2$	C28:0	SFA	-	0.1582	78
79	18.7712	3-Eicosene, (E)-	074685-33-9	$C_{20}H_{40}$	C19:1	Olefinic HC	(5E)-5-Icosene	1.6185	95
80	18.8995	9-Eicosene, (E)-	074685-29-3	$C_{20}H_{40}$	C19:1	Olefinic HC	-	0.6042	95
81	18.9718	1-Nonadecene	018435-45-5	$C_{19}H_{38}$	C18:1	Olefinic HC	Nonadec-1-ene	0.3351	99
82	19.0822	5-Eicosene, (E)-	074685-30-6	$C_{20}H_{40}$	C19:1	Olefinic HC	(5E)-5-Icosene	0.3149	91
83	19.1565	Linoelaidic acid	000506-21-8	$C_{18}H_{32}O_2$	C19:2	PUFA	-	0.2741	83
84	19.3461	13-Tetradecen-1-ol acetate	056221-91-1	$C_{16}H_{30}O_2$	C15:1	MUFA	13-tetradecenyl acetate	0.108	91
85	19.4889	Heptadecyl acetate	000822-20-8	$C_{19}H_{38}O_2$	C18:0	SFA	1-Heptadecanol, acetate	0.2637	55
86	19.8563	1-Heneicosyl formate	077899-03-7	$C_{22}H_{44}O_2$	C21:0	SFA	-	0.2433	83
87	20.0088	Octacosanol	000557-61-9	$C_{28}H_{58}O$	-	Fatty alcohol	-	0.1665	64
88	20.2577	(E)-Hexadec-2-enal	022644-96-8	$C_{16}H_{30}O$	C15:1	Aldehyde	2-Hexadecenal, (2E)-	2.6589	70
89	20.433	1-Heptadecene	006765-39-5	$C_{17}H_{34}$	C16:1	Olefinic HC	Hexahydroaplotaxene	0.7263	96
90	20.5165	Fumaric acid, 2-chloropropyl pentadecyl ester	1000348-57-2	$C_{22}H_{39}ClO_4$	C16:1	Chlorinated FA	-	0.3179	99
91	20.9429	1-Nonadecene	018435-45-5	$C_{19}H_{38}$	C18:1	Olefinic HC	Nonadec-1-ene	0.0618	90
92	21.1498	n-Hexadecanoic acid	000057-10-3	$C_{16}H_{32}O_2$	C15:0	SFA	Hexadecanoic acid	1.7096	49
93	21.3304	1,14-Docosanediol	004452-45-3	$C_{22}H_{46}O_2$	-	Alcohol	-	0.1833	83
94	21.3969	E-2-Octadecadecen-1-ol	1000131-10-2	$C_{18}H_{36}O$	-	Unsaturated alcohol	(E)-2-Octadecen-1-ol	0.1596	91
95	21.5595	Z,E-3,13-Octadecadien-1-ol	1000131-10-4	$C_{18}H_{34}O$	-	Unsaturated alcohol	-	0.4902	94
96	21.7049	Octadecanal	000638-66-4	$C_{18}H_{36}O$	-	Aldehyde	Stearaldehyde	0.479	93
97	21.8448	Z,E-3,13-Octadecadien-1-ol	1000131-10-4	$C_{18}H_{34}O$	-	Unsaturated alcohol	-	0.2951	95
98	21.9562	(Z)-14-Tricosenyl formate	077899-10-6	$C_{24}H_{46}O_2$	C23:1	MUFA	-	0.7134	98
99	22.1235	Z,E-3,13-Octadecadien-1-ol	1000131-10-4	$C_{18}H_{34}O$	-	Unsaturated alcohol	-	0.3597	91
100	22.223	Oxirane, hexadecyl-	007390-81-0	$C_{18}H_{36}O$	-	-	1,2-Epoxyoctadecane	0.5133	95

Table 7.S6 Continued.

Peak No.	Retention time (min)	Systematic name	Cas number	Molecular formula	Shorthand notation	Type of compound	Common/ another name	Area %	Qual
101	22.445	9,12-Octadecadienoic acid (Z,Z)-	000060-33-3	$C_{18}H_{32}O_2$	C17:2	PUFA	cis-9,cis-12-Octadecadienoic acid	0.1567	91
102	22.8846	13-Tetradecen-1-ol acetate	056221-91-1	$C_{16}H_{30}O_2$	C15:1	MUFA	13-tetradecenyl acetate	0.1434	90
103	23.4726	1,19-Eicosadiene	014811-95-1	$C_{20}H_{38}$	C19:2	Olefinic HC	-	0.2035	58
104	23.6896	9-Tricosene, (Z)-	027519-02-4	$C_{23}H_{46}$	C22:1	Olefinic HC	(Z)-9-Tricosene	0.6114	96
105	23.7949	Z,E-3,13-Octadecadien-1-ol	1000131-10-4	$C_{18}H_{34}O$	-	Unsaturated alcohol	-	0.1944	96
106	23.9815	1-Octadecene	000112-88-9	$C_{18}H_{36}$	C17:1	Olefinic HC	α-Octadecene	0.5387	93
107	24.0975	13-Tetradecen-1-ol acetate	056221-91-1	$C_{16}H_{30}O_2$	C15:1	MUFA	13-tetradecenyl acetate	0.1215	95
108	24.3846	10,12-Hexadecadien-1-ol	1000130-89-7	$C_{16}H_{30}O$	-	Unsaturated alcohol	-	0.2111	81
109	24.668	9-Octadecenoic acid, (E)-	000112-79-8	$C_{18}H_{34}O_2$	C17:1	MUFA	trans-δ^9-Octadecenoic acid	1.8724	99
110	24.8923	Octadecanoic acid	000057-11-4	$C_{18}H_{36}O_2$	C17:0	SFA	Stearic acid	1.4125	92
111	25.2036	2-Methyl-Z,Z-3,13-octadecadienol	1000130-90-5	$C_{19}H_{36}O$	-	Unsaturated alcohol	-	0.4774	72
112	25.5456	7-Pentadecyne	022089-89-0	$C_{15}H_{28}$	C14:2	Alkyne HC	-	0.1933	91
113	25.6695	1-Tetracosene	010192-32-2	$C_{24}H_{48}$	C23:1	Olefinic HC	Tetracos-1-ene	0.791	99
114	25.9515	Z,E-3,13-Octadecadien-1-ol	1000131-10-4	$C_{18}H_{34}O$	-	Unsaturated alcohol	-	0.3518	96
115	26.4389	4-[3-Ethoxypropylamino]benzo-1,2,3-triazine	025465-41-2	-	-	-	-	0.1503	90
116	26.7272	Linoelaidic acid	000506-21-8	$C_{18}H_{32}O_2$	C17:2	PUFA	-	0.1296	97
117	27.718	1,19-Eicosadiene	014811-95-1	$C_{20}H_{38}$	C19:2	Olefinic HC	-	0.5501	70
118	28.5992	Methyl 10-trans,12-cis-octadecadienoate	1000336-44-2	$C_{19}H_{34}O_2$	C18:2	PUFA	-	0.0814	90
119	28.8321	Erucic acid	000112-86-7	$C_{23}H_{44}O_2$	C22:1	MUFA	ω-9; cis-13-docosenoic acid	0.8813	98
120	29.0725	1-Hexacosene	018835-33-1	$C_{26}H_{52}$	C25:1	Olefinic HC	Hexacos-1-ene	0.5163	91
121	29.5574	E-7-Dodecen-1-ol acetate	1000131-35-3	$C_{14}H_{26}O_2$	C13:2	PUFA	-	0.3434	95
122	29.7297	(R)-(-)-14-Methyl-8-hexadecyn-1-ol	064566-18-3	$C_{17}H_{32}O$	-	Unsaturated alcohol	-	0.6091	93
123	29.8657	1-Hexacosene	018835-33-1	$C_{26}H_{52}$	C25:1	Olefinic HC	Hexacos-1-ene	0.3089	95
124	29.9465	11,14-Octadecadienoic acid, methyl ester	056554-61-1	$C_{19}H_{34}O_2$	C18:2	PUFA	-	0.5162	89
125	30.4611	cis-9-Hexadecenal	056219-04-6	$C_{16}H_{30}O$	-	Aldehyde	-	0.9871	92
126	30.7303	Octadecanal	000638-66-4	$C_{18}H_{36}O$	-	Aldehyde	-	0.5736	64
127	31.4563	Ethanol, 2-(9-octadecenyloxy)-, (Z)-	005353-25-3	$C_{20}H_{40}O_2$	-	Alcohol	-	0.4892	70

Table 7.S6 Continued.

Peak No.	Retention time (min)	Systematic name	Cas number	Molecular formula	Shorthand notation	Type of compound	Common/ another name	Area %	Qual
128	31.8436	Pentadecanal-	002765-11-9	$C_{15}H_{30}O$	-	Aldehyde	-	1.2908	93
129	32.0336	4-Piperidinamine, N,1-dimethyl-	073579-08-5	$C_7H_{16}N_2$	-	-	-	0.8762	45
130	32.4215	1-Hexacosene	018835-33-1	$C_{26}H_{52}$	C25:1			0.318	91
131	32.9024	Erucic acid	000112-86-7	$C_{23}H_{44}O_2$	C22:1	MUFA	ω-9; cis-13-docosenoic acid	3.0507	94
132	33.0688	Erucic acid	000112-86-7	$C_{23}H_{44}O_2$	C22:1	MUFA	ω-9; cis-13-docosenoic acid	1.4698	96
133	33.4542	Z-14-Octadecen-1-ol acetate	1000131-07-6	$C_{20}H_{38}O_2$	C19:1	MUFA	-	1.0471	94
134	33.6919	1-Tricosene	018835-32-0	$C_{23}H_{46}$	C22:1	MUFA	Tricosene-1	0.8604	94

Analysis of Dynamic Viscosity in Relation to Shear Rate and Stress

Table 7.S7 Variation of the dynamic viscosity of Yellow Dodolla oil to shear rate and stress.

RPM (min^{-1})	Shear rate ($\dot{\gamma}$) (s^{-1})	Shear stress (τ) (Pa)	Dynamic viscosity (η) ($mm^2\ s^{-1}$)	Temperature (T) (°C)
5	27.05	3.974	145.40	24.5
8.3	44.90	5.735	126.15	24.5
13.9	75.19	8.204	108.15	24.5
23.2	125.5	11.811	94.20	24.7
45.3	245.00	20.505	83.75	24.7
64.6	349.40	28.310	80.85	24.8
107.8	583.10	45.540	79.25	24.9
179.6	971.60	74.910	76.45	25.0
297.6	1610	120.800	74.40	23.2
500	2705	-	-	-

Table 7.S8 Variation of the dynamic viscosity of liquid phase product to shear rate and stress under β-Mo_2C/$AlPO_4$-18 catalysis at 300 °C, 21 bar H_2 pressure, and 2.5 hours.

RPM (min^{-1})	Shear rate ($\dot{\gamma}$) (s^{-1})	Shear stress (τ) (Pa)	Dynamic viscosity (η) ($mm^2\ s^{-1}$)	Temperature (T) (°C)
5	27.05	6.048	150.10	26.4
8.3	44.90	5.88	129.20	26.1
13.9	75.19	8.242	110.75	26.1
23.2	125.5	11.885	93.65	25.9
45.3	245.0	20.560	83.80	26.0
64.6	349.4	28.435	80.90	26.1
107.8	583.1	46.425	79.50	25.9
179.6	971.6	75.900	77.95	26.1
297.6	1610	-	-	-
500	2705	-	-	-

Table 7.S9 Variation of the dynamic viscosity of liquid phase product to shear rate and stress under $Ni_3C/AlPO_4$-18 catalysis at 300 °C, 21 bar H_2 pressure, and 2.5 hours.

RPM (min^{-1})	Shear rate ($\dot{\gamma}$) (s^{-1})	Shear stress (τ) (Pa)	Dynamic viscosity (η) ($mm^2\ s^{-1}$)	Temperature (T) (°C)
5	27.05	7.675	281.50	23.8
8.3	44.90	9.965	222.00	23.9
13.9	75.19	13.460	177.50	23.9
23.2	125.50	18.815	148.50	24.1
45.3	245.00	31.340	126.50	24.2
64.6	349.40	41.825	117.50	24.5
107.8	583.10	64.170	108.00	24.5
179.6	971.60	98.775	98.65	25.1
297.6	1610	-	-	-
500	2705	-	-	-

Table 7.S10 Variation of the dynamic viscosity of liquid phase product to shear rate and stress under $WC/AlPO_4$-18 catalysis at 300 °C, 21 bar H_2 pressure, and 2.5 hours.

RPM (min^{-1})	Shear rate ($\dot{\gamma}$) (s^{-1})	Shear stress (τ) (Pa)	Dynamic viscosity (η) ($mm^2\ s^{-1}$)	Temperature (T) (°C)
5	27.05	4.657	159.95	24.8
8.3	44.90	6.320	140.00	24.9
13.9	75.19	8.891	118.45	24.9
23.2	125.50	12.535	98.40	25.0
45.3	245.00	21.230	86.20	25.2
64.6	349.40	28.965	82.75	25.3
107.8	583.10	46.860	80.10	25.3
179.6	971.60	75.935	77.45	25.5
297.6	1610	-	-	-
500	2705	-	-	-

Table 7.S11 Variation of the dynamic viscosity of liquid phase product to shear rate and stress under β-$Mo_2C/AlPO_4$-18 catalysis at 500 °C, 21 bar H_2 pressure, and 2.5 hours.

RPM (min^{-1})	Shear rate ($\dot{\gamma}$) (s^{-1})	Shear stress (τ) (Pa)	Dynamic viscosity (η) ($mm^2\ s^{-1}$)	Temperature (T) (°C)
5	27.05	0.617	24.80	26.1
8.3	44.90	0.835	19.43	25.9
13.9	75.19	1.347	15.90	25.8
23.2	125.5	1.521	12.70	25.9
45.3	245.0	2.681	10.06	25.9
64.6	349.4	3.158	9.14	25.9
107.8	583.1	4.737	8.12	25.7
179.6	971.6	6.695	7	25.7
297.6	1610	9.580	6.10	25.6
500	2705	15.385	5.79	25.6

Table 7.S12 Variation of the dynamic viscosity of liquid phase product to shear rate and stress under $Ni_3C/AlPO_4$-18 catalysis at 500 °C, 21 bar H_2 pressure, and 2.5 hours.

RPM (min^{-1})	Shear rate ($\dot{\gamma}$) (s^{-1})	Shear stress (τ) (Pa)	Dynamic viscosity (η) ($mm^2\ s^{-1}$)	Temperature (T) (°C)
5	27.05	0.835	31.65	25.8
8.3	44.90	0.961	24.60	25.7
13.9	75.19	1.340	18.85	25.8
23.2	125.50	2.050	15.55	25.9
45.3	245.00	3.158	13.00	25.8
64.6	349.40	4.110	12.00	25.9
107.8	583.10	6.025	10.365	25.9
179.6	971.60	8.199	8.66	25.9
297.6	1610	12.000	7.455	25.8
500	2705	19.250	7.29	26.0

Table 7.S13 Variation of the dynamic viscosity of liquid phase product to shear rate and stress under WC/$AlPO_4$-18 catalysis at 500 °C, 21 bar H_2 pressure, and 2.5 hours.

RPM (min^{-1})	Shear rate ($\dot{\gamma}$) (s^{-1})	Shear stress (τ) (Pa)	Dynamic viscosity (η) ($mm^2\ s^{-1}$)	Temperature (T) (°C)
5	27.05	0.544	20.75	26.5
8.3	44.90	0.889	20.45	26.5
13.9	75.19	1.407	18.55	26.5
23.2	125.50	2.086	16.15	26.5
45.3	245.00	3.702	14.95	26.2
64.6	349.40	4.828	13.70	26.3
107.8	583.10	6.966	12.04	26.2
179.6	971.60	9.942	10.23	26.0
297.6	1610	14.895	9.11	26.2
500	2705	23.700	8.81	26.2

Functional Group Characterization using FT-IR Analysis

Table 7.S14 FT-IR spectra of hydroprocessed Yellow Dodolla oil at 300 and 500 ℃, 21 H_2 pressure, and 2.5 hours using β-Mo_2C/$AlPO_4$-18 catalyst.

Observed frequency (cm^{-1})		Possible frequency	Vibrational
Mo-300	**Mo-500**	**range (cm^{-1})**	**assignments**
3008.87	-	3100-3000	week =C–H stretching
-	2954.81	3000–2800	week C–H stretching
2922.61	2922.33	3000–2800	strong C–H stretching
2853.10	2853.14	2950–2850	strong C–H stretching
1744.17	1743.95	1750–1730	strong C=O stretching
-	1710.76	1730–1700	strong C=O stretching
1656.68	-	1680–1640	weak C=C stretching
-	1641.32	1680–16400	week C=C stretching
1464.57	-	1465–1430	methylene vibration,
-	1456.58	1465–1430	methylene vibration,
1417.88	1413.36	1500-1400	aromatic C–C stretching
1377.77	1377.87	-	C-H bending vibration of CH_2
-	1284.91	1320–1210	C–O stretching
1238.07	1236.38	1260-1050	C–O stretching
-	1165.35	1300–1160	C–O stretching
1160.46	-	1300–1160	C–O stretching
1118.64	-	1125–1085	C–O stretching
	1116.99	1125–1085	C–O stretching
-	1105.*05*	1150–1085	C–O–C stretching
1098.43	-	1150–1085	C–O–C stretching
965.00	965.55	970–920	shoulder trans = C–H out-of-plane bending
-	942.96	950–910	O–H bending
-	909.40	-	terminal wag of ethers
-	813.14	860–800	aromatic –C-H out of plane bending
721.70	721.12	725–720	C–H rocking methyl

Table 7.S15 FT-IR spectra of hydroprocessed Yellow Dodolla oil at 300 and 500 ℃, 21 H_2 pressure, and 2.5 hours using $Ni_3C/AlPO_4$-18 catalyst.

Observed frequency (cm^{-1})		Possible frequency range (cm^{-1})	Vibrational assignments
Ni-300	**Ni-500**		
3008.08	-	3100-3000	week =C–H stretching
-	2954.78	3000–2800	week C–H stretching
2922.58	2922.72	3000–2800	strong C–H stretching
2853.15	2853.46	2950–2850	strong C–H stretching
1744.32	1743.96	1750–1730	strong C=O stretching
-	1710.67	1730–1700	strong C=O stretching
1656.68	-	1680–1640	weak C=C stretching
-	1641.32	1680–16400	week C=C stretching
1464.93	-	1465–1430	methylene vibration
-	1456,59	1465–1430	methylene vibration
1418.34	1413.55	1500-1400	aromatic C–C stretching
1377.81	1377.82	-	C-H bending vibration of CH_2
-	1285.42	1320–1210	C–O stretching
1239.01	1236.37	1260-1050	C–O stretching
-	1165.34	1300–1160	C–O stretching
1160.44	-	1300–1160	C–O stretching
1119.66	-	1125–1085	C–O stretching
-	1113.48	1125–1085	C–O stretching
-	1105.04	1150–1085	C–O–C stretching
1098.88	-	1150–1085	C–O–C stretching
966.50	965.61	970–920	shoulder trans = C–H out-of-plane bending
-	942.97	950–910	O–H bending
915.11	-	950–910	O–H bending
-	909.97	-	terminal wag of ethers
-	814.65	860–800	aromatic –C-H out of plane bending
721.33	722.15	725–720	C–H rocking methyl

Table 7.S16 FT-IR spectra of hydroprocessed Yellow Dodolla oil at 300 and 500 ℃, 21 H_2 pressure, and 2.5 hours using WC/$AlPO_4$-18 catalyst.

Observed frequency (cm^{-1})		Possible frequency range (cm^{-1})	Vibrational assignments
W-300	**W-500**		
3007.81	-	3100-3000	week =C–H stretching
-	2955.31	3000–2800	week C–H stretching
2922.55	2922.88	3000–2800	strong C–H stretching
2853.13	2853.56	2950–2850	strong C–H stretching
1744.37	1743.94	1750–1730	strong C=O stretching
-	1711.13	1730–1700	strong C=O stretching
1653.72	-	1680–1640	weak C=C stretching
-	1641.32	1680–1640	week C=C stretching
1464.07	-	1465–1430	methylene vibration
-	1456.77	1465–1430	methylene vibration
1418.45	1413.56	1500-1400	aromatic C–C stretching
1377.83	1377.89	-	C-H bending vibration of CH_2
-	1286.18	1320–1210	C–O stretching
1236.42	1236.35	1260-1050	C–O stretching
-	1165.33	1300–1160	C–O stretching
1159.72	-	1300–1160	C–O stretching
1119.52	-	1125–1085	C–O stretching
-	1119.52	1125–1085	C–O stretching
-	1105.05	1150–1085	C–O–C stretching
1098.57	-	1150–1085	C–O–C stretching
966.33	965.76	970–920	shoulder trans = C–H out-of-plane bending
-	942.98	950–910	O–H bending
914.76	-	950–910	O–H bending
-	909.37	-	terminal wag of ethers
-	814.10	860–800	aromatic –C-H out of plane bending
721.61	721.83	725–720	C–H rocking methyl

Appendix B. Supplementary Information (List of Figures) for Chapters Six and Seven

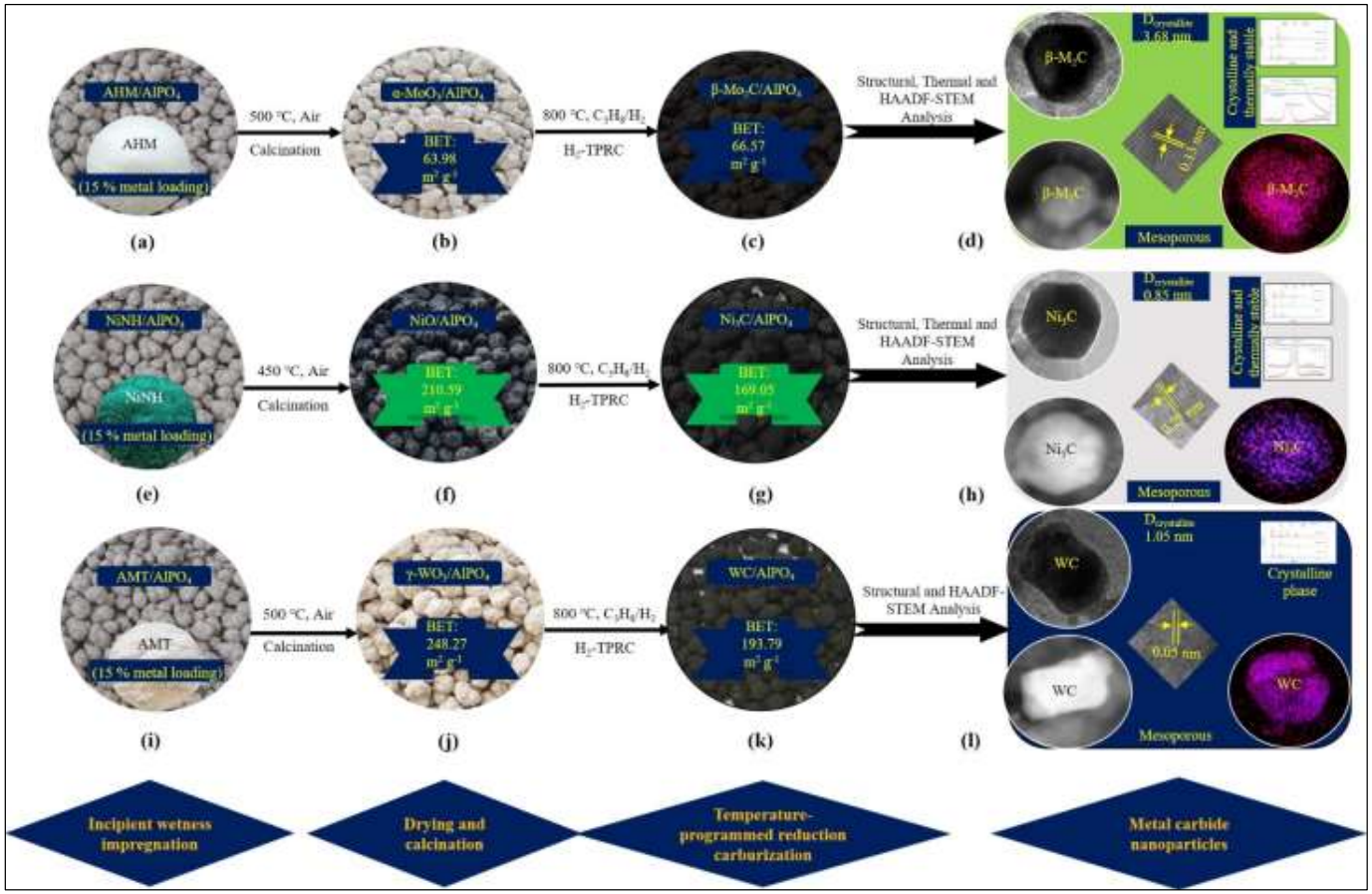

Figure 6.S1 Illustration of the formation process of $AlPO_4$-18 supported metal oxide and metal carbide nanoparticles. Support material and precursor salts (a, e, i), metal oxides (b, f, j), metal carbides (c, g, k), single nanoparticles (d, h, l). AHM- Ammonium molybdate tetrahydrate, NiNH- Nickel nitrate hexahydrate, AMT- Ammonium metatungstate hydrate. $AlPO_4$ stands for $AlPO_4$-18.

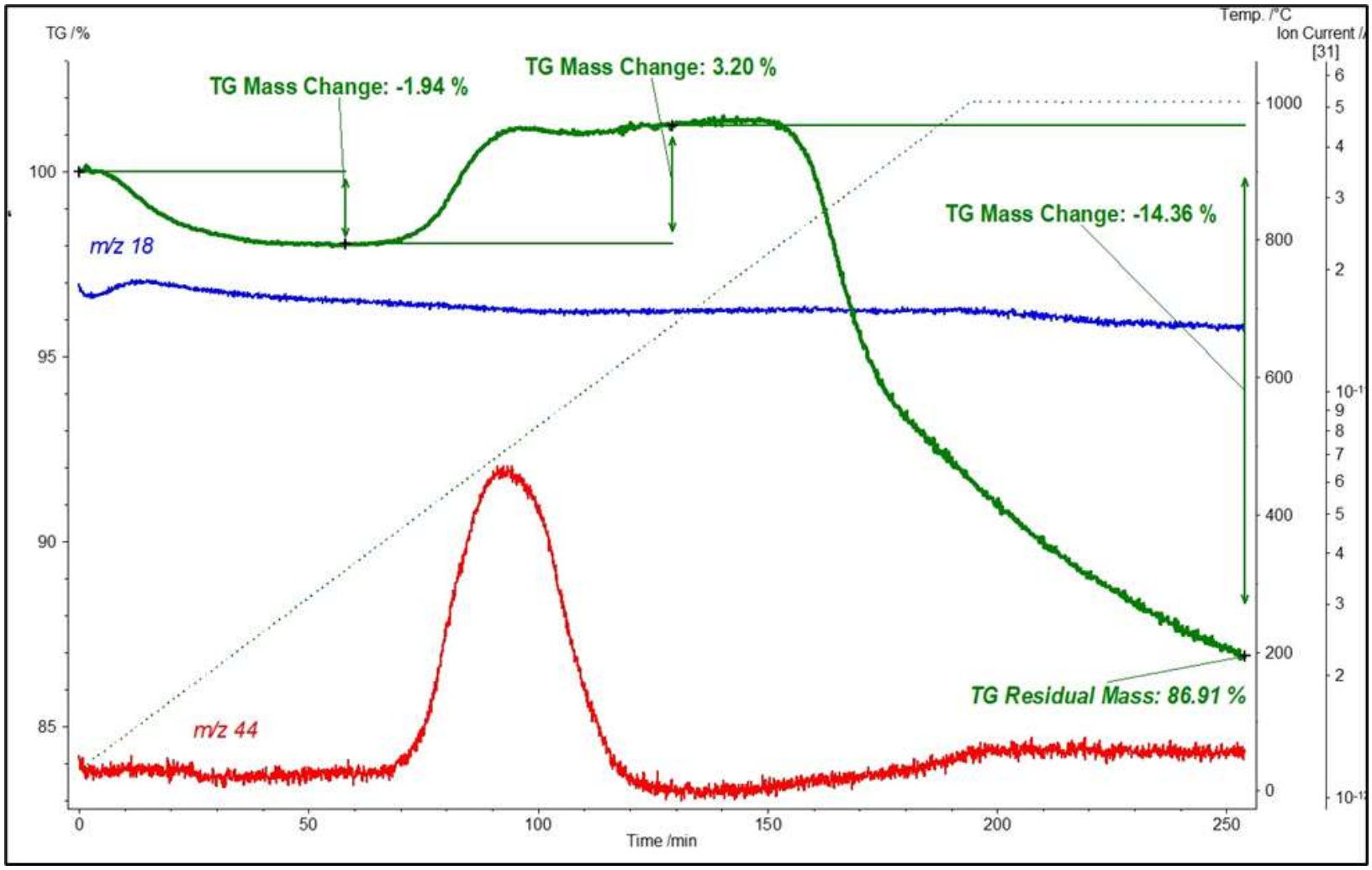

Figure 6.S2 *Ex-situ* TG-MS coupled with temperature programmed oxidation (TPO) for investigation of mass spectra of evolved gases, and mass loss (%) of β-Mo_2C/$AlPO_4$-18 nanoparticles.

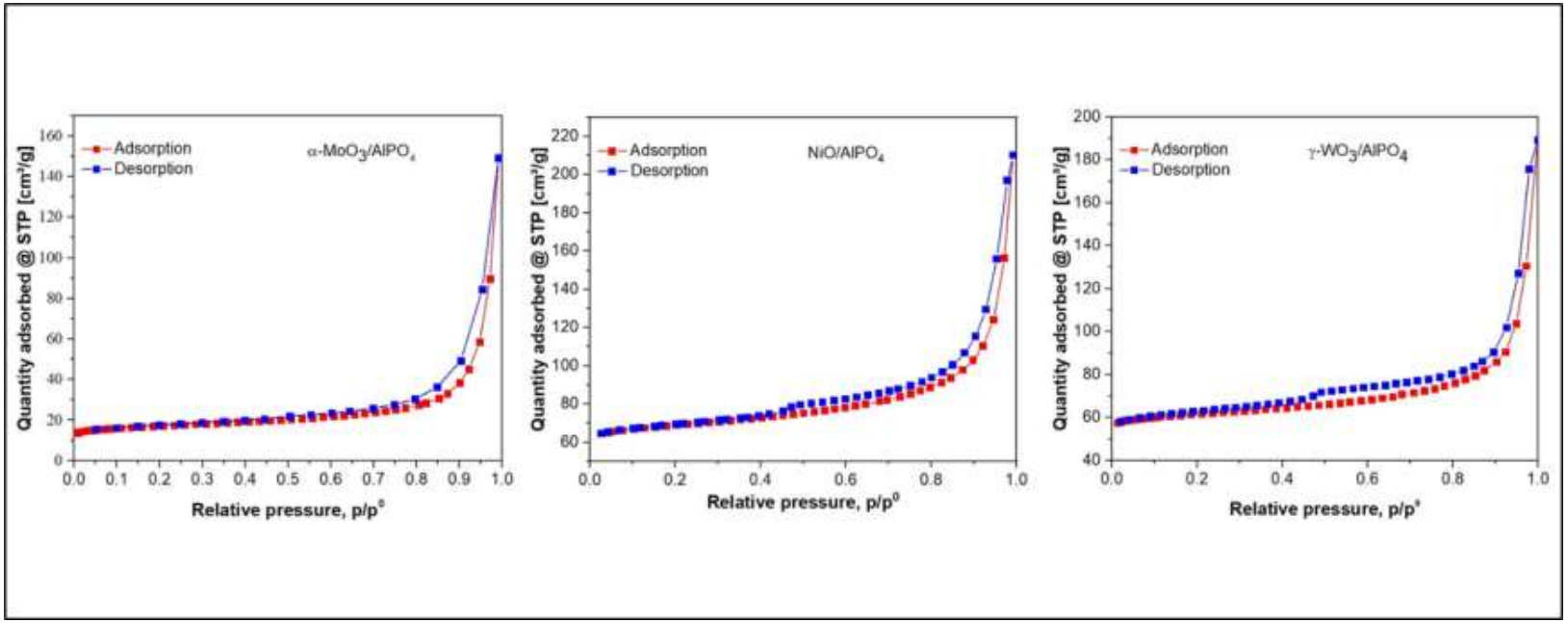

Figure 6.S3 Nitrogen gas adsorption-desorption curves of $AlPO_4$-18 supported calcined nanoparticles. $AlPO_4$ stands for $AlPO_4$-18.

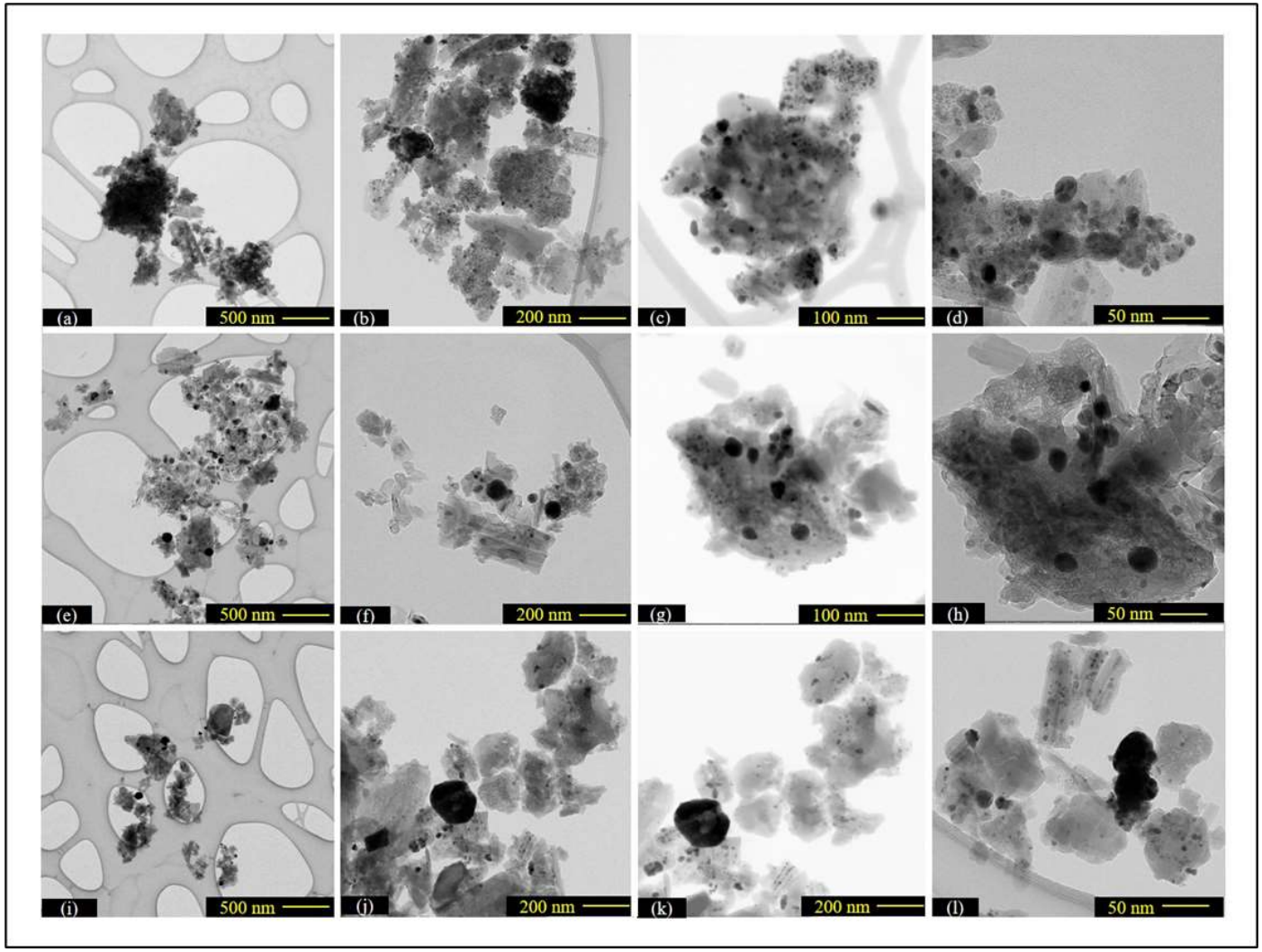

Figure 6.S4 *Ex-situ* TEM nanoparticle images of morphological and structural evolution of β-Mo_2C/$AlPO_4$-18 (a-d); Ni_3C/$AlPO_4$-18 (e-h); and WC/$AlPO_4$-18 (i-l) nanoparticles.

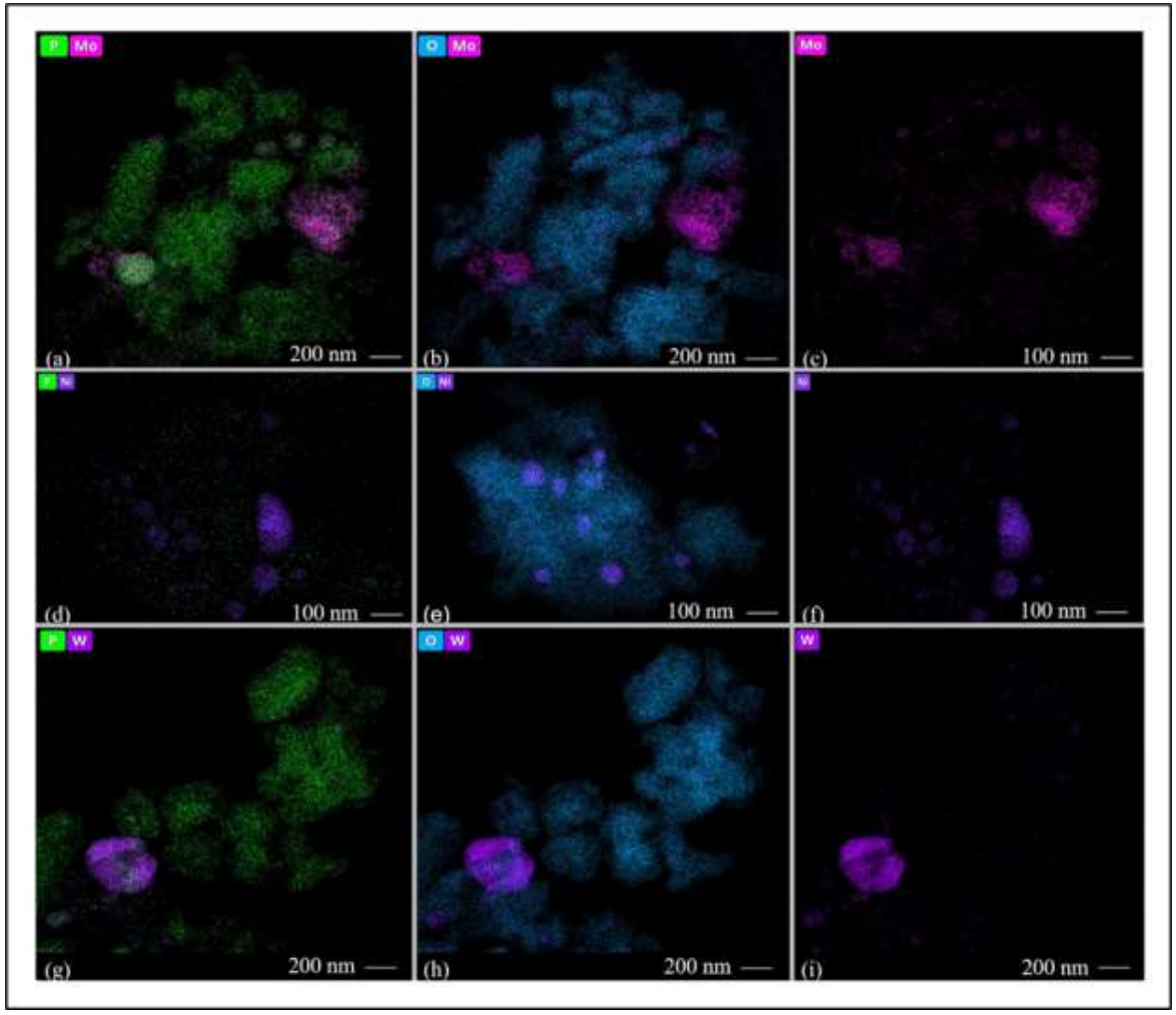

Figure 6.S5 HAADF-STEM with EDX mapping image of β-Mo_2C/$AlPO_4$-18 (a-c), Ni_3C/$AlPO_4$-18 (d-f), and WC/$AlPO_4$-18 (g-i) nanoparticles.

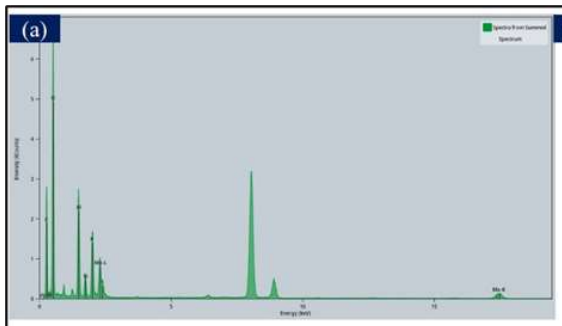

(b)

Element	Electron shell	Atomic fraction (%)	Mass fraction (%)
Mo	K	3.18	14.73
C	K	29.57	17.62
O	K	44.74	35.73
Al	K	21.86	15.91
P	K	8.17	12.65
Si	K	2.47	3.38

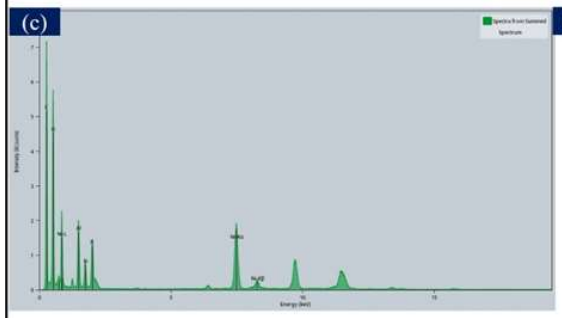

(d)

Element	Electron shell	Atomic fraction (%)	Mass fraction (%)
Ni	K	5.29	16.68
C	K	44.97	29.07
O	K	33.21	28.7
Al	K	8.12	11.83
P	K	6.25	10.46
Si	K	2.16	3.27

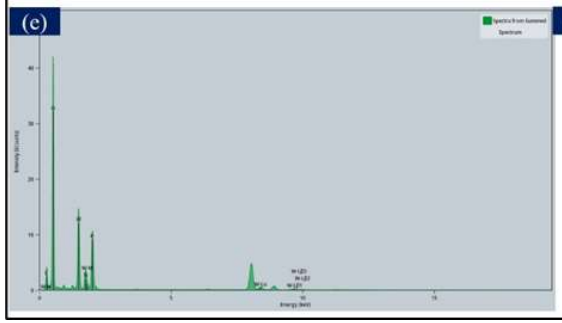

(f)

Element	Electron shell	Atomic fraction (%)	Mass fraction (%)
W	L	0.83	7.36
C	K	9.43	5.85
O	K	61.75	48.13
Al	K	14.37	18.90
P	K	10.31	15.57
Si	K	3.33	4.55

Figure 6.S6 TEM/EDX mapping composition of β-Mo_2C/$AlPO_4$-18 (a-b), Ni_3C/$AlPO_4$-18 (c-d), WC/$AlPO_4$-18 (e-f) nanoparticles.

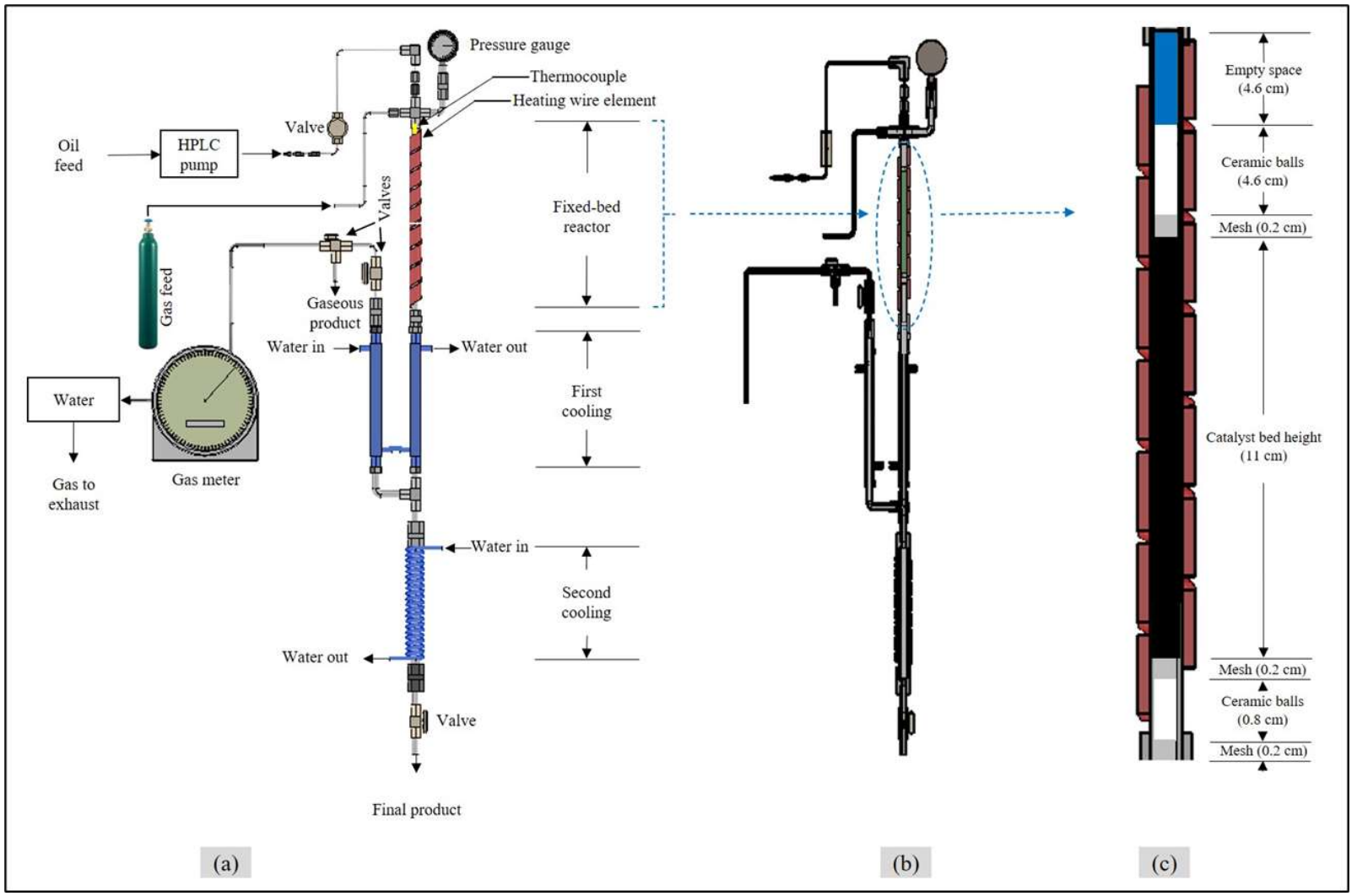

Figure 7.S1 Lab-scale three-phase continuous fixed-bed reactor system. (a) Side view, (b) Cross-sectional view, (c) Magnified view of the interior components and cross-section of the reactor.

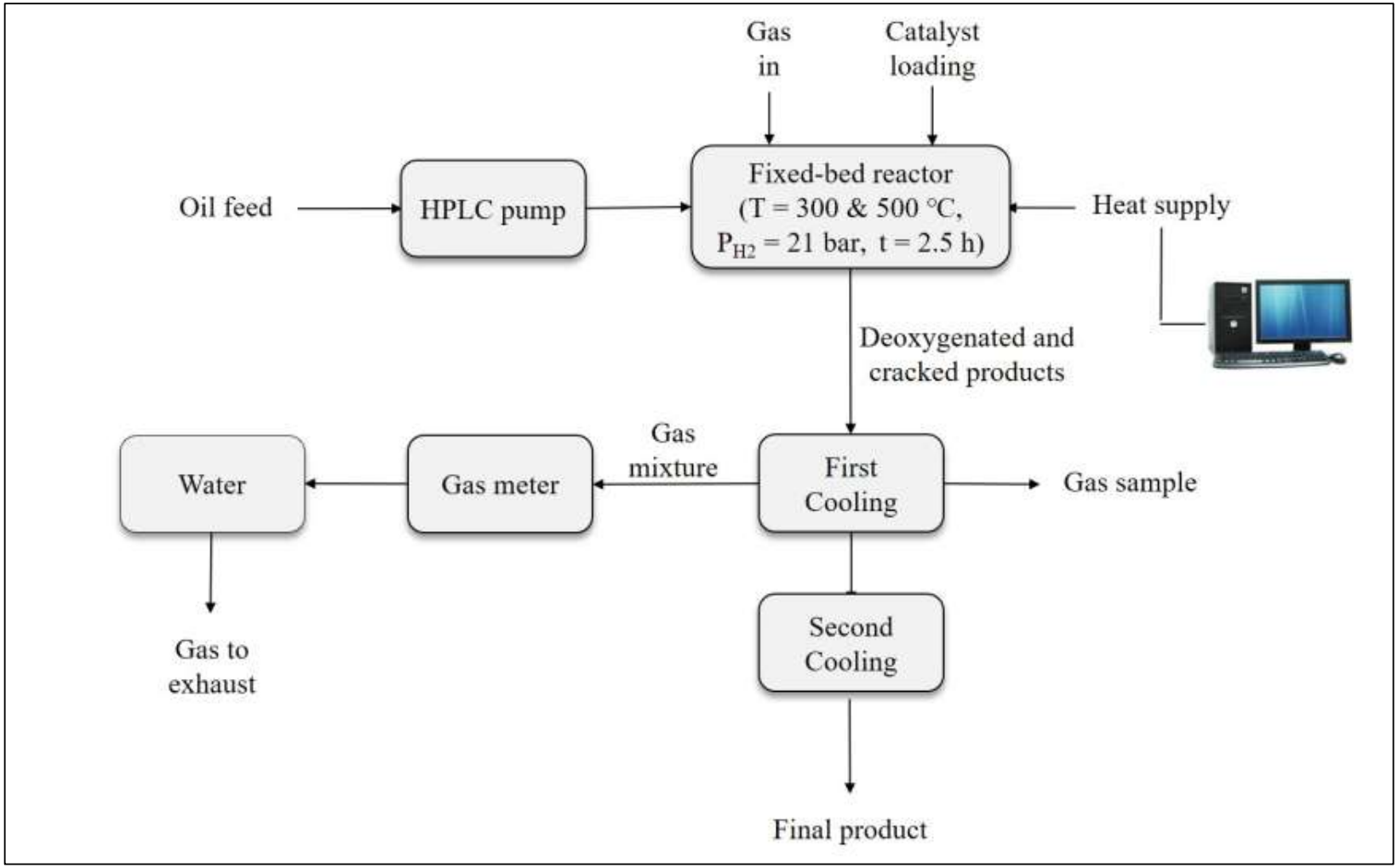

Figure 7.S2 Schematic representation of laboratory-scale three-phase continuous fixed-bed reactor system.

Appendix C. List of Figures

Hexane-Extracted *Brassica carinata* Vegetable Oils

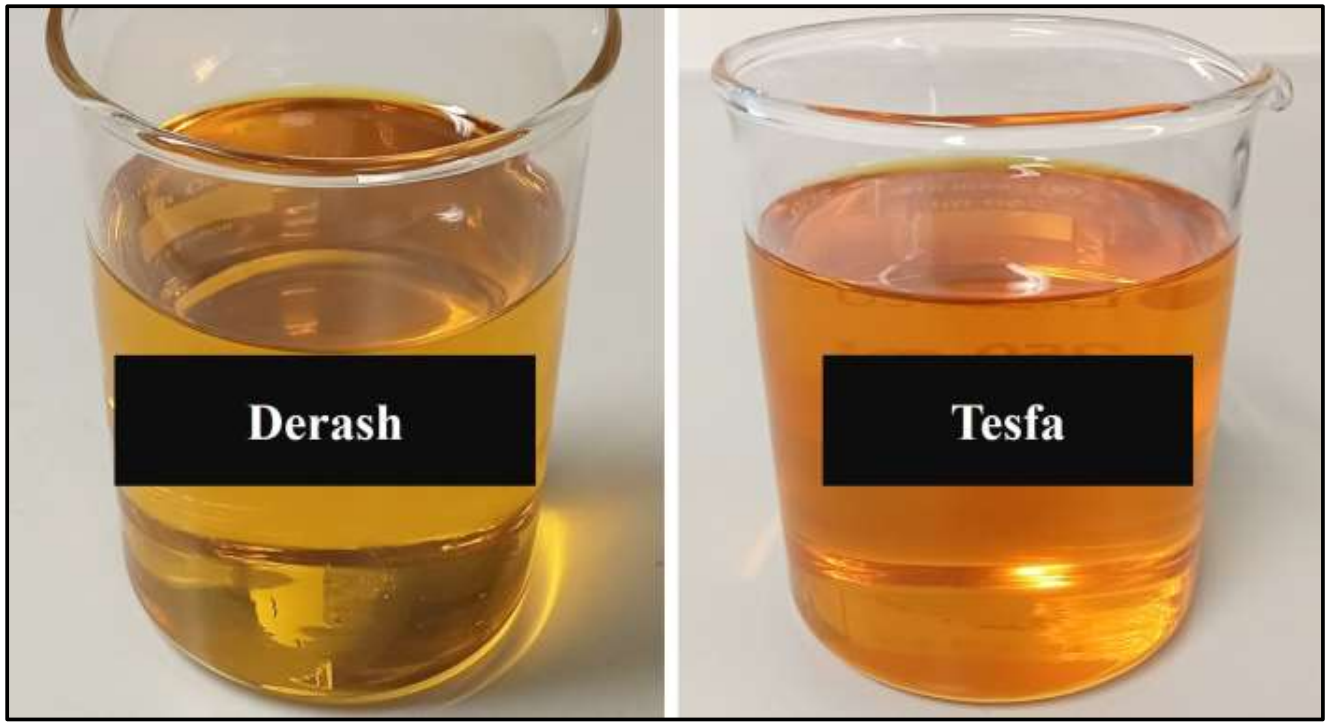
Derash
Tesfa

$AlPO_4$-18 Catalyst Support

$AlPO_4$-18 Supported Calcinated and Carburized Metal Carbide Nanoparticles

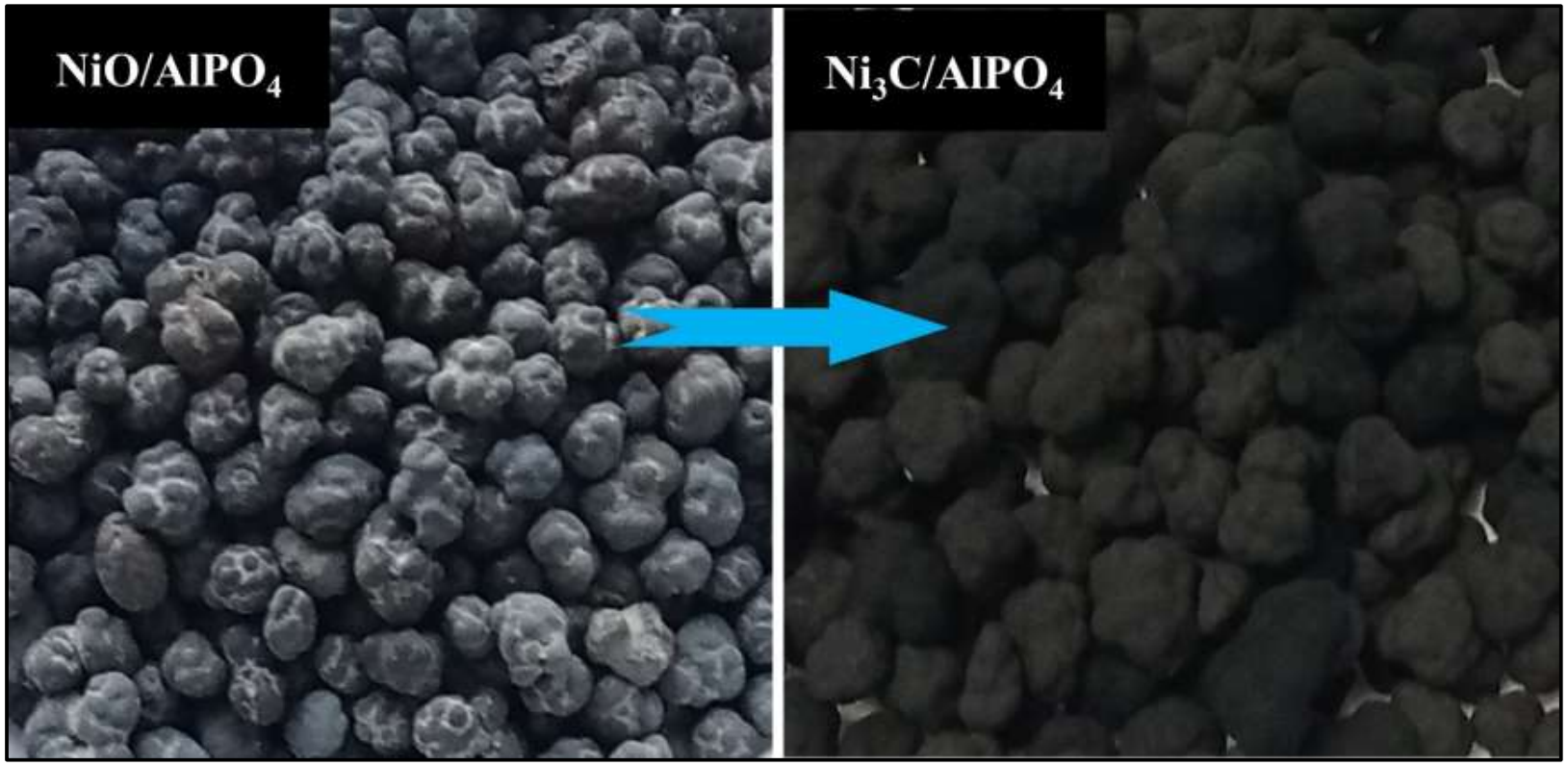
NiO/AlPO4
Ni3C/AlPO4


γ-WO3/AlPO4
WC/AlPO4

HAADF-STEM Elemental Mapping of Supported Metal Carbide Nanoparticles

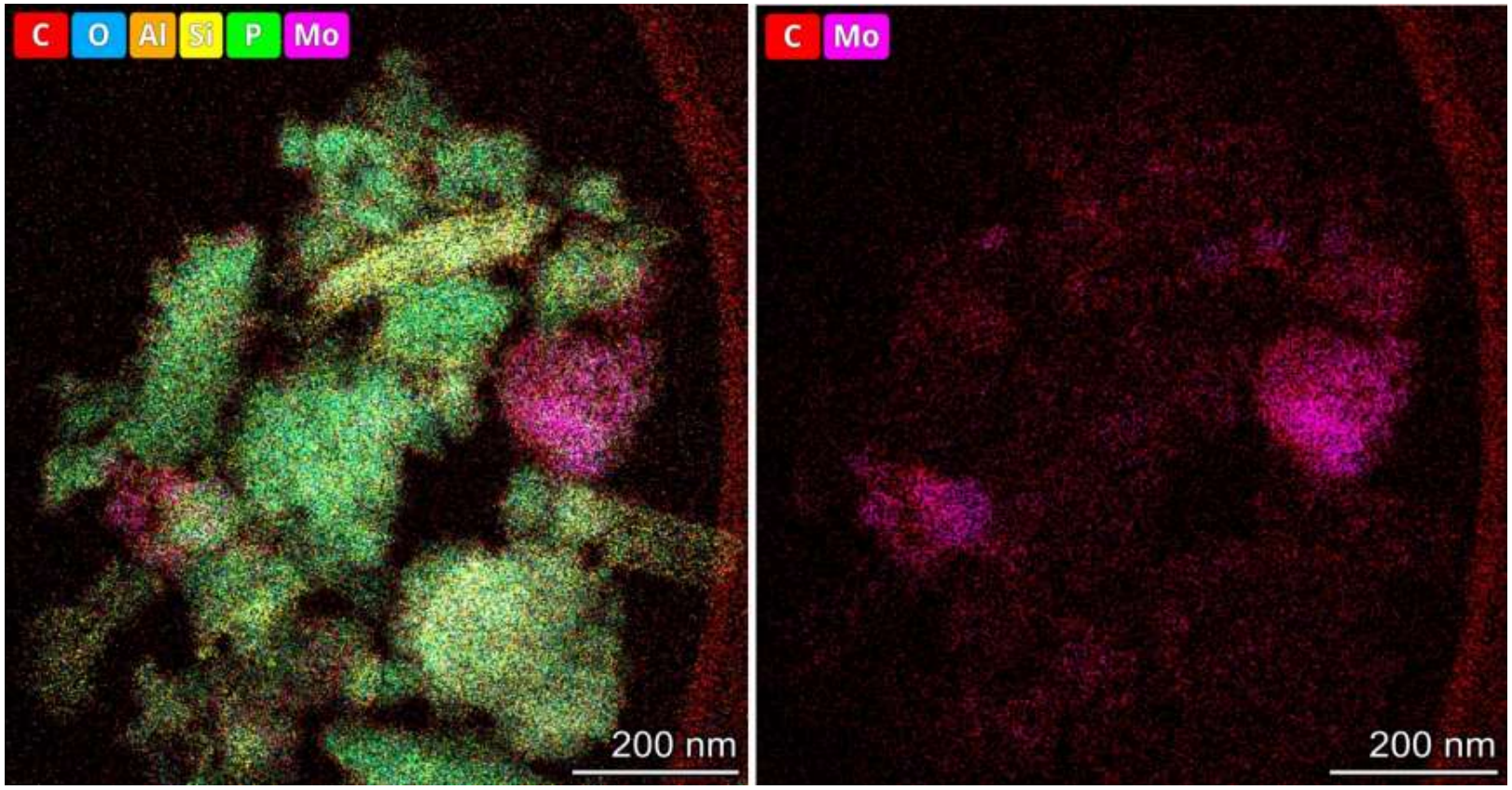

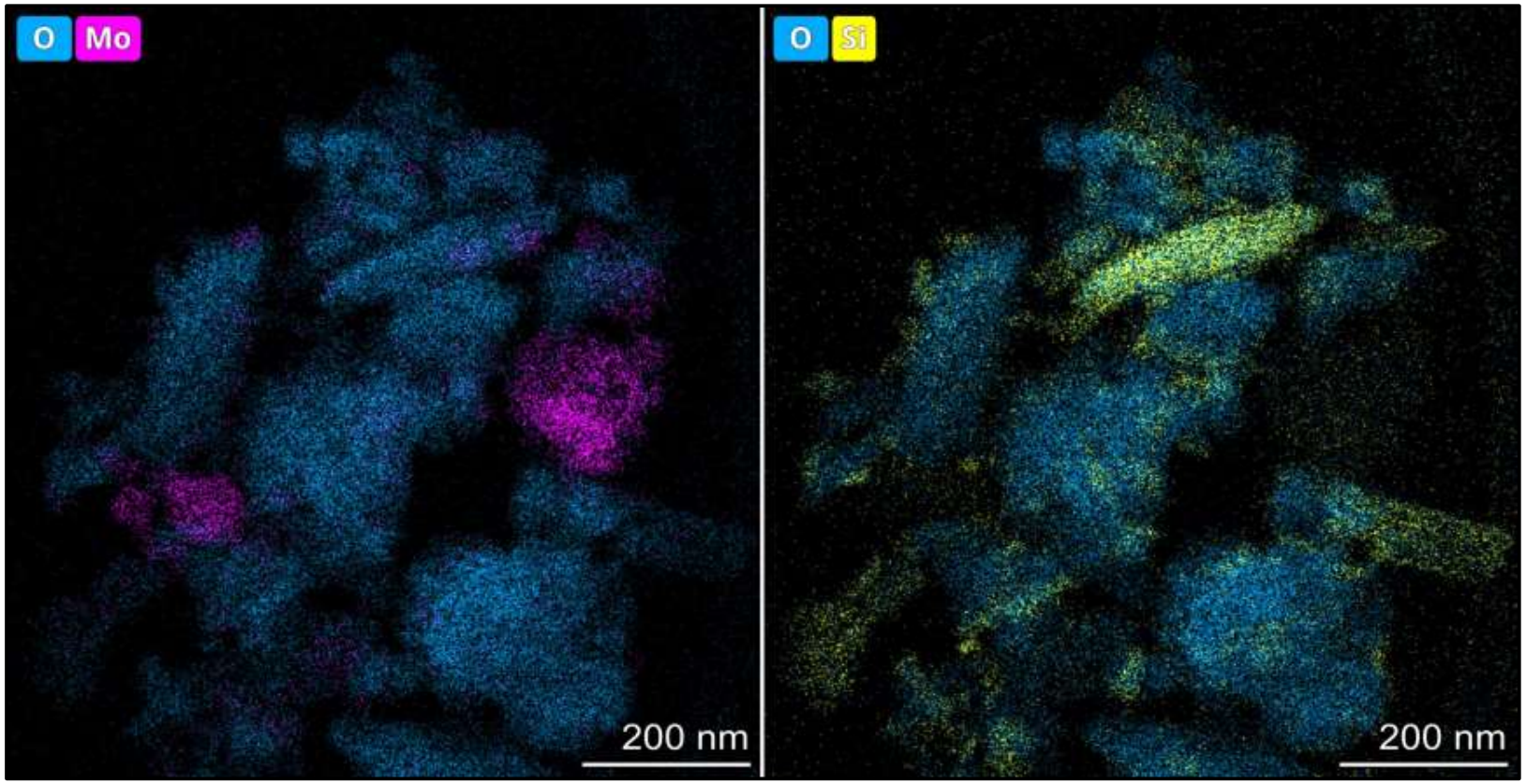
O
Mo
200 nm
O
Si
200 nm

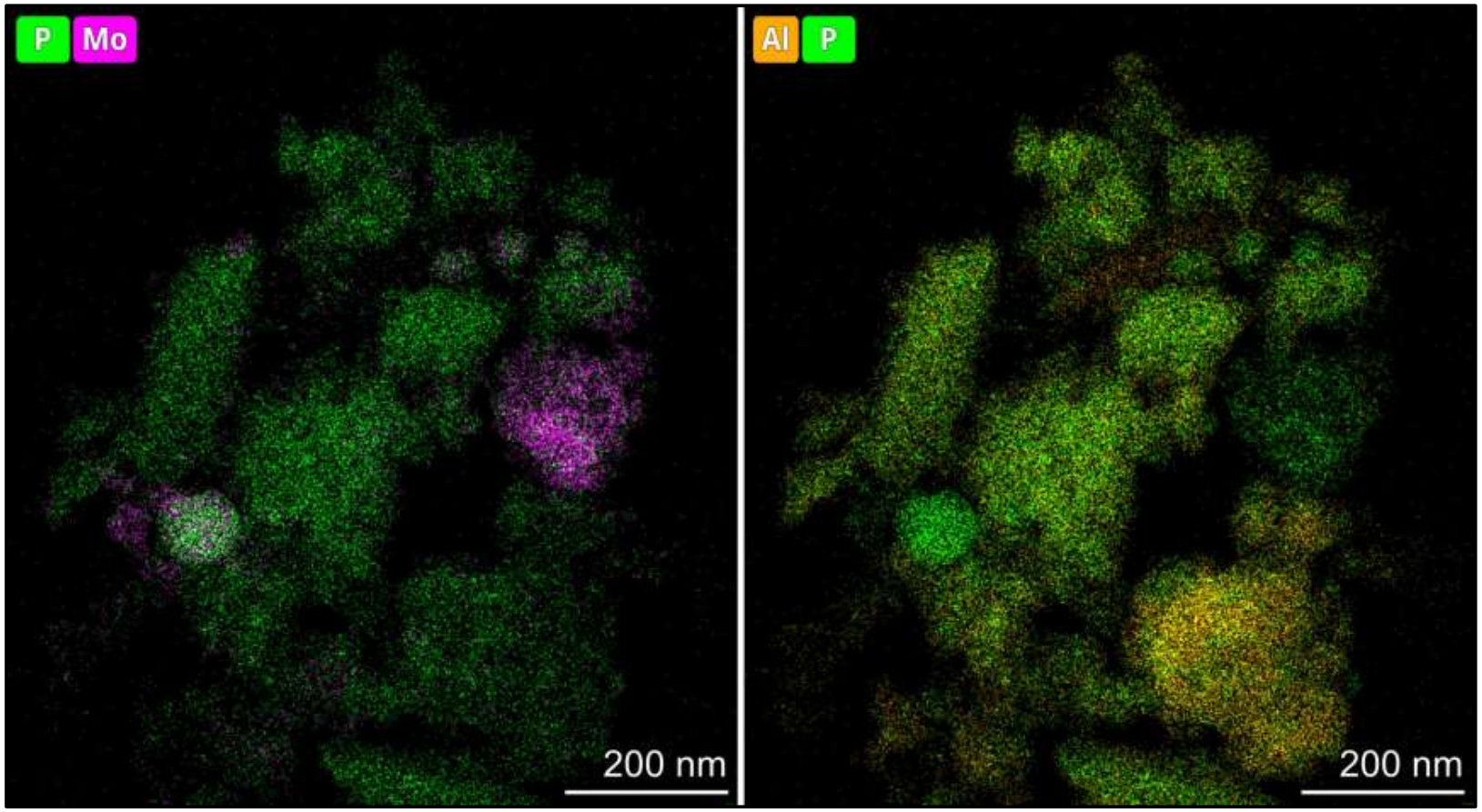
P
Mo
200 nm
Al
P
200 nm

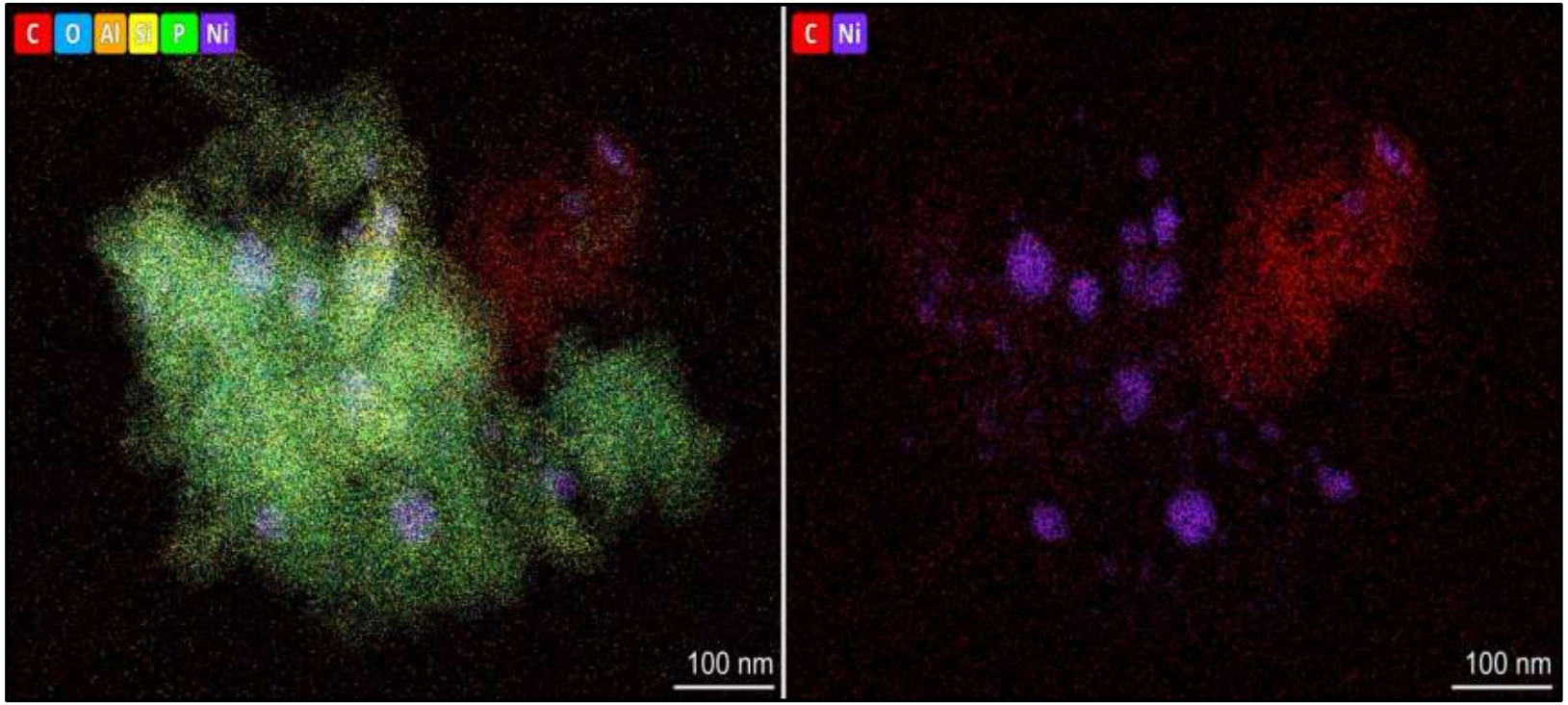
C O Al Si P Ni
100 nm
C Ni
100 nm

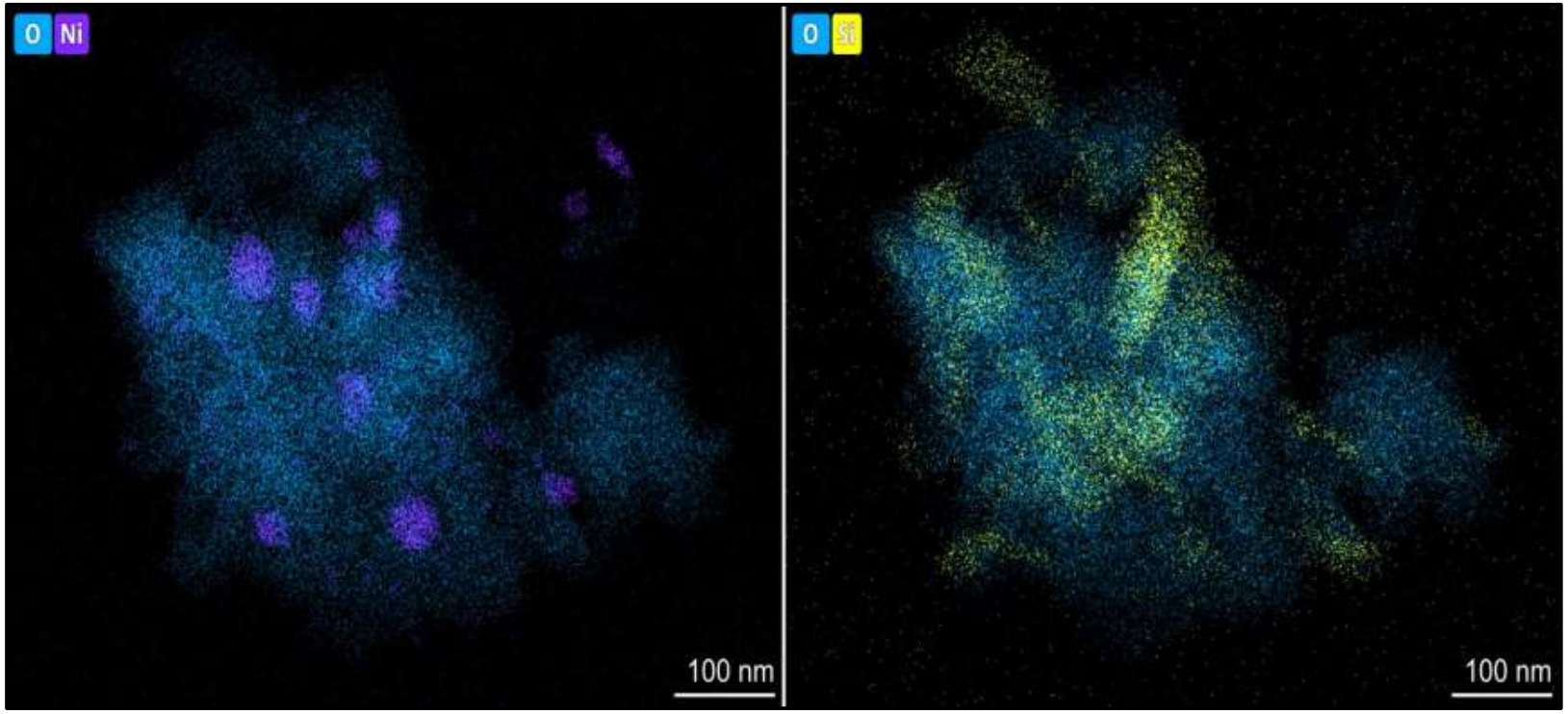
O
Ni
100 nm
O
Si
100 nm

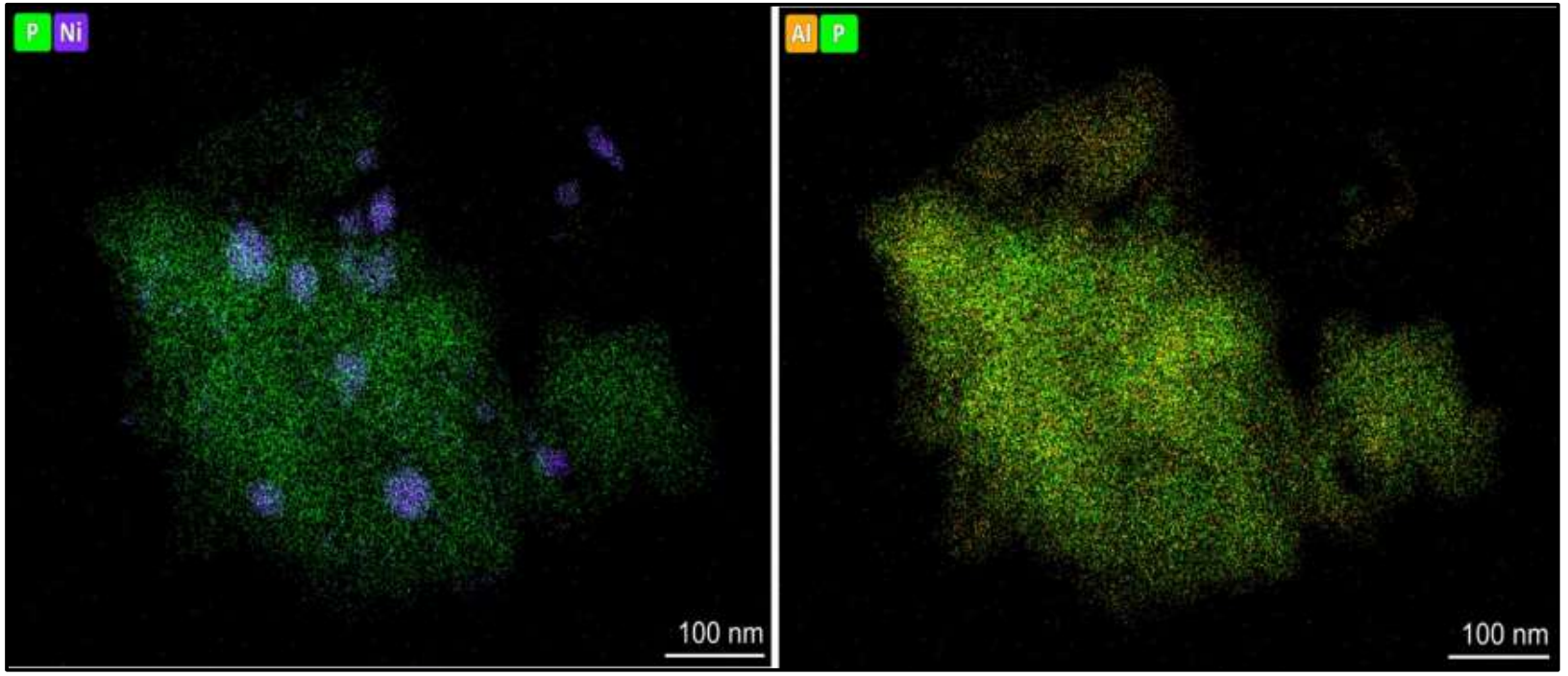
P
Ni
100 nm
Al
P
100 nm

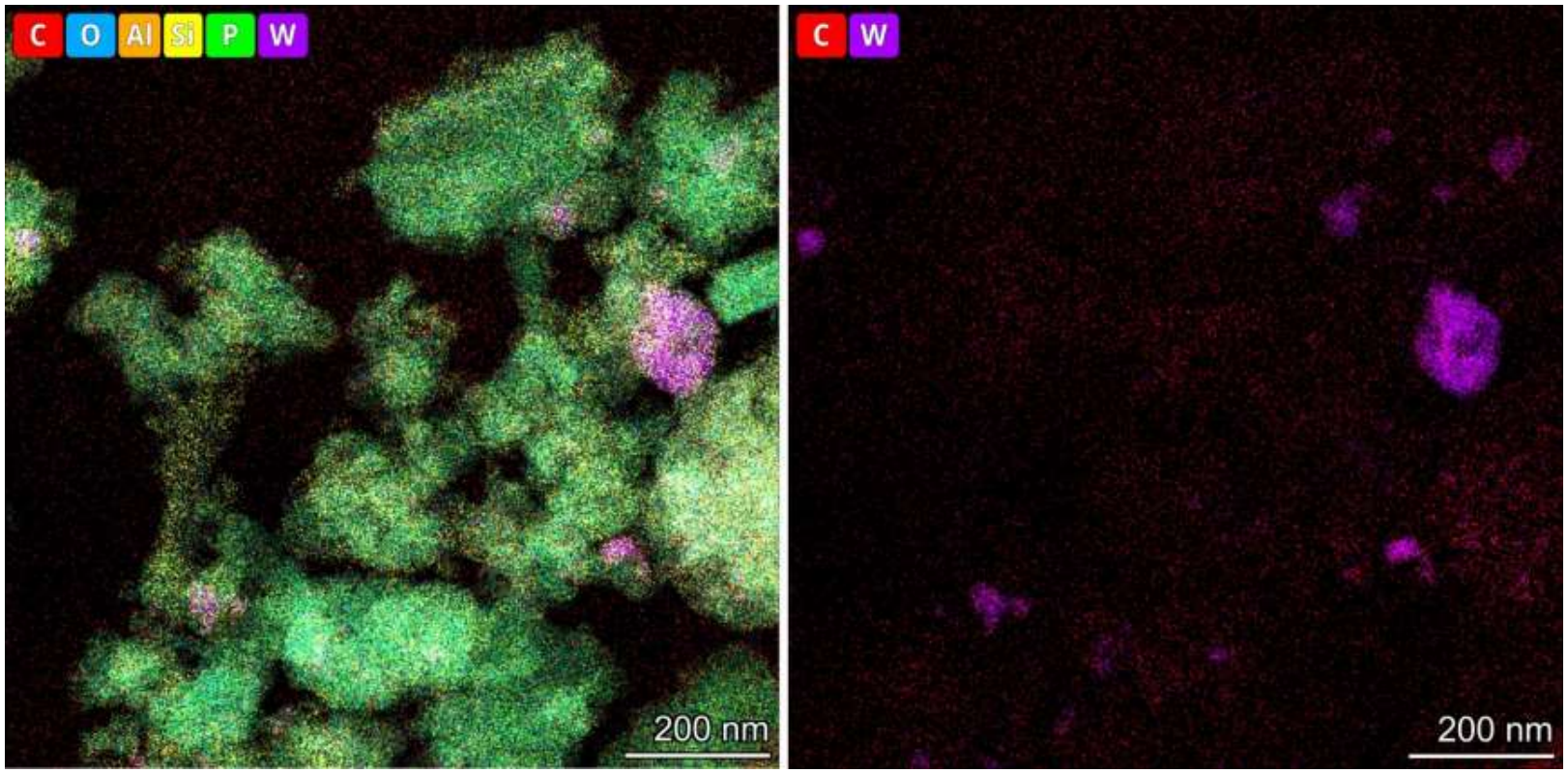
C O Al Si P W
200 nm
C W
200 nm

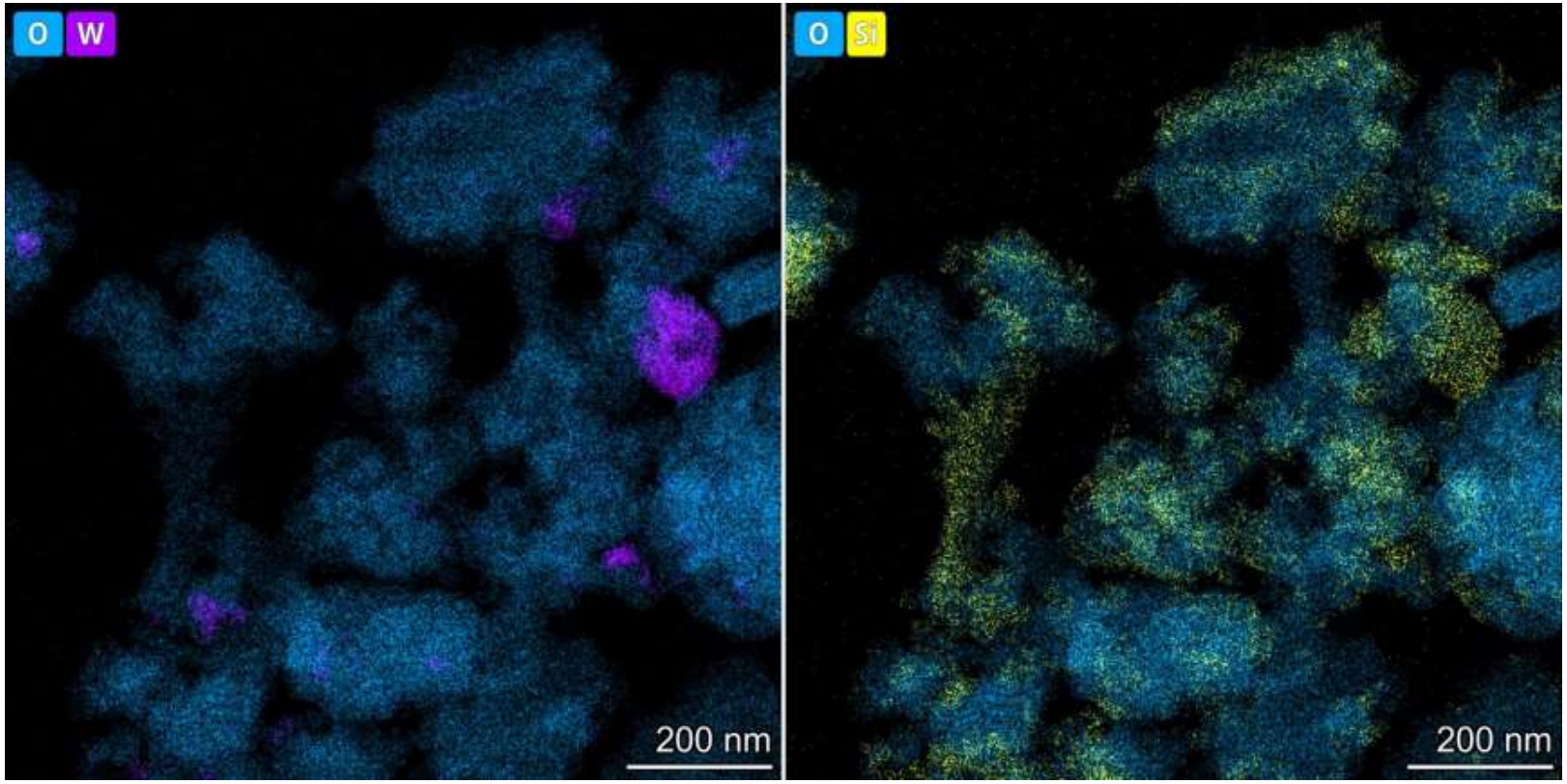
O
W
200 nm
O
Si
200 nm

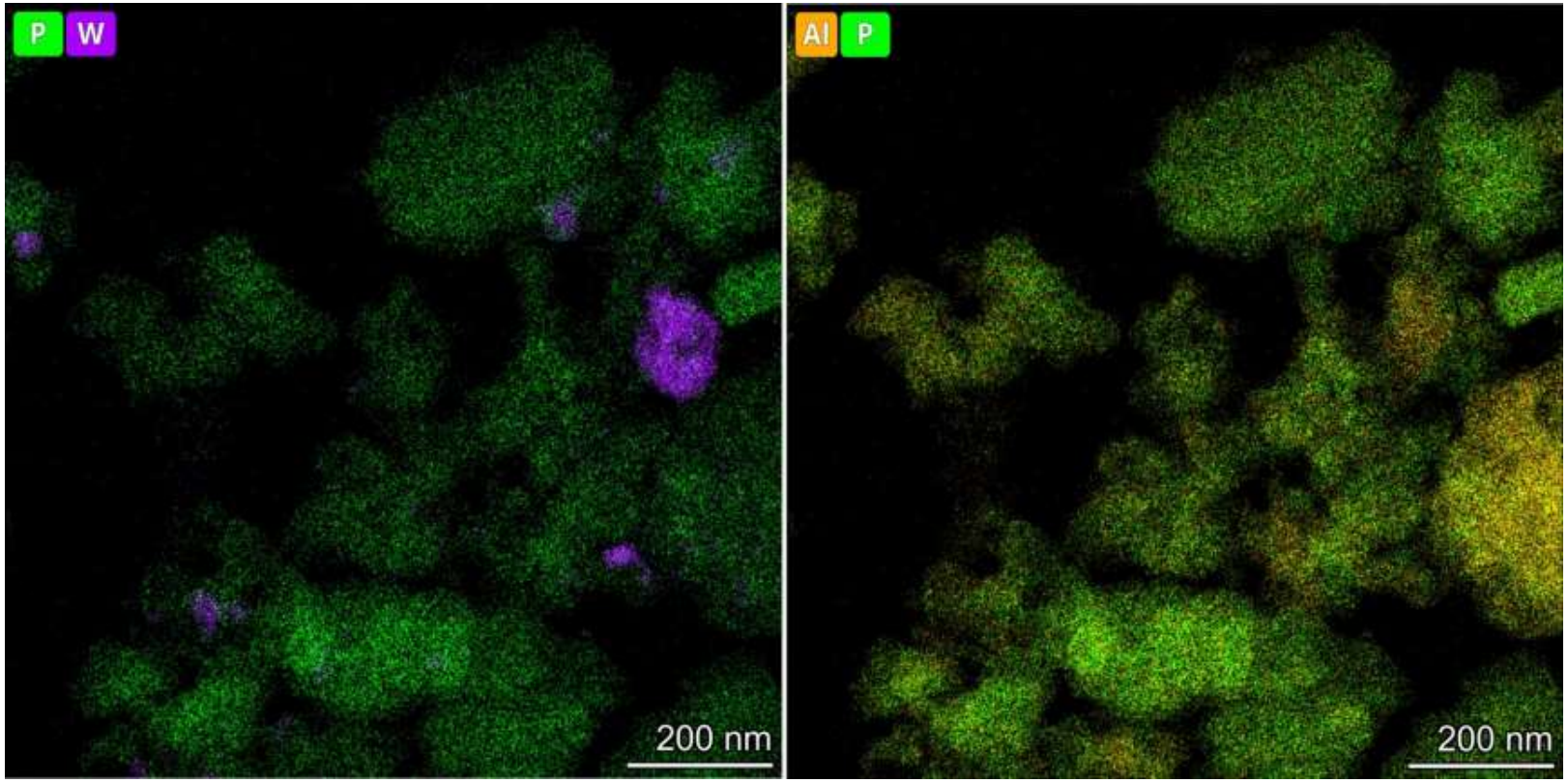
P
W
200 nm
Al
P
200 nm

Oil Feedstock and Hydroprocessed Liquid Phase Products

Oil feedstock **Hydroprocessed at 300 °C** **Hydrocracked at 500 °C**

LIST OF ANNEXES

Annex A: ASTM Users` Guide

A-1: ASTM D4054 – "Standard Practice for Qualification and Approval of New Aviation Turbine Fuels and Fuel Additives"

ASTM D4054 was developed to provide the producer of an alternative jet fuel with guidance regarding testing and property targets necessary to evaluate a candidate alternative jet fuel. D4054 is an iterative process, which requires the candidate fuel developer to test samples of fuel to measure properties, composition, and performance. The testing covers basic specification properties, expanded properties called fit-for-purpose (FFP) properties, engine rig and component test, and if necessary, full-scale engine testing. This is a rigorous process that requires participation and input from many of the stakeholders at ASTM.

ASTM D4054 was developed as a guide by the engine and airplane OEMs (original equipment manufacturers) with ASTM International member support. It provides the producer of an alternative fuel with guidance of what is expected in the form of required testing and OEM involvement. It also includes property targets that are based on OEM experience with the impact of fuel or additives on the design and performance of gas turbine engines. The fuel producer should engage the key organizations within international aviation jet fuel communities that typically support the evaluation and approval of new fuels. These include ASTM International, the Coordinating Research Council (CRC), and Commercial Aviation Alternative Fuels Initiative (CAAFI). A task force within ASTM's Emerging Fuel Subcommittee should be formed to solicit stakeholder input regarding testing and preparation of an ASTM research report. Typically, the OEMs will be a part of that task force. An ASTM research report is the vehicle used to submit the data used for gaining final approval for the new fuel to the ASTM membership. This research report will be reviewed by engine and airplane OEMs, airworthiness organizations, and international fuel specification standards groups. Involvement in these organizations is critical because it gives the fuel producer access to the world's foremost authorities in jet fuel and access to the most current work being performed in the development of new fuels

A-2: ASTM D7566– "Standard Specification for Aviation Turbine Fuel Containing Synthesized Hydrocarbons".

ASTM D7566 was issued in September, 2009. The specification is structured with annexes that define property and compositional requirements for synthetic blending components that can be mixed with conventional, petroleum-derived jet fuel at specified volumes. D7566 includes a provision to allow fuels meeting this specification to be re-identified as conventional fuels when they enter the distribution infrastructure. ASTM International Standard D1655, "Standard Specification for Aviation Turbine Fuels", defines the requirements for petroleum derived, conventional jet fuel. This re-identification provision allows the drop-in fuels listed in D7566 to be seamlessly integrated into the infrastructure and on to the aircraft without the need for separate tracking or regulatory approval. This is because the infrastructure is already designed to support D1655 jet fuel, and virtually all civil aircraft are certified to operate with jet fuel meeting specification D1655. So, once a new, alternative jet fuel is added as an annex to D7566, it is ready to fly on commercial airliners.

Annex B. Conversion Processes Approved for Aviation Alternative Fuel Production

- **Fischer Tröpsch synthesized isoparaffinic kerosene (FT-SPK)** was approved by ASTM for incorporation into ASTM D7566 in September, 2009. In the FT-SPK process, coal, natural gas, or biomass feed stocks are gasified into a syngas comprised of hydrogen and carbon monoxide. This syngas is then catalytically converted to a liquid hydrocarbon fuel blending component in the FT reactor.
- **Hydroprocessed fatty acid esters and fatty acids (HEFA)** was approved by ASTM for incorporation into ASTM D7566 in June, 2011. In the HEFA process, lipid feedstocks such as plant or algae oils, tallow (animal fats), or waste greases such as cooking oils are deoxygenated and then hydroprocessed to produce a pure hydrocarbon fuel blending component.
- **Synthesized is paraffins (SIP)** was approved by ASTM for incorporation into ASTM D7566 in July, 2014.The SIP process utilizes a fermentation to convert a sugar feed stock into a hydrocarbon molecule that can be blended into conventional jet fuel.
- **Fischer Tröpsch synthesized kerosene with aromatics (FT-SPK/A)** was approved by ASTM for incorporation into ASTM D7566 in November, 2015.FT-SPK/A is a variation of the FT process where a fully-synthetic alternative aviation fuel containing aromatics is produced.
- **Alcohol to jet (ATJ)** was approved by ASTM for incorporation into ASTM D7566 in April 2016.The ATJ process utilizes dehydration, oligomerization, and hydroprocessing to convert alcohol feed stocks to a pure hydrocarbon fuel blending component. The ATJ process is currently limited to isobutanol alcohol feed stocks, but is in process of being expanded to include ethanol feed stocks

Annex C. Summary of Jet Fuel Production Pathways.

Category	Pathways	Companies	U.S. or International Agencies	Airline Companies/Manufacturers
Alcohol-to-Jet (ATJ)	Ethanol-to-Jet	Terrabon/MixAlco; Lanza Tech/Swedish Biofuels; Coskata	Defense Advanced Research Projects Agency, FAA	Boeing, Virgin Atlantic
	Butanol-to-Jet	Gevo; Byogy; Albemarle/Cobalt; Solazyme	U.S. Navy/NAWCWD, AFRL, DLA, USAF	Continental Airlines; United Airlines
Oil-to-Jet (OTJ)	Hydroprocessed Renewable Jet (HRJ)	UOP; SG Biofuels; AltAir Fuels; Agrisoma Biosciences; Neste Oil; PetroChina; Sapphire Energy, Syntroleum/Tyson Food; PEMEX; ASA	U.S. Navy, USAF, Netherland Air Force, NASA, Dutch Military, EADs	Boeing, Lufthansa, Virgin Atlantic, Virgin Blue, GE Aviation, Air New Zealand, Rolls-Royce, Continental, CFM, JAL, Airbus, KLM, Pratt & Whitney, Air China, TAM Airlines, Jet Blue Airways, IAE, United Airlines, Air France, Finnair, Air Mexico, Thomson Airways, Porter Airlines, Alaska Airlines, Horizon Air, Etihad Airways, Romanian Air, Bombardier
	Catalytic Hydrothermolysis (CH)	Applied Research Assoc., Aemetis/Chevron Lummus Global	FAA CLEEN, NRC Canada, AFRL	Rolls-Royce, Pratt & Whitney
	Hydrotreated Depolymerized Cellulosic Jet (Pyrolysis or HDCJ)	Kior/Hunt Refining/Petrotech, Envergent, GTI, Dynamotive		N/A
Gas to Jet (GTJ)	FT Synthesis	Syntroleum; SynFuels; Rentech; Shell; Solena	U.S. DOE, U.S. DOD, USAF, Ontario government	Qatar Airways, United Airlines, Airbus, British Airways
	Gas Fermentation	Coskata; INEOS Bio/Lanza Tech; Swedish Biofuels	N/A	Virgin Atlantic
Sugar to Jet (STJ)	Catalytic Upgrading of Sugar to Jet	Virent/Shell, Virdia	AFRL, U.S. DOE	N/A
	Direct Sugar Biological to Hydrocarbons	Amyris/Total, Solazyme, LS9	U.S. Navy, FAA	Boeing; Embraer; Azul Airlines; GE; Trip Airlines

Annex D. Jet Fuel Specifications, Combustion, and Engine Tests.

In addition to defined target compositions, jet fuel specifications and requirements are mostly defined in terms of required performance properties. The specifications required for jet fuels are:

(1) Acceptable minimum energy density by mass,

(2) Maximum allowable freeze point temperature,

(3) Maximum allowable deposits in standard heating tests,

(4) Maximum allowable viscosity,

(5) Maximum allowable sulfur and aromatics content,

(6) Maximum allowable amount of wear in standardized test,

(7) Maximum acidity and mercaptan concentration,

(8) Minimum aromatics content,

(9) Minimum fuel electrical conductivity, and

(10) Minimum allowable flash point (U.S. Department of Defense 2011).

There are three standards for certifying aviation fuel: ASTM D1655, International Air Transport Association Guidance Material (Kerosene Type), and the United Kingdom Ministry of Défense, Defence Standard (Def Stan) 91-91 (ONGC and Quality Control Laboratory 2008; Agusdinata, Zhao, et al. 2011; American Society for Testing and Materials 2013). ASTM Specification D7566 (Standard Specification for Aviation Turbine Fuel Containing Synthesized Hydrocarbons), which targets alternative jet fuel, lists the fuel properties and criteria required to control the production and quality of a renewable fuel for aviation safety (American Society for Testing and Materials 2013) (Source: Review of Bio jet Fuel Conversion Technologies).

Annex E. Jet Fuel Specifications.

(ExxonMobil Aviation 2005; ONGC and Quality Control Laboratory 2008; U.S. Department of Defense 2011; American Society for Testing and Materials 2013; UK Ministry of Defense 2013)

	Jet A-1				JP-8
	ASTM D1655-04a	**IATA**	**Def Stan 91-91**	**ASTM D7566**	**MIL-DTL-83133E specification**
Acidity, Total (mg KOH/g)	0.1, max	0.015, max	0.012, max	0.1, max	0.015, max
Acidity, Total (mg KOH/g)	25, max	25, max	25, max	25, max (8, min)	25, max
Sulphur, Total (wt. %)	0.3, max	0.3, max	0.3, max	0.3, max	0.3, max
Distillation Temperature					
10% Recovery (°C)	205, max	205, max	205, max	205, max	205, max
20% Recovery (°C)	_	_	_	_	_
50% Recovery (°C)	_	_	_	— (15, min)	_
90% Recovery (°C)	_	_	_	— (40, min)	_
Final BP (°C)	300, max	300, max	300, max	300, max	300, max
Flash Point (°C)	38, min	38, min	38, min	38, min	38, min
Freezing Point (°C), max	-47	-47	-47	–40 Jet A ; –47 Jet A-1	-47
Viscosity @ -20°C (cSt)	8, max	8, max	8, max	8, max	8, max
Net Heat of Comb. (MJ/kg)	42.8, min	42.8, min	42.8, min	42.8, min	42.8, min
Density @ 15°C (kg/m3)	775-840	775-840	775-840	775-840	775-840

(**Note:** MIL-DTL-83133E is the standard specifically for JP-8 fuel.)

Annex F. Flight Tests with Bio Jet Fuels through Different Conversion Pathways by Commercial Airlines.

Commercial Airline	Aircraft	Partners	Year	Feedstocks	Bio Jet Fuel Content	Conversion Pathway
Virgin Atlantic	B747-400	Boeing, GE Aviation	2008	Coconut &Babassu	20%	OTJ
Air New Zealand	B747-400	Boeing Rolls-Royce, UOP	2008	Jatropha	50%	OTJ
Continental Airlines	B737-800	Boeing, GE Aviation, CFM, Honeywell UOP	2009	2.5% Algae & 47.5% Jatropha	50%	OTJ
JAL	B747-400	Boeing, Pratt & Whitney, Honeywell UOP, Nikki Universal	2009	42% Camelina, 8% Jatropha, <0.5%Algae	50%	OTJ
KLM	B747-400	GE, Honeywell UOP	2009	Camelina	50%	OTJ
KLM	B737-800	SkyNRG, Dynamic Fuels	2011	Waste cooking oil	50%	OTJ
TAM Airlines	A-320	Airbus, CFM	2010	Jatropha	50%	OTJ
Boeing	B747-8F		2011	Camelina	15%	OTJ
Air France	A-321	SkyNRG	2011	Waste cooking oil	50%	OTJ
Gulfstream Aerospace	Gulfstream G450	Honeywell, NBAA	2012	Camelina	50%	OTJ
AeroMexico	B737-200		2011	Jatropha	30%	OTJ
Air China	B747-400	Boeing, PetroChina	2012	Jatropha	50%	OTJ

Annex F. Continued.

Commercial Airline	Aircraft	Partners	Year	Feedstocks	Bio Jet Fuel Content	Conversion Pathway
Alaska Airlines	B737, Bombardier Q400	Dynamic Fuels, Horizon Air	2011	Algae & waste cooking oil	20%	OTJ
Etihad Airways	B777-300ER	SkyNRG	2012	Recycled vegetable cooking oil	n.a.	OTJ
Paramus Flying Club	Cessna 182	SkyNRG	2013	Waste cooking oil	50%	OTJ
LAN	A-320	Honeywell	2013	Camelina	30%	OTJ
Thai Airways	Boeing-777	SkyNRG	2012	Waste cooking oil	50%	OTJ
NRC Canada	Falcon 20, T-33	Aemetis, AFRL, Rolls-Royce, FAA-CLEEN, Agrisoma Biosciences, Applied Research Assoc., Chevron Lummus Global	2012	Carinata	100%	OTJ (CH)
Azul Airlines	E195 Jet	Amyris, Embraer, GE	2012	Sugarcane	-	STJ
Continental Airlines	B737-800	Solazyme, United Airlines	2011	Sugarcane/Algae	-	ATJ
Virgin Atlantic	-	Lanza Tech, Swedish Biofuels	2011	Industrial waste gas	-	GTJ (fermentation)

GLOSSORY OF TERMS

Abyssinian Mustard Seeds. Commonly known as Abyssinian cabbage, Ethiopian mustard, Ethiopian rape, *Gomenzer*. A high yielding, disease and pest tolerant, oilseed in the central highlands of Ethiopia at altitudes of 2200 to 2800 m above sea level.

ASTM. ASTM International. Previously known as American Society for Testing and Material. Owner of the major Jet fuel specifications ASTM D1655, ASTM D7566, ASTM D4054.

Aviation Fuel. Current aviation fuels, a kerosene-type fuel, commonly referred to as Jet A-1 or Jet A. Jet A-1 is suitable for most turbine engine aircraft. It has a flash point of 38 °C and a freeze point maximum of −47 °C. Jet A is only available in North America and has a higher freeze point (−40 °C).

Biofuel. The term 'biofuel' is generally used to describe non fossil fuels derived from *biomass*, but it's important to note that the sustainability of some of these can vary significantly depending on their source and processing. Aviation is focused on advanced generation biofuels derived from sustainable biomass that do not impact the food supply chain or fresh water resources or contribute to deforestation.

Biomass. Any organic matter that can be converted into fuel.

Bio-SPKA. Synthetic paraffinic kerosene that was produced from a bio-derived oil source.

Brunauer-Emmett-Teller (BET). Surface Area Analysis and Barrett-Joyner-Halenda (BJH) Pore Size and Volume Analysis.

Carbon Footprint. Amount of net carbon dioxide emissions addressed to a specific product or activity

Carbon Neutral. With zero carbon footprint (CO_2 emission = CO_2 absorption)

Carbon Offsetting. In the context of addressing climate change concerns, offsetting is an action by a company or individual to compensate for their emissions by financing a reduction in emissions elsewhere. While carbon offsetting does not require companies to reduce their emissions "in-

house", it provides an environmentally effective option for sectors where the potential for further emissions reductions is limited or the abatement costs are unduly high.

Cloud Point. Temperature at which solids (wax) begin to form and separate from the fuel

CORSIA. Aims to help address any annual increase in total CO_2 emissions from international civil aviation above 2020 levels. Offsetting and carbon markets have been a fundamental component of global, regional and national emissions reduction policies. They have operated for decades for compliance purposes and voluntary emissions reductions, and continue to be an effective mechanism to underpin action against climate change.

"Drop-in" Fuels. A Fuel that can be used with current aircraft and engine technology and does not require modifications to aircraft engines and fuel systems and ground supply infrastructure.

Esterification. Process to produce esters from fatty acids and alcohols, e.g. FAME and FAEE

First Generation Biofuel. Biofuel produced from biomass that may compete with food production, degrade fresh water supply, cause deforestation and/or reduce biodiversity

Fuel. Jet fuel that meets the technical and certification requirements for use in commercial aircraft.

Fischer-Tröpsch Process. A chemical reaction process that uses a catalyst to react carbon monoxide and hydrogen to make hydrocarbons.

Fischer-Tröpsch SPKA. Synthetic paraffinic kerosene that was produced from a starting material using the Fischer-Tropsch process.

Free Fatty Acids. A carboxylic acid with an aliphatic chain that is either unsaturated or saturated in a mixture of triglyceride oil.

Freezing Point. Temperature at which a solid melt on warming

Fossil Fuel. General term for buried combustible geological deposits of organic materials, formed from decayed plants and animals that have been converted to coal, natural gas or crude oil by exposure to heat and pressure in the Earth's crust over hundreds of millions of years.

GtL. Gas to liquid technology

Gasification. Process transforming feedstock into CO and H2 under high temperature

Gas Chromatography-Mass Spectrometry. GC-MS is an analytical technique that combines gas chromatography with mass spectrometry to identify chemical compounds

GCxGC-MSA. Gas chromatography method that utilizes two gas chromatography separation steps followed by analysis by mass spectrometry

Green Transport. A new concept—an initiative to support sustainable economic development without sacrificing the local and global environment.

HEFA Fuels. Fuels produced from vegetable oils via the hydroprocessed esters and fatty acids process.

Hydrocarbons. Molecules made out of carbon and hydrogen, used as fuels

Hydrocracking. Cutting down carbon chains under influence of hydrogen

Hydrotreatment. Saturating and removing impurities in hydrocarbons using hydrogen

Hydroprocessing. Process technology widely used in the refining industry for the production of clean, transportation fuels. The technology utilizes catalysts in the presence of hydrogen to convert a variety of feedstocks, including biologically derived materials, into high-quality fuels.

The International Civil Aviation Organization (ICAO). A UN agency managing the administration and governance of the Convention of International Civil Aviation

Jet A. A kerosene type fuel with a flash point of above 38 °C (100 °F) and a maximum freezing point of -40 °C. Available mostly in the United States. Choice of Jet A in the USA is driven by price and availability.

Jet A-1. A kerosene grade suitable for most turbine engine aircraft. A flash point of above 38 °C (100 °F) and a maximum freezing point of -47 °C. A net heat of combustion of at least 42.8 MJ/kg. Standard specification jet fuel used worldwide. The lower freezing point makes Jet A-1 more suitable for long international flights over polar routes and during winter, but it is more expensive than Jet A.

Jet B. A distillate spanning the naphtha and kerosene fractions of petroleum and having a superior cold weather performance. A freezing point maximum of -50 °C. A net heat of combustion of at

least 42.8 MJ/kg. It has a higher flammability than Jet A and Jet A-1. Significant demand only in very cold climates.

JP-4. The military equivalent of Jet B with added corrosion inhibitors and anti-icing compounds.

JP-5. High flash point kerosene

JP-8. The military equivalent of Jet A-1 with added corrosion inhibitors and anti-icing chemicals

Kerosene. The common name for petroleum-derived jet fuel such as Jet A-1. In addition to its use in aviation, kerosene can be used for a variety of other purposes.

Low Carbon Fuel. Fuels that provide high greenhouse gas lifecycle savings (>60%) when compared with their fossil equivalents.

Marginal Lands. Land with low levels of productivity, poor soil quality, and unsuitable for housing or other uses

Millions of Tons of Oil Equivalent (Mtoe). Unit of energy used to describe the energy content of all fuels, typically on a large scale. It is equal to $4.1868*10^{16}$ Joules.

Neat Bio-SPK. 100 percent Bio-SPK.

Paraffin. Straight-chain alkane hydrocarbons with general formula C_nH_{2n}+2Pyrolysis = heating in absence of oxygen resulting in thermal decomposition

Second Generation Biofuel. Biofuel made from sustainable, non-food biomass such as algae, jatropha, etc.

Specific Energy. Amount of energy per unit weight or volume

Sustainability. In this context is defined as something that can be continually and repeatedly resourced in a manner consistent with economic, social and environmental aims, specifically something that conserves an ecological balance by avoiding depletion of natural resources and does not contribute to climate change.

Sustainable Aviation Fuel (SAF). It is the term preferred by the aviation industry because the scope of the use of this term is broader than aviation biofuels. 'Biofuels' generally refers to fuels produced from biological resources (plant or animal material). However, current technology allows fuel to be produced from other alternative sources, including non-biological resources; thus, the

term is adjusted to highlight the sustainable nature of these fuels. SAF is made by blending conventional kerosene (fossil-based) with renewable hydrocarbon. They are certified as "Jet-A1" fuel and can be used without any technical modifications to aircraft. Other terms such as renewable aviation fuel, renewable jet fuel, alternative fuel, bio jet fuel, and sustainable alternative fuel have similar intended meaning.

Sustainable Fuel. 'Sustainable fuel' can be derived from biomass, but could also be derived from other sustainable sources that have a lower overall carbon footprint than fossil- or some biomass-derived fuels–such as fuels made from bio or non-bio waste streams.

Synthetic Aromatic. A manufactured aromatic hydrocarbon product, i.e. one that contains alternating single and double bonds between carbons. The simplest form of which is known as a benzene ring with six carbon and six hydrogen atoms. Some aromatic compounds in Jet fuel contain more complex fused benzene compounds.

Synthetic Fuel. A manufactured hydrocarbon product which is chemically similar to the fossil equivalent that can be substituted for or mixed with other aviation fuels. It may or may not be produced from sustainable feedstock.

Synthetic Paraffinic Kerosene (SPK). Aviation fuel that contains predominantly paraffins produced from non-petroleum feedstocks.